ParisTech
INSTITUT DES SCIENCES ET TECHNOLOGIES
PARIS INSTITUTE OF TECHNOLOGY

TELECOM ParisTech

2017-ENST-0051

EDITE - ED 130

Doctorat ParisTech

T H È S E

pour obtenir le grade de docteur délivré par

TELECOM ParisTech

Spécialité « Electronique et Communications »

présentée et soutenue publiquement par

Ahmad BAZZI

23 Octobre 2017

Techniques d'estimation de paramètres pour la localisation à l'intérieur via WiFI

Directeur de thèse : **Dirk SLOCK**
Co-encadrement de la thèse : **Lisa MEILHAC**

Jury

M. Mérouane DEBBAH, Professeur, CentraleSupélec	Président du jury
M. Karim ABED-MERAIM, Professeur, Université d'Orléans	Rapporteur
M. Marius PESAVENTO, Professeur, Technische Universität Darmstadt	Rapporteur
M. Pascal LARZABAL, Professeur, ENS Cachan	Examinateur

TELECOM ParisTech
école de l'Institut Télécom - membre de ParisTech

THÈSE

RivieraWaves-CEVA and Telecom ParisTech

Parameter Estimation Techniques for Indoor Localisation via WiFi

by

Ahmad Bazzi

A thesis submitted in partial fulfillment for the
degree of Doctor of Philosophy

in the
EURECOM
Dpt. Communication Systems

March 2018

"Half of knowledge is having ability to say I don't know."

Imam Ali Ibn Abi Taleb (AS)

RivieraWaves-CEVA and Telecom ParisTech

Abstract

EURECOM
Dpt. Communication Systems

Doctor of Philosophy

by Ahmad Bazzi

In an indoor environment, the problem of extracting the Angle-of-Arrival of the Line-of-Sight component between a transmitter and Wi-Fi receiver using a SIMO link is the main concern of this PhD thesis. One main challenge in doing so is due to the rich multipath channel that indoor environments enjoy. Other challenges are limitation of resources, such as number of antennas, available bandwidth, and Signal-to-Noise-Ratio; not to mention the Wi-Fi "imperfections", such as gain/phase mismatches between antennas and synchronisation issues between transmitter and receiver. In this thesis, our main focus is implementing a real-time system that could measure the angle between a transmitter and receiver in the presence of all the previous challenges.

...

Acknowledgements

First and foremost, I would like to express my deepest gratitude to my two Ph.D. advisors, Dr. Lisa Meilhac and Prof. Dirk Slock for their constant support and guidance. Their joint supervision, complementary research approaches and positive thinking gave me the confidence to master challenging problems and allowed me to benefit from an amazing research experience. Also, their precious advices and encouraging words in any moment of my PhD greatly helped me to overcome the 'down' periods every PhD candidate faces during the thesis.

I would like to thank Prof. Mérouane Debbah, Prof. Karim Abed-Meraim, Prof. Jean-Pierre Delmas, and Prof. Pascal Larzabal for having agreed to be part of the jury committee. I feel honoured to have had the opportunity to present my Ph.D. work in front of such prominent scientists. Also, their precious and detailed comments certainly helped to improve the quality of this dissertation.

I would like to gratefully acknowledge the RivieraWaves team, which financially supported part of my Ph.D.; my special thanks go to Olivier Ringot and Dr. Lisa Meilhac (again). I would like to start with Olivier's perseverance and patience with me during the multiple Campaigns we have done throughout the previous three years. If it weren't for Olivier, the last Chapter would not have been possible to reproduce. Furthermore, there are many wonderful things I could say about Lisa. Briefly, if it weren't for her determination and bright ideas, this thesis would have never been completed.

A note of sincere gratitude goes to my parents Fatima and Abed and to my brothers: Ali and Zein and to my sister, Maysa. Their presence in my life is the only thing I need. Even if for them it was quite hard to fully understand many aspects of my PhD, such as the meaning of a deadline, their generosity of heart and constant love were fundamental pillars for me.

Finally, a special thanks goes to my *'wife to be'*, Fatima. I feel that, without her constant kind words and sacrifices, this PhD would have been very hard to finalise. I feel blessed to have such an extraordinary person at my side!

Contents

List of Figures

Abbreviations

AoA	Angle-of-Arrival
ToA	Time-of-Arrival
JADE	Joint Angle and Delay Estimation
JADED	Joint Angle and Delay Estimation and Detection
SIMO	Single-Input-Multiple-Output
OFDM	Orthogonal Frequency-Division Multiplexing
SA	Selective Availability
GPS	Global Positioning System
DoD	Department of Defense
IPS	Indoor Positioning System
BLE	Bluetooth Low Energy
IEEE	Institute of Electrical and Electronics Engineers
RSSI	Received Signal Strength Indication
GRPR	Golden Receiver Power Range
ULA	Uniform Linear Array
MUSIC	MUltiple SIgnal Classification
ESPRIT	Estimation of Signal Parameters via Rotational Invariance Techniques
LS	Least Squares
WLS	Weighted Least Squares
ML	Maximum Likelihood
IQML	Iterative Quadratic Maximum Likelihood
DIQML	Denoised Iterative Quadratic Maximum Likelihood
AP	Alternating Projections
WiFi	Wireless Fidelity

VB	Variational Bayes
MP	Matching Pursuit
OMP	Orthogonal Matching Pursuit
GP	Gradient Pursuit
IHT	Iterative Hard Thresholding
NIHT	Normalised Iterative Hard Thresholding
ISTA	Iterative Shrinkage-Thresholding Algorithm
SABMP	Sparse reconstruction using distribution Agnostic Bayesian Matching Pursuit
FBMP	Fast Matching Bayesian Pursuit
BPDN	Basis Pursuit Denoising
MP	Matrix Pencil
CESS	Computationally Efficient Single Snapshot
MDL	Minimum Description Length
MMDL	Modified Minimum Description Length
CSI	Cubic Spline Interpolation
CFO	Carrier Frequency Offset
SFO	Sampling Frequency Offset
Tx	Transmitter
Rx	Receiver

Symbols

$\mathbb{C}^{M\times N}$	Class of all $M \times N$ complex-valued matrices
$\mathbb{C}^*$	Class of all complex-valued numbers except zero
$\boldsymbol{A}^{\mathrm{T}}$	Transposition of matrix $\boldsymbol{A}$
$\boldsymbol{A}^*$	Conjugatation of matrix $\boldsymbol{A}$
$\boldsymbol{A}^{\mathrm{H}}$	Conjugate-transposition of matrix $\boldsymbol{A}$
$\boldsymbol{A}^+$	*Moore-Penrose* pseudo-inverse of matrix $\boldsymbol{A}$
$\mathrm{Re}\{\boldsymbol{A}\}$	Real part of matrix $\boldsymbol{A}$
$\mathrm{rank}\,\boldsymbol{A}$	Rank of matrix $\boldsymbol{A}$
$\|\boldsymbol{A}\|$	*Frobenius* norm of matrix $\boldsymbol{A}$
$(\boldsymbol{A})_{i,j}$	The $(i,j)^{th}$ element of matrix $\boldsymbol{A}$
$\boldsymbol{I}_k$	The identity matrix in $\mathbb{C}^{k\times k}$
$\boldsymbol{J}_k$	An all-zero matrix in $\mathbb{C}^{k\times k}$ except ones at its anti-diagonal
$\boldsymbol{0}$	The zero matrix with appropriate dimensions
$\boldsymbol{A}\odot\boldsymbol{B}$	The *Hadamard* product of $\boldsymbol{A}$ and $\boldsymbol{B}$
$\boldsymbol{A}\otimes\boldsymbol{B}$	The *Kronecker* product of $\boldsymbol{A}$ and $\boldsymbol{B}$
$\boldsymbol{A}\boxtimes\boldsymbol{B}$	The *Khatri-Rao*, or column-wise *Kronecker* product, product of $\boldsymbol{A}$ and $\boldsymbol{B}$
$\mathcal{N}(\boldsymbol{A})$	The null-space of $\boldsymbol{A}$, i.e. $\boldsymbol{x}\in\mathcal{N}(\boldsymbol{A})$ if $\boldsymbol{A}\boldsymbol{x}=\boldsymbol{0}$
$\boldsymbol{e}_i$	The i^{th} column of $\boldsymbol{I}$
$X \Longrightarrow Y$	If X is true, then Y is true
$X \Longleftrightarrow Y$	Statements X and Y are equivalent
$\mathbb{E}\{X\}$	Expectation of a random variable X
$\mathcal{R}(\boldsymbol{A},\boldsymbol{x})$	*Rayleigh quotient*, $\frac{\boldsymbol{x}^{\mathrm{H}}\boldsymbol{A}\boldsymbol{x}}{\boldsymbol{x}^{\mathrm{H}}\boldsymbol{x}}$
$\mathbb{1}_k$	$k\times 1$ vector of all-ones
$\delta_{i,j}$	The *Dirac* delta (If $i=j$, then $\delta_{i,j}=1$, else 0)

$\|z\|$	Magnitude of complex number z
$\mathcal{CN}(\boldsymbol{\nu}, \boldsymbol{\Sigma})$	Complex Gaussian of mean $\boldsymbol{\nu}$ and covariance matrix $\boldsymbol{\Sigma}$
argmin	Argument of the minimum.
$\max\{A, B\}$	returns A, if $A \geq B$, else returns B. argmax

Argument o

To Mom, Dad, my beloved siblings, and Fatima ...

Chapter 1

Introduction

1.1 Motivation

1.1.1 Brief history

Localisation refers to the process of locating intended object(s) in space. Although most often associated with modern technology, more primitive localisation methods exist. As a matter of fact, the most basic localisation techniques could be achieved without the use of any special instruments; sailors have been using celestial objects for sea-based localisation for a few thousand years. Many specialised tools have been developed to help provide more accurate localisation, including astrolabe, chronometer, sextant, and compass as well as detailed maritime charts and maps [1]. In the late 1960s, the U.S. Department of Defense (DoD) started off with a project to construct a satellite-based localisation system for military purposes; known nowadays as Global Positioning System, or simply GPS. The system witnessed its first use in combat during the Persian Gulf War in 1990. Furthermore, GPS consists of a constellation of 24 satellites that broadcast precise time signals. When the satellites are in view of a suitable GPS receiver, these signals aid position-location, navigation, and precision timing [1]. Not until 1983 has GPS started evolving far beyond its military origins and begun to migrate into the public sector. It is now a worldwide information resource supporting a wide range of civil, scientific, and commercial functions, ranging from air traffic control and real-time navigation on the road to coffee shop discovery in your block.

In response and due 1990, the DoD activated Selective Availability (SA), a purposeful degradation in the civilian GPS signal, which limited the accuracy of most civilian

GPS units to about 100 meters. Luckily SA was triggered off due to the fact that the DoD recognised the important role played by GPS in numerous commercial activities. Thanks to the deactivation of SA, along with the employment of other technologies such as Differential GPS, now allow civilian GPS units to obtain an accuracy of 10 meters or better. So for localisation in an outdoor environment, GPS works extremely well, given that there is an unobstructed line of sight to four or more GPS satellites. However, the signal from the GPS is too weak to penetrate most buildings, hence GPS is useless indoors; a motivation for seeking other techniques for indoor localisation.

An Indoor Positioning system, or simply IPS, is a data acquisition system providing information of people or objects within the indoor environment and obtaining data to occupants to assist in way finding. Said differently and informally, an IPS is a *mini-GPS* working indoors, where a *mini-GPS* might refer to a Wi-Fi receiver. Whereas GPS depends on satellites, IPS is based on "reference anchors" that are network nodes with a known fixed position in the indoor environment. These "anchors" cooperate with each other to identify the position of the intended node. One approach to the architecture of IPS is "Bluetooth Beaconing". Bluetooth was first invented in 1994 to replace short cables. All thanks to Bluetooth-enabled smartphones together with the Bluetooth beacons that can provide the location of smartphone users. In 2010, Nokia introduced an IPS based on Bluetooth Low Energy (BLE) technology, which was one of latest Bluetooth technology operating on low power with low latency in communications. On the other hand, a lot of systems use enhanced Wi-Fi infrastructure to provide location information [4–6]. Wi-Fi positioning takes advantage of the rapid growth in the early 21^{st} century of wireless access points in urban areas.

Ladd et al present a novel technique whereby localisation is achieved using the IEEE 802.11b, known as wireless Ethernet [2]. In their paper, Ladd et al propose the use of measured signal strength of Ethernet packets as a sensor for a localisation system. The 802.11b wireless standard incorporates a mechanism by which a wireless network card can measure the signal strength of all base stations within its broadcast range [3]. Consequently, a mobile system can use this information in an attempt to determine its distance from these fixed based stations. Given these distances and the prior knowledge of the base stations' location, the mobile system can estimate its own current position. Perturbation of the actual position of the mobile system will cause a change in the actual position of the mobile system results in a change in the measured signal strengths and therefore a change in the estimated position. The idea is simply stated but the actual implementation is much more complicated where Ladd et al use the so-called Bayesian inference localisation. They have implemented this approach to achieve an accuracy of about one meter.

Unfortunately, the chief difficulty in localisation with wireless Ethernet is predicting signal strength. "Radio frequency signal strength measured indoors is nonlinear with distance. In addition, it has non-Gaussian noise, resulting from multipath effects and environmental effects, such as building geometry, network traffic, presence of people, and atmospheric conditions" [2]. On top of that, IEEE 802.11b standard operates in the 2.4-GHz frequency band, meaning "Microwave ovens, Bluetooth devices, 2.4-GHz cordless phones, and welding equipment can be sources of interference. Ladd et al came up with an idea where they broke up the area of interest into cells, and then took signal strength readings in each cell, effectively training the system. A mobile system could then take signal strength readings, compare the measured data to the training set, and use Bayesian Inference to determine the location that would most likely produce those measurements.

Future research [2] was highlighted by Lad et al. Studies were conducted at night-time, i.e. a nearly static environment, and in particular in corridors, which means that movement was restricted to narrow straight lines. They point out the interest of studying the behaviour of a system in a more dynamic environment. The advantage of localising via wireless Ethernet should be clear: In contrast to GPS, the system could work in any environment, whether indoors or outdoors, while GPS only operates for outdoor systems. In addition to that, this technology is ubiquitous and, therefore, no additional hardware cost would be needed.

1.1.2 Parameters inferring location

Received Power

Received power is one of the basic and oldest measuring principles to compute the distance between a transmitter and its corresponding receiver. This relation is given by the free space path loss equation using isotropic radiating antennas [7]:

$$P_R = \frac{P_T G_T G_R}{(4\pi d/\lambda)^2}$$

where P_R and P_T are the received and transmitted power, respectively; G_R and G_T are the receive and transmit antenna gains, respectively; λ is the wavelength of the propagating signal; and d is the separating distance between the transmitter and receiver. As a result, a widely used indicator could be derived which is known as Received Signal Strength Indicator (RSSI). It is an 8-bit signed integer that denotes whether the received power level is within or below/above the Golden Receiver Power Range (GRPR)[8].

RSSI indicates 0 if the received power is within the GRPR; positive if it is above and negative if it is below. Although RSSI was intended for power control purposes [9], many Bluetooth devices, such as Bluetooth 1.2 uses RSSI to discover any nearby devices [10] and estimate the separating distance. However, as tested in [8], RSSI doesn't correlate well with distance. The reasons why is that RSSI is a quantized version of the provided received power and therefore the accuracy would mainly depend on the resolution of the quantization. Also, RSSI is highly affected by multipath, which is a main feature of indoor environments.

Time-of-Arrival

The distance d between the mobile target to the measuring unit is directly proportional to the propagation time Δt. So upon measuring Δt, one could easily calculate the separating distance between the mobile target and the measuring unit by:

$$d = c\Delta t$$

where c is the speed of light in vacuum. However, accurate timing synchronization is required between transmitter and receiver clocks to perform ToA estimation [11].

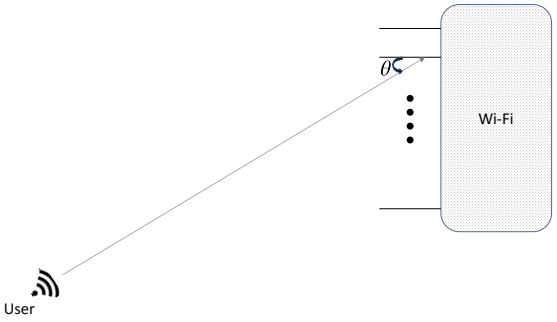

Figure 1.1: User transmitting to Wi-Fi at angle θ

Angle-of-Arrival

Angle of Arrival (or AoA) is a technique based on the relative time delay with respect to an arbitrary antenna chosen as a reference i.e. the time delay at this reference antenna is zero. Assume the SIMO case, as shown in Fig. 1.1, where the user is equipped with

one antenna and receive antennas. Let the transmitted signal at any time be $s(t)$ where it is of the form

$$s(t) = Ae^{j2\pi f_c t}$$

The form of $s(t)$ in the above equation is a valid form of an electromagnetic transmitted signal having two orthogonal components, which are the Inphase (or I) and the Quadrature (or Q). This signal is transmitted with amplitude A and is oscillating on frequency f_c. Following [12], it is easy to show that the received signal is of the form

$$\boldsymbol{r}(t) = \boldsymbol{a}(\theta)s(t)$$

where $\boldsymbol{a}(\theta)$ is the so-called *steering vector*, which is a function of the antenna's position and the AoA, θ.

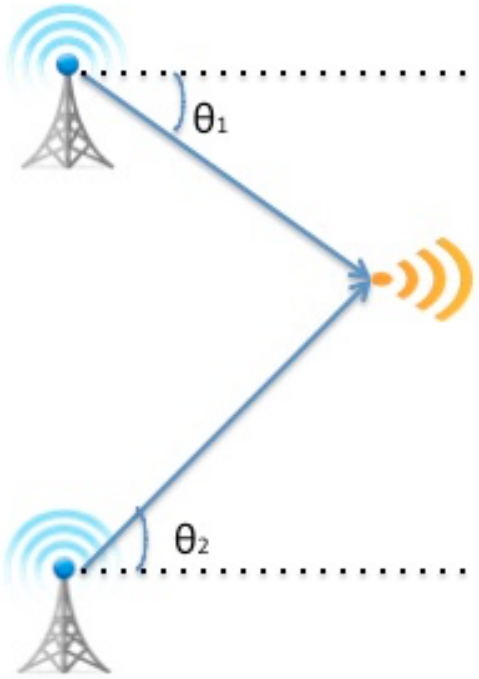

Figure 1.2: Angle-based localisation

Figure 1.3: The two fundamental steps for Position Estimation

After θ is estimated by a suitable *Parameter-Estimation* method by, say, two stations (or WiFis) as depicted in Fig. 1.2, then the position of the user could be easily determined. This means that a 2-step procedure is required to determine a position of a user: a

(i)Parameter-Estimation step followed by a *(ii)Location-Estimation* step. *In this thesis, we focus on the first block, i.e. we are very interested in deriving suitable methods that could yield parameter estimates, which infer the position of the user in the presence of noise, imperfections, impairments, and other difficulties, which will be addressed in the next section.*

1.2 Parameter Estimation: Problems and Methods

The term *Parameter Estimation* refers to the process of utilising sample data to estimate parameters of interest in a certain model, under certain assumptions. It is worth to take a moment and highlight three keywords in the previous statement: *model*, *parameter*, and *assumptions*. One difficulty in indoor localisation is actually confirming a model. For example, Saleh and Valenzuela [13] have modeled the multipath channel as a diffuse one, namely each multipath component is a cluster of rays. Based on their results, they have modeled the ToAs of the clusters as Poisson processes with different, but fixed, rates. The thesis in [14], which is inspired by [13], model the AoAs of the clusters as a Laplacian distribution. However, most (if not all) localisation methods, such as [15–18] assume a specular multipath channel, i.e. each multipath component is only one ray. This seems acceptable due to resolution issues[1] and hence closely spaced sources could be seen as one source.

After confirming a model, or a family of models, parameters involved in these models need to be estimated. This is where parameter estimation methods come in. The Maximum Likelihood (ML) was one of the first methods to be investigated [20]. Even though the ML method is optimal, in the sense that the estimated parameters minimize the Mean-Squared Error (MSE), it did not receive much attention due to the high computational load of the multivariate nonlinear minimisation problem involved, since it requires a q-dimensional search, where q are the number of parameters that enter the model in a non-linear form. Then, a number of interesting beamforming methods were implemented, as solutions to some suitable optimisation problems, such as Bartlett's beamformer [21] and Capon's beamformer [22]. These beamformers require a 1-dimensional (1D) search and are therefore considered to be fast. However, the resolution of these methods are not acceptable with low number of antennas, snapshots, and SNR, which calls for the need of methods with higher accuracy, while maintaining an acceptable computational speed. The 80s witnessed a revolution of the so-called *subspace methods*, which are built on one genuine idea: *"the subspace spanned by the*

[1] In the context of array processing, resolution refers to the ability of discriminating between two closely spaced sources, given a certain SNR [19]

steering vectors of the sources is orthogonal to the noise subspace"[2] The most popular subspace method is the MUltiple SIgnal Classification algorithm, also known as MUSIC [24] by Schmidt, which only requires a 1D search. A root-MUSIC [25] method was implemented by Barabell to replace the 1D search of MUSIC by a polynomial root finding criterion. Paulraj and Kailath invented the ESPRIT [26] (Estimation of Signal Parameters Via Rotational Invariance Techniques) method, which is based on Least-Squares fitting; however, it only operates for Uniform Linear Arrays (ULAs). Even though these methods dominate the aforementioned beamformers in terms of resolution, there are cases where subspace methods fail to operate, such as:

- Coherent sources: which is the case of smart jamming or multipath propagation. A very simple example of two coherent sources are $s_1(t)$ and $s_2(t) = \alpha s_1(t)$, where α is a complex number.
- Single snapshot: since no subspaces could be formed by a single snapshot.

It is worth mentioning that there is a large number of recent research done on subspace methods; we refer the reader to the following papers [27–29].

Another class of parameter estimation methods work on approximating the ML cost function, which are also computationally attractive, but not as attractive as subspace methods. For example, the method by Ziskind and Wax [30] reaches the ML estimate by multiple 1D searches, which is described as Alternating Projections (AP). Another popular technique is the Iterative Quadratic ML (IQML) developed by Bresler and Macovski in [31], where, with a linear parameterisation of the noise subspace, the ML cost function at each iteration is seen as a weighted LS cost function, which is quadratic in the vector of parameters of interest, and thus closed form expressions could be derived. However, the weighting is parameter dependent and hence fixed-point iterations are required.

In addition to parameter estimation methods, one is limited by the number of multipath components allowed in the model. More specifically, let q denote the number of multipath components and N denote the number of antennas at the Wi-Fi; then $q < N$ should be satisfied, otherwise the estimation problem is under-determined, and the estimated solution will not be unique. There is many work done by Pal and Vaidyanathan , such as [32, 33], where they try to estimate the AoAs of q sources, where $q > N$. This is achieved by coprime sampling, i.e. by partitioning the N antennas into two subarrays of sizes N_1 and N_2, where $N = N_1 + N_2$ and (N_1, N_2) are co-prime. The coprime sampling approach suggests specific antenna array configurations, called coprime arrays.

[2] This is explained in details in Chapter 6.

The advantage is that we now have more degrees of freedom, i.e. the number of sources could go up to $q < O(N_1 N_2)$. However, this approach has multiple drawbacks, when our interest is oriented towards indoor localisation via WiFi:

- The sources are assumed to be completely uncorrelated, which is not valid for multipath sources. On the contrary, multipath components are known to be coherent.
- With a small number of antennas, say $N = 3$ antennas, we could not expect to enhance the degrees of freedom by choosing, for instance, $N_1 = 2$ and $N_2 = 1$.
- The AoA between the transmitter and receiver could not be deduced by AoA information only.

On the other hand, Vanderveen, Papadias and Paulraj introduced a novel approach called JADE [34], which stands for Joint Angle and Delay Estimation. They propose to transmit a known signal through a multipath channel, which is received through N antennas at the receiver and M time samples are collected at each antenna. This idea has multiple advantages in the context of indoor localisation via WiFi:

- The degrees of freedom of the number of multipath components could go up to $q < MN$.
- There is no limitation on the geometry of antennas.

We note that JADE is not, in any way, a method. It is simply a smart way of collecting data to increase the number of components that could be resolved. Therefore, it is natural to propose JADE-based methods, such as JADE-ML and JADE-MUSIC in [34] and JADE-ESPRIT in [35]. One should note that the coherence part was not addressed.

Besides the degrees of freedom and coherence of sources, another important aspect to be considered is array perturbation. This is caused by several factors, such as antenna position uncertainty [36], unknown gain/phases between different antennas [37], and mutual coupling between antennas [38]. We address this topic in details in Chapters 6 and 7.

1.3 Contributions of this dissertation

In this thesis, we address all the problems addressed in the previous section in order to derive some methods that perform parameter estimation. In particular,

Chapter 2. In Chapter 2, we tackle a well-known problem involved in array signal processing, which is the detection of number of signals present in the model. Indeed, all the methods mentioned previously require the number of signals to be known a priori. The Minimum Description Length, or MDL [39], is a well-known method for this matter, however it suffers from degradation of performance when the number of available snapshots is, relatively, low. We derive a modified MDL estimator, with the help of random matrix tools [41–43], which improves the estimation of the number of sources when a low number of snapshots $L = \mathcal{O}(N)$ is available.

Publications related to this chapter are:

- A. Bazzi, D. T.M. Slock, L. Meilhac, "Detection of the number of Superimposed Signals using Modified MDL Criterion : A Random Matrix Approach," *IEEE International Conference on Acoustics, Speech, and Signal Processing* (ICASSP), March, 2016.

Chapter 3. In Chapter 3, we address the AoA estimation problem from a compressed sensing point of view. The contributions of this chapter are summarised as follows:

1. After a literature review on some popular compressed sensing methods, we propose a Variational Bayes (VB) method that allows sparse recovery of the desired transmitted signals, which in turn allows estimating their corresponding AoAs.
2. We show that this iterative VB method outperforms existing compressed sensing methods, such as Matching Pursuit (MP) [50], Orthogonal MP (OMP) [51], and some other methods.
3. We also derive a Newton-type Forward Backward Greedy method that performs sparse recovery, given the data.
4. We show, through exhaustive simulations, that the proposed Newton-type method, is not only faster, but attains a lower MSE when compared to methods such as Fast Matching Bayesian Pursuit (FBMP) [67] and Basis Pursuit Denoising (BPDN) [53].

Publications related to this chapter are:

- A. Bazzi, D. T.M. Slock, L. Meilhac, S. Panneerselvan, "A Comparative Study of Sparse Recovery and Compressed Sensing Algorithms with Application to AoA Estimation," *IEEE International Workshop on Signal Processing advances in Wireless Communications* (SPAWC), 2016.

- A. Bazzi, D. T.M. Slock, L. Meilhac, "Sparse Recovery using an Iterative Variational Bayes Algorithm and Application to AoA Estimation," *IEEE Symposium on Signal Processing and Information Technology* (ISSPIT), 2016.
- A. Bazzi, D. T.M. Slock, L. Meilhac, "A Newton-type Forward Backward Greedy Method for Multi-Snapshot Compressed Sensing," *Asilomar conference on signals, systems, and computers* (ASILOMAR), 2017.

Chapter 4. In Chapter 4, we focus on the Joint Angle and Delay Estimation (JADE) problem for localisation purposes. More specifically, we address the single-snapshot and coherence problems mentioned in the previous section. The contributions of this chapter could be summarised as follows:

1. We derive an algorithm that is a modification of the two dimensional Iterative Quadratic ML (2D-IQML) algorithm, where an additional constraint is added for joint ToA and AoA estimation and we show that 2D-IQML gives biased estimates of ToAs/AoAs and performs poorly at low SNR due to noise induced bias.
2. We propose a two dimensional Denoised IQML (2D-DIQML) that gives consistent estimates and outperforms 2D-IQML; (iv) we show that 2D-DIQML is asymptotically globally convergent and hence insensitive to the initialisation.
3. Furthermore, two algorithms, based on 2D Matrix Pencils (MP), for the case of a single snapshot OFDM symbol observed by multiple antennas in a ULA configuration are introduced.
4. For the coherence problem, we derive a "Spatio-Frequential" smoothing technique, when the transmit OFDM symbol is received through multiple coherent signals using a uniform linear antenna array, which is the case of an indoor multipath channel. This smoothing method is inspired from [81] and could be seen as a 2D generalisation of the traditional spatial smoothing technique.
5. We prove in Theorem 4.3 that we could *"lift"* the rank of the sample covariance matrix, so that we could discriminate between coherent sources, and therefore apply subspace methods such as JADE-MUSIC and JADE-ESPRIT.

Publications related to this chapter are:

- A. Bazzi, D. T.M. Slock, L. Meilhac, "Efficient Maximum Likelihood Joint Estimation of Angles and Times of Arrival of Multi Paths," *IEEE GLOBAL Communications Conference* (GLOBECOM), Localization and Tracking : Indoors, Outdoors, and Emerging Networks (LION) Workshop, December, 2015.

- A. Bazzi, D. T. M. Slock, and L. Meilhac, "Single Snapshot Joint Estimation of Angles and Times of Arrival: A 2D Matrix Pencil Approach," *IEEE International Conference on Communications*, 2016.

- A. Bazzi, D. T.M. Slock, L. Meilhac, "On Spatio-Frequential Smoothing for Joint Angles and Times of Arrival Estimation of Multipaths," *IEEE International Conference on Acoustics, Speech, and Signal Processing* (ICASSP), March, 2016.

Chapter 5. In Chapter 5, we propose a novel approach, which builds up on JADE, entitled Joint Angle and Delay Estimation and Detection, or simply JADED. The contributions of this chapter are summarised as follows:

1. Thanks to this approach, we can now estimate the Angles and Times of Arrival of multipath, without prior knowledge of the number of multipath components. To the best of our knowledge, this problem has not been addressed in the open literature.

2. A method called JADED-RIP, makes use of the Rotational Invariance Properties (RIP) of ULAs and OFDM symbols, detects the number of multipath components, and estimates the angles and times of arrival of each path by performing a 2D search.

3. Another method is a Computationally Efficient Single Snapshot (CESS) version of the JADED-RIP, called CESS-JADED-RIP. This method requires a 1D search followed by a least squares fit, and can only be used when a single OFDM symbol is available.

The drawback of the two proposed methods is that they only work for ULA/OFDM systems and they are sub-optimal in a sense they could be further improved by considering the coloured noise, which leads to an ML-JADED estimator.

Publications related to this chapter are:

- A. Bazzi, D. T.M. Slock, L. Meilhac, "JADED-RIP: Joint Angle and Delay Estimator and Detector via Rotational Invariance Properties," *IEEE International Symposium on Signal Processing and Information Technology*, (ISSPIT), 2016.

Chapter 6. In Chapter 6, we address an important aspect that perturbs Angle-of-Arrival estimation, due to antenna coupling, also known as "Mutual Coupling". The contributions of this chapter are summarised as follows:

1. We derive a sub-optimal algorithm that could estimate AoAs in the presence of mutual coupling.

2. We show why this sub-optimal algorithm, along with other ones [88–92], are indeed suboptimal, in the sense that there is an upper bound on the coupling parameters allowed in the model which can be improved. This would not have been clear without Theorem 6.6.

3. Then, we further improve the sub-optimal algorithm and propose an optimal one, in the sense that more coupling parameters are allowed in the model.

4. Also, we refine the estimates of the optimal algorithm by modifying some constraints of the optimisation problem considered.

5. We derive the MSE expression of the optimal algorithm and show that, in some cases, we can attain the *Cramér-Rao* bound of the problem of joint coupling parameters and AoA estimation. The related Theorems are Theorem 6.7, Theorem 6.9 and Theorem 6.10.

6. Finally, we derive an iterative method that could give Maximum Likelihood (ML) estimates of the AoAs, and therefore allowing the presence of coherent sources, which is not the case of all the previous algorithms.

Publications related to this chapter are:

- A. Bazzi, D. T.M. Slock, L. Meilhac, "Online Angle of Arrival Estimation in the Presence of Mutual Coupling," *IEEE International Workshop on Statistical Signal Processing* (SSP), 2016.

- A. Bazzi, D. T.M. Slock, L. Meilhac, "On Mutual Coupling for ULAs: Estimating AoAs in the presence of more coupling parameters," *IEEE International Conference on Acoustics, Speech, and Signal Processing* (ICASSP), 2017.

- A. Bazzi, D. T.M. Slock, L. Meilhac, "Performance Analysis of an AoA estimator in the presence of more mutual coupling parameters," *IEEE International Conference on Acoustics, Speech, and Signal Processing* (ICASSP), 2017.

- A. Bazzi, D. T.M. Slock, L. Meilhac, "On a Mutual Coupling Agnostic Maximum Likelihood Angle of Arrival Estimator by Alternating Projection," *IEEE Global Conference on Signal and Information Processing* (GlobalSIP), 2016.

- A. Bazzi, D. T.M. Slock, L. Meilhac, "A Mutual Coupling Resilient Algorithm for Joint Angle and Delay Estimation," *IEEE Global Conference on Signal and Information Processing* (GlobalSIP), 2016.

Chapter 7. In Chapter 7, we aim at building a real system that could perform joint Angle and Delay of Arrival Estimation and Detection of multipath components. This is simply done, so that we could extract the Angle-of-Arrival of the Line-of-Sight (LoS) component between the transmitter and receiver.

1. We take into account all critical factors that perturb the Joint Angle and Delay estimation problem and formulate a system model accordingly.
2. We propose an offline calibration method to compensate for all such factors.
3. With the help of the CESS-JADED-RIP algorithm, we have successfully been able to estimate the Angles and Times of Arrival of all the multipath components, which allowed for the extraction of the AoA of the LoS component.

There is no published material related to this chapter.

Other Work. For the sake of consistency of this thesis, we have omitted three publications, which are the following:

- A. Bazzi, D. T.M. Slock, L. Meilhac, "On the Effect of Random Snapshot Timing Jitter on the Covariance Matrix for JADE Estimation," *European Signal Processing Conference* (EUSIPCO), September, 2015.
- A. Bazzi, D. T.M. Slock, L. Meilhac, "On Joint Angle and Delay Estimation in the Presence of Local Scattering," *IEEE International Conference on Communications* (ICC), Workshop on Advances in Network Localization and Navigation, 2016.
- L. Meilhac and A. Bazzi, "Downlink transmit beamsteering Apparatus for a multi-user MIMO transmission," Patent in Preparation, 2017.

Chapter 2

Angle-of-Arrival Detection

In this chapter, we study the problem of estimating the number of superimposed signals using noisy observations from N antennas. In particular, we are interested in the case where a low number of snapshots $L = \mathcal{O}(N)$ is available. Our main contribution can be summarised as follows: we derive a modified MDL estimator, with the help of random matrix tools, which improves the estimation of the number of sources.

2.1 System model

2.1.1 Problem formulation

Consider an array that consists of N antennas. Furthermore, assume $q < N$ narrow-band sources, centered around a known frequency, say f_c, attacking the array from different angles, $\boldsymbol{\Theta} = [\theta_1 \dots \theta_q]$. Since narrow-bandedness in the context of array processing means that the propagation delays of the signals across the array are much smaller than the reciprocal of the bandwidth of the signals, it follows that these propagation delays translate into phase shifts that depend on the location.

Now following [23], the received analog signal across all antennas, in the absence of mutual coupling, could be written as

$$\boldsymbol{x}(t) = \sum_{i=1}^{q} \boldsymbol{a}(\theta_i) s_i(t) + \boldsymbol{w}(t) \tag{2.1}$$

where

$$\boldsymbol{x}(t) = \big[x_1(t) \dots x_N(t)\big]^{\mathrm{T}} \tag{2.2}$$

is the received vector across all antennas at time t. Moreover, the vector $\boldsymbol{a}(\theta)$ is referred to as the "steering vector" of the array towards angle θ. It is this vector that allows us to perform Angle-of-Arrival (AoA) estimation, and is given by

$$\boldsymbol{a}(\theta) = \left[1, z_\theta, \dots z_\theta^{N-1}\right]^{\mathrm{T}} \tag{2.3}$$

where $z_\theta = e^{-j2\pi \frac{d}{\lambda}\sin(\theta)}$, d is the inter-element spacing and λ is the signal's wavelength. Moreover, the signal $s_i(t)$ is the signal emitted by the i^{th} source at time t and

$$\boldsymbol{w}(t) = \left[w_1(t) \dots w_N(t)\right]^{\mathrm{T}} \tag{2.4}$$

is background noise across all antennas at time t. Equation (2.1) could be written in a more compact way as follows

$$\boldsymbol{x}(t) = \boldsymbol{A}(\boldsymbol{\Theta})\boldsymbol{s}(t) + \boldsymbol{w}(t) \tag{2.5}$$

where $\boldsymbol{A}(\boldsymbol{\Theta}) \in \mathbb{C}^{N\times q}$ is referred to as "steering matrix" and is given as

$$\boldsymbol{A}(\boldsymbol{\Theta}) = \left[\boldsymbol{a}(\theta_1) \dots \boldsymbol{a}(\theta_q)\right] \tag{2.6}$$

and $\boldsymbol{s}(t) \in \mathbb{C}^{q\times 1}$ is the vector of transmitted signals, viz.

$$\boldsymbol{s}(t) = \left[s_1(t) \dots s_q(t)\right]^{\mathrm{T}} \tag{2.7}$$

Finally, sampling (2.5) at L time instances, say $t = \{0, T, \dots, (L-1)T\}$, where T is the sampling period, we get

$$\boldsymbol{X} = \boldsymbol{A}(\boldsymbol{\Theta})\boldsymbol{S} + \boldsymbol{W} \tag{2.8}$$

where $\boldsymbol{X} = [\boldsymbol{x}(0), \boldsymbol{x}(T), \dots, \boldsymbol{x}\big((L-1)T\big)] \in \mathbb{C}^{N\times L}$ is the data collected over the observed interval of time. Matrices $\boldsymbol{S} \in \mathbb{C}^{q\times L}$ and $\boldsymbol{W} \in \mathbb{C}^{N\times L}$ are similarly defined.

2.1.2 Assumptions

- **A1.** The matrix of spatial signatures, i.e. $\boldsymbol{A}$, is full column rank. This is valid when $q \leq N$ and all angles of arrival are distinct, i.e. $\theta_i \neq \theta_j$ for all $i \neq j$.
- **A2.** The sources are assumed to be non-coherent, i.e. $\boldsymbol{R}_{ss} = \mathbb{E}\{\boldsymbol{s}(t)\boldsymbol{s}^H(t)\}$ is full rank.
- **A3.** The noise is modelled as complex Gaussian vectors, i.i.d over time, with zero-mean and covariance $\sigma^2\boldsymbol{I}_N$. Also, the noise is independent from the signal.

2.1.3 Problem statement

Under the above assumptions, we are now ready to state our problem: *"Given the available snapshots $\boldsymbol{X}$, estimate the number of source signals, i.e. q."*

2.2 Background of main result

We write down the signal covariance matrix as

$$\begin{aligned}\boldsymbol{R}_{xx} &= \mathbb{E}\{\boldsymbol{x}(t)\boldsymbol{x}^H(t)\} \\ &= \mathbb{E}\big(\boldsymbol{A}(\boldsymbol{\Theta})\boldsymbol{s}(t)+\boldsymbol{w}(t)\big)\big(\boldsymbol{A}(\boldsymbol{\Theta})\boldsymbol{s}(t)+\boldsymbol{w}(t)\big)^H \\ &= \mathbb{E}\big\{\boldsymbol{A}(\boldsymbol{\Theta})\boldsymbol{s}(t)\boldsymbol{s}^H(t)\boldsymbol{A}^H(\boldsymbol{\Theta})\big\}+\mathbb{E}\big\{\boldsymbol{A}(\boldsymbol{\Theta})\boldsymbol{s}(t)\boldsymbol{w}^H(t)\big\}+\mathbb{E}\big\{\boldsymbol{w}(t)\boldsymbol{s}^H(t)\boldsymbol{A}^H(\boldsymbol{\Theta})\big\}+\mathbb{E}\big\{\boldsymbol{w}(t)\boldsymbol{w}^H(t)\big\} \\ &= \boldsymbol{A}(\boldsymbol{\Theta})\mathbb{E}\big\{\boldsymbol{s}(t)\boldsymbol{s}^H(t)\big\}\boldsymbol{A}^H(\boldsymbol{\Theta})+\boldsymbol{A}(\boldsymbol{\Theta})\mathbb{E}\big\{\boldsymbol{s}(t)\boldsymbol{w}^H(t)\big\}+\mathbb{E}\big\{\boldsymbol{w}(t)\boldsymbol{s}^H(t)\big\}\boldsymbol{A}^H(\boldsymbol{\Theta})+\mathbb{E}\big\{\boldsymbol{w}(t)\boldsymbol{w}^H(t)\big\} \\ &= \boldsymbol{A}(\boldsymbol{\Theta})\boldsymbol{R}_{ss}\boldsymbol{A}^H(\boldsymbol{\Theta})+\sigma^2\boldsymbol{I}_N\end{aligned} \tag{2.9}$$

where the last equality holds due to assumption **A3**. Now, let $l_1 \geq l_2 \geq \ldots \geq l_N$ denote the eigenvalues of $\boldsymbol{R}_{xx}$. Then, under assumptions **A1** till **A3**, the smallest $N-q$ eigenvalues of $\boldsymbol{R}_{xx}$ are all equal, i.e.

$$l_{q+1} = \ldots = l_N = \sigma^2 \tag{2.10}$$

We also consider that the q largest eigenvalues are distinct, i.e. $l_1 > l_2 > \ldots > l_q$. The most straightforward way in determining the number of signals is based on the multiplicity of the smallest eigenvalues of $\boldsymbol{R}_{xx}$ as done in the MUSIC algorithm [24]. However, in practical scenarios, we only have access to the sample eigenvalues and not the true ones, which makes it more difficult to distinguish the largest q eigenvalues from the smallest $N-q$ ones, especially at low SNR or low number of snapshots.

If k sources are present in the model, then we can write down

$$\boldsymbol{R}_{xx}^{(k)} = \sum_{i=1}^{k}(\lambda_i-\sigma^2)\boldsymbol{v}_i\boldsymbol{v}_i^{\mathrm{H}}+\sigma^2\boldsymbol{I}_{\mathrm{N}} \tag{2.11}$$

where $\boldsymbol{v}_i$ is the eigenvector corresponding to the eigenvalue λ_i of $\boldsymbol{R}_{xx}^{(k)}$. Denoting $\Theta^{(k)}$ the vector to be estimated, then

$$\Theta^{(k)} = [\lambda_1,\ldots,\lambda_k,\sigma^2,\boldsymbol{v}_1^T,\ldots,\boldsymbol{v}_k^T] \tag{2.12}$$

Thanks to assumption **A3**, the likelihood function is as follows

$$f(\boldsymbol{X}|\Theta^{(k)}) = \prod_{i=1}^{L} \frac{1}{\pi^N \det \boldsymbol{R}_{xx}^{(k)}} \exp\{-\boldsymbol{x}(t_i)^H [\boldsymbol{R}_{xx}^{(k)}]^{-1} \boldsymbol{x}(t_i)\} \tag{2.13}$$

The log-likelihood function, with omitted terms that do not depend on $\Theta^{(k)}$, becomes

$$L(\Theta^{(k)}) = -L \log \det\{\boldsymbol{R}_{xx}^{(k)}\} - \mathrm{tr}\{[\boldsymbol{R}_{xx}^{(k))}]^{-1} \hat{\boldsymbol{R}}\} \tag{2.14}$$

where $\hat{\boldsymbol{R}}$ is the sample covariance matrix computed by

$$\hat{\boldsymbol{R}} = \frac{1}{L} \boldsymbol{X}\boldsymbol{X}^H \tag{2.15}$$

Maximising (2.14) gives the maximum likelihood estimates of $\Theta^{(k)}$. As in [40], these estimates are

$$\hat{\lambda}_i = \hat{l}_i, \qquad i = 1 \dots k \tag{2.16}$$

$$\hat{\sigma}^2 = \frac{1}{N-k} \sum_{i=k+1}^{N} \hat{l}_i \tag{2.17}$$

$$\hat{\boldsymbol{v}}_i = \hat{\boldsymbol{u}}_i, \qquad i = 1 \dots k \tag{2.18}$$

where $\hat{l}_1 \geq \dots \geq \hat{l}_N$ and $\hat{\boldsymbol{u}}_1 \dots \hat{\boldsymbol{u}}_N$ are the sample eigenvalues and their corresponding eigenvectors, respectively. In other words, they are the eigenvalues and eigenvectors of the matrix $\hat{\boldsymbol{R}}$. Plugging equations (2.16), (2.17), (2.18) in (2.14), we get

$$L(\hat{\Theta}^{(k)}) = \log \left(\frac{\prod_{i=k+1}^{N} \hat{l}_i^{\frac{1}{N-k}}}{\frac{1}{N-k} \sum_{i=k+1}^{N} \hat{l}_i} \right)^{L(N-k)} \tag{2.19}$$

The model selection based on the MDL principle is the one that minimises the following

$$\mathrm{MDL}(k) = -L(\hat{\Theta}^{(k)}) + \frac{1}{2}\eta \log(L) \tag{2.20}$$

where η is the number of free adjusted parameters in the parameter vector Θ. Substituting (2.19) in (2.20) and plugging in the number of free adjusted parameters η (See [39]), we get

$$\mathrm{MDL}(k) = -\log \left(\frac{\prod_{i=k+1}^{N} \hat{l}_i^{\frac{1}{N-k}}}{\frac{1}{N-k} \sum_{i=k+1}^{N} \hat{l}_i} \right)^{L(N-k)} + \frac{k}{2}(2N-k)\log(L) \tag{2.21}$$

Therefore, according to the MDL criterion, the number of sources q is the argument k that minimises equation (2.21).

2.3 Detection by MMDL

It has been shown in [41] that the sample eigenvalues $\hat{l}_1 \dots \hat{l}_N$ extracted from the sample covariance matrix $\hat{\boldsymbol{R}}$ are (N, L)-inconsistent estimators of the true eigenvalues of the covariance matrix $\boldsymbol{R}_{xx}$, that is, the sample eigenvalues do not converge towards the true ones as $(N, L) \longrightarrow \infty$ at the same rate $(0 < c = \frac{N}{L} < \infty)$. The MDL estimator in (2.21) depends on the sample eigenvalues of $\hat{\boldsymbol{R}}$, therefore, it seems natural that the performance of the MDL estimator would perform poorly in the asymptotic regime, i.e. $(N, L) \longrightarrow \infty$ at the same rate $(0 < c = \frac{N}{L} < \infty)$. In other words, when insufficient number of snapshots L are available with respect to the number of antennas N in such a way that the ratio $c = \frac{N}{L}$ is not negligible, then the MDL estimator would perform poorly. In this section, we present a modified MDL estimator to cope with this aforementioned issue. The modified MDL estimator is based on using improved estimators of eigenvalues of the covariance matrix $\boldsymbol{R}_{xx}$, which turn out to be (N, L)-consistent, as shown in [42].

2.3.1 Additional assumptions

Before presenting the improved estimators of the eigenvalues of the covariance matrix $\boldsymbol{R}_{xx}$, we proceed as in [42] and pose the following assumptions:

- **B1.** The covariance matrix $\boldsymbol{R}_{xx}$ has uniformly bounded spectral norm for all N, i.e. $\mathrm{Sup_N}\|\boldsymbol{R}_{xx}\| < \infty$ where $\|.\|$ denotes spectral norm.
- **B2.** The sample covariance matrix written as

$$\hat{\boldsymbol{R}} = \sqrt{\boldsymbol{R}}_{xx}\boldsymbol{W}\boldsymbol{W}^H\sqrt{\boldsymbol{R}}_{xx} \tag{2.22}$$

  where $\sqrt{\boldsymbol{R}}_{xx}$ denotes the square root of $\boldsymbol{R}_{xx}$. The matrix $\boldsymbol{W}$ is of size $N \times L$ with complex i.i.d. absolutely continous random entries, with each entry having i.i.d. real and imaginary parts of zeros mean, variance $\frac{1}{2L}$, and finite eighth-order moments.
- **B3.** For all distinct $q+1$ eigenvalues of $\boldsymbol{R}_{xx}$, which are $l_1 > \ldots > l_q > l_{q+1} = \sigma^2$, we assume $\inf_{\mathrm{N}}\{\frac{L}{N} - \kappa_N(m)\} > 0$, where $\kappa_N(m)$ is given in (2.23). In (2.23), K_i is the multiplicity of the i^{th} largest eigenvalue of $\boldsymbol{R}_{xx}$, i.e. $K_1 = \ldots = K_q = 1$

and $K_{q+1} = N - q$. Furthermore, $f_1 < f_2 < \ldots < f_q$ are the real-valued roots of equation (2.24).

$$\kappa_N(m) = \begin{cases} \frac{1}{N}\sum_{i=1}^{q+1} \phi_{i,1}, & \text{if} \quad m = 1 \\ \max\Big\{ \sum_{i=1}^{q+1} \phi_{i,m-1}, \sum_{i=1}^{q+1} \phi_{i,m} \Big\}, & \text{if} \quad 1 < m < q+1 \\ \frac{1}{N}\sum_{i=1}^{q+1} \phi_{i,q}, & \text{if} \quad m = q+1 \end{cases} \tag{2.23a}$$

with

$$\phi_{i,k} = K_i \Big(\frac{l_i}{l_i - f_k} \Big)^2 \tag{2.23b}$$

and

$$\frac{1}{N} \sum_{i=1}^{q+1} K_i \frac{l_i^2}{(l_i - f)^3} = 0 \tag{2.24}$$

Assumption **B3** gives us a lower bound on the parameter L. In other words, the parameter L should be at last $\inf_N\{N\kappa_N(m)\}$. This assumption can also be, geometrically, deduced from the asymptotic eigenvalue distribution. It turns out that for a particular eigenvalue λ_k to be separated from its adjacent clusters, one must have assumption **B3** satisfied. For more info on this assumption, the reader is referred to [42].

2.3.2 The MMDL criterion

The following theorem turns out to be useful because it provides improved eigenvalue estimates, which are not only L-consistent, but also (N, L)-consistent. The theorem is as follows:

Theorem 2.1. *Under assumptions **B1** to **B3**, the following quantities are strongly (N, L)-consistent estimators of l_j $(j = 1, \ldots, q+1)$.*

$$\hat{l}_j^{imp} = L\big(\hat{l}_j - \mu_j\big), \quad j = 1 \ldots q \tag{2.25a}$$

and

$$\hat{l}_{q+1}^{imp} = \frac{L}{N-q} \sum_{i=q+1}^{N} \big(\hat{l}_i - \mu_i\big) \tag{2.25b}$$

where $\mu_1 \leq \mu_2 \leq \ldots \leq \mu_N$ are the real-valued solutions of the following equation in μ:

$$\frac{1}{N} \sum_{i=1}^{N} \frac{\hat{l}_i}{\hat{l}_i - \mu} = \frac{1}{c} \tag{2.25c}$$

Proof. See [42] □

With the improved eigenvalue estimates of $\boldsymbol{R}_{xx}$ in hand from (2.25), we can modify equations (2.16) and (2.17) to get

$$\hat{\lambda}_i = L\big(\hat{l}_j - \mu_j\big), \quad j = 1 \dots k \tag{2.26a}$$

$$\hat{\sigma}^2 = \frac{L}{N-k} \sum_{i=k+1}^{N} \big(\hat{l}_i - \mu_i\big) \tag{2.26b}$$

Using these improved estimates in (2.26), one could easily verify that the improved MDL estimtor finally becomes

$$\mathrm{MDL}^{\mathrm{imp}}(k) = -\log\left(\frac{\prod_{i=k+1}^{N} (\hat{l}_i - \mu_i)^{\frac{1}{N-k}}}{\frac{1}{N-k}\sum_{i=k+1}^{N}(\hat{l}_i - \mu_i)} \right)^{L(N-k)} + \frac{k}{2}(2N-k)\log(L) \tag{2.27}$$

and, therefore the number of sources are estimated by

$$\hat{q} = \arg\min_{k} \mathrm{MDL}^{\mathrm{imp}}(k) \tag{2.28}$$

Remark 2.2. As $c \longrightarrow 0$, then we have $\hat{l}_i^{\mathrm{imp}} \longrightarrow \hat{l}_i$ for all $i = 1 \dots q+1$. Consequently, one could show that $\mathrm{MDL}^{\mathrm{imp}}(k) \longrightarrow \mathrm{MDL}(k)$ for all k as $c \longrightarrow 0$.

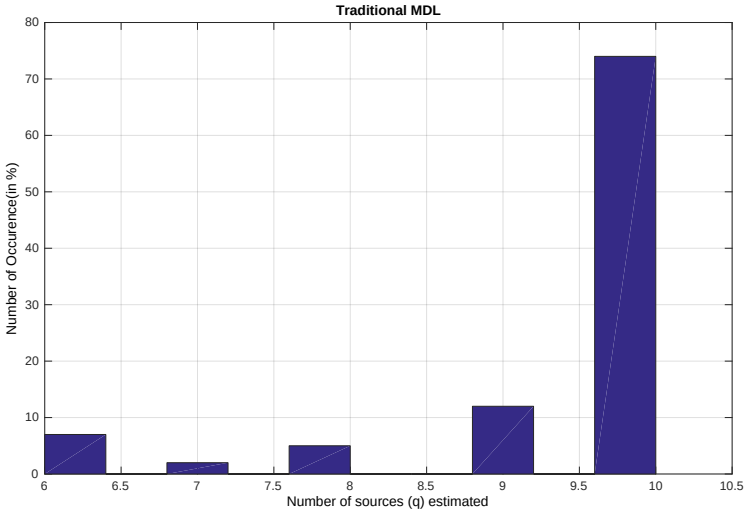

Figure 2.1: Experiment 1: Histogram of the number of signals resolved by the traditional MDL estimator.

We have conducted two experiments: Experiment 1 is dedicated for sufficiently spaced sources, whereas in Experiment 2 we have two sources that are closely spaced.

In order to show the improvement of the modified MDL estimator, we compare it with the traditional one. We have plotted two histograms that show the percentage of occurrence of an estimate of the number of sources $\hat{q}$. Simulations were done under an

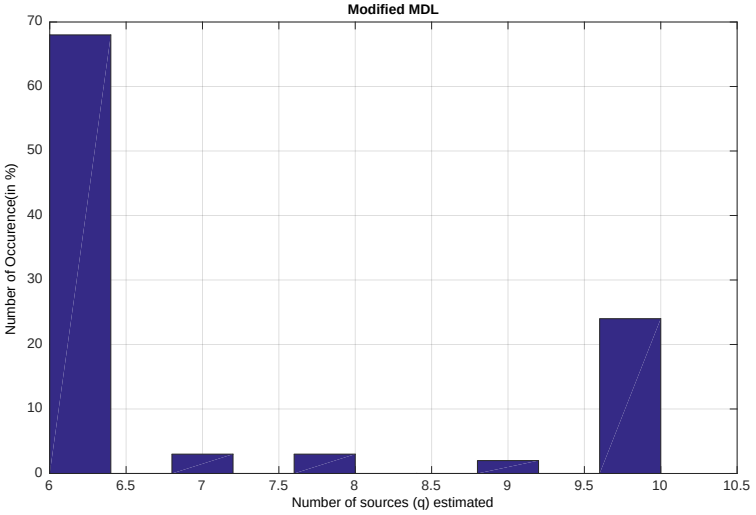

Figure 2.2: Experiment 1: Histogram of the number of signals resolved by the MMDL estimator.

SNR of 10 dB and in the presence of 6 sources with arbitrary (but sufficiently spaced) angles of arrival. The sources were non-coherent and the array geometry consists of $N = 10$ antennas uniformly spaced by half a wavelength. The number of snapshots collected was $L = 10$, i.e. $c = \frac{N}{L} = 1$. The AoAs are fixed to $\theta_1 = 10°$, $\theta_2 = 20°$, $\theta_3 = 30°$, $\theta_4 = 40°$, $\theta_5 = 50°$, and $\theta_6 = 60°$. Note that both histograms were done using 1000 trials.

Figure 2.1 shows the histogram of the percentage of occurrence of $\hat{q}$ using the "traditional" MDL criterion, i.e equation (2.21). Indeed, the performance is poor because only 8% of the estimates of number of sources correspond to the true one, i.e. $\hat{q} = 6$.

On the other hand, Fig 2.2 depicts the histogram of the percentage of occurrence of $\hat{q}$ using the "modified" MDL criterion, i.e equations (2.27) and (2.28). There is a great improvement as almost 68% of the estimates of number of sources correspond to the true one.

Now, in Experiment 2, we have fixed the same parameters as Experiment other, but we changed the AoA of the second source to $\theta_2 = 10.5°$. In both cases, we can see that it is "as if" the first and second source are seen as only one source, because they are closely spaced.

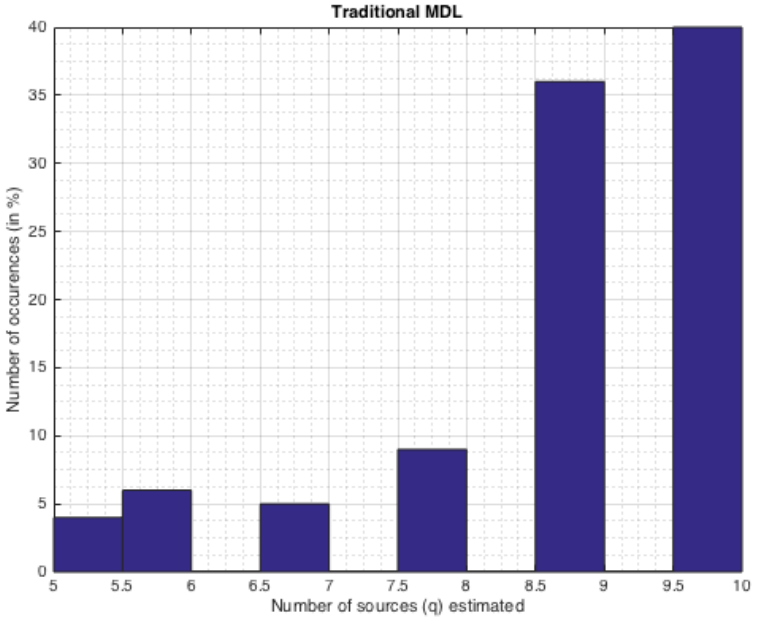

Figure 2.3: Experiment 2: Histogram of the number of signals resolved by the traditional MDL estimator.

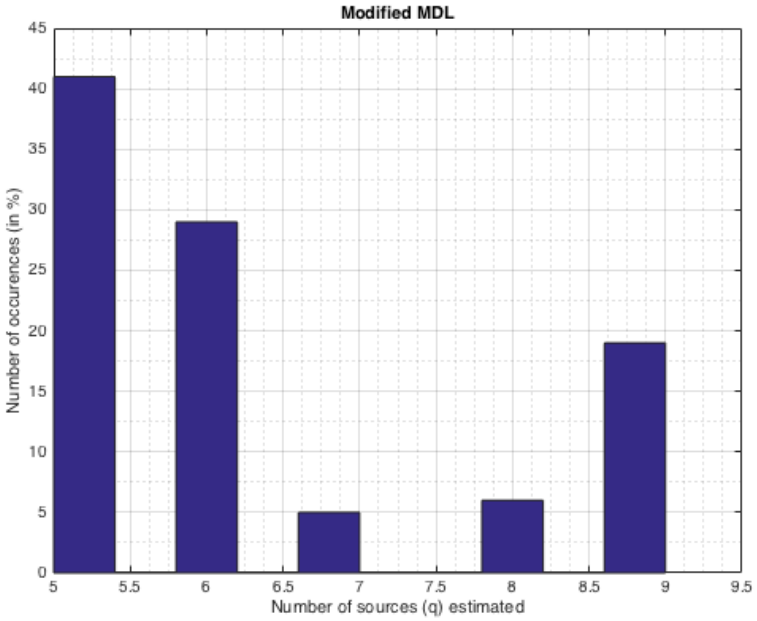

Figure 2.4: Experiment 2: Histogram of the number of signals resolved by the MMDL estimator.

2.4 Conclusions and future directions

In this chapter and with the help of random matrix tools, we have presented a modified MDL (MMDL) estimator for detecting the number of superimposed signals. This

MMDL estimator dominates the traditional MDL especially at the low number of snapshots regime, i.e. when $L = \mathcal{O}(N)$. Simulation results have shown the potential of MMDL over the traditional MDL.

With respect to the results presented in this chapter, interesting future research directions may include: (i) analysing and deriving closed form expressions of the probability of error of the MMDL technique and comparing it with that of the traditional MDL; (ii) studying the regime where the MMDL is considered to be consistent in terms of number of snapshots or SNR.

Chapter 3

Angle-of-Arrival Estimation by Compressed Sensing Techniques

In this chapter, we propose different approaches on estimating the Angle-of-Arrival (AoA) of multiple sources using compressed sensing techniques. The contributions could be summarized as follows: (i) we derive an iterative Variational Bayes (VB) algorithm that allows sparse recovery of the desired transmitted vector; (ii) we show that this iterative VB method outperforms existing compressed sensing methods, such as Matching Pursuit (MP), Orthogonal MP (OMP), etc; (iii) we also derive a Newton-type Forward Backward Greedy method that performs sparse recovery, given the data; (iv) we show, through exhaustive simulations, that the proposed Newton-type method, is not only faster, but attains a lower MSE when compared to methods such as Fast Matching Bayesian Pursuit (FBMP) and Basis Pursuit Denoising (BPDN).

3.1 System model

3.1.1 Problem formulation

As in Chapter 2, we consider q sources impinging an N-element antenna array, and therefore the model reads

$$\boldsymbol{x}(t) = \boldsymbol{A}(\boldsymbol{\Theta})\boldsymbol{s}(t) + \boldsymbol{w}(t) \tag{3.1}$$

where all quantities have been defined in Chapter 2.
Compressed sensing techniques recast the problem in equation (3.1) to the following

$$\boldsymbol{x}(t) = \boldsymbol{\mathcal{A}}\boldsymbol{s}(t) + \boldsymbol{w}(t) \tag{3.2}$$

where $\boldsymbol{\mathcal{A}} \in \mathbb{C}^{N\times K}$ is an over-complete dictionary ($N < K$),

$$\boldsymbol{\mathcal{A}} = [\boldsymbol{a}(\theta^1)\dots\boldsymbol{a}(\theta^K)] \tag{3.3}$$

hopefully[1], containing the q steering vectors in its columns. The vector $\boldsymbol{s}(t) \in \mathbb{C}^{K\times 1}$ is a sparse vector, containing non-zero values at entries corresponding to the true AoAs. For a single-snapshot, equation (3.2) could be seen as

$$\boldsymbol{x} = \boldsymbol{\mathcal{A}}\boldsymbol{s} + \boldsymbol{w} \tag{3.4}$$

and for multiple snapshots, we stack all the observed vectors into a data matrix:

$$\boldsymbol{X} = [\boldsymbol{x}(0), \boldsymbol{x}(T), \dots, \boldsymbol{x}\big((L-1)T\big)] = \boldsymbol{\mathcal{A}}\boldsymbol{S} + \boldsymbol{W} \tag{3.5}$$

where L is the number of collected snapshots. Also $\boldsymbol{S}$ and $\boldsymbol{W}$ are defined in a similar manner to $\boldsymbol{X}$.

3.1.2 Problem statement

The problem could be stated as follows:

- **Single-Snapshot case:** Given the observed vector $\boldsymbol{x}$ and the over-complete dictionary $\boldsymbol{A}$ in equation (3.4), estimate the sparse vector $\boldsymbol{s}$.
- **Multi-Snapshot case:** Given the observed data matrix $\boldsymbol{X}$ and the over-complete dictionary $\boldsymbol{A}$ in equation (3.5), estimate the row-sparse matrix $\boldsymbol{S}$.

3.2 Background of existing methods

Consider the optimisation problem in penalised form given as follows

$$\hat{\boldsymbol{s}} = \arg\min_{\boldsymbol{s}} \|\boldsymbol{x} - \boldsymbol{\mathcal{A}}\boldsymbol{s}\|^2 + \lambda\|\boldsymbol{s}\|_p \tag{3.6}$$

This problem is referred to as l_p-optimisation. When $p = 0$, note that $\|\boldsymbol{s}\|_0$ counts the number of non-zero elements of $\boldsymbol{s}$. Also note that $\|\boldsymbol{s}\|_0$ is a quasi-norm, since the triangular inequality of norms is not satisfied in this case. Solving the problem in (3.6), when $p = 0$, is known to favour sparse solutions the most. However, this comes with a

[1]For example, if $\boldsymbol{\mathcal{A}} = [\boldsymbol{a}(-90°), \boldsymbol{a}(-89°)\dots\boldsymbol{a}(89°), \boldsymbol{a}(90)]$, and we have $q = 1$ source at $\theta_1 = 30.5°$, then the steering vector is in one of the columns of $\boldsymbol{\mathcal{A}}$.

price of having an NP-hard problem in hand to solve. In this paper, we aim to study the performance of three broad categories of compressed sensing algorithms, namely:

- Pursuit-type algorithms.
- Thresholding-type algorithms.
- *Bayesian*-based algorithms.

3.2.1 Pursuit-type algorithms

Pursuit-type algorithms are popular algorithms in the field of compressed sensing. More specifically, matching pursuit algorithms deal with an approximate solution of the l_0-optimisation problem. For uniqueness of the l_0 problem, we refer the reader to [44]. However, basis pursuit relax the l_0-optimisation problem to an l_1-optimisation one. The l_1-optimisation problem is also known as LASSO [45]. For uniqueness of the l_1 problem, we refer the reader to [46]. An advantage of this relaxation is that the problem is now convex. It remains to see when the unique solution provided by the l_1-optimisation problem coincides with that of the l_0 one. The papers in [44, 47] give sufficient conditions for $\hat{\boldsymbol{s}}$ to be a unique solution of the l_0 and l_1-optimisation problems. Moreover, the necessary conditions for that to happen are found in [48, 49].

The pursuit algorithms that are evaluated in the context of AoA estimation in this paper are the following:

- Matching Pursuit (MP) [50]
- Orthogonal MP (OMP) [51]
- Gradient, or directional, Pursuit (GP) [52]
- Basis Pursuit De-Noising (BPDN) [53]

The first three algorithms: MP, OMP, and GP are also referred to as *Greedy* algorithms. These algorithms start by initialising $\hat{\boldsymbol{s}}$ to a zero vector, then estimate a set of non-zero components of $\hat{\boldsymbol{s}}$ by adding new components to those non-zero terms, in an iterative manner [54]. A brief summary of *Greedy* algorithms is given in **Table 1**. Indeed, the algorithms: MP, OMP, and GP differ in how the "Element Selection" and "Coefficient Updates" are done. For example, MP updates one element at each iteration (this entry corresponds to the maximum magnitude of $\boldsymbol{g}^{(\boldsymbol{n})}$). However, OMP updates multiple entries at the same iteration using Least-Square fit. For more information regarding

Table 1: General framework of *Greedy* algorithms

INPUT:
Given the data $\boldsymbol{x}$ and the dictionary $\boldsymbol{\mathcal{A}}$.
INITIALISATION:
$\boldsymbol{r^{(0)}} = \boldsymbol{x}$, $\boldsymbol{\hat{s}^{(0)}} = \boldsymbol{0}$, and $n = 0$.
MAIN LOOP:
while *Stopping Criterion is not met* **do**

- Element Selection: Select the columns of $\boldsymbol{\mathcal{A}}$ based on the largest magnitude of entries of $\boldsymbol{g^{(n)}} = \boldsymbol{\mathcal{A}}^{\mathrm{H}}\boldsymbol{r^{(n)}}$
- Coefficient Update: Obtain a new estimate $\boldsymbol{\hat{s}^{(n)}}$ that minimises $\|\boldsymbol{x} - \boldsymbol{\mathcal{A}s}\|^2$ then increment n.

Greedy methods, we encourage the reader to refer to [54] and [55]. Furthermore, many work has been done on figuring out a good "Stopping Criterion" for *Greedy* algorithms. For example, in [56, 57], a necessary condition was given in order to recover $\boldsymbol{s}$ with error threshold $\delta = 0$, i.e. when $\|\boldsymbol{\hat{s}^{(n)}}\| \leq \delta = 0$.

On the other hand, BPDN aims at an l_1-optimisation problem, or equivalently the following

$$\boldsymbol{\hat{s}} = \arg\min_{\boldsymbol{s}} \|\boldsymbol{s}\|_1 \quad \text{subject to} \quad \|\boldsymbol{x} - \boldsymbol{\mathcal{A}s}\|^2 \leq \epsilon \tag{3.7}$$

The regularization parameter ϵ has to be chosen appropriately depending on the noise, which is a major disadvantage of this algorithm.

3.2.2 Thresholding-type algorithms

The *Greedy* algorithms are easy and computationally efficient. However, they do not promise recovery of $\boldsymbol{s}$ as strong as the l_1-optimisation problem. In this sub-section, we are interested in the following:

- Iterative Hard Thresholding (IHT) [58, 59]
- Normalised IHT (NIHT) [60]
- Iterative Shrinkage-Thresholding Algorithm (ISTA) [61]

It was shown in [62] that solutions of (3.6) are given as follows

$$\boldsymbol{s} = \mathrm{prox}_{\|.\|_p}\Big(\boldsymbol{s} - \gamma\boldsymbol{\mathcal{A}}^{\mathrm{H}}(\boldsymbol{\mathcal{A}s} - \boldsymbol{x})\Big) \tag{3.8}$$

where $\gamma > 0$ and the *proximity* function is given by

$$\text{prox}_{\|.\|_p}(\boldsymbol{z}) = \arg\min_{\boldsymbol{s}} \left(\|\boldsymbol{s}\|_p + \frac{1}{2}\|\boldsymbol{s} - \boldsymbol{z}\|_2^2 \right) \tag{3.9}$$

which has a unique solution $\boldsymbol{s}$ for every $\boldsymbol{z} \in \mathbb{C}^{\text{K}\times 1}$ [63]. Now, equation (3.8) could be solved using fixed-point in an iterative fashion, viz.

$$\boldsymbol{s}^{(n+1)} = \text{prox}_{\|.\|_p}\left(\boldsymbol{s}^{(n)} - \gamma \mathcal{A}^{\text{H}}(\mathcal{A}\boldsymbol{s}^{(n)} - \boldsymbol{x}) \right) \tag{3.10}$$

When $p = 0$, the *proximity* in (3.10) gives the hard threshold, and therefore the IHT algorithm

$$\text{prox}_{\lambda\gamma\|.\|_0}(\boldsymbol{z}) = [\ldots, \boldsymbol{z}_i \mathbb{1}_{|\boldsymbol{z}_i| > \sqrt{2\lambda\gamma}}, \ldots]^{\text{T}} \tag{3.11}$$

However, when $p = 1$, the *proximity* in (3.10) gives the soft threshold. Hence, we obtain the ISTA algorithm

$$\text{prox}_{\lambda\gamma\|.\|_1}(\boldsymbol{z}) = [\ldots, \frac{\boldsymbol{z}_i}{|\boldsymbol{z}_i|}\max(|\boldsymbol{z}_i| - \lambda\gamma, 0), \ldots]^{\text{T}} \tag{3.12}$$

Convergence and recovery properties of IHT are found in [58, 64, 65]. To further enhance IHT, the normalised IHT (NIHT) was obtained by a simple modification [60]. This modification yields a faster algorithm, whilst keeping theoretical performance similar to IHT, in some scenarios.

3.2.3 Bayesian-based algorithms

In this sub-section, the sparse signal $\boldsymbol{s}$ is no longer treated as deterministic, but rather as probabilistic, or random. In other words, a *Bayesian* approach is adopted. Here, we briefly discuss the ideas of:

- Sparse reconstruction using distribution Agnostic Bayesian Matching Pursuit (SABMP) [66]
- Iterative Variational Bayes (VB) with latent variables. [105]

SABMP [66] performs *Bayesian* estimates of the sparse signal $\boldsymbol{s}$ even when it is modelled as non-Gaussian, thus the term "Agnostic". Even more, this method makes use of *a priori* statistics of the noise and the sparsity rate of the signal. More specifically, the signal $\boldsymbol{s}$ is modelled as $\boldsymbol{s} = \boldsymbol{s}_A \odot \boldsymbol{s}_B$, where $\boldsymbol{s}_A$ consists of elements that are drawn from some unknown distribution (Agnostic), whereas $\boldsymbol{s}_B$ are drawn i.i.d. from a *Bernoulli* distribution with success probability p. Note that p controls the sparsity of $\boldsymbol{s}$, and thus

it plays a major role in activating elements[2] of $\boldsymbol{s}$. The SABMP method was shown, through simulations, to outperform BPDN [53] and Fast *Bayesian* Matching Pursuit (FBMP) [67].

On the other hand, we have recently introduced an iterative Variational Bayes (VB) algorithm in [105] with the help of latent variables. Indeed, the paper was inspired by the work in [68–70]. The papers [68–70] focus on introducing latent, or hidden, variables and imposing prior distributions on these variables that favor sparsity. In [105], we also introduce the latent variables discussed in [68–70], which leads to a novel iterative Variational Bayes [71] algorithm that allows recovering $\boldsymbol{s}$ from a single observation $\boldsymbol{x}$ with the help of the latent variables that were introduced.

3.3 Sparse Recovery via Iterative Variational Bayes

3.3.1 The Bayesian perspective

In this section, we shall take a *Bayesian* approach, i.e. the vector $\boldsymbol{s}$ is random and not an unknown deterministic vector. Adopting the *Bayesian* criterion is equivalent to optimising the *maximum aposteriori* (MAP) [23], which is given as

$$\hat{\boldsymbol{s}} = \arg\max_{\boldsymbol{s}} p(\boldsymbol{s}|\boldsymbol{x}) = \arg\max_{\boldsymbol{s}} \frac{p(\boldsymbol{x}|\boldsymbol{s})p(\boldsymbol{s})}{p(\boldsymbol{x})} \tag{3.13}$$

where $p(\boldsymbol{x}|\boldsymbol{s})$ is known as the likelihood function and $p(\boldsymbol{s})$ is referred to as the prior. It was noted in [68] and [69] that the following type of prior favors sparsity

$$p(\boldsymbol{s}) = \prod_{k=1}^{K} p(s_k), \quad p(s_k) = p(s_k|\beta_k)\phi(\beta_k) \tag{3.14}$$

where $\beta_1 \dots \beta_K$ are referred to as latent variables and

$$p(s_k|\beta_k) = \mathcal{N}(s_k; 0, \beta_k^{-1}) \tag{3.15}$$

and $\phi(\beta_k)$ is a nonnegative function. Now, the latent variables $\beta_1 \dots \beta_K$, which are treated as random variables, should have appropriate corresponding pdfs, i.e. $\phi(\beta_1) \dots \phi(\beta_K)$, respectively. As explained in [72], the pdf $\phi(\beta_K)$ should be chosen as the conjugate to the Gaussian distribution. One possibility is the Gamma function, i.e.

$$\phi(\beta_k) = \Gamma(\beta_k; \gamma, \delta) \tag{3.16}$$

[2] By activating elements of $\boldsymbol{s}$, we mean to set these elements to non-zero. Actually, this term was taken from [66].

Moreover, let $\nu = \frac{1}{\sigma^2}$ be the inverse of the noise variance. Also, we allow ν to follow a Gamma prior, viz.

$$p(\nu) = \Gamma(\nu; \zeta, \eta) \tag{3.17}$$

The MAP criterion, with the formulation from equations (3.14) till (3.17) is now

$$p(\boldsymbol{s}, \boldsymbol{\beta}, \nu | \boldsymbol{x}) = \frac{p(\boldsymbol{x}|\boldsymbol{s}, \boldsymbol{\beta}, \nu) p(\boldsymbol{s}, \boldsymbol{\beta}, \nu)}{p(\boldsymbol{x})} \tag{3.18}$$

with $\boldsymbol{\beta} = [\beta_1 \dots \beta_K]$. Assuming independency between the signal vector $\boldsymbol{s}$ and the noise, we can say that

$$p(\boldsymbol{s}, \boldsymbol{\beta}, \nu) = p(\boldsymbol{s}|\boldsymbol{\beta}) p(\boldsymbol{\beta}) p(\nu) \tag{3.19}$$

Finally, we notice that the normalisation factor in equation (3.19) given as

$$p(\boldsymbol{x}) = \int p(\boldsymbol{x}|\boldsymbol{s}, \nu) p(\boldsymbol{s}|\boldsymbol{\beta}) p(\boldsymbol{\beta}) p(\nu) d\boldsymbol{s} d\nu d\boldsymbol{\beta} \tag{3.20}$$

does not have a closed-form expression; hence we propose to use the Variational Bayes methodology.

3.3.2 Variational Bayes methodology

Let $\boldsymbol{y} = [\boldsymbol{\beta}, \nu]$. The log-likelihood function that does not take into account the latent variables $\boldsymbol{y}$, is given as follows [71]

$$\log p(\boldsymbol{x}|\boldsymbol{s}) = \int q(\boldsymbol{y}) \log \Big(\frac{p(\boldsymbol{x}, \boldsymbol{y}|\boldsymbol{s})}{q(\boldsymbol{y})} \Big) d\boldsymbol{y} + \mathrm{KL}\big(q||p\big) \tag{3.21}$$

where $\mathrm{KL}\big(q||p\big)$ is the *Kullback-Leilbler* divergence between $p(\boldsymbol{y}|\boldsymbol{x}, \boldsymbol{s})$ and $q(\boldsymbol{y})$. Since $\mathrm{KL}\big(q||p\big) \geq 0$, then

$$\log p(\boldsymbol{x}|\boldsymbol{s}) \geq \int q(\boldsymbol{y}) \log \Big(\frac{p(\boldsymbol{x}, \boldsymbol{y}|\boldsymbol{s})}{q(\boldsymbol{y})} \Big) d\boldsymbol{y} \tag{3.22}$$

The methodology of Variational Bayes lies in maximising the lower bound in equation (3.22) by imposing a factorised structure on $\boldsymbol{y}$ as follows [71]

$$q(\boldsymbol{y}) = \prod_{k=1}^{K+1} q_k(y_k) \tag{3.23}$$

Substituting the form of $q(\boldsymbol{y})$ in (3.22) and following [71], this lower bound could be expressed as follows:

$$\begin{aligned}\int q(\boldsymbol{y}) \log \Big(\frac{p(\boldsymbol{x},\boldsymbol{y}|\boldsymbol{s})}{q(\boldsymbol{y})}\Big) d\boldsymbol{y} \\ = -\sum_{\substack{k=1\\k\neq i}}^{K+1} \int q_k(y_k) \log q_k(y_k) dy_k - \mathrm{KL}(q_i||\bar{p}_i)\end{aligned} \tag{3.24}$$

with

$$\begin{aligned}\hat{p}_i &\triangleq \mathbb{E}_{y_k\neq y_i}\Big\{\log p(\boldsymbol{x},\boldsymbol{s},\boldsymbol{y})\Big\} \\ &= \int \log\big(p(\boldsymbol{x},\boldsymbol{s},\boldsymbol{y})\big) \prod_{\substack{k=1\\k\neq i}}^{K+1} q_k(y_k) dy_k\end{aligned} \tag{3.25}$$

It is straightforward to see that the lower bound is maximising when $\mathrm{KL}(q_i||\bar{p}_i) = 0$. In other words, each $q_i(y_i)$ should be chosen as

$$\log q_i(y_i) = \mathbb{E}_{y_k\neq y_i}\Big\{\log p(\boldsymbol{x},\boldsymbol{s},\boldsymbol{y})\Big\} + C \tag{3.26}$$

where C is a normalisation constant. Now, following [73], one could solve for $\boldsymbol{s}$, in a Variational Expectation-Maximisation (EM) iterative manner as follows:

- Variational E-step: Given $\boldsymbol{s}^{(n)}$ (i.e. the value of $\boldsymbol{s}$ at iteration n), compute $q_i^{(n)}(y_i)$ for all i using equation (3.26).
- Variational M-step: Given $q_i^{(n)}(y_i)$ for all i, compute $\boldsymbol{s}^{(n+1)}$ that maximises equation (3.24).

Now, we are ready to apply the Variational Bayes methodology to the problem in hand.

3.3.3 The Iterative Variational Bayes method

We first start off by deriving the expressions of $q_i(y_i)$ and $q(\boldsymbol{s})$. Following the factorised structure of $\boldsymbol{y}$ in equation (3.23) and the independency between $\boldsymbol{s}$ and $\boldsymbol{y}$, we can say that the posterier factorises as follows

$$p(\boldsymbol{s},\boldsymbol{y}|\boldsymbol{x},\gamma,\delta,\zeta,\eta) = p(\boldsymbol{s})p(\boldsymbol{y}) = p(\boldsymbol{s})p(\boldsymbol{\beta})p(\nu) \tag{3.27}$$

With the help of equation (3.26), we now analytically evaluate $q(\boldsymbol{s})$ as follows

$$\begin{aligned}\log\, q(\boldsymbol{s}) &= \mathbb{E}_{\boldsymbol{\beta},\nu}\Big\{\log\, p(\boldsymbol{x},\boldsymbol{s},\boldsymbol{y})\Big\}\\ &= \mathbb{E}_{\boldsymbol{\beta},\nu}\Big\{\log\, p(\boldsymbol{x}|\boldsymbol{s},\nu)p(\boldsymbol{s}|\boldsymbol{\beta})\Big\}\\ &= -\frac{1}{2}\mathbb{E}_{\boldsymbol{\beta},\nu}\Big\{\nu\|\boldsymbol{x}-\boldsymbol{\mathcal{A}}\boldsymbol{s}\|^2+\sum_{k=1}^{K}\beta_k|s_k|^2\Big\}\end{aligned} \tag{3.28}$$

With some abuse of notation, $\mathbb{E}_{\boldsymbol{\beta},\nu}$ is the average over the joint distributions $q(\boldsymbol{\beta})$ and $q(\nu)$. In addition, we have omitted the constant in equation (3.28) for the sake of compact presentation. Now, assuming that $\boldsymbol{\beta}$ and ν are independent, we can say

$$\log\, q(\boldsymbol{s}) = -\frac{m_\nu}{2}\|\boldsymbol{x}-\boldsymbol{\mathcal{A}}\boldsymbol{s}\|^2-\frac{1}{2}\sum_{k=1}^{K}m_{\beta_k}|s_k|^2 \tag{3.29}$$

where $m_\nu=\mathbb{E}\{\nu\}$ and $m_{\beta_k}=\mathbb{E}\{\beta_k\}$. With some mathematical steps, one could show that $q(\boldsymbol{s})$ is given as follows

$$\log\, q(\boldsymbol{s}) = -\frac{1}{2}\big(\boldsymbol{s}-\boldsymbol{m_s}\big)^{\mathrm{H}}\boldsymbol{\Sigma}^{-1}\big(\boldsymbol{s}-\boldsymbol{m_s}\big) \tag{3.30}$$

where

$$\boldsymbol{\Sigma}^{-1} = \boldsymbol{\Omega}+m_\nu\boldsymbol{\mathcal{A}}^{\mathrm{H}}\boldsymbol{\mathcal{A}} \tag{3.31}$$

and

$$\boldsymbol{m_s} = m_\nu\boldsymbol{\Sigma}\boldsymbol{\mathcal{A}}^{\mathrm{H}}\boldsymbol{x} \tag{3.32}$$

where $\boldsymbol{\Omega}=\ \mathrm{diag}[m_{\beta_1}\dots m_{\beta_K}]$. Now, we compute $q(\boldsymbol{\beta})$

$$\begin{aligned}&\log\, q(\boldsymbol{\beta})\\ &= \mathbb{E}_{\boldsymbol{s},\nu}\Big\{\log\, p(\boldsymbol{x},\boldsymbol{s},\boldsymbol{y})\Big\}\\ &= \mathbb{E}_{\boldsymbol{s},\nu}\Big\{\sum_{k=1}^{K}\Big(\log\, p(\beta_k)\Big)+\log\, p(\boldsymbol{s}|\boldsymbol{\beta})\Big\}\\ &= \sum_{k=1}^{K}\Big((\gamma-1)\log\,\beta_k-\delta\beta_k+\frac{1}{2}\log\,\beta_k-\beta_k\mathbb{E}|s_k|^2\Big)\end{aligned} \tag{3.33}$$

where the terms $(\gamma-1)\log\,\beta_k$ and $\delta\beta_k$ appear due to K independent Gamma distributions, i.e. $p(\beta_k)$ for $k=1\dots K$. Again, with some abuse of notation, we have ommited constant terms for the sake of compact presentation. With some straightforward algebra, we could say that

$$q(\beta_k) = \Gamma\Big(\beta_k;\frac{2\gamma+1}{2},\frac{2\delta+|(\boldsymbol{m_s})_k|^2+\boldsymbol{\Sigma}_{k,k}}{2}\Big) \tag{3.34}$$

where $(\boldsymbol{m_s})_k$ is the k^{th} entry of vector $\boldsymbol{m_s}$ and $\boldsymbol{\Sigma}_{k,k}$ is the element found in the k^{th} diagonal of $\boldsymbol{\Sigma}$. In a similar manner, we could show that

$$q(\nu) = \Gamma\Big(\nu; \frac{2\zeta+1}{2}, \frac{2\eta + \|\boldsymbol{x} - \boldsymbol{\mathcal{A}}\boldsymbol{m_s}\|^2 + \text{tr}\,\{\boldsymbol{\mathcal{A}}\boldsymbol{\Sigma}\boldsymbol{\mathcal{A}}^{\text{H}}\}}{2}\Big) \tag{3.35}$$

Knowing that for any random variable following a Gamma distribution with parameters λ and μ, i.e. $X \sim \Gamma(x; \lambda, \mu)$, the mean of X, say m_X, is given as $m_X = \frac{\lambda}{\mu}$. Therefore, it is easy to see from equation (3.34) that

$$m_{\beta_k} = \frac{2\gamma + 1}{2\delta + |(\boldsymbol{m_s})_k|^2 + \boldsymbol{\Sigma}_{k,k}} \tag{3.36}$$

Similarly, equation (3.35) implies that

$$m_\nu = \frac{2\zeta + 1}{2\eta + \|\boldsymbol{x} - \boldsymbol{\mathcal{A}}\boldsymbol{m_s}\|^2 + \text{tr}\,\{\boldsymbol{\mathcal{A}}\boldsymbol{\Sigma}\boldsymbol{\mathcal{A}}^{\text{H}}\}} \tag{3.37}$$

Before presenting the algorithm in **Table 1**, we find the following notation useful

$$\boldsymbol{\Theta} = [m_{\beta_1} \ldots m_{\beta_K}, m_\nu, \boldsymbol{s}] \tag{3.38}$$

Furthermore, let $x^{(n)}$ denote the value of the quantity x at iteration n. For convenience, $x^{(0)}$ is the initial value of x. Now, we are ready to state the iterative algorithm that is based on Variational EM as explained in Section IV.A. The algorithm is given in **Table 1**.

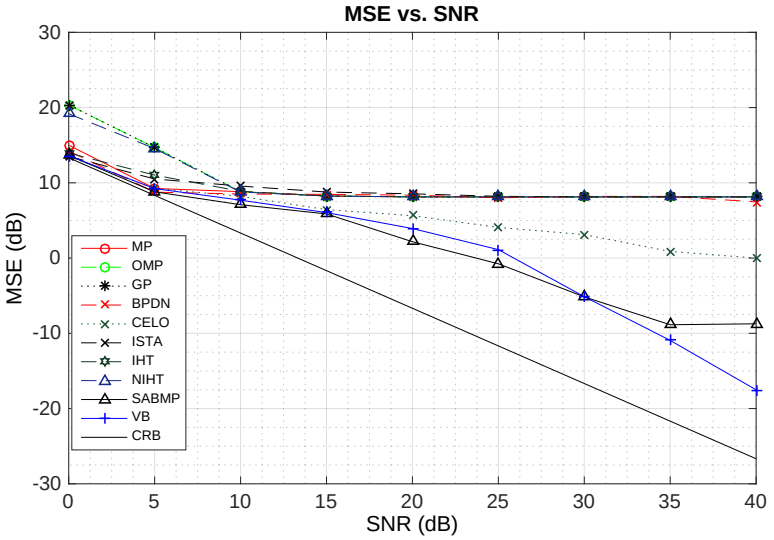

Figure 3.1: Two sources impinging the array from directions $\theta_1 = 0°$ and $\theta_2 = 5°$. The number of antennas is 10.

We have simulated three different scenarios. Furthermore, we fix the following simulation parameters: Consider a Uniform Linear Antenna array composed of N antennas spaced

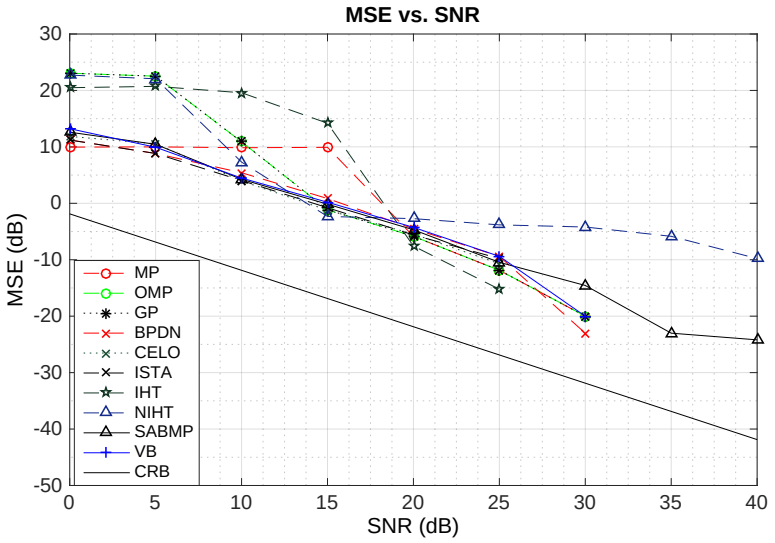

Figure 3.2: Two sources impinging the array from directions $\theta_1 = 0°$ and $\theta_2 = 30°$. The number of antennas is 10.

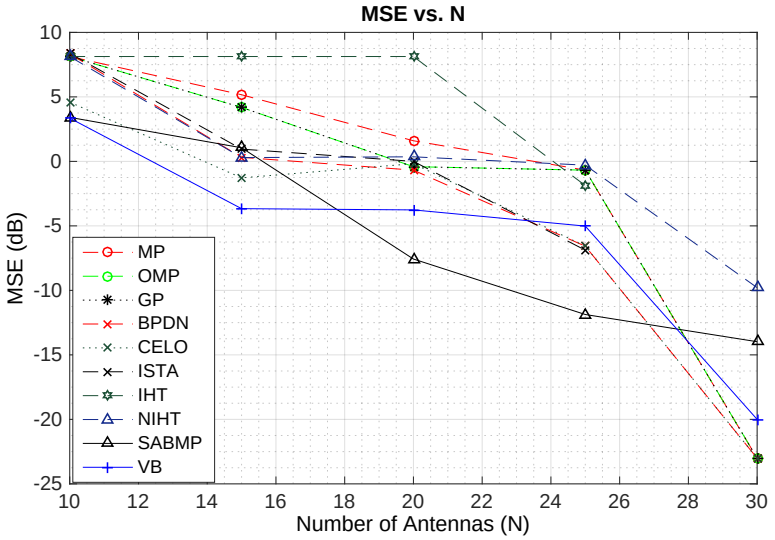

Figure 3.3: Two sources impinging the array from directions $\theta_1 = 0°$ and $\theta_2 = 5°$. The SNR is 20dB.

at half a wavelength. Furthermore, assume $q = 2$ sources attacking the array from directions $\theta_1 = 0°$ and θ_2. The dictionary $\mathcal{A}$ is composed of $K = 91$ atoms discretized from $-45°$ till $+45°$ with a grid step of $1°$. All our experiments are done using $M = 100$ Monte Carlo trials.

In Scenario 1 (Figure 3.1), we fix $N = 10$ antennas and $\theta_2 = 5°$. Moreover, we plot the MSE vs. SNR and we notice that all algorithms except for CELO, SABMP, and VB were not able to resolve the closely spaced sources. This phenomenon is explained through the Restricted Isometry Property (RIP). In short, the RIP condition (in the

context of AoA estimation) relates the number of resolvable sources[3] with the number of antennas N that should be used to resolve these sources. Furthermore, we observe that the MSE of SABMP and VB are close to the Cramer-Rao Bound (CRB), whereas CELO has inferior performance when compared to VB or SABMP. In order to validate the RIP condition, we have simulated Scenarios 2 and 3.

In Scenario 2 (Figure 3.2), we fix $N = 10$ antennas and $\theta_2 = 30°$. One could verify that the RIP condition is now validated for 2 sources when separated at 30°. As one can now see, all the algorithms now recover the sparse signal, and thus properly estimate the AoAs at a sufficiently high SNR. For example, IHT presents no error when SNR $\geq$ 25 dB. Furthermore, MP, OMP, GP, and BPDN present no error when SNR $\geq$ 30 dB.

In Scenario 3 (Figure 3.3), we fix the SNR to be 20 dB and $\theta_2 = 5°$. Furthermore, we plot the MSE vs. the number of antennas (N). We notice that all pursuit and thresholding algorithms promise exact recovery of the closely spaced sources when the number of antennas N exceeds a certain level. For instance, ISTA and IHT promise exact recovery at 20 dB of two sources spaced at 5° when $N > 25$. As for MP, OMP, GP, and BPDN, the required number of antennas should exceed 30 to guarantee exact recovery.

3.4 A Newton-type Forward Backward Greedy Method

In this section, we present a new Greedy method, which is inspired from the Adaptive Forward Backward (AdFoBa) [74] Greedy method. The difference is in the cost function itself, and therefore the forward step would be modified. In addition, we propose a different backward scheme, which seems to correct false peaks.

3.4.1 Optimization problem

The proposed method deals with the multi-snapshots case, i.e. equation (3.5). Furthermore, greedy methods tackle the ℓ_0-optimization problem, namely:

$$\begin{aligned} \underset{\boldsymbol{X}}{\text{minimize}} \quad & \|\boldsymbol{Y} - \boldsymbol{\mathcal{A}}\boldsymbol{X}\|_2^2 \\ \text{subject to} \quad & \|\boldsymbol{X}\|_{2,0} \leq q \end{aligned} \tag{3.39}$$

[3] By number of resolvable sources, we mean the number of sources that could be resolved, given that the angular separation between these sources exceed a certain threshold.

where $\|.\|_{2,0}$ is the $\ell_{2,0}$ norm defined as

$$\|\boldsymbol{X}\|_{2,0} = \text{card } \{k : \|\boldsymbol{X}_{k,:}\|_2 \neq 0\} \tag{3.40}$$

where $\boldsymbol{X}_{k,:}$ is the k^{th} row of $\boldsymbol{X}$ and $\|\|_2$ is the ℓ_2 norm. This means that the $\ell_{2,0}$ norm counts the number of rows that have at least one non-zero entry. In what follows, we discuss the Forward and Backward steps of the proposed Newton-type greedy method.

3.4.2 Forward step

At an n^{th} iteration, we propose to choose an atom[4] that minimizes

$$j^{(n)} = \arg \min_{j \notin \boldsymbol{\Omega}^{(n-1)}} \min_{\boldsymbol{\beta}} \frac{\|\boldsymbol{Y} - \boldsymbol{\mathcal{A}}(\boldsymbol{X}^{(n)} + \boldsymbol{e}_j \boldsymbol{\beta}^H)\|_2^2}{\|[\nabla_{\boldsymbol{X}}(\boldsymbol{Y} - \boldsymbol{\mathcal{A}}\boldsymbol{X})]_{j,:}\|_2^2} \tag{3.41}$$

Note the following

$$\begin{aligned} \min_{\boldsymbol{\beta}} \frac{\|\boldsymbol{Y} - \boldsymbol{\mathcal{A}}(\boldsymbol{X}^{(n)} + \boldsymbol{e}_j \boldsymbol{\beta}^H)\|_2^2}{\|[\nabla_{\boldsymbol{X}}(\boldsymbol{Y} - \boldsymbol{\mathcal{A}}\boldsymbol{X})]_{j,:}\|_2^2} &= \min_{\boldsymbol{\beta}} \|\boldsymbol{Y} - \boldsymbol{\mathcal{A}}(\boldsymbol{X}^{(n)} + \boldsymbol{e}_j \boldsymbol{\beta}^H)\|_2^2 \\ &= \min_{\boldsymbol{\beta}} \text{tr } \left\{ \Big(\boldsymbol{Y} - \boldsymbol{\mathcal{A}}(\boldsymbol{X}^{(n)} + \boldsymbol{e}_j \boldsymbol{\beta}^H)\Big) \Big(\boldsymbol{Y} - \boldsymbol{\mathcal{A}}(\boldsymbol{X}^{(n)} + \boldsymbol{e}_j \boldsymbol{\beta}^H)\Big)^H \right\} \end{aligned} \tag{3.42}$$

Omitting terms that do not depend on $\boldsymbol{\beta}$, we get

$$\min_{\boldsymbol{\beta}} \big(-\boldsymbol{e}_j^H \boldsymbol{\mathcal{A}}^H \boldsymbol{Y} \boldsymbol{\beta} + \boldsymbol{e}_j^H \boldsymbol{\mathcal{A}}^H \boldsymbol{\mathcal{A}} \boldsymbol{X} \boldsymbol{\beta} - \boldsymbol{\beta}^H \boldsymbol{Y}^H \boldsymbol{\mathcal{A}} \boldsymbol{e}_j + \boldsymbol{\beta}^H \boldsymbol{X}^H \boldsymbol{\mathcal{A}}^H \boldsymbol{\mathcal{A}} \boldsymbol{e}_j + \|\boldsymbol{\beta}\|_2^2 \|\boldsymbol{\mathcal{A}} \boldsymbol{e}_j\|_2^2 \big) \tag{3.43}$$

The optimal value of $\boldsymbol{\beta}$ is attained by setting the derivative of the above expression with respect to $\boldsymbol{\beta}$ to zero.

$$\frac{\partial}{\partial \boldsymbol{\beta}} \big(-\boldsymbol{e}_j^H \boldsymbol{\mathcal{A}}^H \boldsymbol{Y} \boldsymbol{\beta} + \boldsymbol{e}_j^H \boldsymbol{\mathcal{A}}^H \boldsymbol{\mathcal{A}} \boldsymbol{X} \boldsymbol{\beta} - \boldsymbol{\beta}^H \boldsymbol{Y}^H \boldsymbol{\mathcal{A}} \boldsymbol{e}_j + \boldsymbol{\beta}^H \boldsymbol{X}^H \boldsymbol{\mathcal{A}}^H \boldsymbol{\mathcal{A}} \boldsymbol{e}_j + \|\boldsymbol{\beta}\|_2^2 \|\boldsymbol{\mathcal{A}} \boldsymbol{e}_j\|_2^2 \big) = 0 \tag{3.44}$$

which gives

$$-2\boldsymbol{Y}^H \boldsymbol{\mathcal{A}} \boldsymbol{e}_j + 2\boldsymbol{X}^H \boldsymbol{\mathcal{A}}^H \boldsymbol{\mathcal{A}} \boldsymbol{e}_j + 2\boldsymbol{\beta}^{\text{opt}} \|\boldsymbol{\mathcal{A}} \boldsymbol{e}_j\|_2^2 = 0 \tag{3.45}$$

Re-arranging terms, we get

$$\boldsymbol{\beta}^{\text{opt}} = \frac{1}{\|\boldsymbol{\mathcal{A}} \boldsymbol{e}_j\|_2^2} \big(\boldsymbol{\mathcal{A}}_{:,j}^H (\boldsymbol{Y} - \boldsymbol{\mathcal{A}}\boldsymbol{X})\big)^H \tag{3.46}$$

[4] Atom refers to a column of the dictionary $\boldsymbol{\mathcal{A}}$

But since the columns of $\boldsymbol{\mathcal{A}}$ are restricted to have a unit norm, then $\|\boldsymbol{\mathcal{A}}\boldsymbol{e}_j\|_2^2 = 1$. Plugging $\boldsymbol{\beta}^{\text{opt}}$ in equation (3.41), we now have

$$j^{(n)} = \arg \min_{j \notin \boldsymbol{\Omega}^{(n-1)}} \frac{\|\boldsymbol{Y} - \boldsymbol{\mathcal{A}}(\boldsymbol{X}^{(n)} + \boldsymbol{e}_j \boldsymbol{\mathcal{A}}_{:,j}^H (\boldsymbol{Y} - \boldsymbol{\mathcal{A}}\boldsymbol{X}))\|_2^2}{\|[\nabla_{\boldsymbol{X}}(\boldsymbol{Y} - \boldsymbol{\mathcal{A}}\boldsymbol{X})]_{j,:}\|_2^2} \tag{3.47}$$

Intuitively, equation (3.47) means that we are *"wiggling"* the weights corresponding to the j^{th} atom, or column, in $\boldsymbol{\mathcal{A}}$ and choosing the atom index that is least affected with this perturbation. Moreover, we have included the Gradient term in the denominator of the above cost function, similar to the *Newton*'s method. Although it may seem natural, this additional term helps in speeding up the convergence of the algorithm, yet achieving better performance as well. After finding this index and appending it in the support set, namely

$$\boldsymbol{\Omega}^{(n)} \leftarrow \boldsymbol{\Omega}^{(n-1)} \cup \{\hat{j}^{(n)}\} \tag{3.48}$$

We estimate an updated version of $\boldsymbol{X}$ as follows

$$\boldsymbol{X}^{(n+1)} = \left(\boldsymbol{\mathcal{A}}_{(:,\boldsymbol{\Omega}^{(n)})}^H \boldsymbol{\mathcal{A}}_{(:,\boldsymbol{\Omega}^{(n)})}\right)^{-1} \boldsymbol{\mathcal{A}}_{(:,\boldsymbol{\Omega}^{(n)})}^H \boldsymbol{Y} \tag{3.49}$$

Also, let $\epsilon^{(n)}$ denote the relative error at iteration n as

$$\epsilon^{(n)} = \left| \|\boldsymbol{Y} - \boldsymbol{\mathcal{A}}\boldsymbol{X}^{(n+1)}\|_2^2 - \|\boldsymbol{Y} - \boldsymbol{\mathcal{A}}\boldsymbol{X}^{(n)}\|_2^2 \right| \tag{3.50}$$

3.4.3 Backward step

To allow flexibility of the proposed greedy method, we propose a backward scheme. The backward scheme will indeed depend on the value of the error $\epsilon^{(n)}$ at iteration (n). If the error is "relatively" small, we can go on to another forward step $n+1$, otherwise a correction is needed. A natural question arises here:

What should $\epsilon^{(n)}$ be compared to ?

Well, we can ask an alternative question, which is the following:

What if the atom added at iteration (n) corresponding to index $j^{(n)}$ increases the cost function $\|\boldsymbol{Y} - \boldsymbol{\mathcal{A}}\boldsymbol{X}\|_2^2$ and not decrease it?

To check for this case, we compare the error $\epsilon^{(n)}$ to an error $\vartheta^{(n)}$, which is computed if the support $\boldsymbol{\Omega}^{(n)}$ contains 1 less element[5]. More precisely, define

$$\vartheta_i^{(n)} = \left| \|\boldsymbol{Y} - \boldsymbol{\mathcal{A}}_{(:,\boldsymbol{\Omega}^{(n)}/\{i\})} \boldsymbol{X}^{(n+1)}_{(\boldsymbol{\Omega}^{(n)}/\{i\},:)}\|_2^2 - \|\boldsymbol{Y} - \boldsymbol{\mathcal{A}}\boldsymbol{X}^{(n)}\|_2^2 \right| \tag{3.51}$$

[5]This could be seen as over-fitting

for all $i \in \mathbf{\Omega}^{(n)}$. Now, choose the smallest error amongst all $\vartheta_i^{(n)}$, i.e.

$$\vartheta^{(n)} = \min \{\vartheta_i^{(n)}\}_{i \in \mathbf{\Omega}^{(n)}} \tag{3.52}$$

and denote

$$i^{(n)} = \underset{i}{\operatorname{argmin}}\, \vartheta_i^{(n)} \tag{3.53}$$

Here, if $\vartheta^{(n)} > \epsilon^{(n)}$ we say that the error at iteration n is acceptable and there doesn't seem to be any over-fitting. On the other hand, if $\vartheta^{(n)} \leq \epsilon^{(n)}$, we should remove this "defected atom", which corresponds to index $i^{(n)}$

$$\mathbf{\Omega}^{(n)} \leftarrow \mathbf{\Omega}^{(n)} / \{i^{(n)}\} \tag{3.54}$$

Re-modify the weighting matrix

$$\boldsymbol{X}^{(n+1)} = \left(\boldsymbol{\mathcal{A}}_{(:,\mathbf{\Omega}^{(n)})}^H \boldsymbol{\mathcal{A}}_{(:,\mathbf{\Omega}^{(n)})}\right)^{-1} \boldsymbol{\mathcal{A}}_{(:,\mathbf{\Omega}^{(n)})}^H \boldsymbol{Y} \tag{3.55}$$

and finally go one step backward

$$n \leftarrow n - 1 \tag{3.56}$$

The forward backward procedure is repeated until error $\epsilon^{(n)} \leq \delta$, where δ is a given tolerance value.

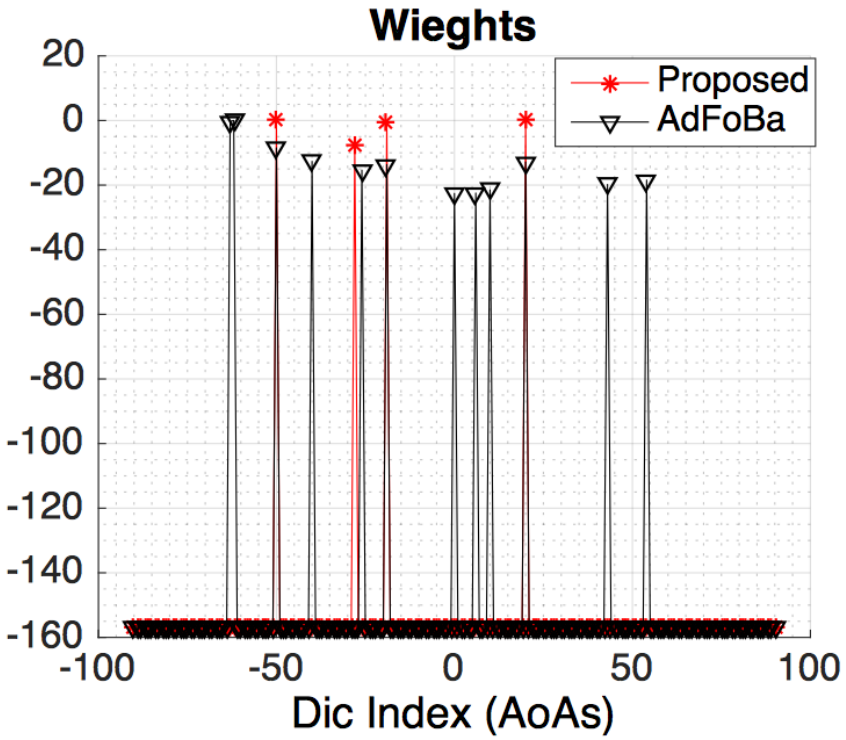

Figure 3.4: Comparison of spectra for $q = 4$ sources.

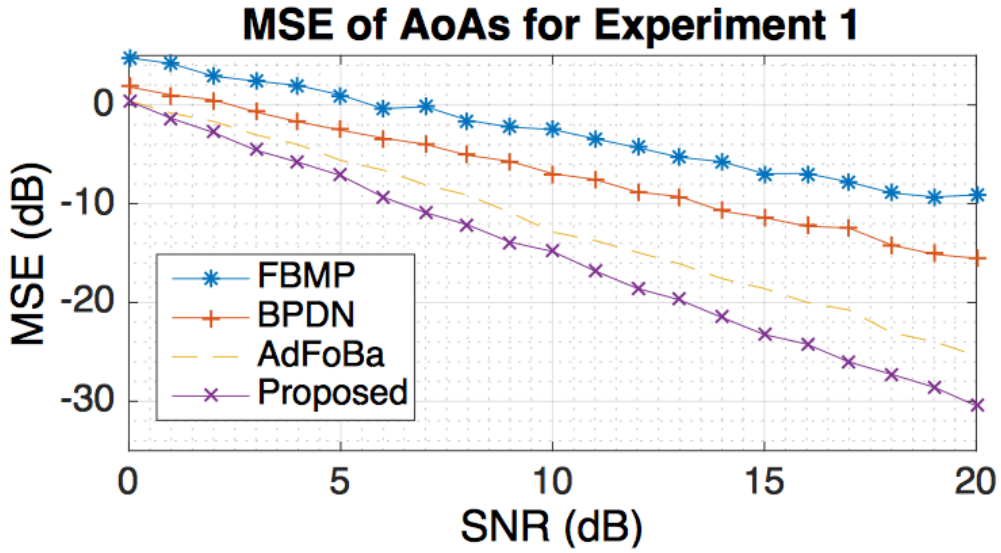

Figure 3.5: MSE of AoAs for Exp. 1

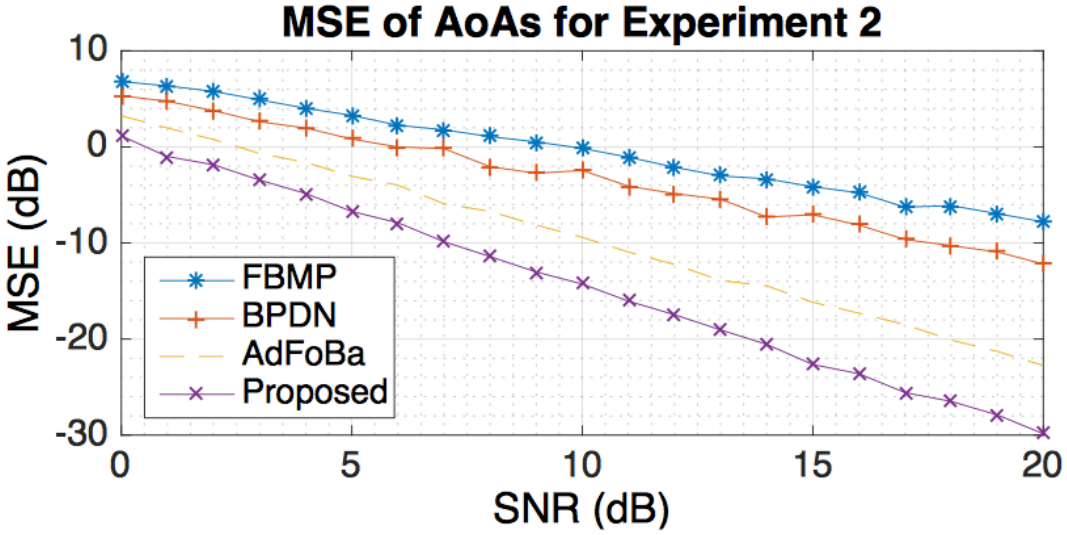

Figure 3.6: MSE of AoAs for Exp. 2

We present some computer simulations to show the efficiency and accuracy of the proposed Newton-type method. In Fig. 3.4, we have used $N = 15$ antennas and a dictionary of size $K = 181$ discritized at steps of 1° . Furthermore, $L = 1$ snapshot was used at SNR $= 20$ dB. We have $q = 4$ sources at $\theta_1 = -50^\circ, \theta_2 = -27^\circ, \theta_3 = -20^\circ, \theta_4 = 20^\circ$. We can clearly see the difference between the proposed Newton-type method and the one AdFoBa [74]. Our method avoids overfitting of sources, whereas the AdFoBa overestimates then number of existing sources.

In Experiment 1 (Fig. 3.5), we are interested in the MSE performance of existing sparse recovery methods compared to the proposed here. We compare the Newton-type Forward Backward proposed method with AdFoBa [74], BPDN [53] and FBMP [67]. Here we have set $L = 10^2$, $N = 10$, $q = 2$ with $\theta_1 = 0^\circ$ and $\theta_2 = 10^\circ$. Also, $K = 181$ as

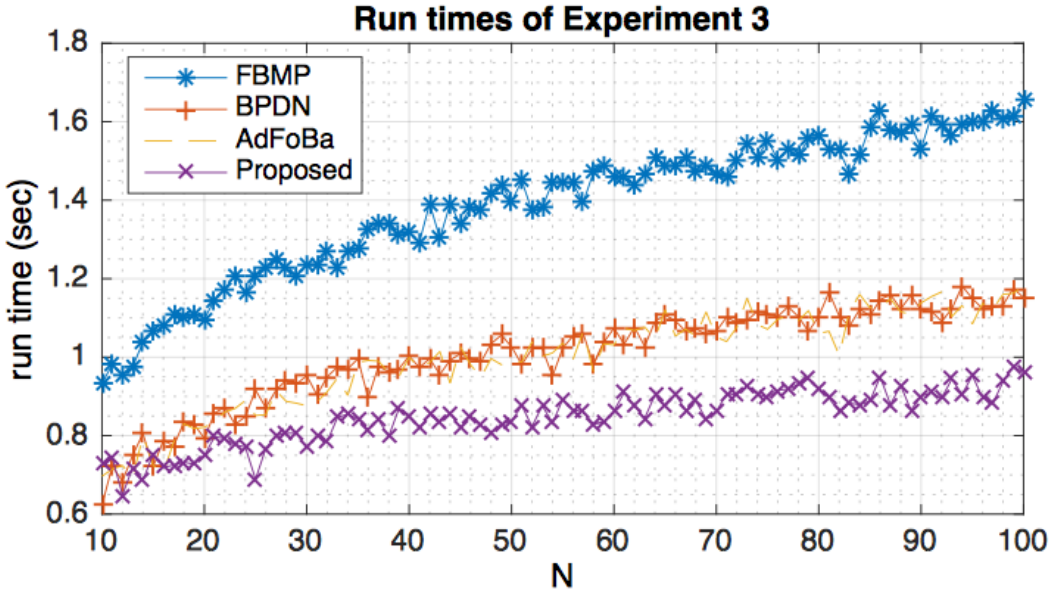

Figure 3.7: Run times of Exp. 3

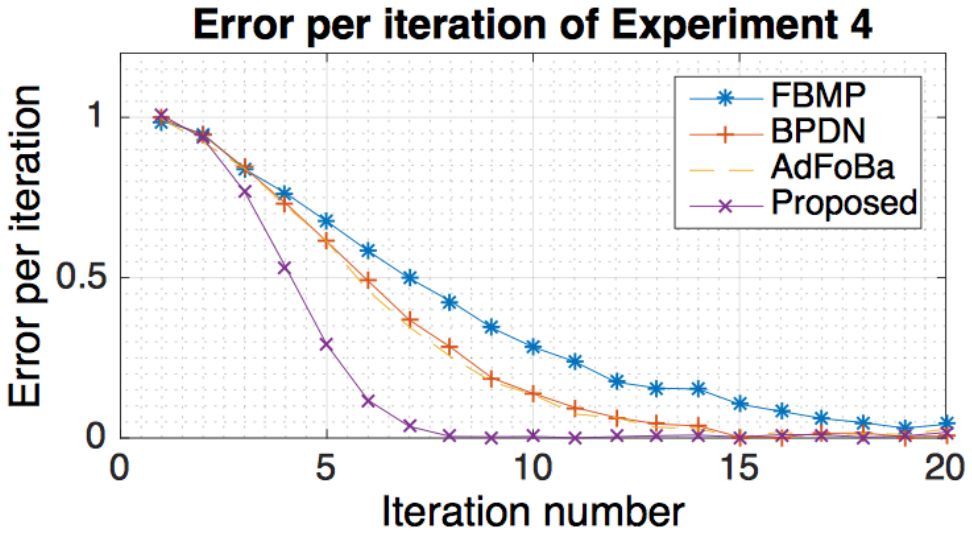

Figure 3.8: Errors per iteration of Exp. 4

before. The MSE is computed using 10^4 Monte Carlo trials. Here, in case of overfitting, we choose the q largest peaks in the weights. We can see that both Forward-Backward schemes (the proposed one and AdFoBa) perform better than BPDN and FBMP, due to their adaptive ability of "correcting themselves" in case of any overfitting or false selected atoms. Moreover, the proposed one performs better than AdFoBa, due to the different backward step criterion. We can see an 5 dB between the proposed method and the AdFoBa at sufficiently high SNR. In Experiment 2 (Fig. 3.6), we have used the same parameters as in Experiment 1, except that we have changed L to $L = 10$. We can also observe the phenomena as above. Note that here we have a higher MSE for all methods due to less observed samples. Nevertheless, we can see that the MSE gaps

between the different methods are still the same as that in Experiment 1. We can see an 8 dB between the proposed method and the AdFoBa at sufficiently high SNR.
Another important aspect is the algorithm complexity or the number of operations required before the algorithm terminates. In Experiment 3 (i.e. Fig. 3.7), we study the speed of the algorithms mentioned above as a function of number of antennas N . To assess generality, we have also averaged the speeds over 10^4 Monte Carlo trials. We can see that the proposed algorithm terminates before all the other ones mentioned above, thanks to the gradient factor in the cost function of equation (3.41). If $N = 100$ antennas were used, we can see a gain of speed of about 0.6 seconds compared to the FBMP algorithm and 0.2 seconds compared to AdFoBa and BPDN.
Finally, in Experiment 4, i.e. Fig. 3.8, we have fixed the parameters as in Experiment 1 and studied the behaviour of the error for different algorithms, in the sense of

$$\epsilon^{(n)} = \left| \|\boldsymbol{Y} - \boldsymbol{\mathcal{A}}\boldsymbol{X}^{(n)}\|_2^2 - \|\boldsymbol{Y} - \boldsymbol{\mathcal{A}}\boldsymbol{X}^{(n-1)}\|_2^2 \right| \tag{3.57}$$

This means that when no improvement occurs, the above error should become negligible. Also, we can see that the proposed algorithm converges in about 8 to 9 iterations. The AdFoBa and the BPDN require around 15 iterations to achieve the same error as the proposed one. Additionally, we can see that the FBMP needs more than 20 iterations to achieve this accuracy.

3.5 Conclusions and future directions

In this Chapter, and with the help of latent variables and Variational Bayes, we have derived an iterative algorithm that could estimate the Angles of Arrival (AoA) of the incoming sources with a single snapshot, without the knowledge of the number of sources, and with closely spaced sources at high SNR.

We have also seen that it is possible that the proposed Newton-type forward backward greedy method performs faster, in terms of convergence and number of operations, and better, in terms of Mean-Squared-Error (MSE) of AoAs.

Future work may be oriented towards performance analysis of the proposed Variational Bayes algorithm and towards taking into account prior knowledge of the number of source signals, which may improve the performance of this algorithm.

Table 2: Proposed Variational Bayes algorithm for AoA Estimation

INPUT:
Given the observed vector $\boldsymbol{x} = \boldsymbol{\mathcal{A}}\boldsymbol{s} + \boldsymbol{n}$.

INITIALISATION:

- Fix
$$\gamma = \delta = \zeta = \eta = 10^{-6}$$
$$n = 0$$
- Initialise
$$m_{\beta_k}^{(0)} = 10^5 \text{ for all } k$$
$$m_{\nu}^{(0)} = \frac{1}{\sigma_n^2}$$

MAIN LOOP:
while $\|\hat{\boldsymbol{\Theta}}^{(n+1)} - \hat{\boldsymbol{\Theta}}^{(n)}\| > \xi$ *(Pre-defined Threshold)* **do**

- Form
$$\boldsymbol{\Omega}^{(n)} = \text{diag}\,[m_{\beta_1}^{(n)} \dots m_{\beta_K}^{(n)}]$$
- Compute $\boldsymbol{\Sigma}$ as in equation (3.31)
$$\boldsymbol{\Sigma}^{(n)} = \left(\boldsymbol{\Omega}^{(n)} + m_{\nu}^{(n)}\boldsymbol{\mathcal{A}}^{\mathrm{H}}\boldsymbol{\mathcal{A}}\right)^{-1}$$
- Compute $\boldsymbol{m_s}$ using (3.32)
$$\boldsymbol{m_s}^{(n)} = m_{\nu}^{(n)}\boldsymbol{\Sigma}^{(n)}\boldsymbol{\mathcal{A}}^{\mathrm{H}}\boldsymbol{x}$$
- For all $k = 1 \dots K$, compute m_{β_k} using (3.36)
$$m_{\beta_k}^{(n+1)} = \frac{2\gamma + 1}{2\delta + |(\boldsymbol{m_s}^{(n)})_k|^2 + \boldsymbol{\Sigma}_{k,k}^{(n)}}$$
- Compute m_{ν} using (3.37)
$$m_{\nu}^{(n+1)} = \frac{2\zeta + 1}{2\eta + \|\boldsymbol{x} - \boldsymbol{\mathcal{A}}\boldsymbol{m_s^{(n)}}\|^2 + \text{tr}\,\{\boldsymbol{\mathcal{A}}\boldsymbol{\Sigma^{(n)}}\boldsymbol{\mathcal{A}}^{\mathrm{H}}\}}$$
- Increment n
$$n \leftarrow n + 1$$

OUTPUT:
The estimate of $\boldsymbol{s}$ is
$$\hat{\boldsymbol{s}} = \boldsymbol{m_s}^{(n)}$$

Chapter 4

Joint Angle and Delay Estimation

In this chapter, we derive several algorithms for the problem of Joint Angle and Delay Estimation (JADE). The contributions, herein, are summarized as follows: (i) we derive an algorithm that is a modification of the two dimensional Iterative Quadratic ML (2D-IQML) algorithm, where an additional constraint is added for joint ToA and AoA estimation; (ii) we show that 2D-IQML gives biased estimates of ToAs/AoAs and performs poorly at low SNR due to noise induced bias; (iii) we derive a two dimensional Denoised IQML (2D-DIQML) that gives consistent estimates and outperforms 2D-IQML; (iv) we show that 2D-DIQML is asymptotically globally convergent and hence insensitive to the initialisation; (v) we derive two algorithms, based on 2D Matrix Pencils (MP), for the case of a single snapshot OFDM symbol observed by multiple antennas in a ULA configuration; (vi) one of the two MP algorithms seems more interesting because it's motivated from an idea that most Wi-Fi systems use a large number of subcarriers compared to the number of antennas; (vii) We present a "Spatio-Frequential" smoothing technique, when the transmit OFDM symbol is received through multiple coherent signals using a uniform linear antenna array, which is the case of an indoor multipath channel.

4.1 System Model

4.1.1 Problem formulation

Consider an OFDM symbol $s(t)$ composed of M subcarriers and centered at a carrier frequency f_c, impinging an antenna array of N antennas via q multipath components, each arriving at different AoAs $\{\theta_i\}_{i=1}^{q}$ and ToAs $\{\tau_i\}_{i=1}^{q}$. In baseband, we could write

the l^{th} received OFDM symbol at the n^{th} antenna as:

$$r_n^{(l)}(t) = \sum_{i=1}^{q} \gamma_i^{(l)} a_n(\theta_i) s(t - \tau_i) + n_n^{(l)}(t) \tag{4.1}$$

where

$$s(t) = \begin{cases} \sum_{m=0}^{M-1} b_m e^{j2\pi m \triangle_f t} & \text{if } t \in [0, T] \\ 0 & \text{elsewhere} \end{cases} \tag{4.2}$$

where $T = \frac{1}{\triangle_f}$ is the OFDM symbol duration, $\triangle_f$ is the subcarrier spacing, b_m is the modulated symbol onto the m^{th} subcarrier, $a_n(\theta)$ is the n^{th} antenna response to an incoming signal at angle θ. The form of $a_n(\theta)$ depends on the array geometry. $\gamma_i^{(l)}$ is the complex coefficient of the i^{th} multipath component. The term $n_n^{(l)}(t)$ is background noise. Plugging (4.2) in (4.1) and sampling $r_n^{(l)}(t)$ at regular intervals of $k \triangleq k\frac{T}{M}$, we get $r_{n,k}^{(l)} \triangleq r_n^{(l)}(k\frac{T}{M})$ as:

$$r_{n,k}^{(l)} = \sum_{i=1}^{q} \sum_{m=0}^{M-1} b_m e^{j2\pi \frac{km}{M}} e^{-j2\pi m \triangle_f \tau_i} \gamma_i^{(l)} a_n(\theta_i) + n_{n,k}^{(l)}. \tag{4.3}$$

Collecting M samples, we can apply an M-point DFT, so observing the m^{th} subcarrier at the n^{th} antenna, we get:

$$R_{n,m}^{(l)} = \sum_{k=0}^{M-1} r_{n,k}^{(l)} e^{-j2\pi m \frac{k}{M}} = b_m \sum_{i=1}^{q} \gamma_i^{(l)} a_n(\theta_i) e^{-j2\pi m \triangle_f \tau_i} + N_{n,m}^{(l)} \tag{4.4}$$

We claim that the transmitted OFDM symbol $s(t)$ is a preamble field of the Wi-Fi 802.11 frame, thus prior knowledge of the modulated symbols $\{b_m\}_{m=0}^{M-1}$ is a valid assumption, since this stream of symbols (each at its corresponding sub-carrier) are repeated in each OFDM symbol placed at the beginning of the Wi-Fi frame for channel estimation and frequency offset purposes. Therefore, at each OFDM symbol reception, we compensate for all such symbols (multiplying by $\frac{b_m^*}{|b_m|^2}$) and hence omit b_m from (4.4). Re-writing (4.4) in a compact matrix form, we have:

$$\boldsymbol{x}(l) = \boldsymbol{H}\boldsymbol{\gamma}(l) + \boldsymbol{n}(l), \quad l = 1 \dots L \tag{4.5}$$

where $\boldsymbol{x}(l)$ and $\boldsymbol{n}(l)$ are $MN \times 1$ vectors

$$\boldsymbol{x}(l) = vec\{\boldsymbol{R}\}, \qquad \boldsymbol{R}^{\langle m,n \rangle} = R_{n,m}^{(l)} \tag{4.6}$$

$$\boldsymbol{n}(l) = vec\{\boldsymbol{N}\}, \qquad \boldsymbol{N}^{\langle m,n \rangle} = N_{n,m}^{(l)} \tag{4.7}$$

$\boldsymbol{H}$ is an $MN \times q$ matrix given as

$$\boldsymbol{H} = \boldsymbol{A} \boxtimes \boldsymbol{C} = [\boldsymbol{a}(\theta_1) \otimes \boldsymbol{c}(\tau_1) \dots \boldsymbol{a}(\theta_q) \otimes \boldsymbol{c}(\tau_q)] \tag{4.8}$$

where $\boldsymbol{a}(\theta)$ and $\boldsymbol{c}(\tau)$ are $N \times 1$ and $M \times 1$, respectively. The n^{th} entry of $\boldsymbol{a}(\theta)$, denoted $\boldsymbol{a}_n(\theta)$, is the response of the n^{th} antenna to a signal arriving at angle θ with respect to the antenna array. We shall assume a Uniform Linear Array (ULA), thus $\boldsymbol{a}_n(\theta) = e^{-jd2\pi f_c(n-1)sin(\theta)}$, where d is the distance between 2 adjacent antennas. Similarly, the m^{th} entry of $\boldsymbol{c}(\tau)$, denoted $\boldsymbol{c}_m(\tau) = e^{-j2\pi\tau(m-1)\triangle_f}$, is the response of the m^{th} subcarrier to a signal arriving with time delay τ. The $q \times 1$ vector $\boldsymbol{\gamma}(l)$ is composed of the multipath coefficients

$$\boldsymbol{\gamma}(l) = [\gamma_1^{(l)} \dots \gamma_q^{(l)}]^T \tag{4.9}$$

Throughout the chapter, we make a distinction between the multi-snapshot case ($L \geq 2$) and the single-snapshot case ($L = 1$). As done in the previous chapter, we omit the time dependence in case of 1 snapshot, i.e.

$$\boldsymbol{x} = \boldsymbol{H}\boldsymbol{\gamma} + \boldsymbol{n} \tag{4.10}$$

4.1.2 Assumptions

We assume the following:

- **A1**: $\boldsymbol{H}$ is full column rank.
- **A2**: The multipath coefficients, $\boldsymbol{\gamma}(l)$, are fixed within a snapshot, and may vary from one snapshot to another.
- **A3**: The number of multipath components q is known.
- **A4**: The vector $\boldsymbol{n}(l)$ is additive Gaussian noise of zero mean and variance $\sigma^2\boldsymbol{I}$, assumed to be white over space, frequencies, and symbols; we also assume that the noise is independent from the multipath coefficients.

Condition **A2** is a valid assumption since the time it takes for an indoor channel to change significantly is of the order of milliseconds [75], whereas the OFDM symbol duration of a snapshot T is of the order of microseconds.

Techniques for estimating the number of sources could be done through hypothesis testing [76] or via information theoretic criteria [77]. However, we assume knowledge of the number of sources, i.e. q is known.

4.1.3 Problem statement

The problem could be stated as follows:

- **Single-Snapshot case:** Given the observed vector $\boldsymbol{x}$ in equation (4.10) and the number of multi-path components q, and their corresponding AoAs and ToAs $\{(\theta_i, \tau_i)\}_{i=1}^{q}$.
- **Multi-Snapshot case:** Given the observed data $\{\boldsymbol{x}(l)\}_{l=1}^{L}$ in equation (4.5) and the number of multi-path components q, and their corresponding AoAs and ToAs $\{(\theta_i, \tau_i)\}_{i=1}^{q}$.

4.2 Efficient Maximum Likelihood Joint AoA and ToA estimation

In a deterministic approach, the signal parameters $\{(\theta_i, \tau_i)\}_{i=1}^{q}$ and multipath components $\{\boldsymbol{\gamma}(l)\}_{l=1}^{L}$ are not sample functions of random processes. Instead, these quantities are modelled as unknown deterministic sequences, and are jointly estimated through the criterion:

$$[\hat{\boldsymbol{H}}, \hat{\boldsymbol{\gamma}}(1), \ldots, \hat{\boldsymbol{\gamma}}(L)] = \underset{\boldsymbol{H}, \boldsymbol{\gamma}(1), \ldots, \boldsymbol{\gamma}(L)}{\arg\min} \sum_{l=1}^{L} \|\boldsymbol{x}(l) - \boldsymbol{H}\boldsymbol{\gamma}(l)\|^2 \tag{4.11}$$

Minimising with respect to $\{\boldsymbol{\gamma}(l)\}_{l=1}^{L}$, we obtain:

$$\hat{\boldsymbol{\gamma}}(l) = (\boldsymbol{H}^H\boldsymbol{H})^{-1}\boldsymbol{H}^H\boldsymbol{x}(l), \quad l = 1 \ldots L \tag{4.12}$$

Treating $\{\boldsymbol{\gamma}(l)\}_{l=1}^{L}$ as nuissance parameters, we substitute its estimate obtained by (4.12) in (4.11) to get:

$$\hat{\boldsymbol{H}} = \underset{\boldsymbol{H}}{\arg\min} \sum_{l=1}^{L} \left\| \boldsymbol{\mathscr{P}}_{\boldsymbol{H}}^{\perp}\boldsymbol{x}(l) \right\|^2 = \underset{\boldsymbol{H}}{\arg\min}\, \mathrm{tr}\left\{ \boldsymbol{\mathscr{P}}_{\boldsymbol{H}}^{\perp}\hat{\boldsymbol{R}}_{xx} \right\} \tag{4.13}$$

where $\boldsymbol{\mathscr{P}}_{\boldsymbol{H}}^{\perp} = \boldsymbol{I}_{MN} - \boldsymbol{H}(\boldsymbol{H}^H\boldsymbol{H})^{-1}\boldsymbol{H}^H$ is the orthogonal projection onto the noise subspace. The matrix $\hat{\boldsymbol{R}}_{xx}$ is the sample covariance matrix obtained by $\hat{\boldsymbol{R}}_{xx} = \frac{1}{L}\sum_{l=1}^{L}\boldsymbol{x}(l)\boldsymbol{x}(l)^H$. Equation (4.13) represents the DML criteria.

4.2.1 Parameterisation of the Noise Subspace

The Deterministic ML (DML) criterion in (4.10) is highly nonlinear, as it requires a $2q$-dimensional search, and its direct optimisation would require cumbersome optimisation techniques. The key to a computationally attractive solution of the DML problem is a parameterisation of the noise subspace, as done in this section. Consider the two

following polynomials:

$$A(z) = \sum_{i=0}^{q} a_i z^{q-i} = \prod_{i=1}^{q} (z - z_{\tau_i}) \tag{4.14a}$$

and

$$B(z) = \sum_{i=0}^{q-1} b_i z^{q-1-i} = \sum_{i=1}^{q} z_{\theta_i} \prod_{k=1, k\neq i}^{q} \frac{(z - z_{\tau_k})}{(z_{\tau_i} - z_{\tau_k})} \tag{4.14b}$$

where $z_{\tau_i} = e^{-j2\pi\tau_i \triangle f}$ and $z_{\theta_i} = e^{-jd2\pi f_c sin(\theta_i)}$. Note that $A(z_{\tau_i}) = 0$ and $B(z_{\tau_i}) = z_{\theta_i}$. The coefficient $a_0 = 1$ so that $A(z)$ is monic. Furthermore, $\boldsymbol{W(f)}$ is a $\big((2N-1)(M-q)+N-1\big) \times MN$ matrix given as

$$\boldsymbol{W(f)} = \left[\frac{\boldsymbol{I}_N \otimes \boldsymbol{A}}{[\boldsymbol{I}_{N-1}|\boldsymbol{0}] \otimes \boldsymbol{B} - [\boldsymbol{0}|\boldsymbol{I}_{N-1}] \otimes \boldsymbol{I}_{M,q-1}}\right] \tag{4.15}$$

where $\boldsymbol{A}$ is $(M-q) \times M$

$$\boldsymbol{A} = \begin{bmatrix} a_q & \cdots & a_1 & a_0 & & 0 \\ & \ddots & & \ddots & \ddots & \\ 0 & & a_q & \cdots & a_1 & a_0 \end{bmatrix} \tag{4.16a}$$

and $\boldsymbol{B}$ is $(M-q+1) \times M$

$$\boldsymbol{B} = \begin{bmatrix} b_{q-1} & \cdots & b_1 & b_0 & & 0 \\ & \ddots & & \ddots & \ddots & \\ 0 & & b_{q-1} & \cdots & b_1 & b_0 \end{bmatrix} \tag{4.16b}$$

Also, $\boldsymbol{f}$ is $2(q+1) \times 1$ given as

$$\boldsymbol{f}^T = \begin{bmatrix} \boldsymbol{a}^T & \boldsymbol{b}^T & 1 \end{bmatrix} \tag{4.16c}$$

$$\boldsymbol{a}^T = \begin{bmatrix} a_0 & \cdots & a_q \end{bmatrix} \tag{4.16d}$$

$$\boldsymbol{b}^T = \begin{bmatrix} b_0 & \cdots & b_{q-1} \end{bmatrix} \tag{4.16e}$$

Finally, $\boldsymbol{I}_{M,q-1}$ is $(M-q+1) \times M$ defined by

$$\boldsymbol{I}_{M,q-1} = [\boldsymbol{I}_{M-q+1} | \overbrace{\boldsymbol{0} \cdots \boldsymbol{0}}^{q-1}] \tag{4.16f}$$

Theorem 4.1. *$\boldsymbol{W(f)}$ has row rank $MN - q$ if $q \leq \frac{M+1}{2}$ and $\boldsymbol{H}$ has full column rank.*

Proof. See [107]. □

Under assumption **A1** and $q \leq \frac{M+1}{2}$, the rows of the matrix $\boldsymbol{W(f)}$ (equivalently, the columns of $\boldsymbol{W}^H\boldsymbol{(f)}$) span the noise subspace, i.e. $\boldsymbol{W(f)H} = \boldsymbol{0}$ and thus we can write $\boldsymbol{\mathscr{P}}_{\boldsymbol{H}}^{\perp} = \boldsymbol{\mathscr{P}}_{\boldsymbol{W}^H\boldsymbol{(f)}}$.

Note that this parameterisation resolves maximally $\frac{M+1}{2}$ paths. It is worth mentioning that if $N > M$, one would want to resolve $\frac{N+1}{2}$ paths (and not $\frac{M+1}{2}$ paths), so a simple modification of the model in (4.5) is done by interchanging $\boldsymbol{a}(\theta)$ and $\boldsymbol{c}(\tau)$ in (4.8), then constructing matrices $\boldsymbol{A}$ and $\boldsymbol{B}$ (equivalently, the polynomials $A(z)$ and $B(z)$) of N and $N-1$ coefficients, respectively. In general, we could find a noise parameterisation that could allow the resolvability of $\frac{max(M,N)+1}{2}$.

4.2.2 2D Iterative Quadratic ML (2D-IQML)

We rewrite the DML cost function in (4.13) as follows

$$\begin{aligned}\min_{\boldsymbol{H}} \operatorname{tr}\Big\{\boldsymbol{\mathscr{P}}_{\boldsymbol{H}}^{\perp}\hat{\boldsymbol{R}}_{xx}\Big\} &= \min_{\boldsymbol{H}} \sum_{l=1}^{L} \Big\|\boldsymbol{\mathscr{P}}_{\boldsymbol{W}^H\boldsymbol{(f)}}\boldsymbol{x}(l)\Big\|^2 \\ &= \min_{\boldsymbol{f}} \sum_{l=1}^{L} \boldsymbol{x}^H(l)\boldsymbol{W}^H\boldsymbol{(f)}\Big(\boldsymbol{W(f)W}^H\boldsymbol{(f)}\Big)^{\dagger}\boldsymbol{W(f)x}(l)\end{aligned} \tag{4.17}$$

where the Moore-Penrose pseudo–inverse has to be introduced since $\boldsymbol{W(f)W}^H\boldsymbol{(f)}$ is singular for $q < \frac{M+1}{2}$, and non-singular for $q = \frac{M+1}{2}$ if M is odd. Note that $\boldsymbol{W(f)x}(l) = \boldsymbol{\mathcal{X}}_l\boldsymbol{f}$, where $\boldsymbol{\mathcal{X}}_l$ is an $((2N-1)(M-q)+N-1) \times (2q+2)$ matrix formed of elements of $\boldsymbol{x}(l)$. Finally, (4.17) boils down to the following

$$\hat{\boldsymbol{f}} = \arg\min_{\boldsymbol{f}} \boldsymbol{f}^H\boldsymbol{\mathcal{Q}}\boldsymbol{f} \tag{4.18a}$$

where

$$\boldsymbol{\mathcal{Q}} = \sum_{l=1}^{L} \boldsymbol{\mathcal{X}}_l^H\Big(\boldsymbol{W(f)W}^H\boldsymbol{(f)}\Big)^{\dagger}\boldsymbol{\mathcal{X}}_l \tag{4.18b}$$

The cost function in (4.18) could be solved in an iterative fashion as

$$\hat{\boldsymbol{f}}_{(n)} = \arg\min_{\boldsymbol{f}} \boldsymbol{f}^H\boldsymbol{\mathcal{Q}}_{(n-1)}\boldsymbol{f} \tag{4.19a}$$

where

$$\boldsymbol{\mathcal{Q}}_{(n-1)} = \sum_{l=1}^{L} \boldsymbol{\mathcal{X}}_l^H\Big(\boldsymbol{W}(\hat{\boldsymbol{f}}_{(n-1)})\boldsymbol{W}^H(\hat{\boldsymbol{f}}_{(n-1)})\Big)^{\dagger}\boldsymbol{\mathcal{X}}_l \tag{4.19b}$$

The vector $\hat{\boldsymbol{f}}_{(n)}$ is the estimated vector of $\boldsymbol{f}$ at iteration (n). A good initialisation would be to set $\boldsymbol{W}(\hat{\boldsymbol{f}}_{(0)})\boldsymbol{W}^H(\hat{\boldsymbol{f}}_{(0)}) = \boldsymbol{I}$. If the constraint $\boldsymbol{e}_1^T\boldsymbol{f} = 1$ was posed to solve (4.19a), then at any iteration (n), the vector $\hat{\boldsymbol{f}}_{(n)}$ would estimate the coefficients in $\boldsymbol{a} = [a_o \dots a_q]^T$

properly, but the rest of its entries corresponding to the coefficients in $\boldsymbol{b} = [b_o \dots b_{q-1}]^T$ would be zero because there is no constraint posed on $\boldsymbol{f}$ in order to take the structure of $\boldsymbol{b} = [b_o \dots b_{q-1}]^T$ into account.

To cope with the aforementioned issue, we add the contraint $(\boldsymbol{J}\boldsymbol{e}_1)^T\boldsymbol{f} = 1$. Note that this constraint is reasonable since, indeed, the last entry of $\boldsymbol{f}$ is 1. In short, we aim to solve (4.19) subject to:

$$\boldsymbol{e}_1^T\boldsymbol{f} = 1 \tag{4.20a}$$

and

$$\boldsymbol{e}_1^T\boldsymbol{J}\boldsymbol{f} = 1 \tag{4.20b}$$

We write the Lagrangian function as

$$L(\boldsymbol{f}, \mu_1, \mu_2) = \boldsymbol{f}^H\boldsymbol{\mathcal{Q}}_{(n-1)}\boldsymbol{f} - \mu_1(\boldsymbol{e}_1^T\boldsymbol{f} - 1) - \mu_2(\boldsymbol{e}_1^T\boldsymbol{J}\boldsymbol{f} - 1) \tag{4.21}$$

where μ_1 and μ_2 are constants. Setting the derivative of $L(\boldsymbol{f}, \mu_1, \mu_2)$ with respect to $\boldsymbol{f}$ to 0, we get

$$\frac{\partial}{\partial \boldsymbol{f}} L(\boldsymbol{f}, \mu_1, \mu_2) = 2\boldsymbol{\mathcal{Q}}_{(n-1)}\boldsymbol{f} - \mu_1\boldsymbol{e}_1 - \mu_2\boldsymbol{J}\boldsymbol{e}_1 = 0 \tag{4.22}$$

So, with some straightforward manipulations, we have

$$\boldsymbol{f} = \mu_1^{'}\boldsymbol{\mathcal{Q}}_{(n-1)}^{-1}\boldsymbol{e}_1 + \mu_2^{'}\boldsymbol{\mathcal{Q}}_{(n-1)}^{-1}\boldsymbol{J}\boldsymbol{e}_1 \tag{4.23}$$

where $\mu_i^{'} = \frac{\mu_i}{2}$. Plugging (4.23) in (4.20a) and (4.20b), we have the following set of equations

$$\begin{bmatrix} \alpha & \gamma \\ \gamma^* & \beta \end{bmatrix} \begin{bmatrix} \mu_1^{'} \\ \mu_2^{'} \end{bmatrix} = \begin{bmatrix} 1 \\ 1 \end{bmatrix} \tag{4.24}$$

where α, β, and γ are given as:

$$\alpha = \boldsymbol{e}_1^T\boldsymbol{\mathcal{Q}}_{(n-1)}^{-1}\boldsymbol{e}_1 \tag{4.25a}$$

$$\beta = \boldsymbol{e}_1^T\boldsymbol{J}\boldsymbol{\mathcal{Q}}_{(n-1)}^{-1}\boldsymbol{J}\boldsymbol{e}_1 \tag{4.25b}$$

$$\gamma = \boldsymbol{e}_1^T\boldsymbol{\mathcal{Q}}_{(n-1)}^{-1}\boldsymbol{J}\boldsymbol{e}_1 \tag{4.25c}$$

Finally, solving (4.24) with respect to $\mu_1^{'}$ and $\mu_2^{'}$, we get the following

$$\hat{\boldsymbol{f}}_{(n)} = \frac{(\beta - \gamma)\boldsymbol{\mathcal{Q}}_{(n-1)}^{-1}\boldsymbol{e}_1 + (\alpha - \gamma^*)\boldsymbol{\mathcal{Q}}_{(n-1)}^{-1}\boldsymbol{J}\boldsymbol{e}_1}{\alpha\beta - |\gamma|^2} \tag{4.26}$$

The 2D-IQML could be summarised as follows:

- *Step1.* Given $\left\{\boldsymbol{x}(l)\right\}_{l=1}^{L}$, form $\left\{\boldsymbol{\mathcal{X}}_l\right\}_{l=1}^{L}$.

- *Step2.* Initialise $\boldsymbol{\mathcal{Q}}_{(0)} = \sum_{l=1}^{L} \boldsymbol{\mathcal{X}}_l^H \boldsymbol{\mathcal{X}}_l$.

- *Step3.* Iterate over (n) to compute $\hat{\boldsymbol{f}}_{(n)}$, using (24) and (25). Stop when $\|\hat{\boldsymbol{f}}_{(n)} - \hat{\boldsymbol{f}}_{(n-1)}\| < \xi$ (Pre-defined Threshold).

- *Step4.* Form the polynomials $A(z)$ and $B(z)$ using the estimate of $\hat{\boldsymbol{f}}_{(n)}$ obtained in the last iteration of *Step3* and equations (13), (15c), (15d), (15e).

- *Step5.* Find the q roots of $A(z_{\hat{\tau}_i}) = 0$, which give estimates of the ToAs as $\left\{z_{\hat{\tau}_i} = e^{-j2\pi\hat{\tau}_i \triangle_f}\right\}_{i=1}^{q}$.

- *Step6.* Compute $B(z_{\hat{\tau}_i}) = z_{\hat{\theta}_i}$, which give estimates of the q AoAs as $\left\{z_{\hat{\theta}_i} = e^{-jd2\pi f_c sin(\hat{\theta}_i)}\right\}_{i=1}^{q}$.

The first iteration of 2D-IQML could be seen as a Subchannel Response Matching (SRM) [79]. Note that, in a first iteration of 2D-IQML, we minimise:

$$\begin{aligned}\frac{1}{L}\sum_{l=1}^{L} \boldsymbol{f}^H \boldsymbol{\mathcal{X}}_l^H \boldsymbol{\mathcal{X}}_l \boldsymbol{f} &\simeq E_l\left\{\boldsymbol{f}^H \boldsymbol{\mathcal{X}}_l^H \boldsymbol{\mathcal{X}}_l \boldsymbol{f}\right\} \\ &= E_l\left\{\boldsymbol{f}^H \boldsymbol{\mathcal{G}}_l^H \boldsymbol{\mathcal{G}}_l \boldsymbol{f}\right\} + \sigma^2 \mathrm{tr}\left\{\boldsymbol{W}^H(\boldsymbol{f})\boldsymbol{W}(\boldsymbol{f})\right\}\end{aligned} \tag{4.27}$$

where $\boldsymbol{g}(l) = \boldsymbol{H}\boldsymbol{\gamma}(l)$ and $\boldsymbol{W}(\boldsymbol{f})\boldsymbol{g}(l) = \boldsymbol{\mathcal{G}}_l \boldsymbol{f}$, with $\boldsymbol{\mathcal{G}}_l$ being a matrix formed by elements of $\boldsymbol{g}(l)$. (4.27) tells us that a balanced $\boldsymbol{f}$ yields asymptotically unbiased and consistent estimates, whereas unbalanced $\boldsymbol{f}$ yield biased and inconsistent estimates. One should also note that different parameterisations of the noise subspace give different estimates of $\boldsymbol{f}$. This initialisation could be seen as a non-weighted version of 2D-IQML. Furthermore, it is easy to see that the optimal value of $\boldsymbol{f}$, denoted hereby $\boldsymbol{f}^o$, is the one that nulls $E_l\{\boldsymbol{f}^H \boldsymbol{\mathcal{G}}_l^H \boldsymbol{\mathcal{G}}_l \boldsymbol{f}\}$. Therefore, in a noiseless scenario, a first iteration of 2D-IQML gives the true value $\boldsymbol{f}^o$. In general, at sufficiently high SNR, 2D-IQML performs well; however, at low SNR, the 2D-IQML estimate is biased. Indeed, consider the asymptotic situation in which the number of subcarriers M grow to infinity. By the law of large numbers, the

2D-IQML criterion becomes essentially equivalent to its expected value, viz.

$$\begin{aligned}&\frac{1}{M}\boldsymbol{f}^H\boldsymbol{\mathcal{X}}_l^H\boldsymbol{\mathcal{R}}^\dagger\boldsymbol{\mathcal{X}}_l\boldsymbol{f}\\&=\mathrm{tr}\Big\{\boldsymbol{W}^H(\boldsymbol{f})\boldsymbol{\mathcal{R}}^\dagger\boldsymbol{W}(\boldsymbol{f})E\{\boldsymbol{x}(l)\boldsymbol{x}^H(l)\}\Big\}+\mathcal{O}(\frac{1}{\sqrt{M}})\\&=\frac{1}{M}\boldsymbol{f}^H\boldsymbol{\mathcal{G}}_l^H\boldsymbol{\mathcal{R}}^\dagger\boldsymbol{\mathcal{G}}_l\boldsymbol{f}+\frac{\sigma^2}{M}\mathrm{tr}\Big\{\boldsymbol{W}^H(\boldsymbol{f})\boldsymbol{\mathcal{R}}^\dagger\boldsymbol{W}(\boldsymbol{f})\Big\}+\mathcal{O}(\frac{1}{\sqrt{M}})\end{aligned}\tag{4.28}$$

where $\boldsymbol{\mathcal{R}}\triangleq\boldsymbol{\mathcal{R}}(\boldsymbol{f})=\boldsymbol{W}(\boldsymbol{f})\boldsymbol{W}^H(\boldsymbol{f})$.
Recall that the minimiser of $\boldsymbol{f}^H\boldsymbol{\mathcal{G}}_l^H\boldsymbol{\mathcal{R}}^\dagger\boldsymbol{\mathcal{G}}_l\boldsymbol{f}$ is $\boldsymbol{f}^o$. Therefore, at high SNR, the 2D-IQML estimate $\boldsymbol{f}$ differs from the optimal $\boldsymbol{f}^o$ by an asymptotically vanishing estimation error, because $\frac{\sigma^2}{M}\mathrm{tr}\{\boldsymbol{W}^H(\boldsymbol{f})\boldsymbol{\mathcal{R}}^\dagger\boldsymbol{W}(\boldsymbol{f})\}$ is negligible. However, this is not the case at low SNR, simply because $\boldsymbol{f}^o$ is not the minimiser of $\frac{\sigma^2}{M}\mathrm{tr}\{\boldsymbol{W}^H(\boldsymbol{f})\boldsymbol{\mathcal{R}}^\dagger\boldsymbol{W}(\boldsymbol{f})\}$, even if $\boldsymbol{\mathcal{R}}\triangleq\boldsymbol{\mathcal{R}}(\boldsymbol{f}^o)$. More explicitely,

$$\begin{aligned}&\min_{\boldsymbol{f}}\Big\{\mathrm{tr}\{\boldsymbol{W}^H(\boldsymbol{f})\boldsymbol{\mathcal{R}}(\boldsymbol{f}^o)^\dagger\boldsymbol{W}(\boldsymbol{f})\}\Big\}\\&<\mathrm{tr}\Big\{\boldsymbol{\mathcal{P}}_{\boldsymbol{W}^H(\boldsymbol{f}^o)}\Big\}=MN-q\end{aligned}\tag{4.29}$$

Finally, we can say from (4.29) that $\frac{\sigma^2}{M}\mathrm{tr}\Big\{\boldsymbol{W}^H(\boldsymbol{f})\boldsymbol{\mathcal{R}}^\dagger\boldsymbol{W}(\boldsymbol{f})\Big\}$ is minimised at $\boldsymbol{f}^1\neq\boldsymbol{f}^o$, so the 2D-IQML criteria is minimised at $\boldsymbol{f}^2\neq\boldsymbol{f}^o$. Hence, due to presence of noise, $\boldsymbol{f}^o$ is not asymptotically near a stationary point of the algorithm and 2D-IQML performs poorly for any initialisation.

We propose here a method to "denoise" the 2D-IQML criterion in a sense that it will correct the 2D-IQML bias and provide a consistent estimate of the vector $\boldsymbol{f}$.

4.2.3 2D-Denoised IQML (2D-DIQML)

Asymptotic Number of Subcarriers (Large M)

The asymptotic noise contribution to the DML criterion is $\sigma^2\mathrm{tr}\{\boldsymbol{\mathcal{P}}_{\boldsymbol{W}^H(\boldsymbol{f})}\}$ (see (4.28)). The denoising strategy consists of removing this asymptotic noise term, or more precisely, an estimate of it i.e. $\hat{\sigma}^2\mathrm{tr}\{\boldsymbol{\mathcal{P}}_{\boldsymbol{W}^H(\boldsymbol{f})}\}$ from the DML criterion, which becomes

$$\begin{aligned}&\min_{\boldsymbol{f}}\sum_{l=1}^{L}\Big\{\mathrm{tr}\Big\{\boldsymbol{\mathcal{P}}_{\boldsymbol{W}^H(\boldsymbol{f})}\big(\boldsymbol{x}(l)\boldsymbol{x}^H(l)-\hat{\sigma}^2\boldsymbol{I}_{MN}\big)\Big\}\Big\}\Leftrightarrow\\&\min_{\boldsymbol{f}}\sum_{l=1}^{L}\Big\{\boldsymbol{f}^H\boldsymbol{\mathcal{X}}_l^H\boldsymbol{\mathcal{R}}^\dagger(\boldsymbol{f})\boldsymbol{\mathcal{X}}_l\boldsymbol{f}-\hat{\sigma}^2\mathrm{tr}\Big\{\boldsymbol{W}^H(\boldsymbol{f})\boldsymbol{\mathcal{R}}^\dagger(\boldsymbol{f})\boldsymbol{W}(\boldsymbol{f})\Big\}\Big\}\end{aligned}\tag{4.30}$$

subject to (4.20a) and (4.20b).
Note that this operation does not change the optimizer of the DML criterion as $\hat{\sigma}^2 \mathrm{tr}\{\boldsymbol{\mathcal{P}}_{\boldsymbol{W}^H(\boldsymbol{f})}\} = \hat{\sigma}^2(MN-q)$ is constant with respect to $\boldsymbol{f}$. We take $\hat{\sigma}^2$ to be a consistent estimate of the noise variance. The denoised DML criterion is now solved in the 2D-IQML way, i.e.

$$\hat{\boldsymbol{f}}_{(n)} = \arg\min_{\boldsymbol{f}} \boldsymbol{f}^H \Big\{ \boldsymbol{\mathcal{Q}}_{(n-1)} - \hat{\sigma}^2 \mathcal{D} \Big\} \boldsymbol{f} \tag{4.31}$$

subject to (4.20a) and (4.20b).
The matrix $\mathcal{D}$ is such that $\boldsymbol{f}''^H \mathcal{D} \boldsymbol{f}' = \mathrm{tr}\{\boldsymbol{W}^H(\boldsymbol{f}'')\boldsymbol{\mathcal{R}}^\dagger(\boldsymbol{f})\boldsymbol{W}(\boldsymbol{f}')\}$. Asymptotically in the number of subcarriers, 2D-DIQML is globally convergent. Indeed, asymptotically it is essentially equivalent to the denoised criterion

$$\frac{1}{M} \boldsymbol{f}^H \Big\{ \boldsymbol{\mathcal{Q}}_{(n-1)} - \hat{\sigma}^2 \mathcal{D} \Big\} \boldsymbol{f} = \frac{1}{M} \boldsymbol{f}^H \boldsymbol{\mathcal{G}}_l^H \boldsymbol{\mathcal{R}}^\dagger \boldsymbol{\mathcal{G}}_l \boldsymbol{f} + \mathcal{O}(\frac{1}{\sqrt{M}}) \tag{4.32}$$

if $\sigma^2 - \hat{\sigma}^2 = \mathcal{O}(\frac{1}{\sqrt{M}})$. Notice, again, that the $\boldsymbol{f}^o$ minimises the first term on the right hand side of (4.32). Therefore, one iteration of 2D-DIQML yields an estimate of the form $\hat{\boldsymbol{f}} = \rho \boldsymbol{f}^o + \mathcal{O}(\frac{1}{\sqrt{M}})$, for some scaling factor ρ. So, *the 2D-DIQML algorithm behaves asymptotically at any SNR as the 2D-IQML algorithm behaves at high SNR.*

Finite Number of Subcarriers

The choice of $\hat{\sigma}^2$ turns out to be crucial. In practice, with large but finite number of subcarriers M, and the true noise variance, the central matrix $\boldsymbol{\mathcal{Q}} - \sigma^2 \mathcal{D}$ in (4.31) is indefinite, thus the minimisation problem is no longer well posed. Simulations show that the performance of 2D-DIQML in that case is very poor. The central matrix $\boldsymbol{\mathcal{Q}} - \hat{\sigma}^2 \mathcal{D}$ should be constrained to be positive semi-definite.

For the consistent estimate of σ^2, we choose here a certain λ that renders $\boldsymbol{\mathcal{Q}} - \lambda \mathcal{D}$ exactly positive semi-definite with one singularity. The 2D-DIQML criterion becomes

$$\hat{\boldsymbol{f}}_{(n)} = \arg\min_{\boldsymbol{f},\lambda} \boldsymbol{f}^H \Big\{ \boldsymbol{\mathcal{Q}}_{(n-1)} - \lambda \mathcal{D} \Big\} \boldsymbol{f} \tag{4.33}$$

subject to (4.20a), (4.20b), and $\boldsymbol{\mathcal{Q}}_{(n-1)} - \lambda \mathcal{D}$ being positive semi-definite.
The solution of λ is $\lambda = \lambda_{min}\Big(\boldsymbol{\mathcal{Q}}_{(n-1)}, \mathcal{D}\Big)$, the minimal generalised eigenvalue of $\boldsymbol{\mathcal{Q}}_{(n-1)}$ and $\mathcal{D}$. After solving for λ, we get $\boldsymbol{f}$ at iteration (n) as

$$\hat{\boldsymbol{f}}_{(n)} = \frac{(\beta' - \gamma')\boldsymbol{\mathcal{S}}_{(n-1)}^{-1} \boldsymbol{e}_1 + (\alpha' - \gamma'^*)\boldsymbol{\mathcal{S}}_{(n-1)}^{-1} \boldsymbol{J} \boldsymbol{e}_1}{\alpha'\beta' - |\gamma'|^2} \tag{4.34}$$

where

$$\boldsymbol{\mathcal{S}}_{(n-1)} = \boldsymbol{\mathcal{Q}}_{(n-1)} - \lambda \boldsymbol{\mathcal{D}} \tag{4.35a}$$

$$\alpha^{'} = \boldsymbol{e}_1^T \boldsymbol{\mathcal{S}}_{(n-1)}^{-1} \boldsymbol{e}_1 \tag{4.35b}$$

$$\beta^{'} = \boldsymbol{e}_1^T \boldsymbol{J} \boldsymbol{\mathcal{S}}_{(n-1)}^{-1} \boldsymbol{J} \boldsymbol{e}_1 \tag{4.35c}$$

$$\gamma^{'} = \boldsymbol{e}_1^T \boldsymbol{\mathcal{S}}_{(n-1)}^{-1} \boldsymbol{J} \boldsymbol{e}_1 \tag{4.35d}$$

Asymptotically, 2D-DIQML becomes

$$\begin{aligned} &\frac{1}{M} \boldsymbol{f}^H (\boldsymbol{\mathcal{X}}_l^H \boldsymbol{\mathcal{R}}^\dagger \boldsymbol{\mathcal{X}}_l - \lambda \boldsymbol{\mathcal{D}}) \boldsymbol{f} \\ &= \frac{1}{M} \boldsymbol{f}^H \boldsymbol{\mathcal{G}}_l^H \boldsymbol{\mathcal{R}}^\dagger \boldsymbol{\mathcal{G}}_l \boldsymbol{f} + \frac{1}{M} (\sigma^2 - \lambda) \boldsymbol{f}^H \boldsymbol{\mathcal{D}} \boldsymbol{f} + \mathcal{O}(\frac{1}{\sqrt{M}}) \end{aligned} \tag{4.36}$$

Notice that, first, optimisation with respect to λ subject to the non-negativity constraint would give $\lambda = \sigma^2 + \mathcal{O}(\frac{1}{\sqrt{M}})$, regardless of any initialisation of $\boldsymbol{f}$. Hence, λ asymptotically nulls the noise contribution, and the optimal value of $\boldsymbol{f}$ is $\boldsymbol{f}^o$. Therefore, global convergence applies for $\boldsymbol{f}$ (to $\boldsymbol{f}^o$) and λ (to σ^2). In other words, at high M, the minimiser of $\boldsymbol{f}$ is $\boldsymbol{f}^o$ and the minimiser of λ is σ^2.

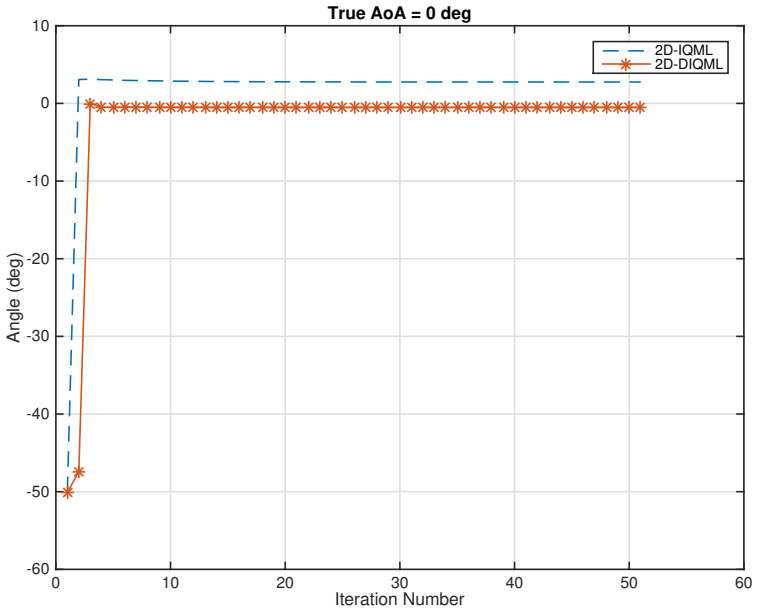

Figure 4.1: 2D-IQML vs. 2D-DIQML on AoA estimation of 1st Path, where true AoA = 0 deg at SNR = -5dB

We have observed that, indeed, *the 2D-DIQML algorithm behaves asymptotically at any SNR as the 2D-IQML algorithm behaves at high SNR*. To that extent, we fix the following simulation parameters:

- $M = 64$ (Large M) subcarriers and $N = 3$ antennas.

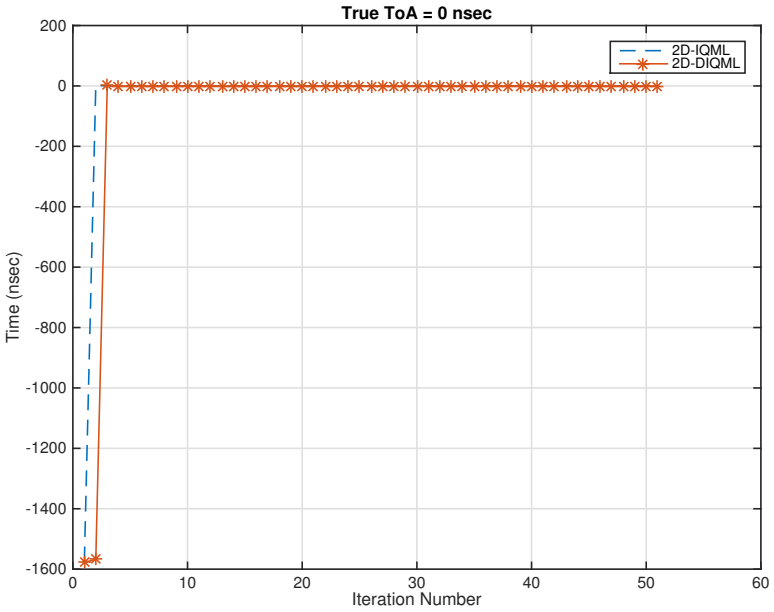

Figure 4.2: 2D-IQML vs. 2D-DIQML on ToA estimation of 1st Path, where true ToA = 0 nsec at SNR = -5dB

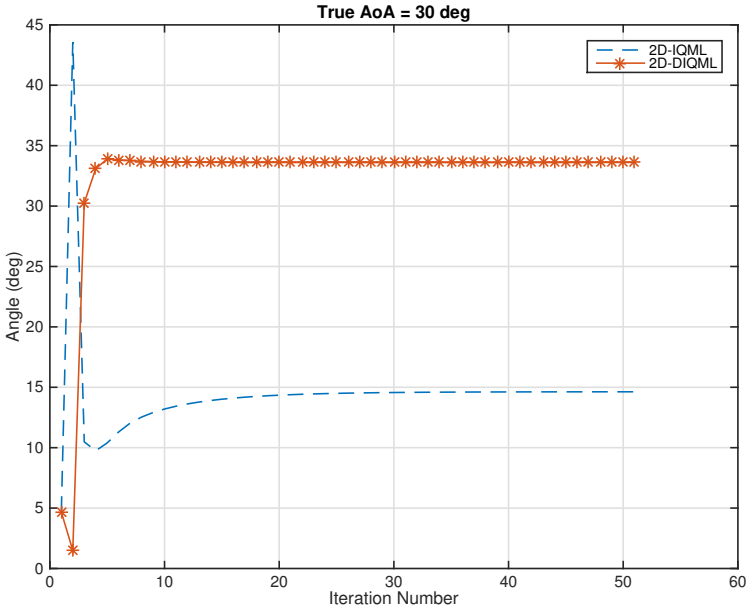

Figure 4.3: 2D-IQML vs. 2D-DIQML on AoA estimation of 2nd Path, where true AoA = 30 deg at SNR = -5dB

- $\triangle_f$= 0.3125MHz and $d = \frac{\lambda}{2}$
- $q = 2$ coherent paths with:
  1. AoAs: $\theta_1 = 0$ and $\theta_2 = 30$ degrees.
  2. ToAs: $\tau_1 = 0$ and $\tau_2 = 100$ nsecs.

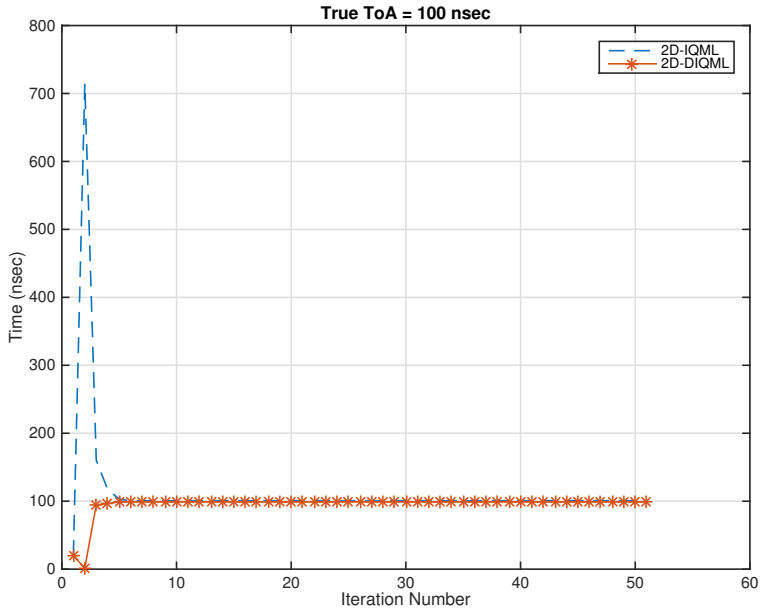

Figure 4.4: 2D-IQML vs. 2D-DIQML on ToA estimation of 2nd Path, where true ToA = 100 deg at SNR = -5dB

- $L = 10$ snapshots.
- $SNR = -5$ dB (Low SNR).

At high SNR, both algorithms perform equally the same, i.e. both give unbiased estimates of ToA/AoAs. Therefore, we have excluded this case from simulations. Nevertheless, it is of vast interest to see how both algorithms perform at low SNR and with a large number of subcarriers. As one can see, the estimated ToAs of both algorithms converge to the true ToA value (see Fig 4.2 and Fig 4.4). However, 2D-IQML AoA estimates are much more biased compared to 2D-DIQML AoA estimates. Indeed, as one could observe in Fig 4.1, the AoA of the first path which was set to be 0 degrees, was estimated to be 4 degrees by 2D-IQML and 0 degrees by 2D-DIQML. Also, by taking a look at Fig 4.3, the AoA of the second path which was set to be 30 degrees, was estimated to be 15 degrees by 2D-IQML and 33 degrees by 2D-DIQML. Finally, we can say that, at low SNR and high number of subcarriers, the 2D-IQML estimates are biased compared to the 2D-DIQML estimates.

4.3 Joint Angle and Delay Estimation by a single-snapshot: 2D Matrix Pencil Approach

In this section, and as the section title suggests, we shall use the single-snapshot model, i.e.

$$\boldsymbol{x} = \boldsymbol{H}\boldsymbol{\gamma} + \boldsymbol{n}$$

where

$$\boldsymbol{H} = \boldsymbol{C}_M \boxtimes \boldsymbol{A}_N \tag{4.37}$$

and all quantities are defined in the first section of this Chapter. In addition, we shall make the sizes of the matrices $\boldsymbol{A}$ and $\boldsymbol{C}$, as well as the sizes of their corresponding columns, explicit. In other words, matrices $(\boldsymbol{C}_K, \boldsymbol{A}_K) \in \mathbb{C}^{\mathrm{K}\times\mathrm{q}}$ where

$$\boldsymbol{C}_K = [\boldsymbol{c}_K(\tau_1) \dots \boldsymbol{c}_K(\tau_q)] \tag{4.38}$$

$$\boldsymbol{A}_K = [\boldsymbol{a}_K(\theta_1) \dots \boldsymbol{a}_K(\theta_q)] \tag{4.39}$$

4.3.1 ToA Estimation using 2D Matrix Pencil

Analytic Formulation

We start by forming a matrix from the data vector $\boldsymbol{x}$ given in equation (4.10). Let $\boldsymbol{X}$ be a $M_p \times K_M$ Hankel block matrix defined as follows

$$\boldsymbol{X} = \begin{pmatrix} \boldsymbol{X}_1 & \boldsymbol{X}_2 & \cdots & \boldsymbol{X}_{K_M} \\ \boldsymbol{X}_2 & \boldsymbol{X}_3 & \cdots & \boldsymbol{X}_{K_M+1} \\ \vdots & \vdots & \ddots & \vdots \\ \boldsymbol{X}_{M_p} & \boldsymbol{X}_{M_p+1} & \cdots & \boldsymbol{X}_M \end{pmatrix} \tag{4.40}$$

where $\boldsymbol{X}_i$ is an $N_p \times K_N$ Hankel matrix given by

$$\boldsymbol{X}_i = \begin{pmatrix} X_{i,1} & X_{i,2} & \cdots & X_{i,K_N} \\ X_{i,2} & X_{i,3} & \cdots & X_{i,K_N+1} \\ \vdots & \vdots & \ddots & \vdots \\ X_{i,N_p} & X_{i,N_p+1} & \cdots & X_{i,N} \end{pmatrix} \tag{4.41}$$

with

$$K_M = M - M_p + 1 \tag{4.42}$$

and

$$K_N = N - N_p + 1 \,. \tag{4.43}$$

The matrix $\boldsymbol{X}$ could be written as

$$\boldsymbol{X} = \boldsymbol{L}\boldsymbol{\Gamma}\boldsymbol{R}^{\mathrm{T}} + \boldsymbol{N} \tag{4.44}$$

where $\boldsymbol{N}$ is a noise matrix with appropriate dimension, and $\boldsymbol{L}$ is an $M_pN_p \times q$ matrix expressed as

$$\boldsymbol{L} = \begin{pmatrix} \boldsymbol{A}_{N_p} \\ \boldsymbol{A}_{N_p}\boldsymbol{D}_\tau \\ \vdots \\ \boldsymbol{A}_{N_p}\boldsymbol{D}_\tau^{M_p-1} \end{pmatrix} \tag{4.45}$$

and $\boldsymbol{R}$ is a $K_MK_N \times q$ matrix given by

$$\boldsymbol{R} = \begin{pmatrix} \boldsymbol{A}_{K_N} \\ \boldsymbol{A}_{K_N}\boldsymbol{D}_\tau \\ \vdots \\ \boldsymbol{A}_{K_N}\boldsymbol{D}_\tau^{K_M-1} \end{pmatrix} \tag{4.46}$$

The matrices $\boldsymbol{\Gamma}$ and $\boldsymbol{D}_\tau$ are $q \times q$ diagonal matrices as

$$\boldsymbol{\Gamma} = \mathrm{diag}\,[\gamma_1 \dots \gamma_q] \tag{4.47}$$

and

$$\boldsymbol{D}_\tau = \mathrm{diag}\,[z_{\tau_1} \dots z_{\tau_q}] \tag{4.48}$$

Let $\boldsymbol{X}_l$ and $\boldsymbol{X}_r$ be two $N_pM_p \times K_N(K_M-1)$ matrices defined as

$$\boldsymbol{X}_l = \boldsymbol{X}^{\langle :,1:K_N(K_M-1)\rangle} \tag{4.49a}$$

$$\boldsymbol{X}_r = \boldsymbol{X}^{\langle :,(K_N+1):K_NK_M\rangle} \tag{4.49b}$$

In a noiseless case, it is easy to see that

$$\boldsymbol{X}_l = \boldsymbol{L}\boldsymbol{\Gamma}\boldsymbol{R}_o^{\mathrm{T}} \tag{4.50a}$$

and

$$\boldsymbol{X}_r = \boldsymbol{L}\boldsymbol{\Gamma}\boldsymbol{D}_\tau\boldsymbol{R}_o^{\mathrm{T}} \tag{4.50b}$$

where

$$\boldsymbol{R}_o = \boldsymbol{R}^{\langle 1:K_N(K_M-1),:\rangle} \tag{4.50c}$$

Consider the following matrix pencil

$$\boldsymbol{X}_r - \lambda \boldsymbol{X}_l = \boldsymbol{L}\boldsymbol{\Gamma}\big(\boldsymbol{D}_\tau - \lambda \boldsymbol{I}_{\mathrm{q}}\big)\boldsymbol{R}_o \tag{4.51}$$

Provided that the two matrices $\boldsymbol{L}$ and $\boldsymbol{R}_o$ are full column rank, i.e. the rank of both matrices is q, then the rank of the matrix pencil $\boldsymbol{X}_r - \lambda \boldsymbol{X}_l$ drops to $q-1$ at $\lambda = z_{\tau_i}$ for all $i = 1 \dots q$.
It is proved in [50] that if the singular value decomposition of $\boldsymbol{X}_l$ is $\boldsymbol{X}_l = \boldsymbol{U}\boldsymbol{\Lambda}\boldsymbol{V}^{\mathrm{H}}$, then the q eigenvalues of the following matrix

$$\boldsymbol{T} = \bar{\boldsymbol{\Lambda}}^{-1}\bar{\boldsymbol{U}}^{\mathrm{H}}\boldsymbol{X}_r\bar{\boldsymbol{V}} \tag{4.52a}$$

where

$$\bar{\boldsymbol{U}} = \boldsymbol{U}^{\langle :,1:q \rangle} \tag{4.52b}$$

$$\bar{\boldsymbol{\Lambda}} = \boldsymbol{\Lambda}^{\langle 1:q,1:q \rangle} \tag{4.52c}$$

$$\bar{\boldsymbol{V}} = \boldsymbol{V}^{\langle :,1:q \rangle} \tag{4.52d}$$

are the values of λ that drop the rank of the matrix pencil $\boldsymbol{X}_r - \lambda \boldsymbol{X}_l$ to $q-1$. In other words, these q values of λ are called the generalised eigenvalues of the matrix pencil $(\boldsymbol{X}_r, \boldsymbol{X}_l)$. As a consequence, the q generalised eigenvalues of $(\boldsymbol{X}_r, \boldsymbol{X}_l)$ are estimates of $\{z_{\tau_i}\}_{i=1}^{q}$. We denote these estimates as $\{\hat{z}_{\tau_i}^{\mathrm{MP}}\}_{i=1}^{q}$.

Conditions for ToA Estimates using 2D Matrix Pencil

Recall that under the assumption that both matrices $\boldsymbol{L}$ and $\boldsymbol{R}_o$ are full column rank, the generalised eigenvalues of the matrix pencil $(\boldsymbol{X}_r, \boldsymbol{X}_l)$ are estimates of $\{z_{\tau_i}\}_{i=1}^{q}$. Before deriving the conditions, we define the following:

Definition: Let P and Q be two integers defined as follows:

- Let q^τ be the number of distinct ToAs, i.e. $\tau^1, \dots, \tau^{q^\tau}$; and let the following integers $P_1, \dots, P_{q^\tau}$ denote their corresponding multiplicity.
  Note that $\sum_{i=1}^{q^\tau} P_i = q$. The maximum number of paths arriving at the same time but with different angles of arrival is $\max_i P_i = P$.
- Similarly, let q^θ be the number of distinct AoAs, i.e. $\theta^1, \dots, \theta^{q^\theta}$; and let the following integers $Q_1, \dots, Q_{q^\theta}$ denote their corresponding multiplicity.
  Note that $\sum_{i=1}^{q^\theta} Q_i = q$. The maximum number of paths arriving at same AoAs but with different ToAs is $\max_i Q_i = Q$.

It is straightforward to see that $\boldsymbol{L}$ and $\boldsymbol{R}_o$ have same structure, but different dimensions, i.e.

$$\boldsymbol{L} = \boldsymbol{C}_{M_p} \boxtimes \boldsymbol{A}_{N_p} \tag{4.53}$$

$$\boldsymbol{R}_o = \boldsymbol{C}_{K_M-1} \boxtimes \boldsymbol{A}_{K_N} \tag{4.54}$$

Remark 4.2. Let $\boldsymbol{H} \in \mathbb{C}^{\mathrm{MN}\times q}$ be a matrix defined as $\boldsymbol{H} = \boldsymbol{C}_M \boxtimes \boldsymbol{A}_N$. The matrix $\boldsymbol{H}$ has full column rank if the following hold:

- *Condition 1*: $q \leq MN$
- *Condition 2*: $P \leq N$
- *Condition 3*: $Q \leq M$

Using the above remark, it is easy to see that both matrices $\boldsymbol{L}$ and $\boldsymbol{R}_o$ are full column rank under the following conditions:

- **B1.** $q \leq \min\{M_pN_p, K_N(K_M-1)\}$
- **B2.** $P \leq \min\{N_p, K_N\}$
- **B3.** $Q \leq \min\{M_p, K_M-1\}$

Therefore, if conditions **B1** till **B3** are satisfied, the ToAs could be estimated through the 2D Matrix Pencil technique described herein.

4.3.2 AoA Estimation using 2D Matrix Pencil

Analytic Formulation

Let $\boldsymbol{Y}$ be a shuffled version of matrix $\boldsymbol{X}$, viz.

$$\boldsymbol{Y} = \boldsymbol{X}\boldsymbol{P} \tag{4.55}$$

where $\boldsymbol{P}$ is a $K_MK_N \times K_MK_N$ permutation matrix defined as follows

$$\boldsymbol{P}^{\mathrm{T}} = \begin{bmatrix} \boldsymbol{E}_1 \\ \boldsymbol{E}_2 \\ \vdots \\ \boldsymbol{E}_{K_N} \end{bmatrix} \tag{4.56a}$$

where

$$\boldsymbol{E}_k = \begin{bmatrix} \boldsymbol{e}_k^T \\ \boldsymbol{e}_{k+K_N}^T \\ \vdots \\ \boldsymbol{e}_{k+K_N(K_M-1)}^T \end{bmatrix} \tag{4.56b}$$

where $\boldsymbol{e}_k$ is the k^{th} column of the identity matrix $\boldsymbol{I}_{K_M K_N}$. Now, as done in equation (4.49), form $\boldsymbol{Y}_l$ and $\boldsymbol{Y}_r$ by

$$\boldsymbol{Y}_l = \boldsymbol{Y}^{\langle :, 1:K_M(K_N-1)\rangle} \tag{4.57a}$$

$$\boldsymbol{Y}_r = \boldsymbol{Y}^{\langle :, (K_M+1):K_N K_M\rangle} \tag{4.57b}$$

Using the same methodology as in equations (4.50), (4.51), and (4.52), one could obtain estimates of the AoAs, i.e. $\{\hat{z}_{\theta_i}^{\mathrm{MP}}\}_{i=1}^{q}$. The conditions for proper estimation of AoAs using the 2D Matrix Pencil technique just described are similar to those in Section 4.3.1 and are given in the following subsection.

Conditions for AoA Estimates using 2D Matrix Pencil

The conditions for AoA estimation using 2D Matrix Pencil are the following:

- **C1**. $q \leq \min\{M_p N_p, K_M(K_N - 1)\}$
- **C2**. $P \leq \min\{N_p, K_N - 1\}$
- **C3**. $Q \leq \min\{M_p, K_M\}$

4.3.3 Proposed Algorithms

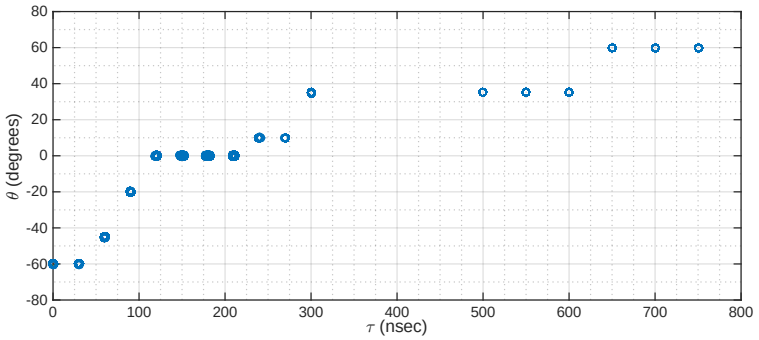

Figure 4.5: Scatter plot of experiment 1 at SNR = 30 dB.

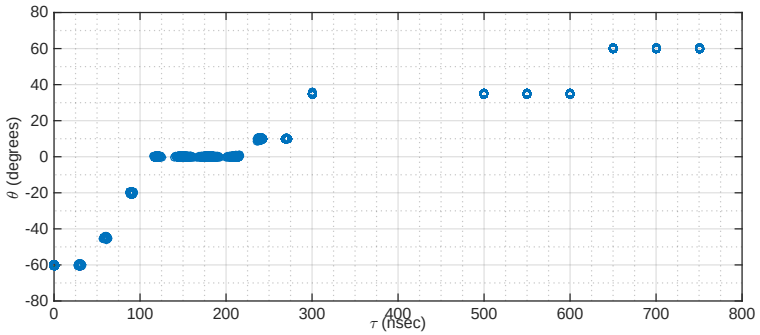

Figure 4.6: Scatter plot of experiment 2 at SNR = 20 dB.

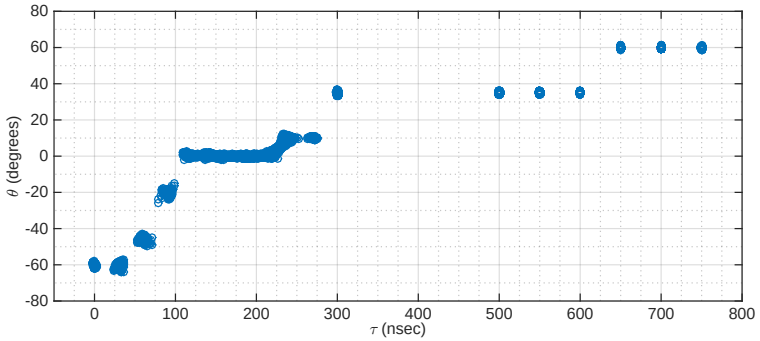

Figure 4.7: Scatter plot of experiment 3 at SNR = 10 dB.

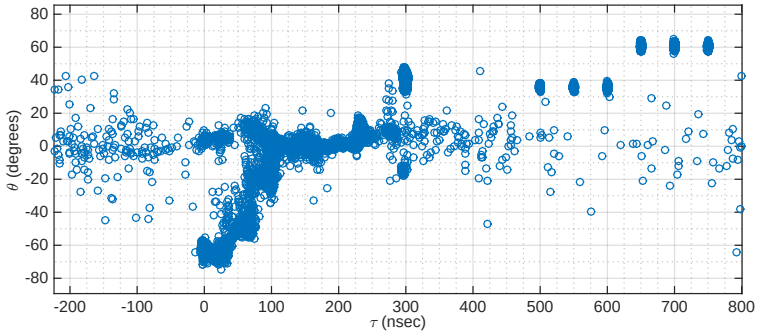

Figure 4.8: Scatter plot of experiment 4 at SNR = 0 dB.

In this section, we present two algorithms that allow joint estimation of the times and angles of arrival. The first algorithm is intended for systems where the number of subcarriers M is much larger than the number of antennas N, i.e. $M \gg N$. This is a reasonable assumption since most Wi-Fi technologies are equipped with 3 up to 8 antennas. Moreover, the number of subcarriers used in a Wi-Fi OFDM symbol varies between 64 and 512. Furthermore, the second algorithm could be used for any configuration, i.e. for any M and N. In addition, conditions for the two algorithms are provided.

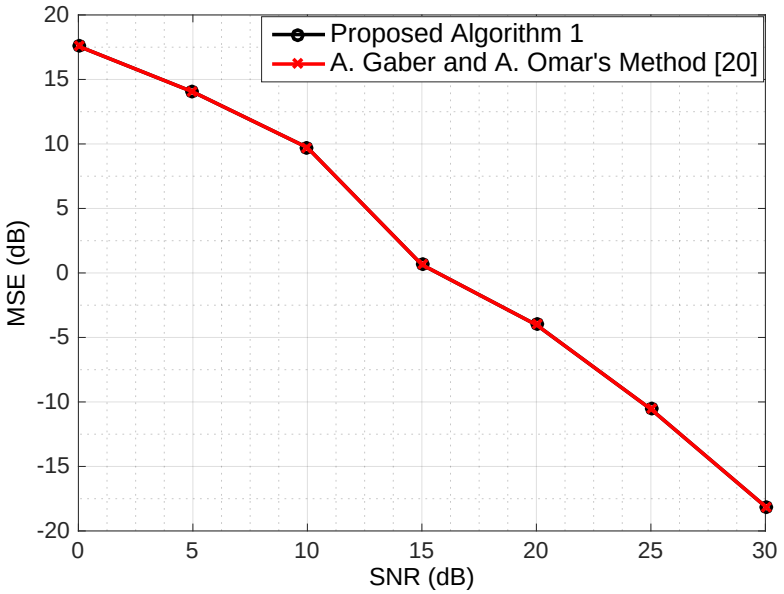

Figure 4.9: MSE of ToAs vs. SNR of experiment 5.

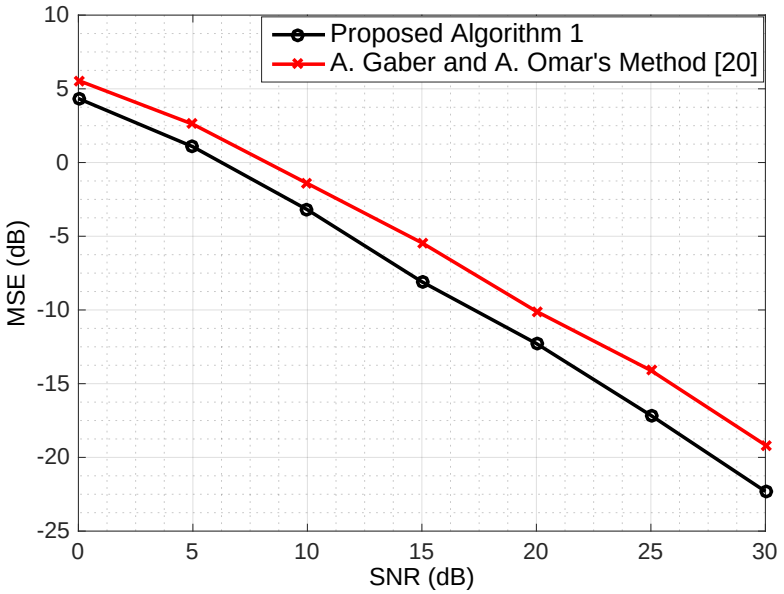

Figure 4.10: MSE of AoAs vs. SNR of experiment 5.

Algorithm 1: ($M \gg N$)

Note that the parameters K_M and K_N (or equivalently M_p and N_p) are free in a noiseless case. However, in a noisy scenario, those parameters should be properly selected. For more details, the reader is referred to [50]. In any case, the parameters K_M and K_N parameters are jointly tuned so that conditions **B1** till **B3** (or **C1** till **C3**) are met, if the purpose is to estimate the ToAs (or AoAs) using 2D Matrix Pencil. If $M \gg N$, one could show that there exist integers K_M and K_N (or equivalently M_p and N_p) where conditions **B1** till **B3** are *less restrictive* than conditions **C1** till **C3**. In other words, if

$M \gg N$, the 2D Matrix Pencil described herein allows estimation of more ToAs than AoAs. Therefore, we propose the following algorithm:

- *Step 1:* Given $\boldsymbol{x}$ and q, form $\boldsymbol{X}$ using equations (4.40) and (4.41).

- *Step 2:* Obtain $\{\hat{z}_{\tau_i}^{\mathrm{MP}}\}_{i=1}^{q}$ using equations (4.49) till (4.52).

- *Step 3:* Estimate the ToAs of the q paths by the following relation:

$$\hat{\tau}_i^{\mathrm{MP}} = -\frac{\mathrm{ang}\{\hat{z}_{\tau_i}^{\mathrm{MP}}\}}{2\pi\ \triangle_f} \tag{4.58}$$

- *Step 4:* Form an $N \times M$ matrix $\boldsymbol{Z}$ by using entries of the snapshot vector $\boldsymbol{x}$ as follows:

$$\boldsymbol{Z} = \begin{pmatrix} X_{1,1} & X_{2,1} & \cdots & X_{M,1} \\ X_{1,2} & X_{2,2} & \cdots & X_{M,2} \\ \vdots & \vdots & \ddots & \vdots \\ X_{1,N} & X_{2,N} & \cdots & X_{M,N} \end{pmatrix} \tag{4.59}$$

Note that $\boldsymbol{Z}$ is written as:

$$\boldsymbol{Z} = \boldsymbol{A}_{\mathrm{N}}\boldsymbol{\Gamma}\boldsymbol{C}_{\mathrm{M}}^{\mathrm{T}} + \boldsymbol{W} \tag{4.60}$$

where $\boldsymbol{W}$ is the noise part. This step comprises in estimating the term $\boldsymbol{G} = \boldsymbol{A}_{\mathrm{N}}\boldsymbol{\Gamma}$ using Least Squares (LS), i.e:

$$\hat{\boldsymbol{G}} = \arg\min_{\boldsymbol{G}} \|\boldsymbol{Z} - \boldsymbol{G}\boldsymbol{C}_{\mathrm{M}}^{\mathrm{T}}\|^2 \tag{4.61}$$

The solution of (4.61) is:

$$\hat{\boldsymbol{G}} = \boldsymbol{Z}\boldsymbol{C}_{\mathrm{M}}^{\dagger} \tag{4.62}$$

where $\boldsymbol{C}_{\mathrm{M}}^{\dagger}$ is the Moore–Penrose pseudoinverse of $\boldsymbol{C}_{\mathrm{M}}^{\mathrm{T}}$ and is given by

$$\boldsymbol{C}_{\mathrm{M}}^{\dagger} = \boldsymbol{C}_{\mathrm{M}}^{*}\left(\boldsymbol{C}_{\mathrm{M}}^{\mathrm{T}}\boldsymbol{C}_{\mathrm{M}}^{*}\right)^{-1} \tag{4.63}$$

Note that $\boldsymbol{C}_{\mathrm{M}}^{\dagger}$ exists if and only if $q \leq M$ and all ToAs are distinct, i.e. $P = 1$. Finally, we use the 2D Matrix Pencil estimates of the ToAs obtained in *Step 3* to compute $\boldsymbol{C}_{\mathrm{M}}^{\mathrm{T}}$ in order to obtain the estimate of $\boldsymbol{G}$ using equation (4.63) then (4.62). In other words, $\boldsymbol{C}_{\mathrm{M}}$ is obtained as

$$\boldsymbol{C}_M = [\boldsymbol{c}_M(\hat{\tau}_1^{\mathrm{MP}}) \ldots \boldsymbol{c}_M(\hat{\tau}_q^{\mathrm{MP}})] \tag{4.64}$$

- *Step 5:* Using $\hat{\boldsymbol{G}}$ from *Step 4*, we solve the following optimisation problem:

$$\begin{aligned}\hat{\boldsymbol{A}}_{\mathrm{N}} &= \arg\min_{\boldsymbol{A}_{\mathrm{N}}} \|\hat{\boldsymbol{G}} - \boldsymbol{A}_{\mathrm{N}}\boldsymbol{\Gamma}\|^2 \\ &= \sum_{i=1}^{q} \arg\min_{\boldsymbol{a}_{\mathrm{N}}(\theta_i)} \|\hat{\boldsymbol{G}}^{\langle :,i\rangle} - \gamma_i \boldsymbol{a}_{\mathrm{N}}(\theta_i)\|^2\end{aligned} \tag{4.65}$$

  Note that the problem is decoupled in terms of $\boldsymbol{a}_{\mathrm{N}}(\theta_i)$ due to the diagonal structure of $\boldsymbol{\Gamma}$. The solution of the problem under a norm constraint, e.g. $\|\boldsymbol{a}_{\mathrm{N}}(\theta_i)\|^2 = N$ for $i = 1 \dots q$, is

$$\hat{\boldsymbol{a}}_{\mathrm{N}}(\theta_i) = \frac{\hat{\boldsymbol{G}}^{\langle :,i\rangle}}{\|\hat{\boldsymbol{G}}^{\langle :,i\rangle}\|} \tag{4.66}$$

- *Step 6:* In the last step, we estimate the AoAs by using an LS fit, i.e.

$$\hat{\boldsymbol{e}}_i = \arg\min_{\boldsymbol{e}_i} \|\mathrm{ang}\{\hat{\boldsymbol{a}}_{\mathrm{N}}(\theta_i)\} - \boldsymbol{T}\boldsymbol{e}_i\|^2, \quad i = 1 \dots q \tag{4.67}$$

  where $\boldsymbol{T} \in \mathbb{C}^{\mathrm{N}\times 2}$ and is given by

$$\boldsymbol{T} = \begin{pmatrix} 0 & 1 \\ 1 & 1 \\ \vdots & \vdots \\ N-1 & 1 \end{pmatrix} \tag{4.68}$$

  and the solution is $\hat{\boldsymbol{e}}_i = [e_{i,1}, e_{i,2}]^{\mathrm{T}} = \boldsymbol{T}^{\dagger}\mathrm{ang}\{\hat{\boldsymbol{a}}_{\mathrm{N}}(\theta_i)\}$ with $\boldsymbol{T}^{\dagger} = (\boldsymbol{T}^{\mathrm{T}}\boldsymbol{T})^{-1}\boldsymbol{T}^{\mathrm{T}}$ and finally θ_i is estimated as follows

$$\hat{\theta}_i = -\sin^{-1}\Big(\frac{e_{i,1}\lambda}{2\pi d}\Big), \qquad i = 1 \dots q \tag{4.69}$$

  Note that the angles in equation (4.67) should be carefully dealt with, i.e. those angles should be within the range $[0, 2\pi]$. In MATLAB, the unwrap command is able to maintain the angles in this range. In short, Algorithm 1 is useful when $M \gg N$. Note that only the ToAs were estimated using the 2D Matrix Pencil technique in *Step 2*. Therefore, the conditions for Algorithm 1 are **B1** till **B3**, in addition to the condition of existance of a pseudoinverse of $\boldsymbol{C}_{\mathrm{M}}$ in *Step 4*. Combining all those conditions, we get the following:

  - **D1**. $q \leq \min\{M_p N_p, K_N(K_M - 1), M\}$
  - **D2**. $P = 1$
  - **D3**. $Q \leq \min\{M_p, K_M - 1\}$

Algorithm 2

In this algorithm, both ToAs and AoAs are estimated using the 2D-Matrix Pencil technique, i.e.

- *Step 1* till *Step 3* are similar to Algorithm 1.

- *Step 4:* Form $\boldsymbol{Y} = \boldsymbol{X}\boldsymbol{P}$ where $\boldsymbol{P}$ is given in equation (4.56).

- *Step 5:* Obtain $\{\hat{z}_{\theta_i}^{\mathrm{MP}}\}_{i=1}^{q}$ using equations (4.57) and (4.52).

- *Step 6:* Estimate the AoAs of the q paths by the following relation:

$$\hat{\theta}_i^{\mathrm{MP}} = -\sin^{-1}\Big(\frac{\mathrm{ang}\{\hat{z}_{\theta_i}^{\mathrm{MP}}\}\lambda}{2\pi d}\Big) \tag{4.70}$$

  Note that the ToAs and AoAs are estimated but are not matched; unlike Algorithm 1, where the matching happens naturally in *Step 5*. In other words, $\hat{\tau}_k^{\mathrm{MP}}$ and $\hat{\theta}_k^{\mathrm{MP}}$ are not necessarily the ToA and AoA of the k^{th} multipath. Therefore, a matching step is required to pair $\{\hat{\tau}_i^{\mathrm{MP}}\}_{i=1}^{q}$ with $\{\hat{\theta}_i^{\mathrm{MP}}\}_{i=1}^{q}$. Fixing the position of $\hat{\tau}_k^{\mathrm{MP}}$ at position k, there are $q!$ possible permutations of $\{\hat{\theta}_i^{\mathrm{MP}}\}_{i=1}^{q}$.

- *Step 7:* The matching criterion is based on evaluating the Maximum Likelihood (ML) cost function for joint angles and times of arrival estimation (see [107] for the JADE ML cost function) by fixing the positions of $\{\hat{\tau}_i^{\mathrm{MP}}\}_{i=1}^{q}$ and permuting $\{\hat{\theta}_i^{\mathrm{MP}}\}_{i=1}^{q}$ as done in the table **SubAlgorithm 1**.

  Since the ToAs and AoAs are both estimated using 2D Matrix Pencil, Algorithm 2 needs conditions **B1** till **B3** and **C1** till **C3**, and therefore

  - **E1**. $q \leq \min\{M_p N_p, K_N(K_M - 1), K_M(K_N - 1)\}$
  - **E2**. $P \leq \min\{N_p, K_N - 1\}$
  - **E3**. $Q \leq \min\{M_p, K_M - 1\}$

This section demonstrates the performance of Algorithm 1 as a function of SNR. The performance of Algorithm 2 was not provided due to lack of space.

In the first four experiments, the array was ULA with $N = 3$ antennas spaced half a wavelength apart. The transmitted OFDM symbol occupies 40 MHz of bandwidth, and uses $M = 64$ subcarriers with uniform spacing $\triangle_f$= 0.625 MHz. The 2D Matrix

Table 3: Step 7 of Algorithm 2

INITIALISATION:
$\boldsymbol{C}_M = [\boldsymbol{c}_M(\hat{\tau}_1^{\mathrm{MP}}) \dots \boldsymbol{c}_M(\hat{\tau}_q^{\mathrm{MP}})]$
$\boldsymbol{A}_N = [\boldsymbol{a}_N(\hat{\theta}_1^{\mathrm{MP}}) \dots \boldsymbol{a}_N(\hat{\theta}_q^{\mathrm{MP}})]$
$\boldsymbol{\Upsilon_1} = \boldsymbol{I}_{\mathrm{q}}$
MAIN LOOP:
for $l = 1$ *to* $q!$ **do**
Step 7.1: $\boldsymbol{H} = \boldsymbol{C}_M \boxtimes (\boldsymbol{A}_N \boldsymbol{\Upsilon}_l)$
Step 7.2: $\boldsymbol{\mathscr{P}_H} = \boldsymbol{I}_{\mathrm{MN}} - \boldsymbol{H}(\boldsymbol{H}^{\mathrm{H}}\boldsymbol{H})^{-1}\boldsymbol{H}^{\mathrm{H}}$
Step 7.3: $\boldsymbol{b}(l) = \left\|\boldsymbol{\mathscr{P}_H}\boldsymbol{x}\right\|^2$
Step 7.4: Choose another permutation matrix $\boldsymbol{\Upsilon}_{l+1}$
FIND BEST MATCH:
Step 7.5: Find $\hat{k} = \arg\max_k \boldsymbol{b}(k)$. This means that all columns of $\boldsymbol{C}_{\mathrm{M}}$ are matched to columns of $\boldsymbol{A}_N \boldsymbol{\Upsilon}_{\hat{k}}$ according to the ML criterion in *Step 7.3*.

Pencil parameters were $M_p = 30$ and $N_p = 2$. The number of multipath components were set to $q = 17$ paths. The ToAs and AoAs of each path are given as follows: The first 11 paths arrive with delays $\{\tau_k = 30(k-1)\ \text{nsec}\}_{k=1}^{11}$ with corresponding AoAs as $\{\theta_k = -60°\}_{k=1}^{2}$, $\theta_3 = -45°$, $\theta_4 = -20°$, $\{\theta_k = 0°\}_{k=5}^{8}$, $\{\theta_k = 10°\}_{k=9}^{10}$, and $\theta_{11} = 35°$. The 6 other paths arrive with delays $\{\tau_k = 500{+}50(k{-}12)\ \text{nsec}\}_{k=12}^{17}$ with corresponding AoAs as $\{\theta_k = 35°\}_{k=12}^{14}$ and $\{\theta_k = 60°\}_{k=15}^{17}$. Moreover, the multipath coefficients $\boldsymbol{\gamma}$ are randomly chosen. For each experiment, a different SNR was set and a scatter plot was depicted using 1000 Monte-Carlo simulations. Each Monte-Carlo simulation plots the ToA and AoA estimates using only one snapshot $\boldsymbol{x}$.

Note that the maximum number of paths arriving at the same time but with different AoAs is $P = 1$, and the maximum number of paths arriving with same AoAs but at different times is $Q = 4$. Moreover, one could easily verify that conditions **D1** till **D3** are satisfied and hence Algorithm 1 is applicable.

In the first experiment, i.e. Figure 4.5, the SNR was set to 30 dB, and we observe almost perfect estimation of all ToAs and AoAs since the variations of the estimates from their true values is negligible. The SNR was 20 dB in the second experiment (Figure 4.6) and we observe almost the same phenomena as the first experiment except for paths 5 till 8 where their AoAs were properly estimated but their ToAs tend to overlap. In the third experiment (Figure 4.7) where the SNR = 10 dB , paths 5 till 10 overlap and ToA/AoA estimates of all paths start to show more deviation from their true values. Finally, in the last experiment (Figure 4.8), the SNR was set to 0 dB and we could observe a clear degradation of the performance of Algorithm 1.

In the last experiment, i.e. experiment 5, we plot two Mean-Squared-Error (MSE) curves, one corresponding to the MSE of the Times-of-Arrival (Figure 4.9) and the other corresponding to the MSE of the Angles-of-Arrival (Figure 4.10). We compare with the first algorithm proposed by A. Gaber and A. Omar in Section III, [80]. The simulation parameters are the same as those in the first four experiments except for q which is now set to 3 sources. In addition, the ToAs are selected as follows: $\tau_1 = 0$ nsec, $\tau_2 = 25$ nsec, and $\tau_3 = 75$ nsec. Furthermore, the corresponding AoAs are chosen to be: $\theta_1 = 0°$, $\theta_2 = 5°$, and $\theta_3 = 10°$. As expected, the MSE of the estimated ToAs using Algorithm 1 and the method in [80] is the same (See Figure 4.9) since *Steps 1* till 3 are similar in both algorithms, and therefore the ToA estimates are the same. However, the estimated AoAs are different, since both algorithms are essentially different. In particular, our proposed Algorithm 1 doesn't require ToA/AoA pairing, since this is automatically done in *Step 6*. Whereas, the method in [80] requires a matching criterion. This may explain why the proposed Algorithm 1 exhibits a lower MSE in AoAs than the one in [80] (See Figure 4.10).

4.4 Spatio-Frequential smoothing: A Remedy for coherent sources

4.4.1 The JADE-MUSIC Algorithm: A Recap

The spatio-frequential covariance matrix is given by

$$\boldsymbol{R}_{xx} = E\{\boldsymbol{x}(l)\boldsymbol{x}^H(l)\} = \boldsymbol{H}\boldsymbol{R}_{\gamma\gamma}\boldsymbol{H}^H + \sigma^2\boldsymbol{I}_{MN} \tag{4.71}$$

where $\boldsymbol{R}_{\gamma\gamma}$ is the covariance matrix of $\boldsymbol{\gamma}(l)$. The matrix given in (4.71) is, usually, estimated through a sample average over snapshots, and is known as the sample covariance matrix, i.e.

$$\boldsymbol{R}_{xx} \simeq \frac{1}{L}\sum_{l=1}^{L}\boldsymbol{x}(l)\boldsymbol{x}^H(l) \tag{4.72}$$

In what follows, $\boldsymbol{R}_{xx}$ will be referred to as the sample covariance matrix, and not the true one. We denote $\lambda_1 > \lambda_2 > \ldots > \lambda_{MN}$ the eigenvalues of $\boldsymbol{R}_{xx}$. Their corresponding eigenvectors are named $\boldsymbol{u}_1, \boldsymbol{u}_2, \ldots, \boldsymbol{u}_{MN}$. The sample covariance matrix in (4.72) is an input to most subspace algorithms for estimating the signal parameters, i.e. AoAs $\{\theta_1 \ldots \theta_q\}$ and ToAs $\{\tau_1 \ldots \tau_q\}$. One of these algorithms is the JADE-MUSIC algorithm, which is a 2-D version of MUSIC. This algorithm is summarised as follows:

(1) Apply an eigenvalue decomposition of $\boldsymbol{R}_{xx}$.

(2) Form the noise subspace matrix, i.e. $\boldsymbol{U}_n = [\boldsymbol{u}_{q+1} \dots \boldsymbol{u}_{MN}]$.
(3) Search for $\{\hat{\theta}_i, \hat{\tau}_i\}_{i=1}^{q}$ by

$$\{(\widehat{\theta}_i, \widehat{\tau}_i)\}_{i=1}^{q} = \arg\max_{\theta,\tau}\{\frac{1}{\|\boldsymbol{U}_n^H[\boldsymbol{a}(\theta) \otimes \boldsymbol{c}(\tau)]\|_F^2}\} \tag{4.73}$$

The MUSIC algorithm is one of many subspace techniques, i.e. the extraction of a signal or noise subspace is required for further processing. Subspace techniques assume that the matrix $\boldsymbol{R}_{\gamma\gamma}$ is full rank, otherwise the estimated subspaces do not reflect the true ones (See [81] for a mathematical argument). Furthermore, rank deficiency of $\boldsymbol{R}_{\gamma\gamma}$ is due to coherence of multiple signals, or to insufficient number of snapshots, i.e. $L < q$. The spatial smoothing pre-processing technique is known to "decorrelate" the sources, and therefore attain full rank of the matrix $\boldsymbol{R}_{\gamma\gamma}$.
In the following section, we present a 2D version of smoothing, i.e. *spatio-frequential* smoothing, and we show its advantage over conventional *spatial* or *frequential* smoothing techniques.

4.4.2 The Spatio-Frequential Preprocessing Technique

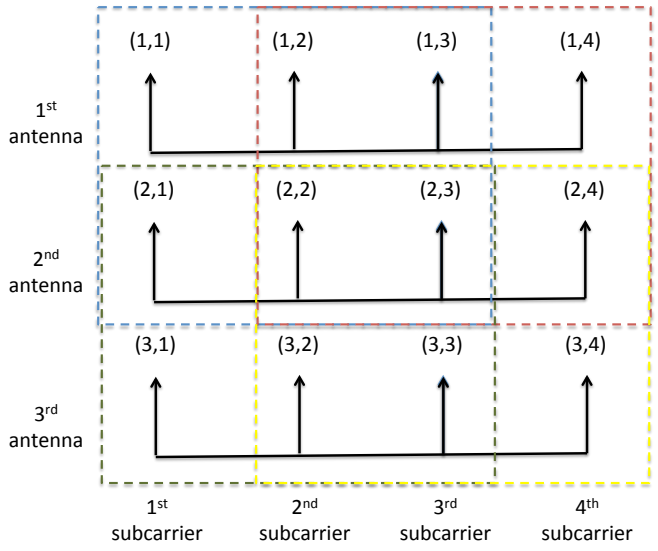

Figure 4.11: A spatio-frequential array of $N = 3$ antennas and $M = 4$ subcarriers partitioned into $N_p = 2$ and $M_p = 3$, hence a total of $K_M K_N = 4$ subarrays.

Recall that equation (4.5) gives the information on all subcarriers at all antennas. We shall use the notation (n, m) to index the m^{th} subcarrier and n^{th} antenna. Let the spatio-frequential array $\{(i, j)\}_{i=1\dots N}^{j=1\dots M}$ of size MN be divided into overlapping subarrays of size M_pN_p (M_p and N_p being the number of subcarriers and antennas in the subarrays,

respectively). Indeed, one could check that the total number of overlapping subarrays is equal to $K_M K_N$, where $K_M = M - M_p + 1$ and $K_N = N - N_p + 1$.

To visualise how the subarrays are formed, we refer the reader to Fig 4.11, where a setting of $N = 3$ antennas and $M = 4$ subcarriers is partitioned into overlapping subarrays of sizes $N_p = 2$ and $M_p = 3$, and therefore a total of $K_M K_N = 4$ subarrays.

Since the effective number of subcarriers and antennas used now are M_p and N_p, respectively, then (4.5) becomes

$$\boldsymbol{x}_{m,n}(l) = \bar{\boldsymbol{H}} \boldsymbol{D}_\tau^{m-1} \boldsymbol{D}_\theta^{n-1} \boldsymbol{\gamma}(l) + \boldsymbol{n}_{m,n}(l) \tag{4.74}$$

where

$$\bar{\boldsymbol{H}} = \begin{bmatrix} \boldsymbol{a}_{N_p}(\theta_1) \otimes \boldsymbol{c}_{M_p}(\tau_1) & \vert & \dots & \vert & \boldsymbol{a}_{N_p}(\theta_q) \otimes \boldsymbol{c}_{M_p}(\tau_q) \end{bmatrix} \tag{4.75}$$

Matrices $\boldsymbol{D}_\tau^{m-1}$ and $\boldsymbol{D}_\theta^{n-1}$ are the $(m-1)^{th}$ and $(n-1)^{th}$ power of the diagonal $q \times q$ matrices $\boldsymbol{D}_\tau$ and $\boldsymbol{D}_\theta$, given by

$$\boldsymbol{D}_\tau = \text{diag}\ \{c_2(\tau_1) \dots c_2(\tau_q)\} \tag{4.76a}$$

$$\boldsymbol{D}_\theta = \text{diag}\ \{a_2(\theta_1) \dots a_2(\theta_q)\} \tag{4.76b}$$

This means that $\boldsymbol{x}_{m,n}(l)$ is an $M_p N_p \times 1$ received vector on the subarray $\{(i,j)\}_{j=n \dots N_p+n-1}^{i=m \dots M_p+m-1}$. The covariance matrix of $\boldsymbol{x}_{m,n}(l)$ in (4.74) after averaging over time snapshots is given as

$$\boldsymbol{R}_{m,n} = \bar{\boldsymbol{H}} \boldsymbol{D}_\tau^{m-1} \boldsymbol{D}_\theta^{n-1} \boldsymbol{R}_{\gamma\gamma} \boldsymbol{D}_\theta^{H^{n-1}} \boldsymbol{D}_\tau^{H^{m-1}} \bar{\boldsymbol{H}}^H + \sigma^2 \boldsymbol{I}_{M_p N_p} \tag{4.77}$$

The *spatio-frequential smoothed covariance* matrix is given by

$$\bar{\boldsymbol{R}} = \frac{1}{K_M K_N} \sum_{m=1}^{K_M} \sum_{n=1}^{K_N} \boldsymbol{R}_{m,n} \tag{4.78}$$

$\bar{\boldsymbol{R}}$ could also be written as

$$\bar{\boldsymbol{R}} = \bar{\boldsymbol{H}} \bar{\boldsymbol{R}}_{\gamma\gamma} \bar{\boldsymbol{H}}^H + \sigma^2 \boldsymbol{I}_{M_p N_p} \tag{4.79}$$

where

$$\bar{\boldsymbol{R}}_{\gamma\gamma} = \frac{1}{K_M K_N} \sum_{m=1}^{K_M} \sum_{n=1}^{K_N} \boldsymbol{D}_\tau^{m-1} \boldsymbol{D}_\theta^{n-1} \boldsymbol{R}_{\gamma\gamma} \boldsymbol{D}_\theta^{H^{n-1}} \boldsymbol{D}_\tau^{H^{m-1}} \tag{4.80}$$

In a single carrier case, i.e. $M = M_p = 1$, it has been proven that the spatial smoothing technique ensures full rank of $\bar{\boldsymbol{R}}_{\gamma\gamma}$ [81], given that $q \leq K_N$.

Analogously, in the single antenna but multi-carrier case, i.e. $N = N_p = 1$, the same technique has been applied in [82] and was referred to as frequency smoothing, in order to acheive full rank of $\bar{\boldsymbol{R}}_{\gamma\gamma}$, when $q \leq K_M$. However, in the general multi-antenna and multi-carrier case, we have the following:

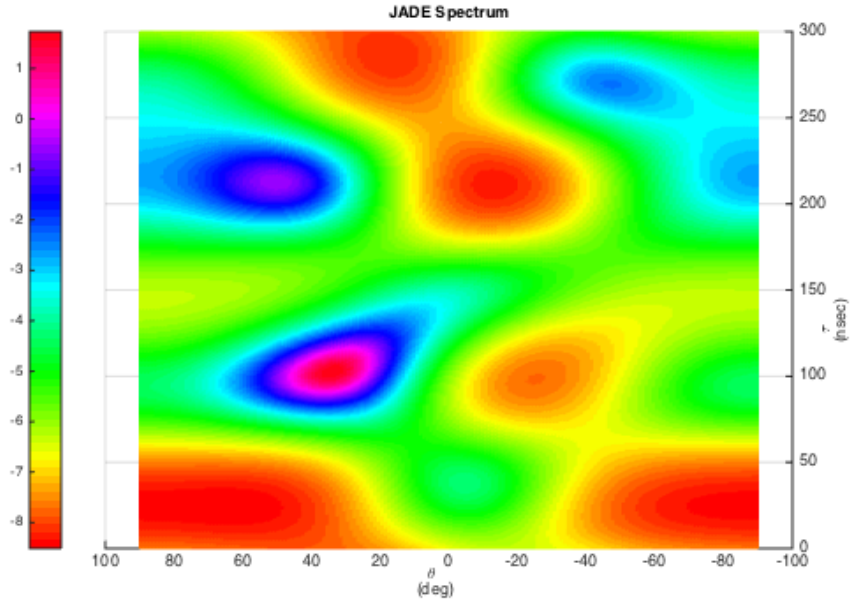

Figure 4.12: Spatial Smoothing with $N_p = 2$.

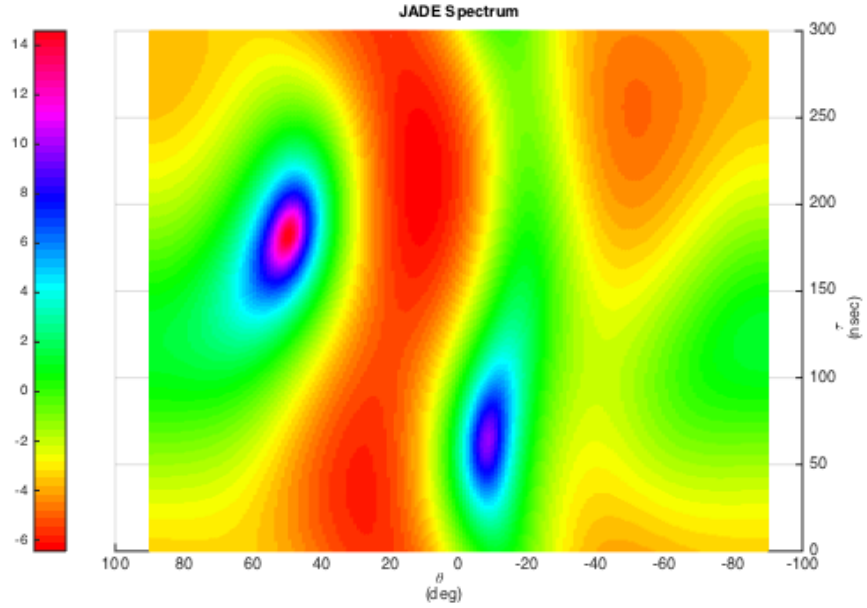

Figure 4.13: Frequency Smoothing with $M_p = 2$.

Theorem 4.3. *If the number of subarrays formed jointly over space and frequency is greater than the number of multipath components, i.e.* $q \leq K_M K_N$, *and the maximum number of paths arriving at the same time but with different angles is less than* K_N, *i.e.*

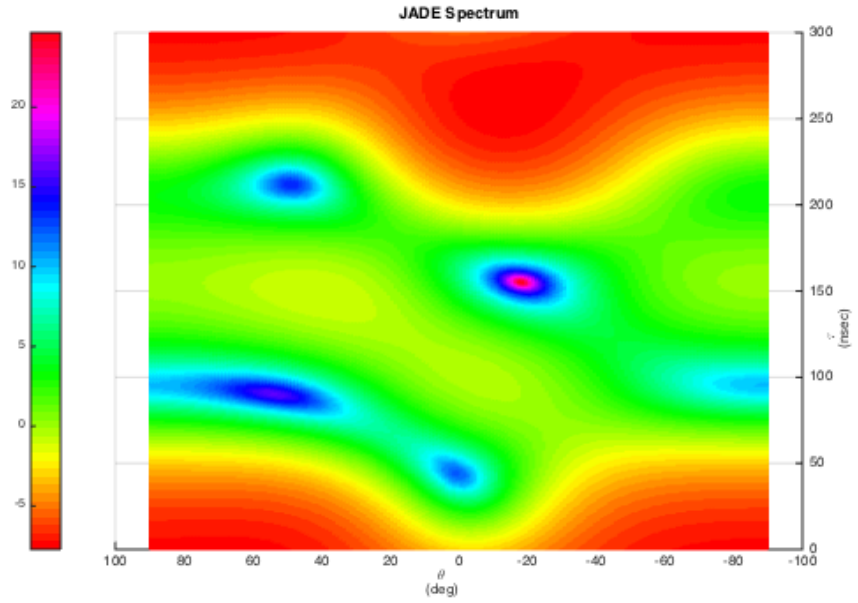

Figure 4.14: Spatio-Frequential Smoothing with $N_p = 2$ and $M_p = 3$.

$\max_i Q_i \leq K_N$, *and the maximum number of paths arriving at the same angles but with different times is less than* K_M, *i.e.* $\max_i P_i \leq K_M$, *then* $\bar{\boldsymbol{R}}_{\gamma\gamma}$ *is of rank* q.

Proof. See Appendix A □

Conditions (i) till (iii) in Appendix A are sufficient to attain full rank of $\bar{\boldsymbol{R}}_{\gamma\gamma}$. But, in order for subspace methods to work properly, one should also have that $\bar{\boldsymbol{H}}$ (see (4.74)) is full column rank. Note that $\bar{\boldsymbol{H}}$ has dimensions $N_pM_p \times q$. In the spirit of Remark 4.2, this is valid when $q \leq M_pN_p$, $\max_i Q_i \leq N_p$, and $\max_i P_i \leq M_p$. In general, one must have:

- $q \leq \min\{K_MK_N, M_pN_p\}$
- $\max_i Q_i \leq \min\{K_N, N_p\}$
- $\max_i P_i \leq \min\{K_M, M_p\}$

Finally, the advantage of *spatio-frequential* smoothing is that it offers K_MK_N subarrays to smooth over, in contrast to *spatial* and *frequential* smoothing that naturally provide K_N and K_M subarrays, respectively. Therefore, one could be able to resolve more coherent sources, as given in **(b.1)**. This advantage is, also, presented through simulations.

Computer simulations are presented to show the advantage of *spatio-frequential* smoothing over the conventional *spatial* and *frequential* smoothing. Simulations have been done

with $N = 3$ antennas and $M = 4$ subcarriers at SNR = 20dB. The subcarrier spacing is chosen $\triangle_f = 3.125$ MHz. We have fixed $q = 4$ paths, where their corresponding angles and times of arrival are $(\theta_1, \tau_1) = (0°, 40 \text{ nsec})$, $(\theta_2, \tau_2) = (60°, 100 \text{ nsec})$, $(\theta_3, \tau_3) = (-20°, 150 \text{ nsec})$ and $(\theta_4, \tau_4) = (50°, 200 \text{ nsec})$. The complex attenuation vector $\boldsymbol{\gamma}$ is fixed to a constant arbitrary value. Finally, $L = 3$ snapshots were collected.

Figure 4.12 shows the JADE spectrum after preprocessing only by spatial smoothing, i.e. $M = M_p = 4$ and $N_p = 2$. Indeed, there is an ambiguity in detecting the 4 peaks corresponding to the true angles and times of arrival due to insufficient number of subarrays to smooth over, i.e. only $K_N = 2 < q$ spatial subarrays are available. The same argument is done when one applies only frequency smoothing, i.e. $N = N_p = 3$ and $M_p = 2$. In that case, one will have $K_M = 3 < q$ subarrays to smooth over. As a result, false peaks appear in figure 4.13.

To this end, we could see that we need at least $q = 4$ subarrays to smooth over. This is done by preprocessing through spatio-frequential smoothing. Choosing $N_p = 2$ and $M_p = 3$ would lead to $K_N K_M = 4$ subarrays in total. After smoothing over space and frequencies, one could observe 4 clear peaks corresponding to the true angles and times of arrival of the 4 paths in figure 4.14.

4.5 Conclusions

In this chapter, we have presented two techniques to solve the highly nonlinear DML algorithm for joint times and angles of arrival: 2D-IQML and 2D-DIQML. Asymptotic performance analysis of both techniques were provided. It has been shown that 2D-IQML gives biased estimates of ToA/AoA and performs poorly at low SNR due to noise. An original "denoising" strategy is proposed, which constrains the Hessian of the cost function to be positive semi-definite. This "denoising" strategy is called 2D-DIQML that has been shown to be globally convergent. Furthermore, 2D-DIQML outperforms 2D-IQML because the former behaves asymptotically at any SNR as the latter behaves at high SNR. Finally, for localisation purposes, joint AoA and ToA information could be used to form a database, where a mapping is done between ToA/AoA vectors and location. Then, this database could be used in an online stage, where joint AoA/ToA estimation is done using the proposed algorithms, followed by a matching criteria that finds the best match in the database to obtain an estimate of the location of a wireless transmitter.

We have also presented two algorithms based on 2D Matrix Pencils. These two algorithms allow joint estimation of times and angles of arrival of multiple paths using only one snapshot. Algorithm 1 resolves more sources than Algorithm 2 in the case where the number of subcarriers is much larger than the number of antennas, which is the case of most Wi-Fi systems. The performance of Algorithm 1 as a function of SNR was studied through simulations.

Finally, we have presented a 2D smoothing preprocessing technique, applied to a *Spatial-Frequential* array, to "decorrelate" multipath components. Then, any 2D subspace algorithm could be applied to estimate the times and angles of arrivals of the different paths. The 2D smoothing technique presented here, naturally, offers more subarrays to smooth over and, therefore, one could be able to resolve more coherent paths.

Chapter 5

Joint Angle and Delay Estimation and Detection

In this chapter, a novel approach entitled "Joint Angle and Delay Estimator and Detector", or simply JADED, is presented. The contributions could be summarized as follows: (i) Thanks to this approach, we can now estimate the Angles and Times of Arrival of multipath, without prior knowledge of the number of multipath components; (ii) a method called JADED-RIP, makes use of the Rotational Invariance Properties (RIP) of ULAs and OFDM symbols, detects the number of multipath components, and estimates the angles and times of arrival of each path by performing a 2D search; (iii) the second method is a Computationally Efficient Single Snapshot (CESS) version of the JADED-RIP, i.e. it requires a 1D search followed by a least squares fit, and can only be used when a single OFDM symbol is available.

5.1 System model

As in the previous Chapter, we consider an OFDM symbol composed of M subcarriers and centered at a carrier frequency f_c, impinging an array of N antennas via q multipath components. Each path arrives at AoA θ_i and ToA τ_i. After applying an FFT and equalization, we can express the l^{th} OFDM symbol as follows

$$\boldsymbol{x}(l) = \boldsymbol{H}\boldsymbol{\gamma}(l) + \boldsymbol{w}(l), \qquad l = 1 \dots L \tag{5.1}$$

where $\boldsymbol{x}(l) \in \mathbb{C}^{MN \times 1}$ is given as

$$\boldsymbol{x}(l) = [X_{1,1}^{(l)} \dots X_{1,N}^{(l)} \dots X_{M,1}^{(l)} \dots X_{M,N}^{(l)}]^{\mathrm{T}} \tag{5.2}$$

with $X_{m,n}^{(l)}$ being the data at the n^{th} antenna and m^{th} subcarrier in the l^{th} OFDM symbol. $\boldsymbol{H} \in \mathbb{C}^{MN \times q}$ contains the ToA/AoA information as

$$\boldsymbol{H} = [\boldsymbol{c}_M(\tau_1) \otimes \boldsymbol{a}_N(\theta_1) \dots \boldsymbol{c}_M(\tau_q) \otimes \boldsymbol{a}_N(\theta_q)] \tag{5.3}$$

where

$$\boldsymbol{a}_N(\theta) = [1, z_\theta \dots z_\theta^{N-1}]^{\mathrm{T}} \quad \text{with} \quad z_\theta = e^{-j2\pi \frac{d}{\lambda} \sin(\theta)} \tag{5.4}$$

$$\boldsymbol{c}_M(\tau) = [1, z_\tau \dots z_\tau^{M-1}]^{\mathrm{T}} \quad \text{with} \quad z_\tau = e^{-j2\pi\tau\triangle_f} \tag{5.5}$$

where $\triangle_f$ is the subcarrier spacing, d is the inter-element spacing, and λ is the signal's wavelength. The $q \times 1$ vector $\boldsymbol{\gamma}(l)$ is composed of the multipath coefficients

$$\boldsymbol{\gamma}(l) = [\gamma_1(l) \dots \gamma_q(l)]^{\mathrm{T}} \tag{5.6}$$

Note that we have made explicit the dimensions of vectors $\boldsymbol{c}_M(\tau)$ and $\boldsymbol{a}_N(\theta)$, i.e. it should be understood that for any integer $K \geq 1$, the vectors $\big(\boldsymbol{c}_K(\tau), \boldsymbol{a}_K(\theta)\big) \in \mathbb{C}^{K \times 1}$. The vector $\boldsymbol{w}(l)$ is additive Gaussian noise of zero mean and covariance $\sigma^2\boldsymbol{I}$, assumed to be white over space, and frequencies. We are now ready to address the problem: *"Given the data $\{\boldsymbol{x}(l)\}_{l=1}^{L}$, estimate the number of multipath components q and the signal parameters $\{(\tau_j, \theta_j)\}_{j=1}^{q}$."*

5.2 JADED-RIP Algorithm Derivation

5.2.1 Data Manipulation

Let $\boldsymbol{X}(l)$ be a matrix formed from the entries of $\boldsymbol{x}(l)$

$$\boldsymbol{X}(l) = \begin{pmatrix} \boldsymbol{X}_1^{(l)} & \boldsymbol{X}_2^{(l)} & \cdots & \boldsymbol{X}_{K_M}^{(l)} \\ \boldsymbol{X}_2^{(l)} & \boldsymbol{X}_3^{(l)} & \cdots & \boldsymbol{X}_{K_M+1}^{(l)} \\ \vdots & \vdots & \ddots & \vdots \\ \boldsymbol{X}_{P_M}^{(l)} & \boldsymbol{X}_{P_M+1}^{(l)} & \cdots & \boldsymbol{X}_M^{(l)} \end{pmatrix} \tag{5.7}$$

where $\boldsymbol{X}_i^{(l)}$ is an $P_N \times K_N$ Hankel matrix given by

$$\boldsymbol{X}_i^{(l)} = \begin{pmatrix} X_{i,1}^{(l)} & X_{i,2}^{(l)} & \cdots & X_{i,K_N}^{(l)} \\ X_{i,2}^{(l)} & X_{i,3}^{(l)} & \cdots & X_{i,K_N+1}^{(l)} \\ \vdots & \vdots & \ddots & \vdots \\ X_{i,P_N}^{(l)} & X_{i,P_N+1}^{(l)} & \cdots & X_{i,N}^{(l)} \end{pmatrix} \tag{5.8}$$

with

$$K_M = M - P_M + 1 \quad \text{and} \quad K_N = N - P_N + 1 \tag{5.9}$$

For simplicity of notation, define the following integers

$$K \triangleq K_M K_N \quad \text{and} \quad P \triangleq P_M P_N \tag{5.10}$$

The matrix $\boldsymbol{X}(l)$ can be written as

$$\boldsymbol{X}(l) = \boldsymbol{L}\boldsymbol{\Gamma}(l)\boldsymbol{R}^{\mathrm{T}} + \boldsymbol{W}(l) \tag{5.11}$$

where $\boldsymbol{L} \in \mathbb{C}^{P\times q}$ and $\boldsymbol{R} \in \mathbb{C}^{K\times q}$ are given as

$$\boldsymbol{L} = [\boldsymbol{h}_P(\tau_1, \theta_1) \dots \boldsymbol{h}_P(\tau_q, \theta_q)] \tag{5.12}$$

$$\boldsymbol{R} = [\boldsymbol{h}_K(\tau_1, \theta_1) \dots \boldsymbol{h}_K(\tau_q, \theta_q)] \tag{5.13}$$

with

$$\boldsymbol{h}_P(\tau, \theta) = \boldsymbol{c}_{P_M}(\tau) \otimes \boldsymbol{a}_{P_N}(\theta) \tag{5.14}$$

$$\boldsymbol{h}_K(\tau, \theta) = \boldsymbol{c}_{K_M}(\tau) \otimes \boldsymbol{a}_{K_N}(\theta) \tag{5.15}$$

The matrix $\boldsymbol{\Gamma}(l) \in \mathbb{C}^{q\times q}$ is a diagonal matrix, i.e.

$$\boldsymbol{\Gamma}(l) = \text{diag}\,[\gamma_1(l), \gamma_2(l) \dots \gamma_q(l)] \tag{5.16}$$

Finally, the matrix $\boldsymbol{W}(l) \in \mathbb{C}^{P\times K}$ is background noise defined in a similar manner as $\boldsymbol{X}(l)$.

5.2.2 Introducing Orthogonal Projectors

Let $\boldsymbol{R}_j$ be a matrix defined as $\boldsymbol{R}$ with omitted j^{th} column. Furthermore, define the orthogonal projector matrix that spans the null space of the columns of $\boldsymbol{R}_j$ as

$$\boldsymbol{\mathcal{P}}_j^{\perp} = \boldsymbol{I}_K - \boldsymbol{R}_j\left(\boldsymbol{R}_j^{\mathrm{T}}\boldsymbol{R}_j\right)^{-1}\boldsymbol{R}_j^{\mathrm{T}} \tag{5.17}$$

In other words, $\boldsymbol{R}_j^{\mathrm{T}}\boldsymbol{\mathcal{P}}_j^{\perp} = \boldsymbol{0}$. Now, let $\boldsymbol{f}_j \in \mathbb{C}^{K\times 1}$ be a vector that lives in the null space of the columns of $\boldsymbol{R}_j$. Therefore, there exists a non-zero vector $\boldsymbol{z} \in \mathbb{C}^{K\times 1}$ such that

$$\boldsymbol{f}_j = \boldsymbol{\mathcal{P}}_j^{\perp}\boldsymbol{z} \tag{5.18}$$

Post-multiplying the vector $\boldsymbol{f}_j$ with the data matrix $\boldsymbol{X}(l)$ yields

$$\begin{aligned}\boldsymbol{X}(l)\boldsymbol{f}_j &= \left(\boldsymbol{L}\boldsymbol{\Gamma}(l)\boldsymbol{R}^{\mathrm{T}}\right)\boldsymbol{f}_j + \boldsymbol{W}(l)\boldsymbol{f}_j \\ &= \boldsymbol{L}_j\boldsymbol{\Gamma}_j(l)\boldsymbol{R}_j^{\mathrm{T}}\boldsymbol{\mathcal{P}}_j^{\perp}\boldsymbol{z} + \alpha_j(l)\boldsymbol{h}_P(\tau_j,\theta_j) + \widetilde{\boldsymbol{w}}(l) \\ &= \alpha_j(l)\boldsymbol{h}_P(\tau_j,\theta_j) + \widetilde{\boldsymbol{w}}(l), \quad l = 1\dots L\end{aligned} \tag{5.19}$$

where $\boldsymbol{L}_j$ is defined in a similar manner as $\boldsymbol{R}_j$ and $\boldsymbol{\Gamma}_j(l) \in \mathbb{C}$ is the same as $\boldsymbol{\Gamma}(l)$ in equation (5.16) but with eliminated j^{th} row and column. Furthermore, $\alpha_j(l) = \gamma_j^{(l)}\boldsymbol{h}_K^{\mathrm{T}}(\tau_j,\theta_j)\boldsymbol{f}_j$. Finally, $\widetilde{\boldsymbol{w}}(l) = \boldsymbol{W}(l)\boldsymbol{f}_j$ is the noise part, which is easily verified to be colored noise.

Equation (5.19) is key to what follows. In other words, we know that a vector $\boldsymbol{f}_j$ exists, which can select the contribution of the j^{th} source. Next, we derive a Least-Square (LS) estimator of all the unknown parameters.

5.2.3 Least-Square Estimator

The parameters concerning the j^{th} source are

$$\boldsymbol{\Theta}_j = [\boldsymbol{f}_j^{\mathrm{T}}, \boldsymbol{\alpha}_j^{\mathrm{T}}, \tau_j, \theta_j] \tag{5.20}$$

where $\boldsymbol{\alpha}_j = [\alpha_j(1)\dots\alpha_j(L)]^{\mathrm{T}}$. Let's stack all unknown parameters into one vector $\boldsymbol{\Theta}$, i.e.

$$\boldsymbol{\Theta} = [\boldsymbol{\Theta}_1, \boldsymbol{\Theta}_2 \dots \boldsymbol{\Theta}_q] = [\boldsymbol{f}^{\mathrm{T}}, \boldsymbol{\alpha}^{\mathrm{T}}, \boldsymbol{\tau}, \boldsymbol{\theta}] \tag{5.21}$$

where

$$\boldsymbol{f} = [\boldsymbol{f}_1^{\mathrm{T}} \dots \boldsymbol{f}_q^{\mathrm{T}}]^{\mathrm{T}} \text{ and } \quad \boldsymbol{\alpha} = [\boldsymbol{\alpha}_1^{\mathrm{T}} \dots \boldsymbol{\alpha}_q^{\mathrm{T}}]^{\mathrm{T}} \tag{5.22}$$

$$\boldsymbol{\tau} = [\tau_1 \dots \tau_q] \quad \text{ and } \quad \boldsymbol{\theta} = [\theta_1 \dots \theta_q] \tag{5.23}$$

All parameters in $\boldsymbol{\Theta}$ have to be jointly estimated. In this section, we propose to estimate these parameters by Least-Squares (LS). In other words, we seek to optimise the following cost function

$$\widehat{\boldsymbol{\Theta}}^{\mathrm{LS}} = \arg\min_{\boldsymbol{\Theta}} g(\boldsymbol{\Theta}) \tag{5.24}$$

where

$$g(\boldsymbol{\Theta}) = \sum_{j=1}^{q}\sum_{l=1}^{L}\left\|\boldsymbol{X}(l)\boldsymbol{f}_j - \alpha_j(l)\boldsymbol{h}_P(\tau_j,\theta_j)\right\|^2 \tag{5.25}$$

and $\widehat{\boldsymbol{\Theta}}^{\mathrm{LS}}$ is the LS estimate of $\boldsymbol{\Theta}$. We re-write $g(\boldsymbol{\Theta})$ in a compact way as follows

$$g(\boldsymbol{\Theta}) = \boldsymbol{f}^{\mathrm{H}}\big(\boldsymbol{I}_q \otimes \boldsymbol{Q}\big)\boldsymbol{f} - 2\,\Re\big(\boldsymbol{f}^{\mathrm{H}}\boldsymbol{C}(\boldsymbol{\tau},\boldsymbol{\theta})\boldsymbol{\alpha}\big) + P\|\boldsymbol{\alpha}\|^2 \tag{5.26}$$

where matrices $\boldsymbol{Q}$ and $\boldsymbol{C}(\boldsymbol{\tau},\boldsymbol{\theta})$ are given by

$$\boldsymbol{Q} = \boldsymbol{\mathcal{X}}^{\mathrm{H}}\boldsymbol{\mathcal{X}} \tag{5.27}$$

$$\boldsymbol{C}(\boldsymbol{\tau},\boldsymbol{\theta}) = \text{blkdiag}\,[\boldsymbol{S}(\tau_1,\theta_1)\ldots\boldsymbol{S}(\tau_q,\theta_q)] \tag{5.28}$$

and matrices $\boldsymbol{\mathcal{X}}$ and $\boldsymbol{S}(\tau,\theta)$ are defined as

$$\boldsymbol{\mathcal{X}} = \Big[\ \boldsymbol{X}^{\mathrm{H}}(1)\ \Big|\ \ldots\ \Big|\ \boldsymbol{X}^{\mathrm{H}}(L)\ \Big]^{\mathrm{H}} \tag{5.29}$$

$$\boldsymbol{S}(\tau,\theta) = \boldsymbol{\mathcal{X}}^{\mathrm{H}}\boldsymbol{\mathcal{H}}(\tau,\theta) \tag{5.30}$$

where

$$\boldsymbol{\mathcal{H}}(\tau,\theta) = \boldsymbol{I}_L \otimes \boldsymbol{h}_P(\tau,\theta) \tag{5.31}$$

Fixing $(\boldsymbol{\alpha},\boldsymbol{\tau},\boldsymbol{\theta})$, we optimise the cost function $g(\boldsymbol{\Theta})$ w.r.t $\boldsymbol{f}$. Hence, setting the derivative of $g(\boldsymbol{\Theta})$ w.r.t $\boldsymbol{f}$ to zero, we get

$$\frac{\partial g(\boldsymbol{\Theta})}{\partial \boldsymbol{f}} = 2\big(\boldsymbol{I}_q \otimes \boldsymbol{Q}\big)\boldsymbol{f} - 2\boldsymbol{C}(\boldsymbol{\tau},\boldsymbol{\theta})\boldsymbol{\alpha} = 0 \tag{5.32}$$

which gives

$$\widehat{\boldsymbol{f}}^{\mathrm{LS}} = \big(\boldsymbol{I}_q \otimes \boldsymbol{Q}\big)^{-1}\boldsymbol{C}(\boldsymbol{\tau},\boldsymbol{\theta})\boldsymbol{\alpha} \tag{5.33}$$

Now, we treat $\widehat{\boldsymbol{f}}^{\mathrm{LS}}$ as a nuissance parameter and plug it in the cost function $g(\boldsymbol{\Theta})$ in equation (5.26), namely

$$\begin{aligned} g(\boldsymbol{\alpha},\boldsymbol{\tau},\boldsymbol{\theta}) &\triangleq g(\widehat{\boldsymbol{f}}^{\mathrm{LS}},\boldsymbol{\alpha},\boldsymbol{\tau},\boldsymbol{\theta}) \\ &= \boldsymbol{\alpha}^{\mathrm{H}}\Big(P\boldsymbol{I}_{qL} - \boldsymbol{C}^{\mathrm{H}}(\boldsymbol{\tau},\boldsymbol{\theta})\big(\boldsymbol{I}_q \otimes \boldsymbol{Q}\big)^{-1}\boldsymbol{C}(\boldsymbol{\tau},\boldsymbol{\theta})\Big)\boldsymbol{\alpha} \end{aligned} \tag{5.34}$$

Due to the block diagonal nature of $\boldsymbol{C}(\boldsymbol{\tau},\boldsymbol{\theta})$, and using

$$\big(\boldsymbol{I}_q \otimes \boldsymbol{Q}\big)^{-1} = \boldsymbol{I}_q \otimes \boldsymbol{Q}^{-1} \tag{5.35}$$

The function $g(\boldsymbol{\alpha},\boldsymbol{\tau},\boldsymbol{\theta})$ decouples into q positive cost functions

$$g(\boldsymbol{\alpha},\boldsymbol{\tau},\boldsymbol{\theta}) = \sum_{j=1}^{q} g_j(\boldsymbol{\alpha}_j,\tau_j,\theta_j) \tag{5.36}$$

Denoting $g_j \triangleq g_j(\boldsymbol{\alpha}_j, \tau_j, \theta_j)$ for ease of notation, we can say

$$\begin{aligned} g_j &= \boldsymbol{\alpha}_j^{\mathrm{H}} \Big(P\boldsymbol{I}_L - \boldsymbol{S}^{\mathrm{H}}(\tau_j, \theta_j) \boldsymbol{Q}^{-1} \boldsymbol{S}(\tau_j, \theta_j) \Big) \boldsymbol{\alpha}_j \\ &= \boldsymbol{\alpha}_j^{\mathrm{H}} \Big(\boldsymbol{\mathcal{H}}^{\mathrm{H}}(\tau_j, \theta_j) \boldsymbol{\mathcal{P}}_{\boldsymbol{\mathcal{X}}}^{\perp} \boldsymbol{\mathcal{H}}(\tau_j, \theta_j) \Big) \boldsymbol{\alpha}_j \end{aligned} \tag{5.37}$$

where the last equality is due to equations (5.27) and (5.30). The projector $\boldsymbol{\mathcal{P}}_{\boldsymbol{\mathcal{X}}}^{\perp}$ is given as

$$\boldsymbol{\mathcal{P}}_{\boldsymbol{\mathcal{X}}}^{\perp} = \boldsymbol{I}_{LP} - \boldsymbol{\mathcal{X}} (\boldsymbol{\mathcal{X}}^{\mathrm{H}} \boldsymbol{\mathcal{X}})^{-1} \boldsymbol{\mathcal{X}}^{\mathrm{H}} \tag{5.38}$$

Fixing $(\boldsymbol{\tau}, \boldsymbol{\theta})$ in $g(\boldsymbol{\alpha}, \boldsymbol{\tau}, \boldsymbol{\theta})$, each function g_j is quadratic in $\boldsymbol{\alpha}_j$. Note that minimising $g(\boldsymbol{\alpha}, \boldsymbol{\tau}, \boldsymbol{\theta})$ w.r.t $\boldsymbol{\alpha}$ is equivalent to minimising each g_j w.r.t $\boldsymbol{\alpha}_j$ since $g_j \geq 0$ for all j. In order to prevent a function g_j to be minimized at the trivial solution $\boldsymbol{\alpha}_j = \boldsymbol{0}$, we form the following *Equality Constrained Quadratic Optimisation* [83] problem

$$\begin{cases} \underset{\boldsymbol{\alpha}_j}{\text{minimize}} & g_j(\boldsymbol{\alpha}_j, \tau_j, \theta_j) \\ \text{subject to} & \boldsymbol{\alpha}_j^{\mathrm{H}} \boldsymbol{e}_1 = 1 \end{cases} \tag{5.39}$$

where $\boldsymbol{e}_1$ is the 1^{st} column of $\boldsymbol{I}_L$. The *Lagrangian* function corresponding to the optimisation problem in (5.39) is the following:

$$\mathcal{L}(\boldsymbol{\alpha}_j, \lambda) = g_j(\boldsymbol{\alpha}_j, \tau_j, \theta_j) - \lambda \big(\boldsymbol{\alpha}_j^{\mathrm{H}} \boldsymbol{e}_1 - 1 \big) \tag{5.40}$$

Setting the derivative of $\mathcal{L}(\boldsymbol{\alpha}_j, \lambda)$ w.r.t $\boldsymbol{\alpha}_j$ to 0, we get

$$\frac{\partial \mathcal{L}(\boldsymbol{\alpha}_j, \lambda)}{\partial \boldsymbol{\alpha}_j} = 2\boldsymbol{\mathcal{H}}^{\mathrm{H}}(\tau_j, \theta_j) \boldsymbol{\mathcal{P}}_{\boldsymbol{\mathcal{X}}}^{\perp} \boldsymbol{\mathcal{H}}(\tau_j, \theta_j) \boldsymbol{\alpha}_j - \lambda \boldsymbol{e_1} = 0 \tag{5.41}$$

which yields

$$\widehat{\boldsymbol{\alpha}}_j^{\mathrm{LS}} = \frac{\lambda}{2} \big(\boldsymbol{\mathcal{H}}^{\mathrm{H}}(\tau_j, \theta_j) \boldsymbol{\mathcal{P}}_{\boldsymbol{\mathcal{X}}}^{\perp} \boldsymbol{\mathcal{H}}(\tau_j, \theta_j) \big)^{-1} \boldsymbol{e_1} \tag{5.42}$$

Plugging this expression of $\widehat{\boldsymbol{\alpha}}_j^{\mathrm{LS}}$ in the constraint of the optimisation problem in equation (5.39), we can solve for the *Lagrangian* multiplier λ as

$$\lambda = \frac{2}{\boldsymbol{e}_1^{\mathrm{H}} \big(\boldsymbol{\mathcal{H}}^{\mathrm{H}}(\tau_j, \theta_j) \boldsymbol{\mathcal{P}}_{\boldsymbol{\mathcal{X}}}^{\perp} \boldsymbol{\mathcal{H}}(\tau_j, \theta_j) \big)^{-1} \boldsymbol{e}_1} \tag{5.43}$$

and therefore $\widehat{\boldsymbol{\alpha}}_j^{\mathrm{LS}}$ is obtained by plugging the expression of λ in equation (5.42), i.e.

$$\widehat{\boldsymbol{\alpha}}_j^{\mathrm{LS}} = \frac{\big(\boldsymbol{\mathcal{H}}^{\mathrm{H}}(\tau_j, \theta_j) \boldsymbol{\mathcal{P}}_{\boldsymbol{\mathcal{X}}}^{\perp} \boldsymbol{\mathcal{H}}(\tau_j, \theta_j) \big)^{-1} \boldsymbol{e}_1}{\boldsymbol{e}_1^{\mathrm{H}} \big(\boldsymbol{\mathcal{H}}^{\mathrm{H}}(\tau_j, \theta_j) \boldsymbol{\mathcal{P}}_{\boldsymbol{\mathcal{X}}}^{\perp} \boldsymbol{\mathcal{H}}(\tau_j, \theta_j) \big)^{-1} \boldsymbol{e}_1} \tag{5.44}$$

hence $\widehat{\boldsymbol{\alpha}}^{\mathrm{LS}}$ is obtained by stacking all $\widehat{\boldsymbol{\alpha}}_j^{\mathrm{LS}}$ into one vector as in equation (5.22). As done before, we treat $\widehat{\boldsymbol{\alpha}}^{\mathrm{LS}}$ as nuissance parameters and thus we substitute them in $g(\boldsymbol{\alpha}, \boldsymbol{\tau}, \boldsymbol{\theta})$

to get $g(\boldsymbol{\tau},\boldsymbol{\theta}) \triangleq g(\widehat{\boldsymbol{\alpha}}^{\mathrm{LS}},\boldsymbol{\tau},\boldsymbol{\theta})$, where

$$g(\boldsymbol{\tau},\boldsymbol{\theta}) = \sum_{j=1}^{q} \frac{1}{\boldsymbol{e}_1^{\mathrm{H}}\big(\boldsymbol{\mathcal{H}}^{\mathrm{H}}(\tau_j,\theta_j)\boldsymbol{\mathcal{P}}_{\boldsymbol{\mathcal{X}}}^{\perp}\boldsymbol{\mathcal{H}}(\tau_j,\theta_j)\big)^{-1}\boldsymbol{e}_1} \tag{5.45}$$

The LS estimates of the ToAs $\boldsymbol{\tau}$ and AoAs $\boldsymbol{\theta}$ are simply

$$(\widehat{\boldsymbol{\tau}}^{\mathrm{LS}},\widehat{\boldsymbol{\theta}}^{\mathrm{LS}}) = \arg\min_{\boldsymbol{\tau},\boldsymbol{\theta}} g(\boldsymbol{\tau},\boldsymbol{\theta}) \tag{5.46}$$

Since $g(\boldsymbol{\tau},\boldsymbol{\theta})$ is decoupled into q identical functional forms, given in the last equality in equation (5.45), then one can jointly estimate the ToAs/AoAs by performing a 2D-search as

$$\{(\widehat{\tau}_j^{\mathrm{LS}},\widehat{\theta}_j^{\mathrm{LS}})\}_{j=1}^{\widehat{q}} = \arg\max_{\tau,\theta} f_{\mathrm{JADED}}(\tau,\theta) \tag{5.47}$$

where

$$f_{\mathrm{JADED}}(\tau,\theta) = \boldsymbol{e}_1^{\mathrm{H}}\big(\boldsymbol{\mathcal{H}}^{\mathrm{H}}(\tau,\theta)\boldsymbol{\mathcal{P}}_{\boldsymbol{\mathcal{X}}}^{\perp}\boldsymbol{\mathcal{H}}(\tau,\theta)\big)^{-1}\boldsymbol{e}_1 \tag{5.48}$$

and $\widehat{q}$ is an estimate of q obtained by the number of peaks in $f_{\mathrm{JADED}}(\tau,\theta)$.

5.3 Computationally Efficient Single Snapshot JADED-RIP (CESS-JADED-RIP)

The JADED-RIP algorithm requires a 2D search over the variables (τ,θ). It turns out that for a single snapshot, i.e. $L = 1$, we can propose a computationally more efficient method, which we call here Computationally Efficient Single Snapshot JADED-RIP, or simply CESS-JADED-RIP. For a single snapshot and using equation (5.31), $f_{\mathrm{JADED}}(\tau,\theta)$ can be expressed as

$$f_{\mathrm{JADED}}(\tau,\theta) = \frac{1}{\boldsymbol{h}_P^{\mathrm{H}}(\tau,\theta)\boldsymbol{\mathcal{P}}_{\boldsymbol{\mathcal{X}}}^{\perp}\boldsymbol{h}_P(\tau,\theta)} \tag{5.49}$$

Using the structure of $\boldsymbol{h}_P(\tau,\theta)$ in equation (5.14), we can write the denominator in equation (5.49) as follows

$$\boldsymbol{h}_P^{\mathrm{H}}(\tau,\theta)\boldsymbol{\mathcal{P}}_{\boldsymbol{\mathcal{X}}}^{\perp}\boldsymbol{h}_P(\tau,\theta) = \boldsymbol{a}_{P_N}^{\mathrm{H}}(\theta)F(\tau)\boldsymbol{a}_{P_N}(\theta) \tag{5.50}$$

where

$$F(\tau) = \big(\boldsymbol{c}_{P_M}(\tau)\otimes\boldsymbol{I}_{P_N}\big)^{\mathrm{H}}\boldsymbol{\mathcal{P}}_{\boldsymbol{\mathcal{X}}}^{\perp}\big(\boldsymbol{c}_{P_M}(\tau)\otimes\boldsymbol{I}_{P_N}\big) \tag{5.51}$$

Maximising (5.49) is equivalent to minimizing (5.50), hence we aim at solving

$$\begin{cases} \underset{\boldsymbol{a}_{P_N}(\theta)}{\text{minimize}} & \boldsymbol{a}_{P_N}^{\mathrm{H}}(\theta) F(\tau) \boldsymbol{a}_{P_N}(\theta) \\ \text{subject to} & \boldsymbol{a}_{P_N}^{\mathrm{H}}(\theta) \boldsymbol{e}_1 = 1 \end{cases} \tag{5.52}$$

Following similar steps as in equations (5.40) till (5.44), the vector $\widehat{\boldsymbol{a}}_{P_N}(\theta)$ that solves the above problem is given as

$$\widehat{\boldsymbol{a}}_{P_N}(\theta) = \frac{F^{-1}(\tau)\boldsymbol{e}_1}{\boldsymbol{e}_1^{\mathrm{H}} F^{-1}(\tau)\boldsymbol{e}_1} \tag{5.53}$$

Substituting $\widehat{\boldsymbol{a}}_{P_N}(\theta)$ in the objective function of the problem in equation (5.52) gives us a cost function in τ, and therefore the ToAs are estimated as follows

$$\{\widehat{\tau}_j\}_{j=1}^{\widehat{q}} = \arg\max_{\tau} w(\tau) \tag{5.54}$$

where

$$w(\tau) = \boldsymbol{e}_1^{\mathrm{H}} F^{-1}(\tau)\boldsymbol{e}_1 \tag{5.55}$$

Now, we are left with the estimation of the AoAs. Notice that equation (5.53) maps τ to θ, therefore for each $\widehat{\tau}_j$, we can obtain $\widehat{\boldsymbol{a}}_{P_N}(\widehat{\theta}_j)$ as

$$\widehat{\boldsymbol{a}}_{P_N}(\widehat{\theta}_j) = \frac{F^{-1}(\widehat{\tau}_j)\boldsymbol{e}_1}{\boldsymbol{e}_1^{\mathrm{H}} F^{-1}(\widehat{\tau}_j)\boldsymbol{e}_1}, \qquad j = 1 \dots \widehat{q} \tag{5.56}$$

Then, we estimate $\widehat{\theta}_j$ from $\widehat{\boldsymbol{a}}_{P_N}(\widehat{\theta}_j)$. This is done by forming the vector of phases of $\widehat{\boldsymbol{a}}_{P_N}(\widehat{\theta}_j)$ as follows

$$\left[\widehat{\boldsymbol{\phi}}_j\right]_k = -\frac{1}{2\pi d}\tan^{-1}\Big(\frac{\Im\big(\left[\widehat{\boldsymbol{a}}_{P_N}(\widehat{\theta}_j)\right]_k\big)}{\Re\big(\left[\widehat{\boldsymbol{a}}_{P_N}(\widehat{\theta}_j)\right]_k\big)}\Big), \quad j = 1 \dots \widehat{q} \tag{5.57}$$

After the operation in equation (5.57), we have $\widehat{\boldsymbol{\phi}}_j$ in the following form: $\widehat{\boldsymbol{\phi}}_j = \boldsymbol{\rho}\sin(\widehat{\theta}_j)$, where $\boldsymbol{\rho} = [0 \dots (P_N - 1)]^{\mathrm{T}}$. Finally, we extract $\widehat{\theta}_j$ from $\widehat{\boldsymbol{\phi}}_j$ by the following LS fit

$$\widehat{\theta}_j = \arg\min_{\widehat{\theta}_j} \left\| \widehat{\boldsymbol{\phi}}_j - \boldsymbol{\rho}\sin(\widehat{\theta}_j) \right\|^2, \qquad j = 1 \dots \widehat{q} \tag{5.58}$$

The solution is easily verified to be

$$\widehat{\theta}_j = \sin^{-1}\Big(\boldsymbol{\rho}^{\dagger}\widehat{\boldsymbol{\phi}}_j\Big) = \sin^{-1}\Big(\frac{6\boldsymbol{\rho}^{\mathrm{T}}\widehat{\boldsymbol{\phi}}_j}{P_N(P_N-1)(2P_N-1)}\Big) \tag{5.59}$$

where $\boldsymbol{\rho}^{\dagger} = (\boldsymbol{\rho}^{\mathrm{T}}\boldsymbol{\rho})^{-1}\boldsymbol{\rho}^{\mathrm{T}}$.

Table 4: Summary of the JADED-RIP algorithm

INITIALISATION:

Step 1. Given the data $\{\boldsymbol{x}(l)\}_{l=1}^{L}$, form matrices $\{\boldsymbol{X}(l)\}_{l=1}^{L}$ using equations (5.7) and (5.8).

Step 2. Compute the projector matrix $\boldsymbol{\mathcal{P}}_{\boldsymbol{\mathcal{X}}}^{\perp}$ given in equation (5.38).

MAIN LOOP:

Step 3. On a 2D discretized grid, find the $\widehat{q}$ peaks of $f_{\text{JADED}}(\tau,\theta)$:

$$\left\{(\hat{\theta}_j,\hat{\tau}_j)\right\}_{j=1}^{\widehat{q}} = \arg\max_{\theta,\tau} \boldsymbol{e}_1^{\text{H}}\left(\boldsymbol{\mathcal{H}}^{\text{H}}(\tau,\theta)\boldsymbol{\mathcal{P}}_{\boldsymbol{\mathcal{X}}}^{\perp}\boldsymbol{\mathcal{H}}(\tau,\theta)\right)^{-1}\boldsymbol{e}_1$$

where $\boldsymbol{\mathcal{H}}(\tau,\theta)$ is given in equation (5.31).

Table 5: Summary of the CESS-JADED-RIP algorithm

INITIALISATION:

Similar to JADED-RIP.

MAIN LOOP:

Step 3. On a 1D discretized grid, find the $\widehat{q}$ peaks of $w(\tau)$:

$$\left\{\widehat{\tau}_j\right\}_{j=1}^{\widehat{q}} = \arg\max_{\tau} \boldsymbol{e}_1^{\text{H}} F^{-1}(\tau)\boldsymbol{e}_1$$

where $F(\tau)$ is given in equation (5.51).

Step 4. For each $\widehat{\tau}_j$, estimate $\widehat{\theta}_j$ using equations (5.56) till (5.59).

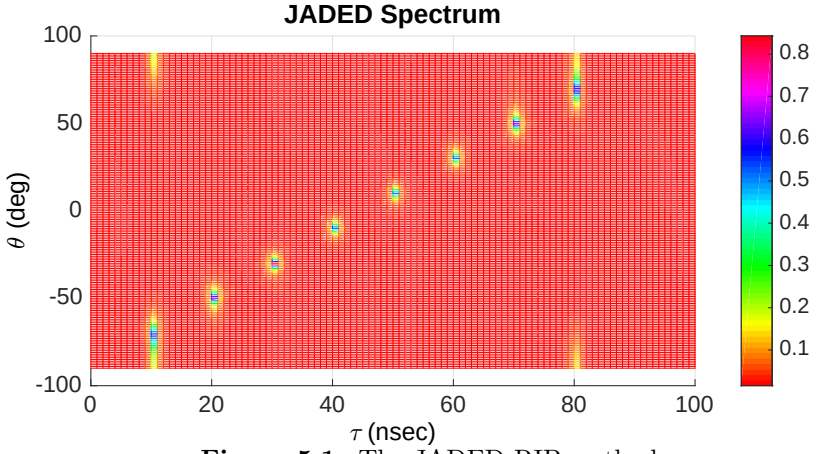

Figure 5.1: The JADED-RIP method.

5.4 Identifiability conditions

In this section, we derive identifiability conditions for unique estimation and detection of $(\boldsymbol{\tau},\boldsymbol{\theta})$ for JADED-RIP and CESS-JADED-RIP. The first set of conditions are given to guarantee a unique representation of equation (5.19), which happens when projectors $\{\boldsymbol{\mathcal{P}}_j^{\perp}\}_{j=1}^{q}$, given in equation (5.17), are uniquely defined. In other terms, these projectors should be full column rank. A sufficient condition for that to occur is when $\boldsymbol{R}$ is full column rank.

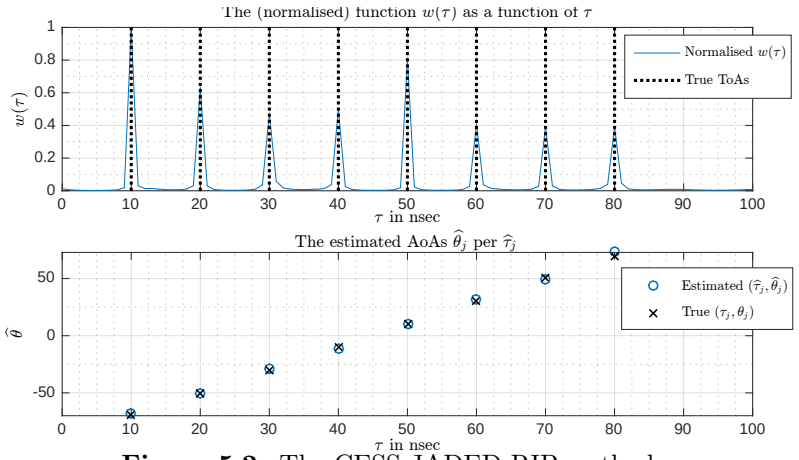

Figure 5.2: The CESS-JADED-RIP method.

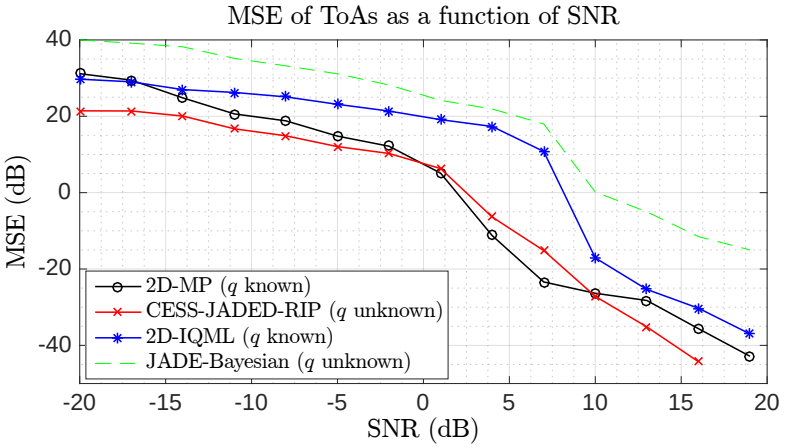

Figure 5.3: MSE of ToAs

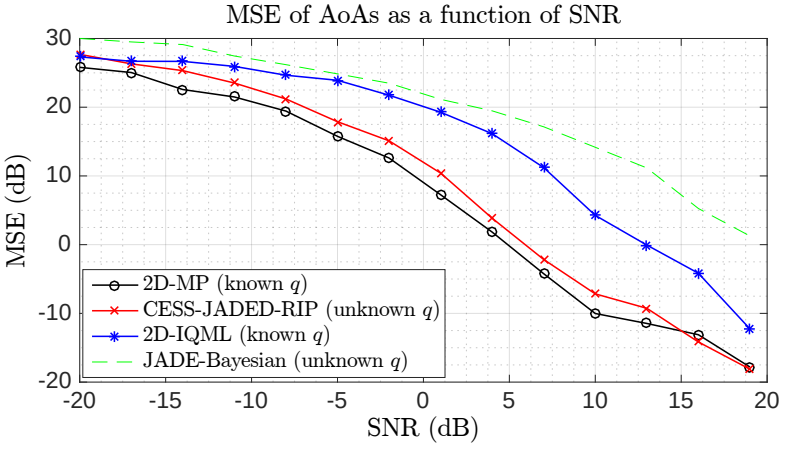

Figure 5.4: MSE of AoAs

The second projector that should be uniquely defined is the data projector matrix, namely $\boldsymbol{\mathcal{P}}_{\boldsymbol{\mathcal{X}}}^{\perp}$, given in equation (5.38). A necessary condition is when $\boldsymbol{\mathcal{X}}$ is a tall matrix,

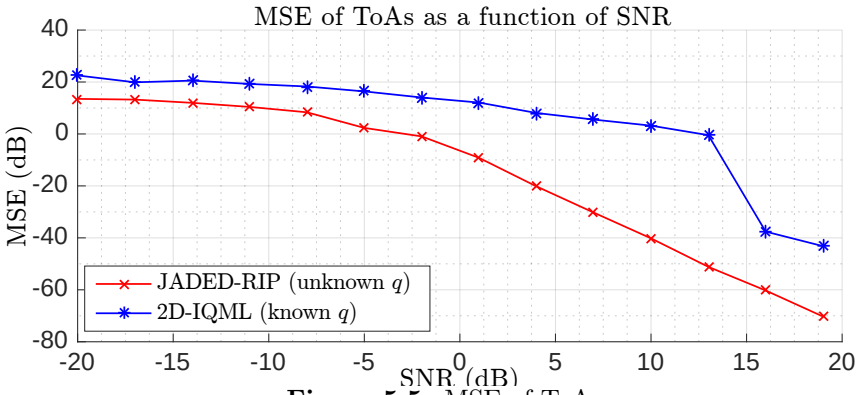

Figure 5.5: MSE of ToAs

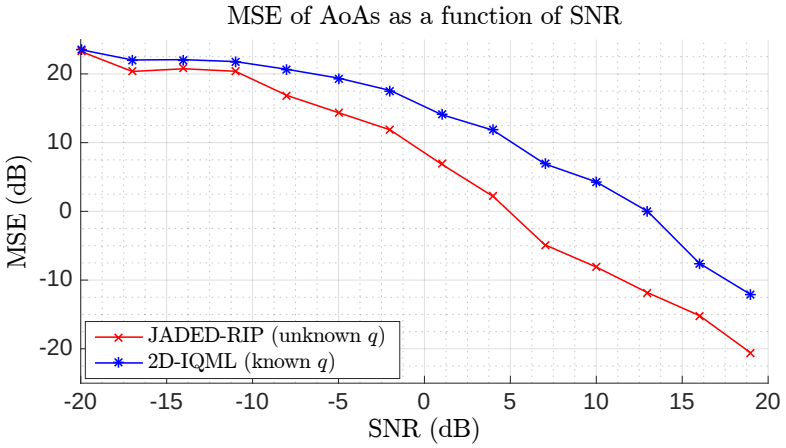

Figure 5.6: MSE of AoAs

namely $LP > K$. Combining Remark 4.2 and the condition of the existance of the data projector, the JADED-RIP algorithm should satisfy the following:

- **A1**: $q \leq K_M K_N < LP_M P_N$
- **A2**: $Q_\tau \leq K_N$ and $Q_\theta \leq K_M$

As for CESS-JADED-RIP, the parameter Q_τ should be 1, since the ToAs are estimated through a 1D search over $w(\tau)$ given in equation (5.55). Therefore, this approach does not allow multiple paths arriving at the same time. Finally, the CESS-JADED-RIP method should satisfy the following:

- **B1**: $q \leq K_M K_N < P_M P_N$
- **B2**: $Q_\tau = 1$ and $Q_\theta \leq K_M$

We have conducted the following three experiments:

In Experiment 1, i.e. Fig 5.1 and Fig 5.2, we plot the different spectra of the proposed algorithms. More precisely, Fig 5.1 plots the 2D-spectrum of the JADED-RIP given in equation (5.48). Also, Fig 5.2 plots the 1D-spectrum given in equation (5.55) (in order to estimate the ToAs) and the scatter plot to estimate the AoAs using the LS fit in equation (5.59). We have fixed $q = 8$ paths, where $\tau_k = 10k$ nsec and $\theta_k = -70+20(k-1)$ degrees, for $k = 1 \dots 8$. Also the multipath coefficients are chosen to be i.i.d Gaussian of zero mean. The number of antennas used is $N = 3$ with $d = 0.5$ and the OFDM symbol comprises of $M = 64$ subcarriers occupying a bandwidth of 200 MHz, i.e. $\triangle_f = 3.125$ MHz. We have chosen $P_M = 40$ and $P_N = 2$. The SNR is set to 5 dB. We have collected $L = 10$ OFDM symbols for the JADED-RIP method. It is interesting to see that we do not observe an overestimation of q in both methods, i.e. the peaks correspond to the true and only the true signal parameters.

In Experiment 2, i.e. Fig 5.3 and Fig 5.4, we plot the MSE of ToA/AoA estimates of CESS-JADED-RIP as a function of SNR. Moreover, the MSE is compared with other existing methods, such as the 2D-MP [108], the 2D-IQML [107], and a straightforward extension of [84] to the 2D case, which we refer to as JADE-Bayesian. We have averaged over 10^3 Monte-Carlo trials. These methods are particularly chosen for this experiment, since they could deal with a single snapshot. We recall that 2D-MP and 2D-IQML require the knowledge of q, whereas JADED and JADE-Bayesian estimate q from data. Note that the value of q is prior known for both 2D-MP and 2D-IQML. To this end, we fix $q = 2$ paths, with $(\tau_1, \theta_1) = (10\text{nsec}, -70^\circ)$ and $(\tau_2, \theta_2) = (20\text{nsec}, 20^\circ)$. The values of N, M, P_N, P_M, d and $\triangle_f$ are the same as those in Experiment 1. The multipath parameters are set to $\boldsymbol{\gamma} = [1; 0.8e^{j\frac{\pi}{4}}]$, i.e. coherent sources. In addition, only $L = 1$ OFDM symbol is available. We see that the performance of CESS-JADED-RIP is very close to that of 2D-MP in terms of MSE of ToA and AoA, according to Fig 5.3 and Fig 5.4, respectively. Also, we can see that CESS-JADED-RIP outperforms 2D-IQML and JADE-Bayesian.

In Experiment 3, i.e. Fig 5.5 and Fig 5.6, we plot the MSE of ToA/AoA estimates of JADED-RIP and 2D-IQML as a function of SNR, when multiple snapshots are available. This is why we have excluded 2D-MP and JADE-Bayesian, since they only operate with one snapshot. The same parameters are set as in Experiment 2, except for L, which is set to 10. By referring to Fig 5.5 and Fig 5.6, one could observe that the JADED-RIP outperforms 2D-IQML in terms of MSE of ToAs and AoAs, at any given SNR.

5.5 Peak Detection and Resolvability

Indeed, a natural question that arrises here is how are we going to detect the number of sources. Since the JADED approach is automated to give peaks around the AoA/ToA, then a heuristic approach of picking the peaks is to set a certain threshold, which is determined through practice. This step should be done after normalising the JADED spectrum such that the highest peak is equal to 1. In addition, we have observed that peaks corresponding to true locations have almost the same altitude, which could further ease the detection criterion. We would also like to note that false peaks are inevitable at low SNR.

5.6 Conclusions and future directions

There are some contributions that should be highlighted: We have proposed a novel approach for joint estimation and detection of Angles and Times of arrival, i.e. JADED. Two methods were derived so as to solve the JADED problem using Rotational Invariance Properties (RIP), which arises when a ULA receives known OFDM symbols. The JADED-RIP method performs a 2D search of a suitable cost function, where each peak indicates a present source with corresponding ToA/AoA. The second algorithm, CESS-JADED-RIP, is a faster version of JADED-RIP, which can be used for single snapshot scenarios only. The algorithms function properly in the presence of coherent sources, since subspace extraction is not needed, as in the case of MUSIC, ESPRIT, and other subspace methods.

Future work should address the following points:

- Improving JADED-RIP, by taking into account the colored noise in equation (**??**), which leads to an ML estimator.
- Deriving analytic MSE expressions and the optimal values of P_N and P_M.
- Proposing a JADED algorithm that operates for arbitrary arrays, such as uniform circular arrays.
- Taking into account hardware imperfections, such as antenna calibration and mutual coupling, synchronization errors, etc. This could further empower JADED as a competitive candidate among other indoor positioning methods.

Chapter 6

Mutual Coupling

In this chapter, we study an important aspect that perturbs Angle-of-Arrival estimation, due to antenna coupling, also known as "Mutual Coupling". The contributions are summarised as follows: (i) we derive a sub-optimal algorithm that could estimate AoAs in the presence of mutual coupling; (ii) we show why this sub-optimal algorithm, along with other ones, are indeed suboptimal, in the sense that there is an upper bound on the coupling parameters allowed in the model; (iii) then, we further improve the sub-optimal algorithm and propose an optimal one, in the sense that more coupling parameters are allowed in the model; (iv) then, we refine the estimates of the optimal algorithm by modifying some constraints of the optimisation problem considered; (v) we derive the MSE expression of the optimal algorithm and show that, in some cases, we can attain the Cramér-Rao bound of the problem of joint coupling parameters and AoA estimation; (vi) finally, we derive an iterative method that could give Maximum Likelihood (ML) estimates of the AoAs, and therefore allowing the presence of coherent sources, which is not the case of all the previous algorithms.

6.1 System model

6.1.1 Problem formulation

The previous chapters considered an ideal model, in the sense that no mutual coupling was included in the model. Recall equation (2.8), which is the AoA estimation problem, i.e.

$$\boldsymbol{X} = \boldsymbol{A}(\boldsymbol{\Theta})\boldsymbol{S} + \boldsymbol{W}$$

where all quantities have been defined in Chapter 2. Equation (2.8) assumes an ideal model, in the sense that each antenna acts independently of all the others. In reality, the current developed in an antenna element depends on its own excitation and on the contributions from adjacent antennas. As a consequence, an ideal model is no longer valid. This phenomenon is called "Mutual Coupling" between array elements, and it enters the model as follows [85]

$$\widetilde{\boldsymbol{X}} = \boldsymbol{T}(\boldsymbol{c})\boldsymbol{A}(\boldsymbol{\Theta})\boldsymbol{S} + \boldsymbol{W} \tag{6.1}$$

where $\boldsymbol{T}(\boldsymbol{c}) \in \mathbb{C}^{N\times N}$ captures the effect of mutual coupling, and is known as the "Mutual Coupling Matrix" (MCM). Due to the linear and uniform configuration of the different elements of the array, the MCM $\boldsymbol{T}(\boldsymbol{c})$ is given by a symmetric Toeplitz matrix, i.e.

$$\boldsymbol{T}(\boldsymbol{c}) = \begin{bmatrix} c_0 & c_1 & c_2 & \cdots & c_{p-1} & 0 & \cdots & 0 \\ c_1 & c_0 & c_1 & \cdots & c_{p-2} & c_{p-1} & \cdots & 0 \\ \vdots & & & \ddots & \ddots & & & \vdots \\ 0 & \cdots & c_{p-1} & c_{p-2} & \cdots & c_1 & c_0 & c_1 \\ 0 & \cdots & 0 & c_{p-1} & \cdots & c_2 & c_1 & c_0 \end{bmatrix} \tag{6.2}$$

Let c_i be the coupling coefficient between two elements placed i inter-element spacings apart. Since the amplitude of the coupling parameters tend to decay as a function of increasing distance, namely

$$1 > |c_1| > \ldots > |c_{N-1}| \tag{6.3}$$

then a well-approximation of $\boldsymbol{T}(\boldsymbol{c})$ is a banded symmetric Toeplitz matrix [86, 87] with bandwidth p. In other words, antennas that are placed at least p inter-element spacings apart do not interfere, i.e. $c_i = 0$ for all $i \geq p$. In what follows, the MCM of a ULA configuration is modelled as banded symmetric Toeplitz matrix of bandwidth p and denoted as $\boldsymbol{T}(\boldsymbol{c})$, where $\boldsymbol{c} = [1, c_1 \ldots c_{p-1}]^{\mathrm{T}}$ is the vector of coupling parameters.

6.1.2 Assumptions

For both problems above, we shall assume the following:

- **A1**: Matrix $\boldsymbol{A}$ is full column rank.
- **A2**: The noise $\boldsymbol{w}(l)$ is modelled as a white circular complex Gaussian process of zero mean and covariance $\sigma^2\boldsymbol{I}$ and independent from the source signals.
- **A3**: For simplicity, the number of source signals q is known.
- **A4**: The source signals are allowed to be partially correlated, but not coherent.

6.1.3 Problem statement

We are now ready to address our online calibration problem:
"Given $\boldsymbol{X}$, q, and p, estimate the angles of arrival $\boldsymbol{\Theta}$ of the incoming signals in the presence of mutual coupling $\boldsymbol{T}(\boldsymbol{c})$."

6.2 The MUSIC Algorithm

6.2.1 Preliminaries

This subsection serves as a review of the MUSIC algorithm, in the absence of mutual coupling. In other words, the model in equation (2.8) is assumed. The covariance matrix of the received data could be written as

$$\begin{aligned} \boldsymbol{R_{xx}} &\triangleq \mathbb{E}\{\boldsymbol{x}(t)\boldsymbol{x}^{\mathrm{H}}(t)\} \\ &= \boldsymbol{A}(\boldsymbol{\Theta})\boldsymbol{R_{ss}}\boldsymbol{A}^{\mathrm{H}}(\boldsymbol{\Theta}) + \sigma^2\boldsymbol{I} \end{aligned} \tag{6.4}$$

where the second equality is due to *Assumption 5* and

$$\boldsymbol{R_{ss}} \triangleq \mathbb{E}\{\boldsymbol{s}(t)\boldsymbol{s}^{\mathrm{H}}(t)\} \tag{6.5}$$

is the source covariance matrix. Using spectral decomposition, the matrix $\boldsymbol{R_{xx}}$ is expressed as

$$\begin{aligned} \boldsymbol{R_{xx}} &= \left[\begin{array}{c|c} \boldsymbol{U_s} & \boldsymbol{U_n} \end{array}\right] \left[\begin{array}{c|c} \boldsymbol{\Sigma_s} & \boldsymbol{0} \\ \hline \boldsymbol{0} & \boldsymbol{\Sigma_n} \end{array}\right] \left[\begin{array}{c|c} \boldsymbol{U_s} & \boldsymbol{U_n} \end{array}\right]^{\mathrm{H}} \\ &= \boldsymbol{U_s}\boldsymbol{\Sigma_s}\boldsymbol{U_s}^{\mathrm{H}} + \boldsymbol{U_n}\boldsymbol{\Sigma_n}\boldsymbol{U_n}^{\mathrm{H}} \end{aligned} \tag{6.6}$$

The partitioning in equation (6.6) is done because $\boldsymbol{R_{xx}}$ is composed of two major parts: Signal and Noise. The signal part $\boldsymbol{A}(\boldsymbol{\Theta})\boldsymbol{R_{ss}}\boldsymbol{A}^{\mathrm{H}}(\boldsymbol{\Theta})$ is rank q, under *Assumptions 1* and *3*. Therefore, due to the noise part $\sigma^2\boldsymbol{I}$, one can say that $\boldsymbol{\Sigma_s}$ is a $q \times q$ diagonal matrix composed of eigenvalues strictly greater than σ^2 and $\boldsymbol{\Sigma_n} = \sigma^2\boldsymbol{I}_{N-q}$. The eigenvectors $\boldsymbol{U_s}$ and $\boldsymbol{U_n}$ are, often, referred to as the *signal* and *noise subspaces*, respectively.
In the absence of mutual coupling, the key to MUSIC is the following observation:

$$\|\boldsymbol{U_n}^{\mathrm{H}}\boldsymbol{a}(\theta)\|^2 = 0 \Longrightarrow \theta \in \boldsymbol{\Theta} \tag{6.7}$$

In practice, one could estimate the covariance quantities through sample averaging, viz.

$$\widehat{\boldsymbol{R}}_{\boldsymbol{xx}} = \frac{1}{L}\boldsymbol{X}\boldsymbol{X}^{\mathrm{H}} = \widehat{\boldsymbol{U}}_{\boldsymbol{s}}\widehat{\boldsymbol{\Sigma}}_{\boldsymbol{s}}\widehat{\boldsymbol{U}}_{\boldsymbol{s}}^{\mathrm{H}} + \widehat{\boldsymbol{U}}_{\boldsymbol{n}}\widehat{\boldsymbol{\Sigma}}_{\boldsymbol{n}}\widehat{\boldsymbol{U}}_{\boldsymbol{n}}^{\mathrm{H}} \tag{6.8}$$

MUSIC estimates the angles-of-arrival $\boldsymbol{\Theta}$ through peak finding, as follows

$$\{\widehat{\theta}_i\}_{i=1}^{q} = \arg\max_{\theta} \frac{1}{\boldsymbol{a}^{\mathrm{H}}(\theta)\widehat{\boldsymbol{U}}_{\boldsymbol{n}}\widehat{\boldsymbol{U}}_{\boldsymbol{n}}^{\mathrm{H}}\boldsymbol{a}(\theta)} \tag{6.9}$$

6.2.2 Mutual Coupling in the sense of MUSIC

The previous subsection tells us that one can estimate the angles-of-arrival in the absence of mutual coupling by performing a 1D-search according to equation (6.9). Now, for the ease of exposition, let $\bar{\boldsymbol{a}}(\theta)$ denote the steering vector in the presence of mutual coupling, i.e.

$$\bar{\boldsymbol{a}}(\theta) = \boldsymbol{T}(\boldsymbol{c})\boldsymbol{a}(\theta) \tag{6.10}$$

Similarly, define $\bar{\boldsymbol{A}}(\boldsymbol{\Theta})$ as follows

$$\bar{\boldsymbol{A}}(\boldsymbol{\Theta}) = \boldsymbol{T}(\boldsymbol{c})\boldsymbol{A}(\boldsymbol{\Theta}) = [\bar{\boldsymbol{a}}(\theta_1)\dots\bar{\boldsymbol{a}}(\theta_q)] \tag{6.11}$$

Taking into account mutual coupling, i.e. the model in equation (6.1), one could follow the same steps from equation (6.4) till (6.8) in order to say that the angles-of-arrival could be estimated as follows

$$\{\widehat{\theta}_i\}_{i=1}^{q} = \arg\max_{\theta} \frac{1}{\bar{\boldsymbol{a}}^{\mathrm{H}}(\theta)\widehat{\boldsymbol{U}}_{\boldsymbol{n}}\widehat{\boldsymbol{U}}_{\boldsymbol{n}}^{\mathrm{H}}\bar{\boldsymbol{a}}(\theta)} \tag{6.12}$$

where $\widehat{\boldsymbol{U}}_{\boldsymbol{n}}$ is the sample estimate of $\boldsymbol{U}_{\boldsymbol{n}}$. Throughout the rest of this paper, $\boldsymbol{U}_{\boldsymbol{n}}$ is the noise subspace, namely $\boldsymbol{U}_{\boldsymbol{n}}\boldsymbol{U}_{\boldsymbol{n}}^{\mathrm{H}} = \boldsymbol{P}_{\bar{\boldsymbol{A}}}^{\perp} = \boldsymbol{I} - \boldsymbol{P}_{\bar{\boldsymbol{A}}}$, where

$$\boldsymbol{P}_{\bar{\boldsymbol{A}}} = \bar{\boldsymbol{A}}(\bar{\boldsymbol{A}}^{\mathrm{H}}\bar{\boldsymbol{A}})^{-1}\bar{\boldsymbol{A}}^{\mathrm{H}} \tag{6.13}$$

However, applying MUSIC directly as in equation (6.12) to the problem in hand is not possible, since the functional form of the steering vector is not known. In other terms, we have partial knowledge of vector $\bar{\boldsymbol{a}}(\theta)$, which is that it is a known *Vandermonde* vector $\boldsymbol{a}(\theta)$ pre-multiplied by an unknown banded symmetric Toeplitz matrix $\boldsymbol{T}(\boldsymbol{c})$, as in equation (6.10). Nevertheless, MUSIC implies the following

$$\|\boldsymbol{U}_{\boldsymbol{n}}^{\mathrm{H}}\boldsymbol{T}(\boldsymbol{m})\boldsymbol{a}(\theta)\|^2 = 0 \Longrightarrow \{\theta \in \boldsymbol{\Theta} \text{ and } \boldsymbol{m} = \boldsymbol{c}\} \tag{6.14}$$

In order to proceed, we find the following theorem useful:

Theorem 6.1. *Let* $\boldsymbol{\alpha} = [\alpha_0, \alpha_1 \dots \alpha_{p-1}]^T \in \mathbb{C}^{p\times 1}$ *and* $\boldsymbol{a} \in \mathbb{C}^{N\times 1}$. *Define the corresponding matrix* $\boldsymbol{T}(\boldsymbol{\alpha})$. *Then the following is true for any* $1 \leq p \leq N$

$$\boldsymbol{T}(\boldsymbol{\alpha})\boldsymbol{a} = \boldsymbol{B}_p\boldsymbol{\alpha} \tag{6.15}$$

where $\boldsymbol{B}_p = \mathcal{G}_p(\boldsymbol{a})$. *where*

$$\boldsymbol{B}_p = \left[\begin{array}{c|c|c|c} \boldsymbol{a} & \boldsymbol{S}_1\boldsymbol{a} & \dots & \boldsymbol{S}_{p-1}\boldsymbol{a} \end{array} \right] \tag{6.16}$$

and $\boldsymbol{S}_k \in \mathbb{C}^{N\times N}$ *is an all-zero matrix except at the* k^{th} *sub- and super-diagonals, which are set to 1.*

Proof. See Appendix B. □

Using this theorem, we can say that

$$\bar{\boldsymbol{a}}(\theta) = \boldsymbol{T}(\boldsymbol{c})\boldsymbol{a}(\theta) = \boldsymbol{B}(\theta)\boldsymbol{c} \tag{6.17}$$

where

$$\boldsymbol{B}(\theta) = \mathcal{G}_p(\boldsymbol{a}(\theta)) \tag{6.18}$$

Therefore, equation (6.14) could be re-written as

$$\|\boldsymbol{U}_{\boldsymbol{n}}^{\mathrm{H}}\boldsymbol{B}(\theta)\boldsymbol{m}\|^2 = 0 \Longrightarrow \{\theta \in \boldsymbol{\Theta} \text{ and } \boldsymbol{m} = \boldsymbol{c}\} \tag{6.19}$$

Said differently and in a more compact way, equation (6.19) also means

$$\left\| \begin{bmatrix} \boldsymbol{U}_{\boldsymbol{n}}^{\mathrm{H}}\boldsymbol{B}(\theta_1) \\ \vdots \\ \boldsymbol{U}_{\boldsymbol{n}}^{\mathrm{H}}\boldsymbol{B}(\theta_q) \end{bmatrix} \boldsymbol{m} \right\|^2 = 0 \Longrightarrow \boldsymbol{m} = \boldsymbol{c} \tag{6.20}$$

Therefore, one way to formulate the problem is

$$(\mathcal{P}_1): \min_{\boldsymbol{m},\bar{\theta}_1\dots\bar{\theta}_q} \boldsymbol{m}^{\mathrm{H}}\widehat{\boldsymbol{S}}(\bar{\theta}_1 \dots \bar{\theta}_q)\boldsymbol{m} \tag{6.21}$$

where

$$\widehat{\boldsymbol{S}}(\theta_1 \dots \theta_q) = \begin{bmatrix} \widehat{\boldsymbol{U}}_{\boldsymbol{n}}^{\mathrm{H}}\boldsymbol{B}(\theta_1) \\ \vdots \\ \widehat{\boldsymbol{U}}_{\boldsymbol{n}}^{\mathrm{H}}\boldsymbol{B}(\theta_q) \end{bmatrix}^{\mathrm{H}} \begin{bmatrix} \widehat{\boldsymbol{U}}_{\boldsymbol{n}}^{\mathrm{H}}\boldsymbol{B}(\theta_1) \\ \vdots \\ \widehat{\boldsymbol{U}}_{\boldsymbol{n}}^{\mathrm{H}}\boldsymbol{B}(\theta_q) \end{bmatrix} = \sum_{j=1}^{q} \widehat{\boldsymbol{K}}(\theta_j) \tag{6.22}$$

where

$$\widehat{\boldsymbol{K}}(\theta) = \boldsymbol{B}(\theta)\widehat{\boldsymbol{U}}_{\boldsymbol{n}}\widehat{\boldsymbol{U}}_{\boldsymbol{n}}^{\mathrm{H}}\boldsymbol{B}(\theta) \tag{6.23}$$

Assuming true subspaces (i.e. $\widehat{\boldsymbol{U}}_{\boldsymbol{n}} = \boldsymbol{U}_{\boldsymbol{n}}$) and excluding the trivial solution $\boldsymbol{m} = \boldsymbol{0}$, it is clear that one solution of problem $(\mathcal{P}_1)$ is attained when $\boldsymbol{m} = \boldsymbol{c}$ and $[\bar{\theta}_1 \dots \bar{\theta}_q] = [\theta_1 \dots \theta_q] = \boldsymbol{\Theta}$. Said differently, $\boldsymbol{S}(\boldsymbol{\Theta})$ admits a null space of dimension 1 spanned by the vector of coupling parameters, $\boldsymbol{c}$.
In any case, this is a multidimensional problem in the AoA parameters, and a number of papers have resorted to an alternative and sub-optimal problem, namely

$$(\mathcal{P}_2): \min_{\boldsymbol{m},\theta} \boldsymbol{m}^{\mathrm{H}} \widehat{\boldsymbol{K}}(\theta) \boldsymbol{m} \tag{6.24}$$

The sub-optimality here has a nice interpretation: It is "as if" the coupling parameters are treated to be angular-dependent and therefore, one does not acknowledge that the vector of coupling parameters $\boldsymbol{c}$ is fixed for any θ. Consequently, the objective function in $(\mathcal{P}_2)$ would have been a reasonable choice if the coupling parameters are a function of θ, i.e. $\boldsymbol{c} = \boldsymbol{c}(\theta)$. *Surprisingly, a problem involving angular-dependent coupling parameters suggests a computationally less optimisation problem in terms of the AoA parameters.* Indeed, this approach is sub-optimal when $\boldsymbol{c}$ is independent of θ.

6.3 A suboptimal MUSIC-based approach

6.3.1 Algorithm derivation

Let us consider problem $(\mathcal{P}_2)$ under an affine constraint

$$\begin{aligned} \underset{\boldsymbol{m},\theta}{\text{minimize}} \quad & \boldsymbol{m}^{\mathrm{H}} \widehat{\boldsymbol{K}}(\theta) \boldsymbol{m} \\ \text{subject to} \quad & \boldsymbol{e}_1^H \boldsymbol{m} = 1 \end{aligned} \tag{6.25}$$

The Lagrangian function corresponding to the optimisation problem in (6.25) is the following:

$$\mathcal{L}(\boldsymbol{m}, \alpha) = \boldsymbol{m}^{\mathrm{H}} \boldsymbol{K}(\theta) \boldsymbol{m} - \alpha\left(\boldsymbol{e}_{\boldsymbol{1}}^{\mathbf{H}} \boldsymbol{m} - 1\right) \tag{6.26}$$

Setting the derivative of $\mathcal{L}(\boldsymbol{m}, \boldsymbol{\alpha})$ with respect to $\boldsymbol{m}$ to 0, we get

$$\frac{\partial}{\partial \boldsymbol{m}} \mathcal{L}(\boldsymbol{m}, \alpha) = 2\boldsymbol{K}(\theta)\boldsymbol{m} - \alpha \boldsymbol{e}_{\boldsymbol{1}} = 0 \tag{6.27}$$

Equation (6.27) gives the optimal coupling parameters, $\boldsymbol{m}^*$, for a given θ, in terms of the optimal Lagrangian multiplier α^* as

$$\boldsymbol{m}^* = \frac{\alpha^*}{2} \boldsymbol{K}(\theta)^{-1} \boldsymbol{e}_{\boldsymbol{1}} \tag{6.28}$$

Now plugging the expression of $\boldsymbol{m}^*$ in the constraint of the optimisation problem in (6.25) yields the optimal value of α^*

$$\alpha^* = \frac{2}{\mathbf{e_1^H} \boldsymbol{K}(\theta)^{-1} \mathbf{e_1}} \tag{6.29}$$

Therefore, $\boldsymbol{m}^*$ is now given as

$$\boldsymbol{m}^* = \frac{\boldsymbol{K}(\theta)^{-1} \mathbf{e_1}}{\mathbf{e_1^H} \boldsymbol{K}(\theta)^{-1} \mathbf{e_1}} \tag{6.30}$$

Finally, plugging the expression of $\boldsymbol{m}^*$ in the MUSIC cost function in (6.24), we get

$$\{\hat{\theta}_i\}_{i=1}^{q} = \arg\max_{\theta} \mathbf{e_1^H} \boldsymbol{K}(\theta)^{-1} \mathbf{e_1} \tag{6.31}$$

To prove the existance and uniqueness of $\boldsymbol{m}^*$, we need the following Lemma:

Lemma 6.2. *[83] Consider the "Equality Constrained Quadratic Optimisation" problem given in equation (6.25). Equations (6.27) and the constraint in equation (6.25) together are written in matrix form as:*

$$\underbrace{\begin{bmatrix} \boldsymbol{K}(\theta) & -\mathbf{e_1} \\ \mathbf{e_1^H} & 0 \end{bmatrix}}_{\triangleq \boldsymbol{\mathcal{M}}} \begin{bmatrix} \boldsymbol{m} \\ \alpha \end{bmatrix} = \begin{bmatrix} \mathbf{0} \\ 1 \end{bmatrix} \tag{6.32}$$

The coefficient matrix $\boldsymbol{\mathcal{M}}$ is referred to as the KKT matrix [83].
Let $[\boldsymbol{m}^*, \alpha^*]^T$ denote a solution of (6.32).
The following holds:

- *The KKT matrix $\boldsymbol{\mathcal{M}}$ is nonsingular, and therefore invertible.*
- *The solution $[\boldsymbol{m}^*, \alpha^*]^T$ is the unique global solution of the equality constrained quadratic problem in equation (6.25).*

if and only if:

- *Assumption 1: The matrix $\mathbf{e_1^H}$ has linearly independent rows.*
- *Assumption 2: The matrix $\boldsymbol{K}(\theta)$ is positive definite in the null space of $\mathbf{e_1^H}$, i.e. $\boldsymbol{z}^H \boldsymbol{K}(\theta) \boldsymbol{z} > 0$ for all $\boldsymbol{z} \neq 0$ satisfying $\mathbf{e_1^H} \boldsymbol{z} = 0$.*

Using the above **Lemma**, we have the following Theorem:

Theorem 6.3. *The solution $[\boldsymbol{m}^*, \alpha^*]^T$ is the unique global solution if and only if $q + p < N + 1$ and $p \leq \frac{N}{2}$.*

Proof. See Appendix C □

6.3.2 Discussion

Theorem 6.3 p rovides a sufficient and necessary condition for the existance and uniqueness of the coupling parameters $\boldsymbol{m}^*$ using the proposed algorithm, i.e. $p+q < N+1$ and $p \leq \frac{N}{2}$. However, the identifiability condition in [88] is the following: $2p + q \leq N + 1$. One could, thus, easily verify that the proposed algorithm could resolve more sources.

We would strongly like to note that we have not addressed the coupling estimation part as the optimisation was first done over $\boldsymbol{m}$, then the solution of $\boldsymbol{m}$ (i.e. $\boldsymbol{m}^*$) was substituted back in the MUSIC cost function. In other words, the vector $\boldsymbol{m}^*$ was treated as a nuissance parameter. The problem of estimating the coupling parameters $\boldsymbol{m}$ is beyond the scope of this paper. Once again, our aim is estimating the AoAs of multiple sources in the presence of mutual coupling.

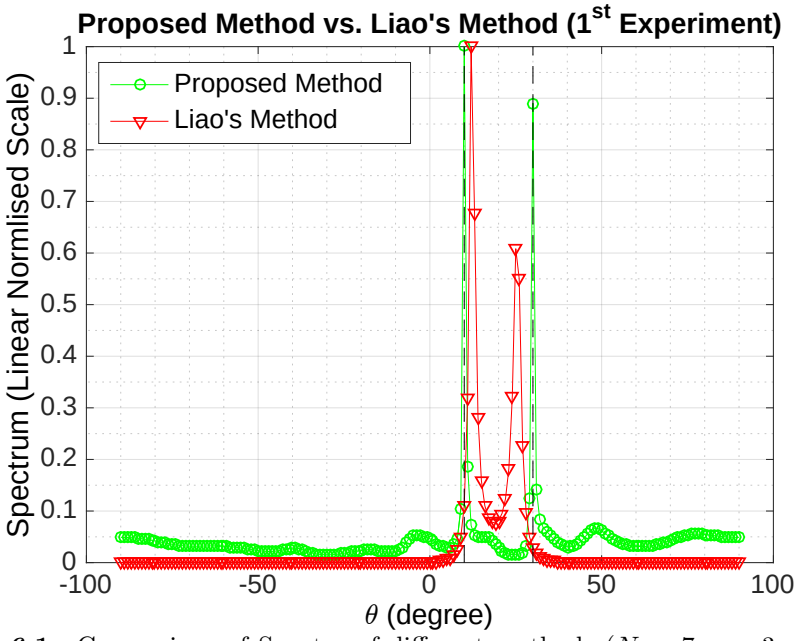

Figure 6.1: Comparison of Spectra of different methods ($N = 7, p = 3, q = 2, L = 100$). Vertical dashed lines correspond to the true AoAs.

Now, we present our simulation results regarding the proposed method and compare with the method presented by Liao *et Al.* [88]. In the first experiment, consider a ULA array that is composed of $N = 7$ antennas spaced at $\frac{\lambda}{2}$. Furthermore, assume two sources impinging the array at $\theta_1 = 10°$ and $\theta_2 = 30°$. As for the mutual coupling, we fix $p = 3$, with $t_1 = -0.95 - 1.29j$ and $t_2 = -0.05 + 0.25j$. The SNR is set to 9 dB and the number of snapshots $L = 100$. Figure 6.1 depicts the spectrum of our method versus Liao's method for this situation. The vertical dashed lines correspond to the true AoAs.

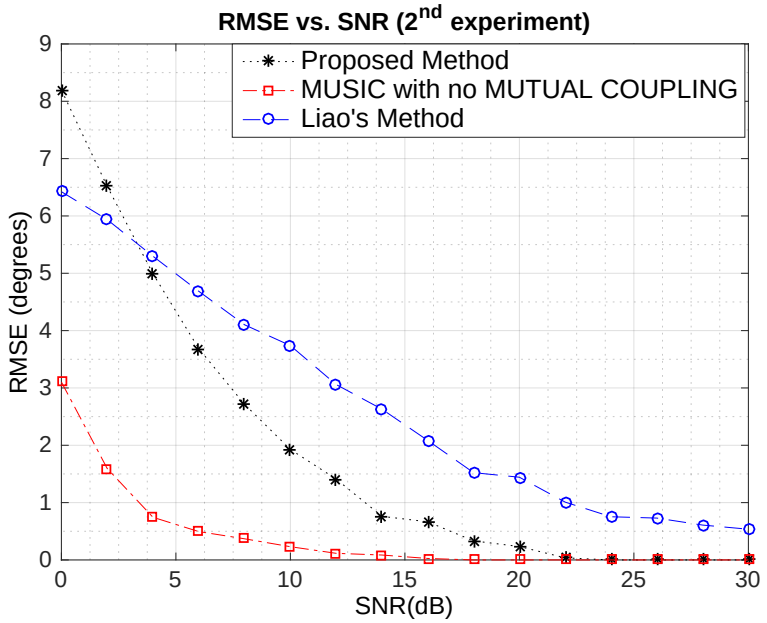

Figure 6.2: RMSE on a linear scale vs. SNR of experiment 2.

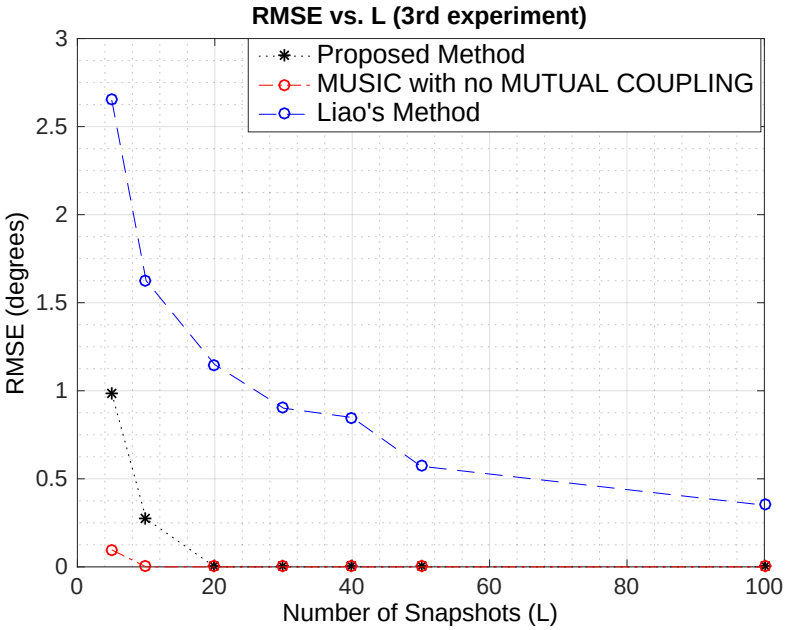

Figure 6.3: RMSE on a linear scale vs. Number of Snapshots of experiment 3.

We can clearly see that our method peaks at the true AoAs, whereas Liao's method is biased away from the true values.

In the second experiment (i.e. Figure 6.2), we fix $N = 10$ antennas, $q = 3$ sources arriving at $\theta_1 = 10°$, $\theta_2 = 20°$, and $\theta_3 = 30°$. The number of coupling parameters is $p = 3$. The number of snapshots $L = 100$. The number of Monte-Carlo trials is $M = 500$. In addition, at each trial, the coupling parameters are chosen randomly to assess generality of our RMSE curves. We notice that our proposed method exhibits an improvement of around 1.5°, in average, in terms of RMSE when 5 dB $<$ SNR $<$ 20 dB.

Interestingly, when SNR > 22 dB, our method coincides with MUSIC ("coupling-free" MUSIC, that is) and the RMSE is 0, whereas Liao's method still shows some error of around 0.75° RMSE.

In the third experiment (i.e. Figure 6.3) ,we plot RMSE vs. number of snapshots (L) at fixed SNR. The parameters q, $\boldsymbol{\Theta}$, N, M, and p are the same as those in the 2^{nd} experiment. The SNR is set to 30 dB. Again, we observe that our proposed method performs better than Liao's. When the number of snapshots exceeds 20, our method shows zero RMSE and coincides with "coupling-free" MUSIC. However, Liao's method shows error even when the number of snapshots reach 100.

6.4 An optimal MUSIC-based approach

6.4.1 Preliminaries

Theorem 6.4. *Let* $\boldsymbol{\alpha}_p = [\alpha_0, \alpha_1 \dots \alpha_{p-1}]^T$ *and* $\boldsymbol{a} = [1, z \dots z^{N-1}]^T$. *Define the corresponding matrix* $\boldsymbol{T}(\boldsymbol{\alpha}_p)$. *Then for any* $1 \leq p \leq N$, *the following holds*

$$\boldsymbol{T}(\boldsymbol{\alpha}_p)\boldsymbol{a} = g(z, \boldsymbol{\alpha}_p)\boldsymbol{a} - \boldsymbol{M}_p\widetilde{\boldsymbol{\alpha}}_p \tag{6.33}$$

where the polynomial $g(z, \boldsymbol{\alpha})$ *is given by*

$$g(z, \boldsymbol{\alpha}_p) = \alpha_0 + \sum_{k=1}^{p-1} \alpha_k (z^k + z^{-k}) \tag{6.34}$$

The matrix $\boldsymbol{M}_p \in \mathbb{C}^{N \times (p-1)}$ *is defined as*

$$\boldsymbol{M}_p = \left[\frac{\boldsymbol{U}_p}{\boldsymbol{0}}\right] + \left[\frac{\boldsymbol{0}}{\boldsymbol{L}_p}\right] \tag{6.35}$$

with

$$\boldsymbol{U}_p = \begin{bmatrix} z^{-1} & z^{-2} & \dots & z^{-(p-1)} \\ 0 & z^{-1} & \dots & z^{-(p-2)} \\ \vdots & \ddots & \ddots & \vdots \\ 0 & \cdots & 0 & z^{-1} \end{bmatrix} \tag{6.36}$$

$$\boldsymbol{L}_p = \begin{bmatrix} 0 & \cdots & 0 & z^N \\ \vdots & \iddots & \iddots & \vdots \\ 0 & z^N & \dots & z^{N+p-3} \\ z^N & z^{N+1} & \dots & z^{N+p-2} \end{bmatrix} \tag{6.37}$$

and

$$\widetilde{\boldsymbol{\alpha}}_p = [\alpha_1, \alpha_2 \dots \alpha_{p-1}]^T \tag{6.38}$$

Proof. See Appendix D □

Theorem 6.4 is key to Theorem 6.5, which comes next:

Theorem 6.5. *Let* $\boldsymbol{a} = [1, z \dots z^{N-1}]^T$ *and* $\boldsymbol{B}_p = \mathcal{G}_p(\boldsymbol{a})$. *Then,* $\boldsymbol{B}_p$ *has the following spectral characteristics:*

1. *If* $p \leq \frac{N+1}{2}$, *then* $\boldsymbol{B}_p$ *is full column rank.*
2. *If* $p = \frac{N+2}{2}$ *and* z *is an* N^{th} *unit root (i.e.* $z^N = 1$*) then* $rank(\boldsymbol{B}_p) = \frac{N}{2}$. *The null space is given in equation (E.11). Otherwise, it is full column rank.*
3. *We distinguish 2 cases when* $p > \frac{N+2}{2}$*:*
   (a) *N is even:*
      i. *If* $z^N \neq \pm 1$, *then* $\boldsymbol{B}_p$ *is full column rank.*
      ii. *If* $z^N = -1$, *then* $rank(\boldsymbol{B}_p) = \frac{N}{2} + 1$. *The null space is given in equation (E.30).*
      iii. *If* $z^N = 1$, *then* $rank(\boldsymbol{B}_p) = \frac{N}{2}$. *The null space is given in equation (E.34).*
   (b) *N is odd:*
      i. *If* $z^N = \pm 1$, *then* $rank(\boldsymbol{B}_p) = \frac{N+1}{2}$. *The null space is given in equation (E.35).*
      ii. *Otherwise,* $\boldsymbol{B}_p$ *is full column rank.*

Proof. See Appendix E □

Theorem 6.6. *For ULA type configurations, i.e.* $\boldsymbol{a}(\theta) = [1, z_\theta, \dots z_\theta^{N-1}]^T$ *with* $z_\theta = e^{-j2\pi \frac{d}{\lambda} sin(\theta)}$. *Define the following sets*

$$\boldsymbol{\Theta_+} = \left\{ sin^{-1}\left(\frac{k\lambda}{Nd}\right), \quad k = -\frac{N}{2} \dots \frac{N}{2} \right\} \tag{6.39}$$

$$\boldsymbol{\Theta_-} = \left\{ sin^{-1}\left(\frac{(k+\frac{1}{2})\lambda}{Nd}\right), \quad k = -\frac{N}{2} \dots \frac{N}{2} \right\} \tag{6.40}$$

$$\boldsymbol{\Theta_\pm} = \left\{ \boldsymbol{\Theta_+} \cup \boldsymbol{\Theta_-} \right\} \tag{6.41}$$

The matrix $\boldsymbol{B}(\theta) = \mathcal{G}_p(\boldsymbol{a}(\theta))$ *has the following characteristics:*

- *If* $p < \frac{N+2}{2}$, *the matrix* $\boldsymbol{B}(\theta)$ *is full column rank.*

- *When* $p \geq \frac{N+2}{2}$*, we distinguish the following cases:*
  - *If* N *is even and* $\theta \in \boldsymbol{\Theta_+}$*, then rank*$(\boldsymbol{B}(\theta)) = \frac{N}{2}$.
  - *If* N *is even and* $\theta \in \boldsymbol{\Theta_-}$*, then rank*$(\boldsymbol{B}(\theta)) = \frac{N}{2} + 1$.
  - *If* N *is odd and* $\theta \in \boldsymbol{\Theta_\pm}$*, then rank*$(\boldsymbol{B}(\theta)) = \frac{N+1}{2}$.
  - *Else* $\boldsymbol{B}(\theta)$ *is full column rank.*

Proof. See Appendix F □

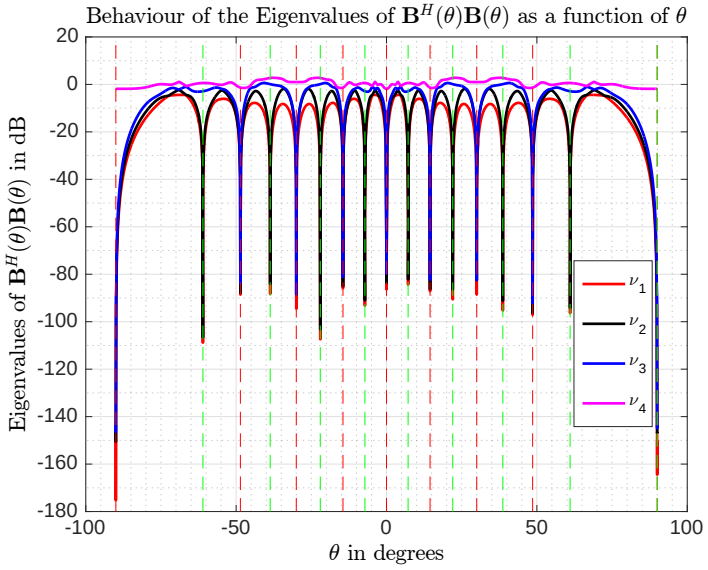

(a) $N = 8$ and $p = 7$

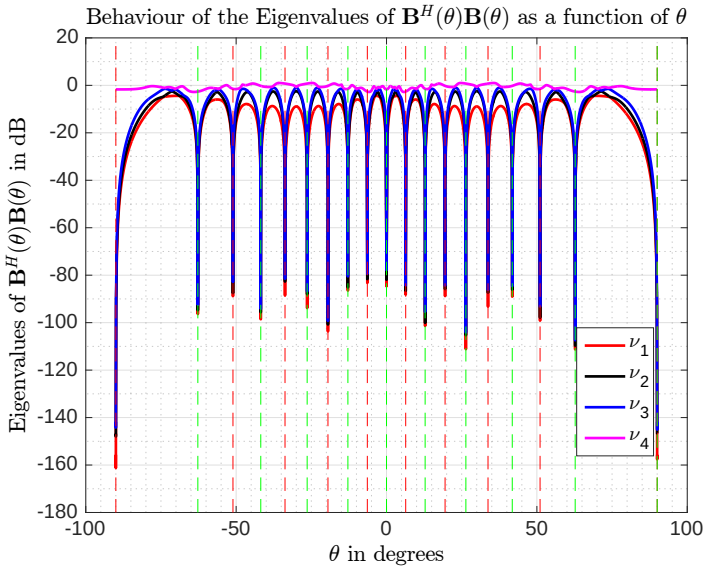

(b) $N = 9$ and $p = 8$

Figure 6.4: Eigenvalues of $\boldsymbol{B}^{\mathrm{H}}(\theta)\boldsymbol{B}(\theta)$ as a function of θ for different values of N and p.

It is important to understand the behaviour of matrix $\boldsymbol{B}(\theta)$ as function of θ. Let $\nu_1 \leq \nu_2 \leq \ldots \leq \nu_p$ be the eigenvalues of $\boldsymbol{B}^{\mathrm{H}}(\theta)\boldsymbol{B}(\theta)$. In order to partially verify ***Theorem 6.6***, we have depicted two figures where $p > \frac{N+2}{2}$. In Fig. 6.4a, we fix $N = 8$ (even) and $p = 7$. The red and green dashed vertical lines correspond to angles in $\boldsymbol{\Theta_+}$ and $\boldsymbol{\Theta_-}$, respectively. Observe that when θ approaches angles in $\boldsymbol{\Theta_+}$, we have three eigenvalues, i.e. ν_1, ν_2, and ν_3, dropping to zero. This implies that, when $\theta \in \boldsymbol{\Theta_+}$, the rank of $\boldsymbol{B}(\theta)$ is $p - 3 = 4 = \frac{N}{2}$. However, when when $\theta \in \boldsymbol{\Theta_-}$, only two eigenvalues, namely ν_1 and ν_2, go to zero. In this case, the rank of $\boldsymbol{B}(\theta)$ is $p - 2 = 5 = \frac{N}{2} + 1$. Also note that ν_4 is strictly positive. In Fig. 6.4b, we fix $N = 9$ (odd) and $p = 8$. Again, ν_4 is strictly positive. When $\theta \in \boldsymbol{\Theta_\pm}$, three eigenvalues go to zero, implying that the rank of $\boldsymbol{B}(\theta)$ is $p - 3 = 5 = \frac{N+1}{2}$.

6.4.2 Algorithm derivation

The previous subsection reveals an important phenomenon of matrix $\boldsymbol{B}(\theta)$. According to ***Theorem 6.6***, if $\theta_k \in \boldsymbol{\Theta_\pm}$ and $p \geq \frac{N+2}{2}$, then $\boldsymbol{B}(\theta_k)$ admits a null-space. Therefore, optimising the cost function given in $(\mathcal{P}_2)$, without choosing an appropriate constraint, gives false AoAs. Mathematically speaking, the cost function in $(\mathcal{P}_2)$ is exactly zero for all $\theta_k \in \boldsymbol{\Theta_\pm}$ when $p \geq \frac{N+2}{2}$. To circumvent this issue, we form the following optimisation problem

$$\begin{cases} \underset{\boldsymbol{m},\theta}{\text{minimize}} & \boldsymbol{m}^{\mathrm{H}}\widehat{\boldsymbol{K}}(\theta)\boldsymbol{m} \\ \text{subject to} & \boldsymbol{e}_1^{\mathrm{H}}\boldsymbol{B}(\theta)\boldsymbol{m} = 1 \end{cases} \tag{6.42}$$

It is easy to see that, for any θ, the trivial solution $\boldsymbol{m} = \boldsymbol{0}$ and the vectors that lie in the null space of $\boldsymbol{B}(\theta)$ (i.e. $\boldsymbol{B}(\theta)\boldsymbol{m} = 0$) are not feasible solutions because they do not satisfy the constraint. Therefore, optimising the above problem will exclude the latter false solutions.

The *Lagrangian* function corresponding to the optimisation problem in (6.42) is the following:

$$\mathcal{L}(\boldsymbol{m}, \nu) = \boldsymbol{m}^{\mathrm{H}}\widehat{\boldsymbol{K}}(\theta)\boldsymbol{m} - \nu\big(\boldsymbol{e}_1^{\mathrm{H}}\boldsymbol{B}(\theta)\boldsymbol{m} - 1\big) \tag{6.43}$$

Setting the derivative of $\mathcal{L}(\boldsymbol{m}, \nu)$ with respect to $\boldsymbol{m}$ to 0, we get

$$\frac{\partial}{\partial \boldsymbol{m}}\mathcal{L}(\boldsymbol{m}, \nu) = 2\widehat{\boldsymbol{K}}(\theta)\boldsymbol{m} - \nu\boldsymbol{B}^{\mathrm{H}}(\theta)\boldsymbol{e}_1 = 0 \tag{6.44}$$

Equation (6.44) gives the optimal coupling parameters, $\boldsymbol{m^o}$, for a given θ, in terms of the optimal Lagrangian multiplier ν^o as

$$\boldsymbol{m^o} = \frac{\nu^o}{2}\widehat{\boldsymbol{K}}^{-1}(\theta)\boldsymbol{B}^{\mathrm{H}}(\theta)\boldsymbol{e}_1 \tag{6.45}$$

It is easy to prove that

$$\boldsymbol{B}^{\mathrm{H}}(\theta)\boldsymbol{e}_1 = \boldsymbol{a}_p^*(\theta) \tag{6.46}$$

where $\boldsymbol{a}_p(\theta)$ is a $p\times 1$ vector defined as in equation (2.3). The expression of ν^o is obtained by plugging equations (6.45) and (6.46) in the constraint of the problem in (6.42), viz.

$$\nu^o = \frac{2}{\boldsymbol{a}_p^{\mathrm{T}}(\theta)\widehat{\boldsymbol{K}}^{-1}(\theta)\boldsymbol{a}_p^*(\theta)} \tag{6.47}$$

Therefore, $\boldsymbol{m^o}$ is now given as

$$\boldsymbol{m^o} = \frac{\widehat{\boldsymbol{K}}^{-1}(\theta)\boldsymbol{a}_p^*(\theta)}{\boldsymbol{a}_p^{\mathrm{T}}(\theta)\widehat{\boldsymbol{K}}^{-1}(\theta)\boldsymbol{a}_p^*(\theta)} \tag{6.48}$$

Substituting $\boldsymbol{m^o}$ in the objective function of (6.42), the q AoAs could be estimated as follows

$$\{\widehat{\theta}_k\}_{k=1}^{q} = \arg\min_{\theta} \frac{1}{f(\theta)} \tag{6.49a}$$

where

$$f(\theta) = \boldsymbol{a}_p^{\mathrm{T}}(\theta)\widehat{\boldsymbol{K}}^{-1}(\theta)\boldsymbol{a}_p^*(\theta) \tag{6.49b}$$

Note that $\widehat{\boldsymbol{K}}(\theta)$ is not invertible for the cases given in ***Theorem 6.6*** and when $\theta \in \boldsymbol{\Theta}$ at infinite SNR. For that, we adopt diagonal loading as done in [94], namely $\big(\boldsymbol{K}(\theta)+\epsilon\boldsymbol{I}\big)^{-1}$, where $\epsilon > 0$ is small. Additionally, it has been mentioned in [94] that there is generally no known method for determining the optimal value of ϵ, and it is usually determined experimentally. We have found that $\epsilon = 10^{-14}$ serves as a good value.

6.4.3 Properties of the algorithm

For a better understanding of the behaviour of the cost function given in equation (6.49), we reveal some of its properties

Property 1: *For $p = 1$, i.e. no mutual coupling, the function $f(\theta)$ "boils down" to the traditional MUSIC cost function in equation (6.9).*

Proof. Trivial. □

Property 2: *This property characterizes the null space of* $\boldsymbol{K}(\theta)$ *for* $p+q \leq N$ *as a function of* θ

$$\mathcal{N}(\boldsymbol{K}(\theta_i)) = \begin{cases} \{\boldsymbol{0}\}, & \text{if } \theta_i \notin \boldsymbol{\Theta} \cup \boldsymbol{\Theta}_{\pm} \\ \{\boldsymbol{0} \cup \boldsymbol{c}\}, & \text{if } \theta_i \in \boldsymbol{\Theta} \text{ and } \theta_i \notin \boldsymbol{\Theta}_{\pm} \\ \mathcal{N}\big(\boldsymbol{B}(\theta_i)\big), & \text{if } \theta_i \notin \boldsymbol{\Theta} \text{ and } \theta_i \in \boldsymbol{\Theta}_{\pm} \\ \mathcal{N}\big(\boldsymbol{B}(\theta_i)\big) \cup \{\boldsymbol{c}\}, & \text{if } \theta_i \in \boldsymbol{\Theta} \cap \boldsymbol{\Theta}_{\pm} \end{cases} \tag{6.50}$$

Note that if $p < \frac{N+2}{2}$, *then* $\mathcal{N}\big(\boldsymbol{B}(\theta_i)\big) = \{\boldsymbol{0}\}$. *Also note that this property assumes true subspaces, i.e.* $\widehat{\boldsymbol{K}}(\theta) = \boldsymbol{K}(\theta) = \boldsymbol{B^H}(\theta)\boldsymbol{U_n}\boldsymbol{U_n}^H\boldsymbol{B}(\theta)$.

Proof. See Appendix G □

Property 3: *Assuming true subspaces (i.e.* $\widehat{\boldsymbol{U}}_{\boldsymbol{n}} = \boldsymbol{U_n}$*), the function* $f(\theta)$ *is bounded when* $\theta \notin \boldsymbol{\Theta}$ *and unbounded when* $\theta \in \boldsymbol{\Theta}$.

Proof. See Appendix H □

Property 4: *The condition so that* $f(\theta)$ *uniquely identifies the AoAs is that* $p+q \leq N$.

Proof. This is so because the cost function in equation (6.49) depends on the inversion of $\boldsymbol{K}(\theta)$. Hence, in the case where $\theta \notin \boldsymbol{\Theta} \cup \boldsymbol{\Theta_{\pm}}$, the matrix $\boldsymbol{U_n}^{\mathrm{H}}\boldsymbol{B}(\theta)$ is full column rank when $p \leq N-q$. As for the case when $\theta \in \boldsymbol{\Theta} \cup \boldsymbol{\Theta_{\pm}}$, we have the argument in ***Property 3***. □

Remark: The existing methods in [89–91] and the suboptimal method in Section 6.3.1 can not identify the true AoAs, when the number of coupling parameters $p > \frac{N}{2}$. According to ***Property 2***, the cost functions of these exsiting methods would yield peaks whenever $\theta \in \boldsymbol{\Theta_{\pm}}$ and $p > \frac{N}{2}$. One could not, simply, remove these peaks because they would affect the estimation, when the true AoAs are close to those in $\boldsymbol{\Theta_{\pm}}$.

6.4.4 MSE Analysis

It is well known that the noise subspace could be decomposed into two parts:

$$\widehat{\boldsymbol{U}}_{\boldsymbol{n}} = \boldsymbol{U_n} + \widetilde{\boldsymbol{U}}_{\boldsymbol{n}} \tag{6.51}$$

where the first part, $\boldsymbol{U_n}$, is the true noise subspace and the second one, $\widetilde{\boldsymbol{U}}_{\boldsymbol{n}}$, is the error term. Using this decomposition and other asymptotic properties (i.e. for large L or high SNR) which will appear in this section, we wish to derive an asymptotic MSE expression for the AoA estimates obtained from equation (6.49). In other words, we seek an asymptotic expression of $\mathbb{E}\{(\widetilde{\theta}_k)^2\}$, where $\widetilde{\theta}_k$ is the error part

$$\widehat{\theta}_k = \theta_k + \widetilde{\theta}_k \tag{6.52}$$

Since $\{\widehat{\theta}_k\}_{k=1}^{q}$ are minimum points of $f^{-1}(\theta)$, then

$$\frac{\partial f^{-1}(\widehat{\theta}_k)}{\partial \theta} \triangleq \frac{\partial f^{-1}(\theta)}{\partial \theta}\Big|_{\theta=\widehat{\theta}_k} = 0 \tag{6.53}$$

As done in [95], since $\widehat{\theta}_k$ is an estimate of θ_k, we could, asymptotically, expand the above derivative in the neighborhood of the true θ_k using *Taylor* series

$$\frac{\partial f^{-1}(\widehat{\theta}_k)}{\partial \theta} = \frac{\partial f^{-1}(\theta_k)}{\partial \theta} + \frac{\partial^2 f^{-1}(\theta_k)}{\partial \theta^2}(\widehat{\theta}_k - \theta_k) + \dots \tag{6.54}$$

which gives an approximate expression of the error $\widetilde{\theta}_k = \widehat{\theta}_k - \theta_k$

$$\widetilde{\theta}_k \backsimeq -\frac{\frac{\partial f^{-1}(\theta_k)}{\partial \theta}}{\frac{\partial^2 f^{-1}(\theta_k)}{\partial \theta^2}} = -\frac{f'(\theta_k)}{f''(\theta_k) - 2\frac{(f'(\theta_k))^2}{f(\theta_k)}} \tag{6.55}$$

where $f'(\theta_k)$ and $f''(\theta_k)$ are the 1^{st} and 2^{nd} order derivatives of $f(\theta)$ evaluated at point θ_k, respectively.

Property 5: *The derivatives $f'(\theta)$ and $f''(\theta)$ are given as*

$$f'(\theta) = g_1(\theta) + g_2(\theta) \tag{6.56}$$

$$f''(\theta) = h_1(\theta) + h_2(\theta) + h_3(\theta) \tag{6.57}$$

where $g_1(\theta)$ and $g_2(\theta)$ are given in equation (I.5) and $h_1(\theta)$, $h_2(\theta)$, and $h_3(\theta)$ are given in equation (I.6).

Proof. See Appendix I. □

The expressions of $f'(\theta)$ and $f''(\theta)$ in equations (6.56) and (6.57), respectively, turn out to be too complicated to analyze the error in equation (6.55). However, some simplifications could be done, asymptotically, thanks to the following theorem

Theorem 6.7. *Let λ_j and $\boldsymbol{v}_j$ be the j^{th} smallest eigenvalue and its corresponding normalized eigenvector of $\boldsymbol{K}(\theta_k)$. Similarly, define $\widehat{\lambda}_j$ and $\widehat{\boldsymbol{v}}_j$ for $\widehat{\boldsymbol{K}}(\theta_k)$. The smallest*

eigenvalue $\widehat{\lambda}_1$ *and its eigenvector* $\widehat{\boldsymbol{v}}_1$ *could be approximated as*

$$\widehat{\lambda}_1 = \frac{1}{\|\boldsymbol{c}\|^2}\boldsymbol{c}^H\boldsymbol{B}^H(\theta_k)\widetilde{\boldsymbol{U}}_{\boldsymbol{n}}\boldsymbol{P}_k^{\perp}\widetilde{\boldsymbol{U}}_{\boldsymbol{n}}^H\boldsymbol{B}(\theta_k)\boldsymbol{c} + \mathcal{O}(\|\widetilde{\boldsymbol{U}}_{\boldsymbol{n}}\|^3) \tag{6.58}$$

$$\widehat{\boldsymbol{v}}_1 = \frac{1}{\|\boldsymbol{c}\|}\Big(\boldsymbol{c} - \sum_{i=\Delta+2}^{p}\frac{\boldsymbol{v}_i^H\boldsymbol{B}^H(\theta_k)\boldsymbol{U}_{\boldsymbol{n}}\widetilde{\boldsymbol{U}}_{\boldsymbol{n}}^H\boldsymbol{B}(\theta_k)\boldsymbol{c}}{\lambda_i}\boldsymbol{v}_i\Big) + \mathcal{O}(\widetilde{\boldsymbol{U}}_{\boldsymbol{n}}^2) \tag{6.59}$$

where $\boldsymbol{P}_k^{\perp} = \boldsymbol{I} - \boldsymbol{P}_k$ *and*

$$\boldsymbol{P}_k = \boldsymbol{U}_{\boldsymbol{n}}^H\boldsymbol{B}(\theta_k)\boldsymbol{K}^{+}(\theta_k)\boldsymbol{B}^H(\theta_k)\boldsymbol{U}_{\boldsymbol{n}} \tag{6.60}$$

and Δ *is the dimension of* $\mathcal{N}\big(\boldsymbol{B}(\theta_k)\big)$*, which is* 0 *when* $p \leq \frac{N+2}{2}$ *or* $\{p > \frac{N+2}{2}$ *and* $\theta_k \notin \boldsymbol{\Theta}_{\pm}\}$ *and non-zero otherwise (according to* ***Theorem 6.6****). Note that* $\mathcal{O}(\|\widetilde{\boldsymbol{U}}_{\boldsymbol{n}}\|^k)$ *and* $\mathcal{O}(\widetilde{\boldsymbol{U}}_{\boldsymbol{n}}^k)$ *are scalar and vector terms, respectively, in which* $\widetilde{\boldsymbol{U}}_{\boldsymbol{n}}$ *appears* k *times in each term.*

Proof. See Appendix J. □

This theorem reveals a behaviour of $\widehat{\lambda}_1$, i.e. it acts as $\mathcal{O}(\|\widetilde{\boldsymbol{U}}_{\boldsymbol{n}}\|^2)$. Using ***Theorem 4***, and some straightforward algebra, we have the following asymptotic approximations of $f(\theta)$, $f'(\theta)$, and $f''(\theta)$

$$f(\theta) = \frac{1}{\widehat{\lambda}_1\|\boldsymbol{c}\|^2}\mu_k + \mathcal{O}\big(\|\widetilde{\boldsymbol{U}}_{\boldsymbol{n}}\|^{-1}\big) \tag{6.61}$$

$$f'(\theta) = -\frac{2}{\widehat{\lambda}_1^2\|\boldsymbol{c}\|^4}\mu_k\mathrm{Re}\{\widetilde{\rho}_k\} + \mathcal{O}\big(\|\widetilde{\boldsymbol{U}}_{\boldsymbol{n}}\|^{-2}\big) \tag{6.62}$$

$$f''(\theta) = \frac{2}{\widehat{\lambda}_1^3\|\boldsymbol{c}\|^4}\mu_k\Big(\frac{4}{\|\boldsymbol{c}\|^2}(\mathrm{Re}\{\widetilde{\rho}_k\})^2 - \widehat{\lambda}_1\upsilon_k\Big) + \mathcal{O}\big(\|\widetilde{\boldsymbol{U}}_{\boldsymbol{n}}\|^{-3}\big) \tag{6.63}$$

where

$$\mu_k = \|\boldsymbol{c}^{\mathrm{H}}\boldsymbol{a}_p^*(\theta_k)\|^2 \tag{6.64}$$

$$\widetilde{\rho}_k = \boldsymbol{c}^{\mathrm{H}}\boldsymbol{B}^{\mathrm{H}}(\theta_k)\widetilde{\boldsymbol{U}}_{\boldsymbol{n}}\boldsymbol{P}_k^{\perp}\boldsymbol{U}_{\boldsymbol{n}}^{\mathrm{H}}\boldsymbol{D}(\theta_k)\boldsymbol{c} \tag{6.65}$$

$$\upsilon_k = \boldsymbol{c}^{\mathrm{H}}\boldsymbol{D}^{\mathrm{H}}(\theta_k)\boldsymbol{U}_{\boldsymbol{n}}\boldsymbol{P}_k^{\perp}\boldsymbol{U}_{\boldsymbol{n}}^{\mathrm{H}}\boldsymbol{D}(\theta_k)\boldsymbol{c} \tag{6.66}$$

Substituting these expressions in equation (6.55), we arrive at

$$\widetilde{\theta}_k \simeq \frac{\mathrm{Re}\{\widetilde{\rho}_k\}}{\upsilon_k} \tag{6.67}$$

In order to proceed, we use the following lemma, which gives the probabilistic distribution of the columns of $\widetilde{\boldsymbol{U}}_{\boldsymbol{n}}$

Lemma 6.8. *Let $\widetilde{\boldsymbol{n}}_i$ be the i^{th} column of $\widetilde{\boldsymbol{U}}_{\boldsymbol{n}}$. Asymptotically, the vectors $\boldsymbol{U}_{\boldsymbol{s}}\boldsymbol{U}_{\boldsymbol{s}}^H\widetilde{\boldsymbol{n}}_i$ are jointly Gaussian distributed with zero means and covariance matrices given by*

$$\mathbb{E}\Big\{\big(\boldsymbol{U}_{\boldsymbol{s}}\boldsymbol{U}_{\boldsymbol{s}}^H\widetilde{\boldsymbol{n}}_i\big)\big(\boldsymbol{U}_{\boldsymbol{s}}\boldsymbol{U}_{\boldsymbol{s}}^H\widetilde{\boldsymbol{n}}_j\big)^H\Big\} = \frac{\sigma^2}{L}\boldsymbol{U}\delta_{i,j} \tag{6.68}$$

$$\mathbb{E}\Big\{\big(\boldsymbol{U}_{\boldsymbol{s}}\boldsymbol{U}_{\boldsymbol{s}}^H\widetilde{\boldsymbol{n}}_i\big)\big(\boldsymbol{U}_{\boldsymbol{s}}\boldsymbol{U}_{\boldsymbol{s}}^H\widetilde{\boldsymbol{n}}_j\big)^T\Big\} = \boldsymbol{0} \tag{6.69}$$

where

$$\boldsymbol{U} = \boldsymbol{U}_{\boldsymbol{s}}\boldsymbol{\Sigma}_{\boldsymbol{s}}\big(\boldsymbol{\Sigma}_{\boldsymbol{s}} - \sigma^2\boldsymbol{I}\big)^{-2}\boldsymbol{U}_{\boldsymbol{s}}^H \tag{6.70}$$

Proof. See [95]. □

This lemma is key to the following theorem, which gives the MSE expression $\mathbb{E}\big\{(\widetilde{\theta}_k)^2\big\}$

Theorem 6.9. *The estimates $\big\{\widehat{\theta}_k\big\}_{k=1}^q$ estimated through $f(\theta)$ by equation (6.49) are asymptotically unbiased. Furthermore, the MSE expression $\mathbb{E}\big\{(\widetilde{\theta}_k)^2\big\}$ is given as*

$$\mathbb{E}\big\{(\widetilde{\theta}_k)^2\big\} \triangleq var_f^{(p)}(\widehat{\theta}_k) = \frac{\sigma^2}{2L}\frac{\bar{\boldsymbol{a}}^H(\theta_k)\boldsymbol{U}\bar{\boldsymbol{a}}(\theta_k)}{\bar{\boldsymbol{d}}^H(\theta_k)\boldsymbol{U}_{\boldsymbol{n}}\boldsymbol{P}_k^{\perp}\boldsymbol{U}_{\boldsymbol{n}}^H\bar{\boldsymbol{d}}(\theta_k)} \tag{6.71}$$

where $\bar{\boldsymbol{a}}(\theta_k)$ and $\boldsymbol{U}$ are defined in equations (6.10) and (6.70), respectively. Also, $\bar{\boldsymbol{d}}(\theta_k) = \frac{\partial\bar{\boldsymbol{a}}(\theta)}{\partial\theta}\Big|_{\theta=\widehat{\theta}_k}$.

Proof. See Appendix K. □

It is interesting and easy to see that when $p = 1$, the above MSE expression coincides with the MSE expression of MUSIC derived in [95]. In other words, if $p = 1$, we have $\bar{\boldsymbol{a}}(\theta_k) = \boldsymbol{a}(\theta_k)$, $\bar{\boldsymbol{d}}(\theta_k) = \boldsymbol{d}(\theta_k)$, and $\boldsymbol{P}_k^{\perp} = \boldsymbol{I}$, hence

$$\mathrm{var}_f^{(1)}(\widehat{\theta}_k) = \frac{\sigma^2}{2L}\frac{\boldsymbol{a}^{\mathrm{H}}(\theta_k)\boldsymbol{U}\boldsymbol{a}(\theta_k)}{\boldsymbol{d}^{\mathrm{H}}(\theta_k)\boldsymbol{U}_{\boldsymbol{n}}\boldsymbol{U}_{\boldsymbol{n}}^{\mathrm{H}}\boldsymbol{d}(\theta_k)} = \mathrm{var}_{\mathrm{MU}}(\widehat{\theta}_k;\boldsymbol{a}) \tag{6.72}$$

where $\mathrm{var}_{\mathrm{MU}}(\widehat{\theta}_k;\boldsymbol{a})$ is read as follows: The variance of $\widehat{\theta}_k$ obtained by MUSIC by utilising a steering vector $\boldsymbol{a}(\theta)$. We adopt this notation because the MSE expression, $\mathrm{var}_f^{(p)}(\widehat{\theta}_k)$, could also be expressed as

$$\mathrm{var}_f^{(p)}(\widehat{\theta}_k) = \Big(\frac{1}{1-\gamma_k}\Big)\mathrm{var}_{\mathrm{MU}}(\widehat{\theta}_k;\bar{\boldsymbol{a}}) \tag{6.73}$$

where

$$0 \leq \gamma_k = \mathcal{R}\Big(\boldsymbol{P}_k, \boldsymbol{U}_{\boldsymbol{n}}^{\mathrm{H}}\bar{\boldsymbol{d}}(\theta_k)\Big) < 1 \tag{6.74}$$

where the bounds in equation (6.74) are due to the fact that γ_k is a *Rayleigh quotient*, which is always bounded between the minimum and maximum eigenvalues of $\boldsymbol{P}_k$. Since $\boldsymbol{P}_k$ is a projector matrix, then the eigenvalues are either 0 or 1. Note that $\gamma_k = 1$ only when $N - q = \text{rank}(\boldsymbol{P}_k) = p - 1$, thus violating the identifiability condition given in ***Property 4***.

Observation: It is very important to observe that $\text{var}_{\text{MU}}(\widehat{\theta}_k; \bar{\boldsymbol{a}})$ appearing in equation (6.73) is, indeed, the MSE of $\widehat{\theta}_k$ estimated through MUSIC with *known mutual coupling parameters*. Therefore, the quantity $\frac{1}{1-\gamma_k}$ quantifies the loss of performance, or "gap" in terms of MSE, between the proposed method in equation (6.49) and the MUSIC algorithm with *known mutual coupling parameters*.

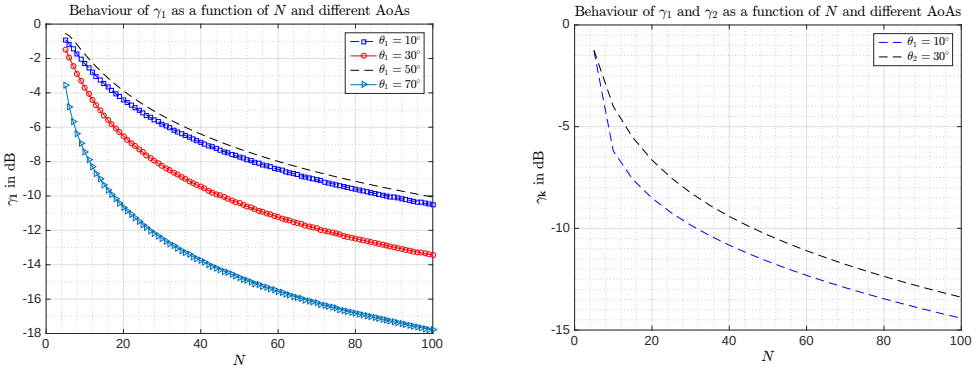

(a) $q = 1$ **(b)** $q = 2$

Figure 6.5: The behaviour of γ_k for fixed $p = 3$ as a function of N.

In Fig. 6.5, we study the behaviour of γ_k given in equation (6.74) by fixing $p = 3$ and increasing N, i.e. $\frac{p}{N} \to 0$. Fig. 6.5a plots γ_1 for one source $q = 1$, but different AoAs. The coupling parameters are set to

$$\boldsymbol{c} = \left[1;\ -0.08 + 0.5j;\ -0.14 - 0.3j\right]^{\text{T}} \tag{6.75}$$

In addition, Fig. 6.5b plots γ_1 and γ_2 when $q = 2$ sources are present. The coupling parameters are set to

$$\boldsymbol{c} = \left[1;\ 0.28 + 0.41j;\ 0.18 + 0.2j\right]^{\text{T}} \tag{6.76}$$

We observe that in both cases $\gamma_k \to 0$ as $\frac{p}{N} \to 0$. Furthermore, the rate of decay depends on the AoA, number of sources, and the coupling parameters.

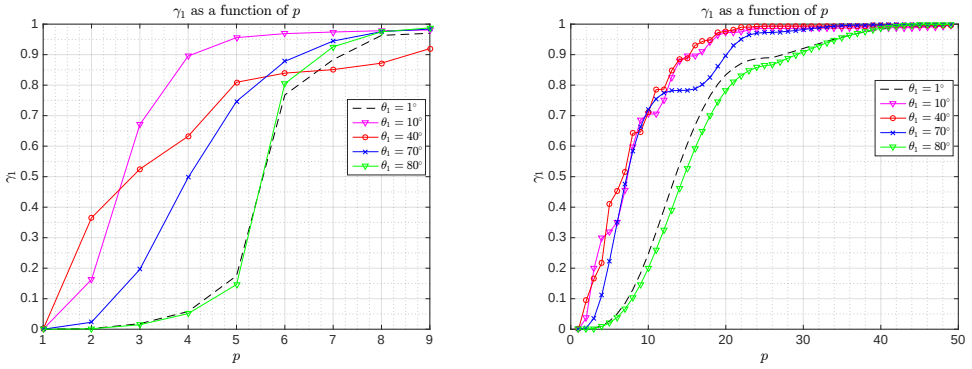

(a) $N = 10$ **(b)** $N = 50$

Figure 6.6: The behaviour of γ_k for fixed N as a function of p.

In Fig. 6.6, we study the behaviour of γ_k by fixing N and increasing p. We have simulated two different scenarios when $q = 1$ source is present. The coupling parameters are generated by first forming a vector $\overline{\boldsymbol{c}}$, such that $\left\{\overline{c}_k = \frac{1}{k+1}e^{j2\pi\phi_k}\right\}_{k=1}^{N}$, where ϕ_k is randomly chosen. Then, in order to compute γ_k, for $p = p_0$, we choose the first p_0 elements of $\overline{\boldsymbol{c}}$ to form the vector $\boldsymbol{c} \in \mathbb{C}^{p_0 \times 1}$. In Fig. 6.6a and Fig. 6.6b, we have set $N = 10$ and $N = 50$, respectively. We also observe that γ_k is increasing as p increases for fixed N. This results in an increase of the MSE given in equation (6.71), when p increases due to the factor $\left(\frac{1}{1-\gamma_k}\right)$, as we shall next.

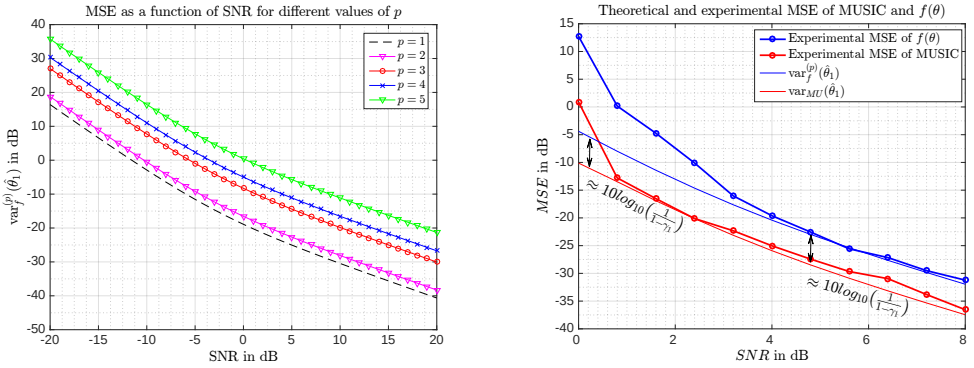

(a) $N = 6$, $q = 1$, and $\theta_1 = 50°$ **(b)** $N = 6$, $q = 1$, $\theta_1 = 10°$, and $p = 3$.

Figure 6.7: MSE of the proposed method in equation (6.71) for different values of p and θ_1

The MSE of the proposed algorithm in equation (6.49), namely $\text{var}_f^{(p)}(\widehat{\theta}_k)$, is simulated in Fig. 6.7. In Fig. 6.7a, we set $N = 6$, $q = 1$, and $\theta_1 = 50°$. The number of snapshots is $L = 10^3$. The coupling parameters are chosen from vector

$$\overline{\boldsymbol{c}} = [1;\ -0.08 + 0.5j;\ -0.14 - 0.3j;\ -0.04 + 0.04j;\ 0.03 - 0.02j]^{\mathrm{T}} \tag{6.77}$$

as done in the case of Fig. 6.6. This figure tells us that a higher MSE is obtained for increasing p. In Fig. 6.7b, we quantify this loss of performance. We have $q = 1$ source impinging an array of $N = 6$ at $\theta_1 = 10°$. The number of snapshots is $L = 10^2$. The

number of coupling parameters is $p = 3$ with $\boldsymbol{c}$ equal to that in the scenario depicted in Fig. 6.5a. We have plotted the experimental and theoretical MSE of MUSIC with *known coupling parameters* and the proposed algorithm in equation (6.49). For the experimental MSE, we have averaged over 10^3 Monte-Carlo simulations. This figure validates the gap between the MSE of MUSIC and the proposed algorithm, which is about $\frac{1}{1-\gamma_1}$, for sufficiently high SNR. The value of γ_1 could be extracted from Fig. 6.5a, since we have used the same coupling parameters. We could see that $\gamma_1 \simeq 0.758$ for $\theta_1 = 10^\circ$, which gives $10\log_{10}\big(\frac{1}{1-\gamma_1}\big) \simeq 6$dB. This factor is the loss of performance compared to MUSIC with *known coupling parameters*. Furthermore, we could also observe that the experimental and theoretical MSE curves are in agreement for sufficiently high SNR.

6.4.5 Comparison with the Cramér-Rao Bound

The *Cramér-Rao* Bound (CRB) on the AoA estimates of a model that includes unknown mutual coupling, i.e. equation (6.1) was derived in [96]. The CRB is given as

$$\mathrm{var}_{\mathrm{CRB}}(\widehat{\theta}_k) = \frac{\sigma^2}{2L}\Big(\big[\bar{\boldsymbol{D}}^{\mathrm{H}}\boldsymbol{P}_{\bar{\boldsymbol{A}}}^{\perp}\bar{\boldsymbol{D}} \odot \boldsymbol{R}_{\boldsymbol{ss}}\big]^{-1}\Big)_{k,k} \tag{6.78}$$

where $\boldsymbol{P}_{\bar{\boldsymbol{A}}}^{\perp} = \boldsymbol{I} - \boldsymbol{P}_{\bar{\boldsymbol{A}}}$ is given in equation (6.2) and $\bar{\boldsymbol{A}}$ is given in equation (6.11). Also

$$\bar{\boldsymbol{D}} = \Big[\ \tfrac{\partial \bar{\mathbf{a}}(\theta_1)}{\partial \theta_1}\ \Big|\ \ldots\ \Big|\ \tfrac{\partial \bar{\mathbf{a}}(\theta_q)}{\partial \theta_q}\ \Big] \tag{6.79}$$

Following similar steps as in [95], we re-write the MSE equation, $\mathrm{var}_f^{(p)}(\widehat{\theta}_k)$, in a way that turns out to be useful when comparing to the CRB

$$\mathrm{var}_f^{(p)}(\widehat{\theta}_k) = \frac{\sigma^2}{2L}\frac{\big(\boldsymbol{R}_{\boldsymbol{ss}}^{-1}\big)_{k,k} + \sigma^2\big(\boldsymbol{R}_{\boldsymbol{ss}}^{-1}(\bar{\boldsymbol{A}}^{\mathrm{H}}\bar{\boldsymbol{A}})^{-1}\boldsymbol{R}_{\boldsymbol{ss}}^{-1}\big)_{k,k}}{\bar{\boldsymbol{d}}^{\mathrm{H}}(\theta_k)\boldsymbol{U}_{\boldsymbol{n}}\boldsymbol{P}_k^{\perp}\boldsymbol{U}_{\boldsymbol{n}}^{\mathrm{H}}\bar{\boldsymbol{d}}(\theta_k)} \tag{6.80}$$

Large Number of Antennas

We study the performance of the algorithm proposed in equation (6.49) in the asymptotic regime when $\frac{p}{N} \to 0$, i.e. $N \to \infty$ for fixed p. We have the following Theorem, which is a generalisation of the case with no mutual coupling in [95]

Theorem 6.10. *The limits of* $var_{CRB}(\widehat{\theta}_k)$ *and* $var_f^{(p)}(\widehat{\theta}_k)$ *are given as*

$$var_{CRB}(\widehat{\theta}_k) \xrightarrow[\frac{p}{N}\to 0]{} \frac{6\sigma^2}{N^3 L|\boldsymbol{h}_k^H \boldsymbol{c}|^2} \frac{1}{\left(\boldsymbol{R_{ss}}\right)_{k,k}} \tag{6.81}$$

$$var_f^{(p)}(\widehat{\theta}_k) \xrightarrow[\frac{p}{N}\to 0]{} \frac{6\sigma^2}{N^3 L|\boldsymbol{h}_k^H \boldsymbol{c}|^2} \left(\boldsymbol{R_{ss}}^{-1}\right)_{k,k} \tag{6.82}$$

$$\gamma_k \xrightarrow[\frac{p}{N}\to 0]{} 0 \tag{6.83}$$

where

$$\boldsymbol{h}_k = \boldsymbol{a}_p(\theta_k) + \boldsymbol{a}_p^*(\theta_k) - \boldsymbol{e}_1 \tag{6.84}$$

Proof. See Appendix L. □

Using this theorem, we have that

$$\frac{\mathrm{var}_f^{(p)}(\widehat{\theta}_k)}{\mathrm{var}_{\mathrm{CRB}}(\widehat{\theta}_k)} = \left(\boldsymbol{R_{ss}}\right)_{k,k} \left(\boldsymbol{R_{ss}}^{-1}\right)_{k,k} \tag{6.85}$$

and hence the CRB is attained for uncorrelated signals (i.e. $\boldsymbol{R_{ss}}$ is diagonal), when $\frac{p}{N} \to 0$.

High SNR

For high SNR and uncorrelated signals, one could show the following relation

$$\frac{\mathrm{var}_f^{(p)}(\widehat{\theta}_k)}{\mathrm{var}_{\mathrm{CRB}}(\widehat{\theta}_k)} = \left(1 + \frac{\left((\bar{\boldsymbol{A}}^{\mathrm{H}}\bar{\boldsymbol{A}})^{-1}\right)_{k,k}}{\mathrm{SNR}_k}\right)\left(\frac{1}{1-\gamma_k}\right) \tag{6.86}$$

where $\mathrm{SNR}_k = \frac{(\boldsymbol{R_{ss}})_{k,k}}{\sigma^2}$. For high SNR, the ratio in equation (6.86) is controlled by the factor $\frac{1}{1-\gamma_k}$, i.e. the "gap" between the MSE of the proposed algorithm and the CRB is $\frac{1}{1-\gamma_k}$.

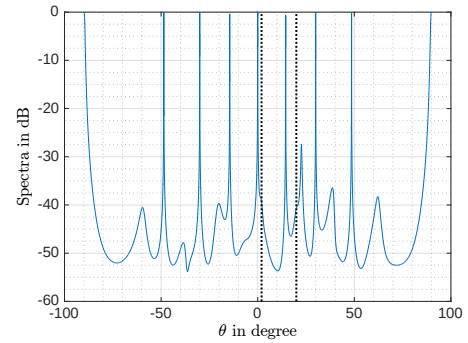

(a) Proposed sub-optimal method

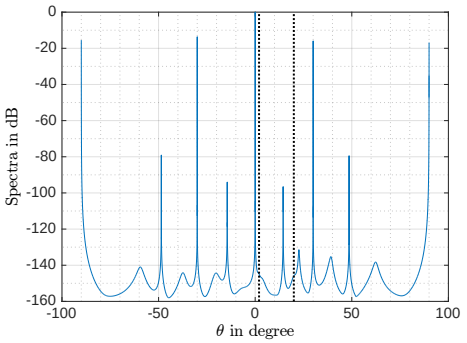

(b) Method in [89]

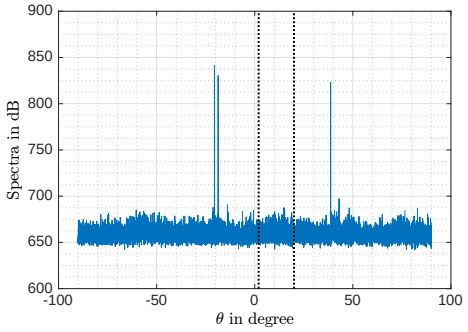

(c) Method in [88]

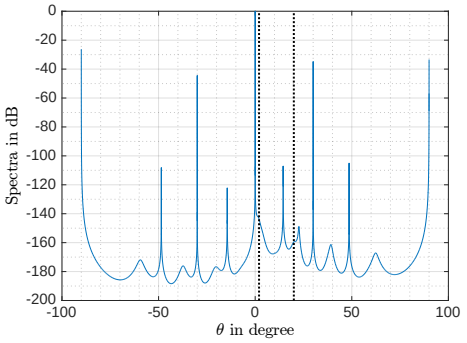

(d) RARE [90, 91]

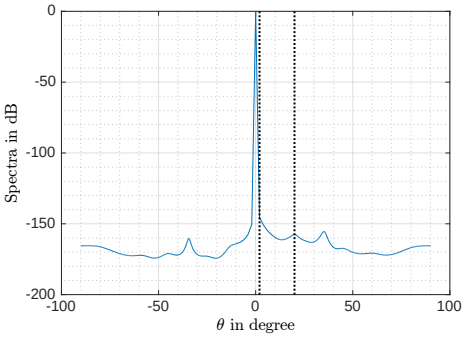

(e) Recursive RARE [92]

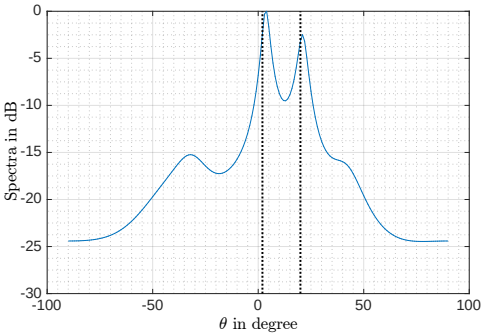

(f) Method in [93]

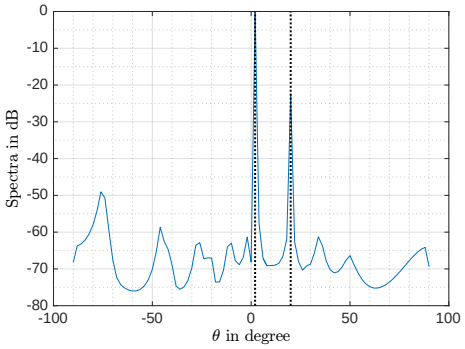

(g) Proposed method $f(\theta)$ in eqn (6.49)

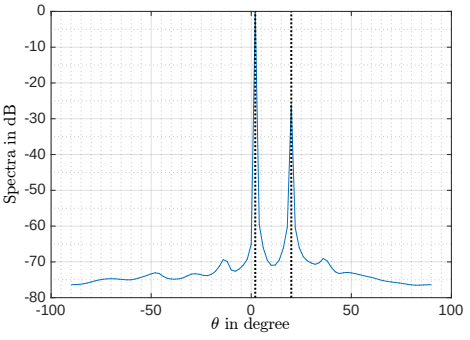

(h) Refinement of proposed method

Figure 6.8: Different normalized spectra (in dB) of methods that estimate AoAs in the presence of mutual coupling.

In Fig. 6.8, different spectra of methods that estimate AoAs in the presence of mutual coupling are depicted for a particular scenario. There are two sources $\theta_1 = 2^\circ$ and

$\theta_2 = 20°$ attacking a ULA composed of $N = 8$ antennas. The ULA suffers from mutual coupling with $p = \frac{N+2}{2} = 5$ coupling parameters given as

$$\boldsymbol{c} = [1;\ -0.44 + 0.23j;\ 0.33 + 0.01j;\ -0.23 - 0.1j;\ 0.1 + 0.16j]^{\mathrm{T}} \tag{6.87}$$

The SNR is set to 10 dB and the collected number of snapshots is $L = 500$. We observe that the methods in Figures 6.8a, 6.8b, and 6.8d yield fake peaks when $\theta \in \boldsymbol{\Theta}_+$ according to ***Theorem 6.6***. In addition, there is no peaks corresponding to the true positions. This is so because fake peaks may overlap with the true ones, when the latter are sufficiently close to the former. Furthermore, the recursive RARE depicted in Fig. 6.8e is initialized by RARE, and therefore selecting a false peak in the first iteration may deteriorate the performance of recursive RARE in further iterations. As we can see, recursive RARE has not successfully identified the true positions. Moreover, the method in [88] depicted in Fig. 6.8c does not perform well at all. As stated earlier, this is so because the method requires that $2p + q \leq N + 1$. On the other hand, the iterative method in [93] gives broad and biased peaks away from the true positions. Moreover, the proposed method in equation (6.49) depicted in Fig. 6.8g gives peaks at the true positions. The ratio between the highest true peak and the highest fake peak is about 50dB. Additionally, the ratio between the 2^{nd} highest true peak and the highest fake peak is about 25dB. Indeed, there is a great improvement between the proposed method and the previously mentioned one. Finally, the refined method discussed in Section VII could further diminish the fake peaks as we can see in Fig. 6.8h. In addition, the refined method also exhibits better performance in terms of bias and MSE of AoAs and coupling parameters, when compared to all these methods.

6.4.6 Refining the AoA estimates by alternating minimisation

As explained in Section III.B, the optimisation problem formed in $(\mathcal{P}_2)$ is suboptimal. This is due to the fact that it, implicitly, assumes that each AoA is exposed to different mutual coupling parameters, namely $\boldsymbol{c} = \boldsymbol{c}(\theta)$. Fortunately, problem $(\mathcal{P}_1)$ is optimal, since it forces the same coupling parameters on all the AoAs. In this section, we propose an efficient algorithm that aims at optimising problem $(\mathcal{P}_1)$.

Consider the following problem:

$$\begin{cases} \underset{\boldsymbol{m},\theta_1 \ldots \theta_q}{\text{minimize}} & \boldsymbol{m}^{\mathrm{H}} \widehat{\boldsymbol{S}}(\boldsymbol{\Theta}) \boldsymbol{m} \\ \text{subject to} & \Big(\sum_{k=1}^{q} \boldsymbol{e}_1^{\mathrm{H}} \boldsymbol{B}(\theta_k) \Big) \boldsymbol{m} = 1 \end{cases} \tag{6.88}$$

The constraint here is a generalisation of that in problem (6.42) in a sense that it prevents the cost function to be zero when the AoA variables $\boldsymbol{\Theta}$ are "simultaneously"

in the set $\boldsymbol{\Theta}_{\pm}$, i.e. when $\theta_1 \in \boldsymbol{\Theta}_{\pm} \dots \theta_q \in \boldsymbol{\Theta}_{\pm}$. Following similar steps as in equations (6.43)till (6.48), the optimal coupling parameters are given as

$$\boldsymbol{m^o} = \frac{\widehat{\boldsymbol{S}}^{-1}(\boldsymbol{\Theta})\boldsymbol{A}_p^*(\boldsymbol{\Theta})\mathbb{1}_q}{\mathbb{1}_q^{\mathrm{T}}\boldsymbol{A}_p^{\mathrm{T}}(\boldsymbol{\Theta})\widehat{\boldsymbol{S}}^{-1}(\boldsymbol{\Theta})\boldsymbol{A}_p^*(\boldsymbol{\Theta})\mathbb{1}_q} \tag{6.89}$$

where $\boldsymbol{A}_p(\boldsymbol{\Theta})$ is similarly defined as $\boldsymbol{A}(\boldsymbol{\Theta})$ in equation (2.6) but of size $p \times q$. Plugging this expression of $\boldsymbol{m^o}$ in the objective function of (6.88), we get

$$\widehat{\boldsymbol{\Theta}} = \arg\max_{\boldsymbol{\Theta}} \left\{ \mathbb{1}_q^{\mathrm{T}}\boldsymbol{A}_p^{\mathrm{T}}(\boldsymbol{\Theta})\widehat{\boldsymbol{S}}^{-1}(\boldsymbol{\Theta})\boldsymbol{A}_p^*(\boldsymbol{\Theta})\mathbb{1}_q \right\} \tag{6.90}$$

which involves a $q-$dimensional search in the AoA parameters. We, hereby, propose q "$1-$dimensional" searches done by alternating minimisations: At an iteration i, the following AoAs are estimated from previous iterations:

$$\widehat{\boldsymbol{\Theta}}_{\bar{i}} = [\widehat{\theta}_1 \dots \widehat{\theta}_{i-1}] \tag{6.91}$$

Estimate $\widehat{\theta}_i$ as

$$\widehat{\theta}_i = \arg\max_{\theta} \left\{ \mathbb{1}_i^{\mathrm{T}}\boldsymbol{A}_p^{\mathrm{T}}(\widehat{\boldsymbol{\Theta}}_{\bar{i}}, \theta)\widehat{\boldsymbol{S}}^{-1}(\widehat{\boldsymbol{\Theta}}_{\bar{i}}, \theta)\boldsymbol{A}_p^*(\widehat{\boldsymbol{\Theta}}_{\bar{i}}, \theta)\mathbb{1}_i \right\} \tag{6.92}$$

by picking $\widehat{\theta}_i \notin \widehat{\boldsymbol{\Theta}}_{\bar{i}}$ because values in $\widehat{\boldsymbol{\Theta}}_{\bar{i}}$ also maximize the above cost function. It is easy to see that the first iteration of this algorithm, i.e. $i = 1$, is equivalent to maximising $f(\theta)$. However, the difference is that, the first approach involves picking q peaks from $f(\theta)$, whereas, the alternating minimisation algorithm in equation (6.92) picks one peak at each iteration, and therefore refining the estimates of each AoA. Moreover, this approach could also estimate the coupling parameters. This is done by using all estimated AoAs, say $\widehat{\boldsymbol{\Theta}}$ and inserting them into equation (6.89), namely

$$\widehat{\boldsymbol{c}} = \frac{\widehat{\boldsymbol{S}}^{-1}(\widehat{\boldsymbol{\Theta}})\boldsymbol{A}_p^*(\widehat{\boldsymbol{\Theta}})\mathbb{1}_q}{\mathbb{1}_q^{\mathrm{T}}\boldsymbol{A}_p^{\mathrm{T}}(\widehat{\boldsymbol{\Theta}})\widehat{\boldsymbol{S}}^{-1}(\widehat{\boldsymbol{\Theta}})\boldsymbol{A}_p^*(\widehat{\boldsymbol{\Theta}})\mathbb{1}_q} \tag{6.93}$$

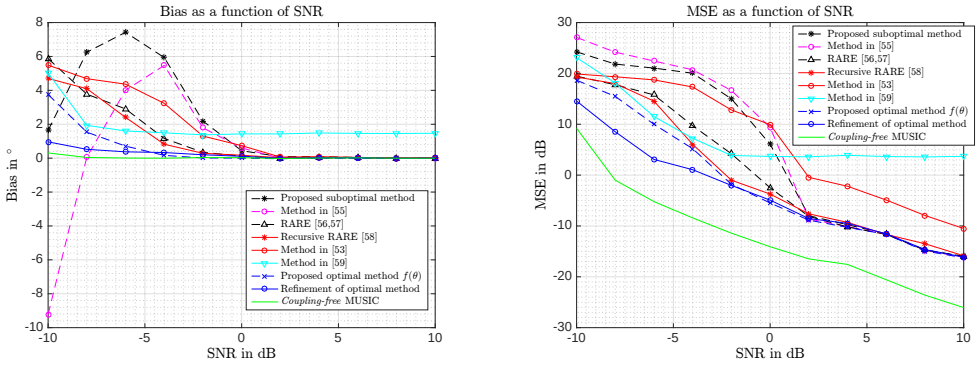

(a) Bias in ° of AoA estimates as a function of SNR.

(b) MSE in dB of AoA estimates as a function of SNR.

Figure 6.9: Bias and MSE of the AoA estimates as a function of SNR for Experiment 1

In Experiment 1, we fix the following parameters: $N = 8$, $q = 2$ i.i.d. uncorrelated Gaussian sources impinge the array at $\theta_1 = 5°$ and $\theta_2 = 20°$. The collected number of snapshots is $L = 10^3$, and the number of coupling parameters is $p = 3$ with

$$\boldsymbol{c} = \left[1;\ 0.2 + 0.46j;\ 0.33 + 0.04j\right]^{\mathrm{T}} \tag{6.94}$$

According to Fig. 6.9a, all methods, except for [93], show no bias when SNR> 2dB. However, it is interesting to observe that the proposed method and its refinement are the least biased. In terms of the MSE of AoA estimates, which is depicted in Fig. 6.9b, we also observe that the proposed method and its refinement exhibit less MSE for any SNR. Interestingly, all algorithms (except for [88] and [93]), are exposed to the same MSE, when the SNR exceeds 2dB.

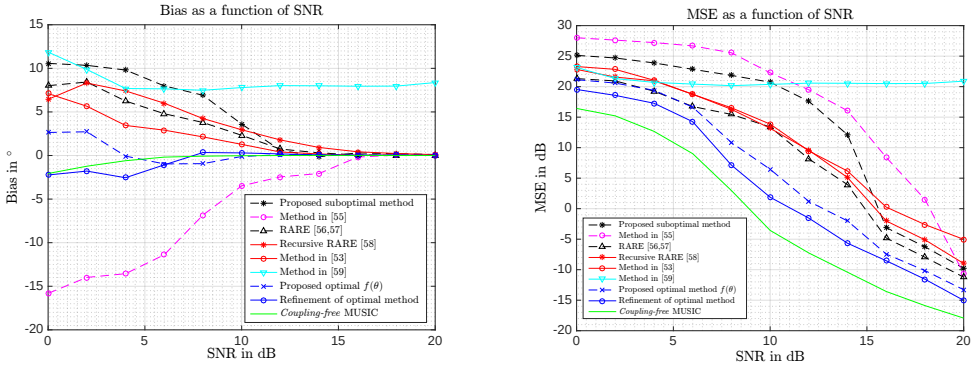

(a) Bias in ° of AoA estimates as a function of SNR.

(b) MSE in dB of AoA estimates as a function of SNR.

Figure 6.10: Bias and MSE of the AoA estimates as a function of SNR for Experiment 2

In Experiment 2, we fix the same parameters as in Experiment 1, except now that the 2 sources are correlated. The sources are Gaussian with covariance matrix

$$\boldsymbol{R_{ss}} = \begin{bmatrix} 1 & \rho \\ \rho^* & 1 \end{bmatrix} \tag{6.95}$$

where the correlation coefficient is set to $|\rho| = 0.8$. Again, the method in [93] does not perform well at all (in terms of bias and MSE). This is so because the method was based on the assumption that $\boldsymbol{R_{ss}}$ is diagonal, and therefore correlation between sources is not allowed. On the other hand, all other methods require higher SNR when sources are correlated, since they are MUSIC-based methods. For example, the proposed method in equation (6.49) requires an SNR of -2 dB to achieve 0 dB MSE, when the sources are un-correlated (Experiment 1). On the other hand, and in order to achieve the same MSE for correlated sources with correlation coefficient $|\rho| = 0.8$, an SNR of 13 dB is needed. This is so because the MSE of this method depends on $\boldsymbol{R_{ss}}^{-1}$, and hence a higher MSE is obtained as correlation between sources increase. According to Fig. 6.10a and 6.10b, we also observe that the proposed and refined methods are the least biased and enjoy better MSE performance than other methods.

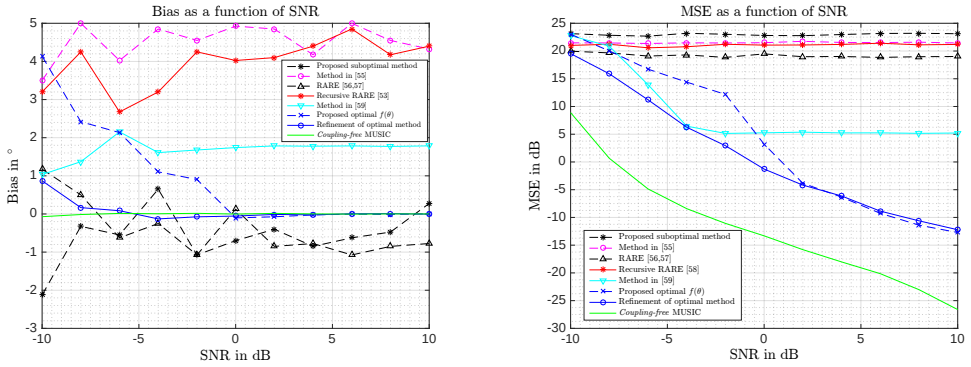

(a) Bias in ° of AoA estimates as a function of SNR.

(b) MSE in dB of AoA estimates as a function of SNR.

Figure 6.11: Bias and MSE of the AoA estimates as a function of SNR for Experiment 3

In Experiment 3, we fix the same parameters as in Experiment 1, except for $p = \frac{N+2}{2} = 5$, with

$$\boldsymbol{c} = \begin{bmatrix} 1;\ 0.2 + 0.46j;\ 0.33 + 0.04j;\ 0.12 + 0.01j;\ 0.01 + 0.03 \end{bmatrix}^{\mathrm{T}} \tag{6.96}$$

According to Figures 6.11a and 6.11b, we see that all algorithms, except for [93] and the proposed ones, do not operate properly in terms of bias and MSE. This is so since p was chosen to be $\frac{N+2}{2}$. Therefore, according to ***Theorem 6.6***, the matrix $\boldsymbol{B}(\theta)$, and consequently $\widehat{\boldsymbol{K}}(\theta)$ admits a null-space whenever $\theta \in \boldsymbol{\Theta_+}$, and therefore the mentioned methods will always choose peaks corresponding to angles in $\theta \in \boldsymbol{\Theta_+}$. At sufficiently high SNR, we see that the MSE of the proposed algorithm and the refined method coincide

(Fig. 6.11b). Additionally, the refined method outperforms all other algorithms in terms of bias and MSE of AoAs and coupling parameters.

6.5 Mutual Coupling Agnostic AoA estimator

6.5.1 The Maximum Likelihood Estimator

Now let us denote

$$\widetilde{\boldsymbol{A}}(\boldsymbol{\Theta}) = \boldsymbol{T}(\boldsymbol{c})\boldsymbol{A}(\boldsymbol{\Theta}) \tag{6.97}$$

we can say that the received signal $\widetilde{\boldsymbol{X}}$, under assumption **A2**,

$$\widetilde{\boldsymbol{X}} \sim \mathcal{N}\Big(\tilde{\boldsymbol{A}}(\boldsymbol{\Theta})\boldsymbol{S}, \sigma^2\boldsymbol{I}_N\Big), \quad l = 1 \dots L \tag{6.98}$$

To simplify notation, we stack all signal and noise parameters into one vector, say

$$\Omega = \Big[\boldsymbol{\Theta}^{\mathrm{T}}, \boldsymbol{c}^{\mathrm{T}}, \mathrm{vec}(\boldsymbol{S}), \sigma^2\Big]^{\mathrm{T}} \tag{6.99}$$

We can now express the joint probability distibution function of all the snapshots $\boldsymbol{X}$, given the unknown signal and noise parameters Ω as

$$f\Big(\widetilde{\boldsymbol{X}}|\Omega\Big) = \prod_{l=1}^{L} \frac{1}{\pi \det\big\{\sigma^2\boldsymbol{I}_N\big\}} \exp\Big\{-\frac{1}{\sigma^2}\big\|\tilde{\boldsymbol{x}}(l) - \tilde{\boldsymbol{A}}(\boldsymbol{\Theta})\boldsymbol{s}(l)\big\|^2\Big\} \tag{6.100}$$

The Deterministic ML estimates of the noise and signal parameters, i.e. $\hat{\Omega}^{\mathrm{ML}}$, are obtained through the following criterion

$$\hat{\Omega}^{\mathrm{ML}} = \arg\max_{\Omega} f\Big(\widetilde{\boldsymbol{X}}|\Omega\Big) \tag{6.101}$$

Finally, $\hat{\Omega}^{\mathrm{ML}}$ is given by the following

$$\hat{\Omega}^{\mathrm{ML}} = \Big[\hat{\boldsymbol{\Theta}}^{\mathrm{T}}, \hat{\boldsymbol{m}}^{\mathrm{T}}, \mathrm{vec}(\hat{\boldsymbol{S}}), \hat{\sigma}^2\Big]^{\mathrm{T}} \tag{6.102a}$$

$$\hat{\sigma}^2 = \frac{1}{NL}\big\|\boldsymbol{X} - \tilde{\boldsymbol{A}}(\hat{\boldsymbol{\Theta}})\hat{\boldsymbol{S}}\big\|^2 \tag{6.102b}$$

$$\hat{\boldsymbol{S}} = \Big(\tilde{\boldsymbol{A}}^{\mathrm{H}}(\hat{\boldsymbol{\Theta}})\tilde{\boldsymbol{A}}(\hat{\boldsymbol{\Theta}})\Big)^{-1}\tilde{\boldsymbol{A}}^{\mathrm{H}}(\hat{\boldsymbol{\Theta}})\boldsymbol{X} \tag{6.102c}$$

$$[\hat{\boldsymbol{\Theta}}, \hat{\boldsymbol{c}}] = \arg\max_{\boldsymbol{\Theta}, \boldsymbol{c}} \mathrm{tr}\Big\{\boldsymbol{\mathscr{P}}_{\tilde{\boldsymbol{A}}(\boldsymbol{\Theta})}\hat{\boldsymbol{R}}\Big\} \tag{6.102d}$$

where $\boldsymbol{\mathscr{P}}_{\tilde{\boldsymbol{A}}(\boldsymbol{\Theta})}$ is the projector onto the signal subspace, i.e. the space spanned by columns of $\boldsymbol{\mathscr{P}}_{\tilde{\boldsymbol{A}}(\boldsymbol{\Theta})}$

$$\boldsymbol{\mathscr{P}}_{\tilde{\boldsymbol{A}}(\boldsymbol{\Theta})} = \tilde{\boldsymbol{A}}(\boldsymbol{\Theta})\Big(\widetilde{\boldsymbol{A}}^{\mathrm{H}}(\boldsymbol{\Theta})\tilde{\boldsymbol{A}}(\boldsymbol{\Theta})\Big)^{-1}\widetilde{\boldsymbol{A}}^{\mathrm{H}}(\boldsymbol{\Theta}) \tag{6.102e}$$

and $\widehat{\boldsymbol{R}}_{\boldsymbol{xx}}$ is the sample covariance matrix of the data given in equation (6.8).
Note that once the estimate $[\hat{\boldsymbol{\Theta}}, \hat{\boldsymbol{c}}]$ is obtained by solving (6.102d), then one could plug $[\hat{\boldsymbol{\Theta}}, \hat{\boldsymbol{c}}]$ in (6.102b) and (6.102c) to obtain the ML estimate of the noise variance and signal matrix, respectively. It turns out that the optimisation problem in (6.102d) is highly nonlinear, as it requires a $\big(q+2(p-1)\big)$-dimensional search[1], and its direct optimisation would require cumbersome optimisation techniques. It is worth stressing a point here: *The rest of the paper focuses on solving* (6.102d) *in order to estimate* $\boldsymbol{\Theta}$*, by treating* $\boldsymbol{c}$ *as a nuissance parameter. Our aim is to estimate the AoAs of multiple sources in the presence of mutual coupling, thus the term "Mutual Coupling Agnostic".*

6.5.2 Proposed iterative method

In the absence of mutual coupling, i.e. $p = 1$ and $\boldsymbol{c} = 1$, Ziskind and Wax have proposed to optimise (6.102d) in order to estimate $\boldsymbol{\Theta}$ via Alternating Projection [30]. That is, the value of θ_i at the k^{th} iteration is obtained by solving the following 1-dimensional optimisation problem

$$\hat{\theta}_i^{(k)} = \arg\max_{\theta_i} \frac{\boldsymbol{a}^{\mathrm{H}}(\theta_i)\boldsymbol{\mathscr{P}}^{\perp}_{\boldsymbol{A}_{\bar{i}}}\widehat{\boldsymbol{R}}_{\boldsymbol{xx}}\boldsymbol{\mathscr{P}}^{\perp}_{\boldsymbol{A}_{\bar{i}}}\boldsymbol{a}(\theta_i)}{\boldsymbol{a}^{\mathrm{H}}(\theta_i)\boldsymbol{\mathscr{P}}^{\perp}_{\boldsymbol{A}_{\bar{i}}}\boldsymbol{a}(\theta_i)} \tag{6.103}$$

where $\mathscr{P}^{\perp}_{\boldsymbol{Y}} = \boldsymbol{I} - \mathscr{P}_{\boldsymbol{Y}}$ and $\boldsymbol{A}_{\bar{i}}$ is obtained by omitting the i^{th} column from matrix $\widetilde{\boldsymbol{A}}(\boldsymbol{\Theta}^{(k)})$. The vector $\boldsymbol{\Theta}^{(k)}$ represents the estimated AoAs at iteration k, in an attempt of estimating the i^{th} AoA. In other words, at iteration k and sub-iteration i, vector $\boldsymbol{\Theta}^{(k)}$ could be expressed as

$$\hat{\boldsymbol{\Theta}}^{(k)} = [\hat{\theta}_1^{(k)}, \hat{\theta}_2^{(k)} \ldots \hat{\theta}_{i-1}^{(k)}, \hat{\theta}_i^{(k-1)}, \hat{\theta}_{i+1}^{(k-1)} \ldots \hat{\theta}_q^{(k-1)}]^{\mathrm{T}} \tag{6.104}$$

Naturally, the algorithm is iterative. At each iteration, the 1-dimensional search in (6.103) is done per AoA $(i = 1 \ldots q)$ in a successive manner until the vector $\hat{\boldsymbol{\Theta}}^{(k)}$ converges.

Notice that, in the presence of mutual coupling, we could follow similar steps as in [30] to get

$$[\hat{\theta}_i^{(k)}\ ,\ \hat{\boldsymbol{c}}_i^{(k)}] = \arg\max_{[\theta_i, \boldsymbol{c}]} \frac{\tilde{\boldsymbol{a}}^{\mathrm{H}}(\theta_i)\boldsymbol{\mathscr{P}}^{\perp}_{\tilde{\boldsymbol{A}}_{\bar{i}}}\widehat{\boldsymbol{R}}_{\boldsymbol{xx}}\boldsymbol{\mathscr{P}}^{\perp}_{\tilde{\boldsymbol{A}}_{\bar{i}}}\tilde{\boldsymbol{a}}(\theta_i)}{\tilde{\boldsymbol{a}}^{\mathrm{H}}(\theta_i)\boldsymbol{\mathscr{P}}^{\perp}_{\tilde{\boldsymbol{A}}_{\bar{i}}}\tilde{\boldsymbol{a}}(\theta_i)} \tag{6.105}$$

[1] It is a $\big(q+2(p-1)\big)$-dimensional search: q is due to the number of parameters in $\boldsymbol{\Theta}$ and $2(p-1)$ is the number of real and imaginary unknown parameters in $\boldsymbol{c}$.

where the maximisation is also done over the coupling parameters $\boldsymbol{c}$. Thanks to Theorem 6.1, we can say that

$$\tilde{\boldsymbol{a}}(\theta) = \boldsymbol{T}(\boldsymbol{c})\boldsymbol{a}(\theta) = \boldsymbol{B}(\theta)\boldsymbol{c} \tag{6.106}$$

where $\boldsymbol{B}(\theta)$ is given in equation (6.18). Equation (6.105) is re-written as

$$[\hat{\theta}_i^{(k)}\ , \hat{\boldsymbol{c}}_i^{(k)}] = \arg\max_{[\theta_i, \boldsymbol{c}]} \frac{\boldsymbol{c}^{\mathrm{H}}\boldsymbol{Q}(\theta_i)\boldsymbol{c}}{\boldsymbol{c}^{\mathrm{H}}\boldsymbol{K}(\theta_i)\boldsymbol{c}} \tag{6.107a}$$

where

$$\boldsymbol{Q}(\theta_i) = \boldsymbol{B}^{\mathrm{H}}(\theta_i)\boldsymbol{\mathscr{P}}^{\perp}_{\tilde{\boldsymbol{A}}_{\bar{i}}}\widehat{\boldsymbol{R}}_{\boldsymbol{xx}}\boldsymbol{\mathscr{P}}^{\perp}_{\tilde{\boldsymbol{A}}_{\bar{i}}}\boldsymbol{B}(\theta_i) \tag{6.107b}$$

$$\boldsymbol{K}(\theta_i) = \boldsymbol{B}^{\mathrm{H}}(\theta_i)\boldsymbol{\mathscr{P}}^{\perp}_{\tilde{\boldsymbol{A}}_{\bar{i}}}\boldsymbol{B}(\theta_i) \tag{6.107c}$$

Maximising first with respect to $\boldsymbol{c}$ according to the following criterion

$$\begin{cases} \underset{\boldsymbol{c}\in\mathbb{C}^{p\times 1}}{\text{maximise}} & \boldsymbol{c}^{\mathrm{H}}\boldsymbol{Q}(\theta_i)\boldsymbol{c} \\ \text{subject to} & \boldsymbol{c}^{\mathrm{H}}\boldsymbol{K}(\theta_i)\boldsymbol{c} = 1 \end{cases} \tag{6.108}$$

gives rise to the following cost function

$$\hat{\theta}_i^{(k)} = \arg\max_{\theta_i} \lambda_{\max}\Big(\boldsymbol{Q}(\theta_i); \boldsymbol{K}(\theta_i)\Big) \tag{6.109a}$$

where $\lambda_{\max}(\boldsymbol{Y}; \boldsymbol{Z})$ is the maximum generalised eigenvalue of the matrix pencil (or matrix pair) $(\boldsymbol{Y}; \boldsymbol{Z})$. Then, the vector $\hat{\boldsymbol{c}}_i^{(k)}$ is estimated after maximising (6.109a) and obtaining $\hat{\theta}_i^{(k)}$, viz.

$$\hat{\boldsymbol{c}}_i^{(k)} = \boldsymbol{v}_{\max}\Big(\boldsymbol{Q}(\hat{\theta}_i^{(k)}); \boldsymbol{K}(\hat{\theta}_i^{(k)})\Big) \tag{6.109b}$$

where $\boldsymbol{v}_{\max}(\boldsymbol{Y}; \boldsymbol{Z})$ is the generalised eigenvector corresponding to the maximum generalised eigenvalue of the matrix pencil $(\boldsymbol{Y}; \boldsymbol{Z})$. The vector $\hat{\boldsymbol{c}}_i^{(k)}$ is also normalised with respect to its first element. Then, an update is done on the vector $\hat{\boldsymbol{\Theta}}^{(k)}$ by replacing $\theta_i^{(k-1)}$ with $\theta_i^{(k)}$.

After estimating $\hat{\theta}_i^{(k)}$ and $\hat{\boldsymbol{c}}_i^{(k)}$, an update should be done on the corresponding column of $\tilde{\boldsymbol{A}}$ according to equation (6.106) as follows

$$\big[\tilde{\boldsymbol{A}}\big]_{(:,i)} \leftarrow \boldsymbol{T}(\hat{\boldsymbol{c}}_i^{(k)})\boldsymbol{a}(\hat{\theta}_i^{(k)}) \tag{6.110}$$

Then, increment $i \leftarrow i + 1$ and do the same procedure to estimate the next AoA. If $i > q$, then $i \leftarrow 1$, and $k \leftarrow k + 1$. The procedure is repeated until the vector $\hat{\boldsymbol{\Theta}}^{(k)}$ shows no satisfying improvement. The algorithm is summarised in the table **Algorithm 6**.

Algorithm 6: Implementation of the Proposed Agnostic Mutual Coupling ML AoA Estimator by Alternating Projection

DATA: Collect $\boldsymbol{X}$ and compute $\widehat{\boldsymbol{R}}_{\boldsymbol{xx}}$ according to equation (6.8).

INITIALISATION:
$k \leftarrow 0$; $\tilde{\boldsymbol{A}} \leftarrow \emptyset$; $\boldsymbol{\mathscr{P}}^{\perp} \leftarrow \boldsymbol{I}$; $\hat{\boldsymbol{\Theta}}^{(k)} \leftarrow \emptyset$;
for $i = 1$ *to* q **do**

- **Step I.1:** Estimate $\hat{\theta}_i^{(k)}$ via 1D search using (6.109a), where:
  - $\boldsymbol{Q}(\theta) = \boldsymbol{B}^{\mathrm{H}}(\theta)\boldsymbol{\mathscr{P}}^{\perp}\widehat{\boldsymbol{R}}_{\boldsymbol{xx}}\boldsymbol{\mathscr{P}}^{\perp}\boldsymbol{B}(\theta)$.
  - $\boldsymbol{K}(\theta) = \boldsymbol{B}^{\mathrm{H}}(\theta)\boldsymbol{\mathscr{P}}^{\perp}\boldsymbol{B}(\theta)$.
- **Step I.2:** Obtain $\hat{\boldsymbol{c}}_i^{(k)}$ using equation (6.109b) and $\hat{\theta}_i^{(k)}$.
- **Step I.3:** Update the following quantities:
  - $[\tilde{\boldsymbol{A}}]_{(:,i)} \leftarrow \boldsymbol{T}(\hat{\boldsymbol{c}}_i^{(k)})\boldsymbol{a}(\hat{\theta}_i^{(k)})$.
  - $\boldsymbol{\mathscr{P}}^{\perp} \leftarrow \boldsymbol{I} - \tilde{\boldsymbol{A}}(\tilde{\boldsymbol{A}}^{\mathrm{H}}\tilde{\boldsymbol{A}})^{-1}\tilde{\boldsymbol{A}}^{\mathrm{H}}$.
  - $[\boldsymbol{\Theta}^{(k)}]_{(i,1)} \leftarrow \hat{\theta}_i^{(k)}$.

MAIN LOOP:
do

- $\hat{\boldsymbol{\Theta}}^{\text{old}} \leftarrow \hat{\boldsymbol{\Theta}}^{(k)}$
- $k \leftarrow k + 1$

for $i = 1$ *to* q **do**

- Compute $\boldsymbol{\mathscr{P}}^{\perp} \leftarrow \boldsymbol{I} - \tilde{\boldsymbol{A}}_{\bar{i}}(\tilde{\boldsymbol{A}}_{\bar{i}}^{\mathrm{H}}\tilde{\boldsymbol{A}}_{\bar{i}})^{-1}\tilde{\boldsymbol{A}}_{\bar{i}}^{\mathrm{H}}$, where $\tilde{\boldsymbol{A}}_{\bar{i}}$ is obtained by omitting the i^{th} column from matrix $\tilde{\boldsymbol{A}}$.
- Do **Step I.1** to estimate $\hat{\theta}_i^{(k)}$.
- Do **Step I.2** to obtain $\hat{\boldsymbol{c}}_i^{(k)}$.
- Update $[\tilde{\boldsymbol{A}}]_{(:,i)} \leftarrow \boldsymbol{T}(\hat{\boldsymbol{c}}_i^{(k)})\boldsymbol{a}(\hat{\theta}_i^{(k)})$ and $[\boldsymbol{\Theta}^{(k)}]_{(i,1)} \leftarrow \hat{\theta}_i^{(k)}$ as done in **Step I.3**.

while $\|\hat{\boldsymbol{\Theta}}^{(k)} - \hat{\boldsymbol{\Theta}}^{\text{old}}\| > \xi$

We have conducted three experiments by fixing the following simulation parameters: $N = 7$ antennas, $q = 2$ sources, and the RMSE is averaged over 200 trials. In all the experiments, we compare the RMSE of the AoA estimates with the *Cramér-Rao* bound that takes into account joint estimation of AoAs and coupling parameters [96]. This threshold indeed depends on several factors, such as separation, correlation, and number of sources.

In the 1^{st} experiment (Fig. 6.12), we have fixed the AoAs to $\theta_1 = 0°$ and $\theta_2 = 20°$. The sources are uncorrelated and are generated as independent and identically distributed (i.i.d) according to a Gaussian distibution. The number of snapshots is $L = 100$. Also,

the number of coupling parameters are $p = 3$ with $\mathbf{c} = [1, 0.3115 + 0.3911j, -0.3063 - 0.1314j]$. We can see that the RMSE of both AoA estimates via the proposed method are close to their corresponding CRBs when SNR exceeds 5 dB

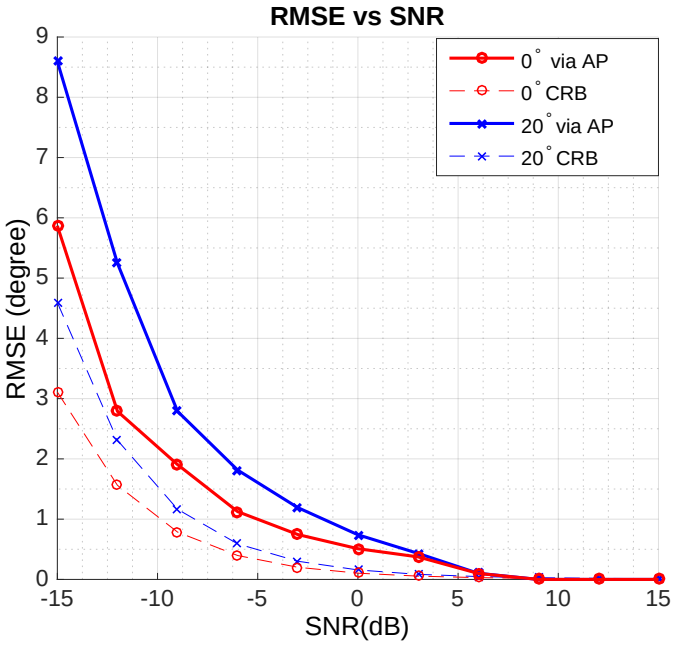

Figure 6.12: RMSE of AoAs on a log-scale vs. SNR of the 1^{st} experiment.

.

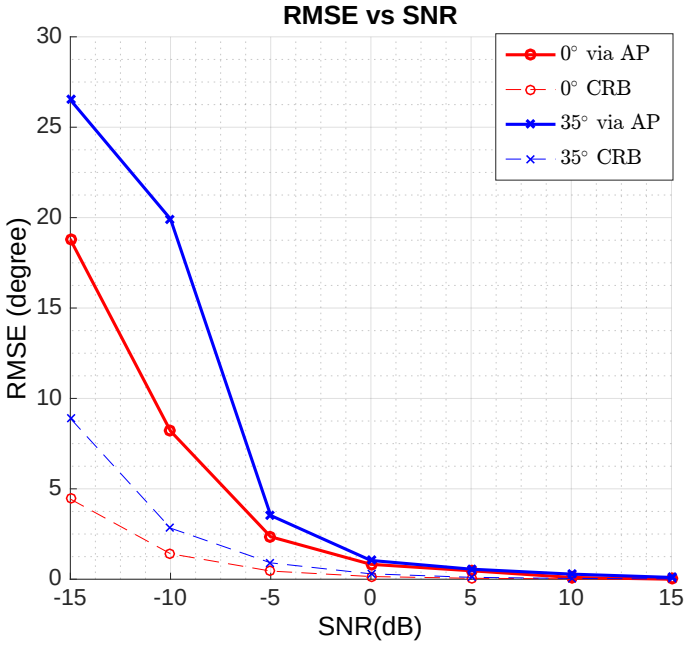

Figure 6.13: RMSE of AoAs on a log-scale vs. SNR of the 2^{nd} experiment.

In the 2^{nd} experiment (Fig. 6.13), the two sources are coherent. the AoAs are now more separated compared to the 1^{st} experiment, namely $\theta_1 = 0°$ and $\theta_2 = 35°$. The number of snapshots is $L = 100$. Moreover, the number of coupling parameters are $p = 2$, with

$\mathbf{c} = [1, 0.1563 - 0.475j]$. We can see that the RMSE per SNR is higher than those of the 1^{st} experiment, even though we have less coupling parameters and AoAs being more separated. This is due to coherency of the sources. However, we see that the RMSE of both AoA estimates are close to their corresponding CRBs, when SNR exceeds 15 dB.

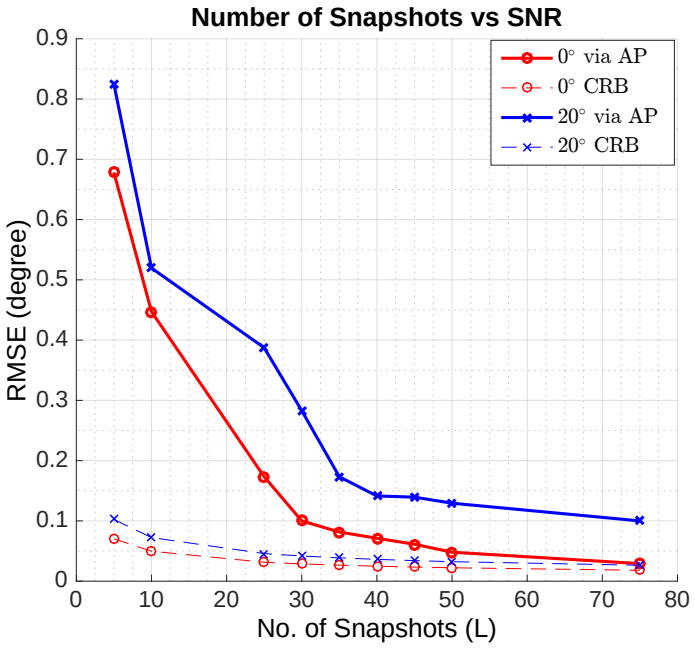

Figure 6.14: RMSE of AoAs on a log-scale vs. SNR of the 3^{rd} experiment.

In the 3^{rd} experiment (Fig. 6.14), we plot the RMSE v.s. number of snapshots L, with SNR fixed to 5 dB. The sources are uncorrelated and are generated as i.i.d according to a Gaussian distibution. The AoAs are brought back to the values of experiment 1, i.e. $\theta_1 = 0°$ and $\theta_2 = 20°$, but with less coupling parameters, i.e. $p = 2$ with $\mathbf{c} = [1, 0.3561 - 0.22j]$. The RMSE of $\hat{\theta}_1$ is close to its corresponding CRB, when L exceeds 75, however, $\hat{\theta}_2$ still shows some error of about 0.1°.

6.6 Conclusions and future directions

There are several new results in this paper that should be highlighted.

- We have derived a suboptimal MUSIC-based method for estimating Angles-of-Arrival in the presence of mutual coupling in Section 6.3.1.
- We have presented and proven two theorems, namely Theorem 6.4 and Theorem 6.5, that allowed us to characterize the spectral behaviour of an important matrix, i.e. $\boldsymbol{B}(\theta)$, through an important theorem, i.e. Theorem 6.6, which explains why other algorithms, such as [89–91] including the suboptimal method in Section 6.3.1, suffer from *"non-identifiability"* (i.e. when $p > \frac{N}{2}$) through that particular matrix.

- In the light of these results, we propose an optimal algorithm (Section 6.4), in the sense that it does not suffer from this *"non-identifiability"* issue. This algorithm could estimate the Angles-of-Arrival of q sources in the presence of p mutual coupling parameters, given that $p+q \leq N$. We have also proved some properties that are related to the cost function $f(\theta)$ (the optimal method) to give a better insight on how the proposed method operates.

- We have derived a closed-form asymptotic MSE expression of the proposed algorithm with the help of the paper in [95] and some *Perturbation Theory* tools. Moreover, we have shown that the estimates of the Angles-of-Arrival through peak finding of $f(\theta)$ are asymptotically unbiased.

- We observed the "gap" between the MSE of the proposed method and the MSE of MUSIC with *known mutual coupling parameters*. This is given by equation (6.73). For the k^{th} source, this "gap" is given by $\left(\frac{1}{1-\gamma_k}\right)$.

- Furthermore, the derived MSE reveals that the proposed algorithm attains the *Cramér-Rao* bound of joint mutual coupling and Angle-of-Arrival estimation when $\frac{p}{N} \to 0$ for uncorrelated signals. However, for high SNR, this is not generally the case.

- We have improved the optimal method, in Section 6.4.6, by a method that is guaranteed to give a lower MSE on Angles-of-Arrival estimates by taking into account a better constraint of the optimization problem in hand.

- Finally, we have proposed an iterative algorithm based on Alternating Projection in order to optimise the Deterministic Maximum Likelihood cost function that takes into account mutual coupling. Throughout the operation of the algorithm, mutual coupling parameters were treated as nuissance parameters, thus the name *"Mutual Coupling Agnostic"*. Furthermore, the sources are allowed to be coherent.

Future directions may include: (i) regarding the mutual coupling problem from a different perspective, namely reducing the mutual coupling effect instead of considering a joint coupling/AoA estimation problem; (ii) including other phenomena that perturb AoA estimation, such as gain/phase mismatch between different antennas.

Chapter 7

Localizing via Wi-Fi

In this chapter, we aim at building a real system that could perform joint Angle and Delay of Arrival Estimation and Detection of multipath components. This is simply done, so that we could extract the Angle-of-Arrival of the Line-of-Sight (LoS) component between the transmitter and receiver. The contributions are summarised as follows: (i) we take into account all critical factors that perturb the Joint Angle and Delay estimation problem and formulate a system model accordingly; (ii) then, we propose an offline calibration method to compensate for all such factors; (iii) finally, and with the help of the CESS-JADED-RIP algorithm, we have successfully been able to estimate the Angles and Times of Arrival of all the multipath components, which allowed for the extraction of the AoA of the LoS component.

7.1 Analytical Modelling

7.1.1 Transmit Signal

Let the baseband OFDM symbol be defined as followed:

$$s(t) = \sum_{m=-\frac{M}{2}}^{\frac{M}{2}} b_m e^{j2\pi m\Delta_f t} \mathbf{\Pi}(\frac{m\Delta_f}{B}) \tag{7.1}$$

where $\Delta_f = \frac{1}{T}$ is the subcarrier spacing and T is the symbol period (i.e. $T = 3.2\mu$sec.) Moreover, parameter M indicates the total number of subcarriers (including the non-useful ones within the band of interest). In the above equation, the time index t could

span any real positive value, i.e. $t > 0$. Due to the periodicity of the exponential term, we get the following relation,

$$s(\alpha T) = s(\alpha T + T), \qquad 0 \leq \alpha \leq 1 \tag{7.2}$$

We would like to, explicitly, express consecutive OFDM symbols that form an OFDM frame. Assuming we have transmitted L consecutive symbols, the overall transmit frame is expressed as

$$f(t) = \sum_{l=0}^{L-1} s(t - lT), \qquad 0 \leq t \leq LT \tag{7.3}$$

Note that the rect function $\mathbf{\Pi}(f)$ is defined as

$$\mathbf{\Pi}(f) = \begin{cases} 1 & \text{if } |f| < \frac{1}{2} \\ \frac{1}{2} & \text{if } |f| = \frac{1}{2} \\ 0 & \text{if } |f| > \frac{1}{2} \end{cases} \tag{7.4}$$

In reality, the function $\mathbf{\Pi}(f)$ is seen as an ideal low pass filter (sinc filter) with zero ripple in the pass and stop bands and zero transition width. In practical scenarios, this ideal filter is not realisable, and instead we shall use $G(f)$ to denote the actual pulse shaping filters in frequency domain[1]. Since Therefore, the baseband signal has the following form now

$$\begin{aligned} f(t) &= \sum_{l=0}^{L-1} s(t - lT), \qquad 0 \leq t \leq LT \\ &= \sum_{l=0}^{L-1} \sum_{m=-\frac{M}{2}}^{\frac{M}{2}} b_m e^{j2\pi m\Delta_f (t-lT)} G(m\Delta_f), \qquad 0 \leq t \leq LT \\ &= \sum_{l=0}^{L-1} \sum_{m=-\frac{M}{2}}^{\frac{M}{2}} \widetilde{b}_m e^{j2\pi m\Delta_f t}, \qquad 0 \leq t \leq LT \end{aligned} \tag{7.5}$$

where the last equality is due to the fact that $\Delta_f T = 1$ and $\widetilde{b}_m = G(m\Delta_f) b_m$. As one can see, the same OFDM symbol $s(t)$ is transmitted L times. The final form of the transmit frame is in broadband, viz.

[1] In case of transmit or receive filters, we do not make the difference and we assume that $G(f)$ is a cascade of filters.

$$x(t) = f(t)e^{j2\pi f_c t} \tag{7.6}$$

In all what follows, we assume absence of noise only for the sake of compact presentation.

7.1.2 Channel Propagation

We assume a specular channel model, i.e. let $h_n(t)$ be the channel seen by the n^{th} antenna

$$h_n(t) = \sum_{k=1}^{q} \gamma_k a_n(\theta_k)\delta(t - \tau_k) \tag{7.7}$$

where γ_k is the complex coefficient of the k^{th} path and the parameters θ_k, τ_k indicates the time of arrival (ToA) and the angle of arrival (AoA) of the k^{th}. Note that the ToA is measured from the moment of transmission of the frame. The function $a_n(\theta)$ is the response of the n^{th} receiving antenna due to a path arriving at angle θ_k. Finally, $\delta(t)$ is the Dirac-delta function defined as

$$\delta(t - \tau) = \begin{cases} 1 & \text{if } t = \tau \\ 0 & \text{else} \end{cases} \tag{7.8}$$

The received signal at the n^{th} antennas could be expressed as

$$y_n(t) = h_n(t) * x(t) \tag{7.9}$$

where $*$ denotes convolution. We could write $y_n(t)$ as

$$\begin{aligned} y_n(t) &= h_n(t) * x(t) \\ &= \big(\sum_{k=1}^{q} \gamma_k a_n(\theta_k)\delta(t - \tau_k)\big) * x(t) \\ &= \sum_{k=1}^{q} \gamma_k a_n(\theta_k)\big(\boldsymbol{\delta(t - \tau_k) * x(t)}\big) \end{aligned} \tag{7.10}$$

To compute the above term $\big(\delta(t - \tau_k) * x(t)\big)$ and "get rid" of the convolution sign, we make use of the shifting property of the convolution, namely

$$\int_{-\infty}^{\infty} f(x)\delta(x - a)\, dx = f(a) \tag{7.11}$$

Using the definition of the convolution, we have that

$$f(t) * g(t) := \int_0^t f(t-s)g(s)\,ds, \tag{7.12}$$

Using this definition, we compute the quantity we are interested in

$$\begin{aligned} \boldsymbol{\delta(t-\tau_k) * x(t)} &= x(t) * \delta(t-\tau_k) \\ &= \int_0^t x(t-s)\delta(s-\tau_k)\,ds. \end{aligned} \tag{7.13}$$

Now, consider the two following cases,

- If $t < \tau_k$, then $\delta(s-\tau_k) = 0$ since $0 \leq s \leq t < \tau_k$ and hence

$$\int_0^t x(t-s)\delta(s-\tau_k)\,ds \equiv 0 \tag{7.14}$$

- If $t \geq \tau_k$, then using the shifting property,

$$\int_0^t x(t-s)\delta(s-\tau_k)\,ds = x(t-s)\Big|_{s=\tau_k} = x(t-\tau_k) \tag{7.15}$$

We conclude that

$$\boldsymbol{\delta(t-\tau_k) * x(t)} = \begin{cases} x(t-\tau_k) & t \geq \tau_k \\ 0 & t < \tau_k \end{cases} \tag{7.16}$$

Now since the signal $x(t)$ is present within $0 \leq t \leq LT$, and zero otherwise, then we could say

$$\boldsymbol{\delta(t-\tau_k) * x(t)} = x(t-\tau_k) \tag{7.17}$$

without the need to impose the two cases. So,

$$y_n(t) = \sum_{k=1}^{q} \gamma_k a_n(\theta_k) x(t-\tau_k) \tag{7.18}$$

7.1.3 Receiver

In this subsection, we should describe carefully the different blocks associated at the receiver's side.

Down-Conversion of the RF signal

Upon the reception of the analog signal $y_n(t)$ for $1 \leq n \leq N$ across all antennas, a downconversion is needed to center the signal $y_n(t)$ around the zero frequency. Ideally, all clocks per antenna paths should have a crystal embedded and running at f_c. However, this is not usually the case. In other words, assume that the oscillator is running at frequency f_c^n at the n^{th} antenna path[2], then a downconversion at the n^{th} path reads

$$y_n^{\text{down}}(t) = y_n(t)e^{-j2\pi f_c^n t} \tag{7.19}$$

where the superscript "down" indicates "down-conversion". We would like to see the effect of the mismatching in downconversion (i.e. when $f_c^n \neq f_c$ for all n). Using equation (7.18) in (7.19) we get

$$y_n^{\text{down}}(t) = \big(\sum_{k=1}^{q} \gamma_k a_n(\theta_k)x(t-\tau_k)\big)e^{-j2\pi f_c^n t} \tag{7.20}$$

Now using equation (7.6), we get

$$\begin{aligned} y_n^{\text{down}}(t) &= \big(\sum_{k=1}^{q} \gamma_k a_n(\theta_k)x(t-\tau_k)\big)e^{-j2\pi f_c^n t} \\ &= \sum_{k=1}^{q} \gamma_k a_n(\theta_k)f(t-\tau_k)e^{j2\pi f_c(t-\tau_k)}e^{-j2\pi f_c^n t} \\ &= \sum_{k=1}^{q} \gamma_k a_n(\theta_k)f(t-\tau_k)e^{j2\pi (f_c-f_c^n)t}e^{-j2\pi f_c\tau_k} \end{aligned} \tag{7.21}$$

As mentioned in Section **??**, the difference $\epsilon_f^n \equiv f_c - f_c^n$ causes Carrier Frequency Offset (CFO). Also let's absorb the term $e^{-j2\pi f_c\tau_k}$ into the multipath coefficients γ_k, due to its independence of time. To this end, let's denote

$$\bar{\gamma}_k = \gamma_k e^{-j2\pi f_c\tau_k} \tag{7.22}$$

Therefore, equation (7.21) becomes

$$y_n^{\text{down}}(t) = \sum_{k=1}^{q} \bar{\gamma}_k a_n(\theta_k)f(t-\tau_k)e^{j2\pi\epsilon_f^n t} \tag{7.23}$$

As we can see, the CFO ϵ_f^n causes a drift in time domain.

[2]In the case of a common oscillator, we have that $f_c^1 = f_c^2 = \ldots = f_c^N = f_c'$

Sampling the RF signal

The sampling process of the RF signal is a block that is of fundamental importance, as it allows us for further signal processing. Nominally, and according to the *Nyquist* criterion, we should sample at a rate that is at least the signal bandwidth so that we do not loose any information carried by the signal. This means that the sampling frequency, $f_s = \frac{1}{T_s}$ should satisfy

$$f_s \geq B \tag{7.24}$$

where $B = M\Delta_f$ is the bandwidth of the OFDM signal $x(t)$ or, equivalently, $y_n^{\text{down}}(t)$. In this document, we assume that the nominal sampling frequency is chosen to be $f_s = B$ and hence

$$T_s = \frac{1}{B} = \frac{1}{M\Delta_f} \tag{7.25}$$

It is impossible to guarantee an exact sampling period T_s. As in the case of CFO, the deviation of the crystal's oscillation frequency from the true one causes a sampling mismatch. More formally, assume that the sampling period is T_s^n at the n^{th} antenna path[3]. Then sampling $y_n^{\text{down}}(t)$ in (7.23) at T_s^n reads

$$y_n^{\text{down}}(p) \triangleq y_n^{\text{down}}(t = pT_s^n + \beta_n) = \sum_{k=1}^{q} \bar{\gamma}_k a_n(\theta_k) f(pT_s^n + \beta_n - \tau_k) e^{j2\pi\epsilon_f^n(pT_s^n + \beta_n)} \tag{7.26}$$

Using equation (7.5) in (7.26), we get

$$\begin{aligned} y_n^{\text{down}}(p) &= \sum_{k=1}^{q} \bar{\gamma}_k \widetilde{a}_n(\theta_k) \sum_{m=-\frac{M}{2}}^{\frac{M}{2}} \widetilde{b}_m e^{j2\pi m\Delta_f(pT_s^n - \tau_k)} e^{j2\pi\epsilon_f^n pT_s^n} \\ &= e^{j2\pi\epsilon_f^n pT_s^n} \sum_{k=1}^{q} \bar{\gamma}_k \widetilde{a}_n(\theta_k) \sum_{m=-\frac{M}{2}}^{\frac{M}{2}} \widetilde{b}_m e^{j2\pi m\Delta_f(pT_s^n - \tau_k)} \end{aligned} \tag{7.27}$$

where $\widetilde{a}_n(\theta) = a_n(\theta)e^{j2\pi\beta_n(\epsilon_f^n)}$. Assuming that $\epsilon_T^n = T_s - T_s^n$, then if $\epsilon_T^n \neq 0$, we can say that the system is prone to Sampling Frequency Offset (SFO). This destroys the orthogonality of the subcarriers, thereby resulting in inter-carrier interference (ICI).

[3]In the case of a common oscillator for sampling, we have that $T_s^1 = T_s^2 = \ldots = T_s^N = T_s'$

Focusing on the last sum in equation (7.27), we can say

$$\begin{aligned}\sum_{m=-\frac{M}{2}}^{\frac{M}{2}} \widetilde{b}_m e^{j2\pi mp\Delta_f T_s^n} e^{-j2\pi m\Delta_f \tau_k} &= \sum_{m=-\frac{M}{2}}^{\frac{M}{2}} \widetilde{b}_m e^{j2\pi mp\Delta_f (T_s-\epsilon_T^n)} e^{-j2\pi m\Delta_f \tau_k} \\ &= \sum_{m=-\frac{M}{2}}^{\frac{M}{2}} \widetilde{b}_m e^{j2\pi mp\Delta_f T_s(1-\delta_T^n)} e^{-j2\pi m\Delta_f \tau_k} \\ &= \sum_{m=-\frac{M}{2}}^{\frac{M}{2}} \widetilde{b}_m e^{j2\pi \frac{mp}{M}(1-\delta_T^n)} e^{-j2\pi m\Delta_f \tau_k} \\ &= \sum_{m=-\frac{M}{2}}^{\frac{M}{2}} \widetilde{b}_m e^{j2\pi \frac{mp}{M}} e^{-j2\pi \frac{mp}{M}\delta_T^n} e^{-j2\pi m\Delta_f \tau_k}\end{aligned} \tag{7.28}$$

where $\delta_T^n = \frac{\epsilon_T^n}{T_s}$. Using (7.27) and (7.28), we can say that

$$y_n^{\text{down}}(p,l) = e^{j2\pi\epsilon_f^n pT_s^n} . \sum_{k=1}^{q} \sum_{m=-\frac{M}{2}}^{\frac{M}{2}} \widetilde{b}_m e^{j2\pi \frac{mp}{M}} e^{-j2\pi \frac{mp}{M}\delta_T^n} e^{-j2\pi m\Delta_f \tau_k} \bar{\gamma}_k \widetilde{a}_n(\theta_k) \tag{7.29}$$

A compact representation would be[4]

$$y_n(p,l) = \left(e^{j2\pi\epsilon_f^n (p+lM)T_s^n}\right)\left(\widetilde{\boldsymbol{f}}_{p,n}^T(l)\widetilde{\boldsymbol{B}}\boldsymbol{C}\boldsymbol{G}\widetilde{\boldsymbol{a}}_n\right) \tag{7.30}$$

[4]We omit the "down" super-scipt

where

$$\widetilde{\boldsymbol{f}}_{p,n}(l) = \begin{bmatrix} (z.z_{\delta_n})^{-\frac{M}{2}(p+lM)} \\ (z.z_{\delta_n})^{(-\frac{M}{2}+1)(p+lM)} \\ \vdots \\ (z.z_{\delta_n})^{-(p+lM)} \\ (z.z_{\delta_n})^{(p+lM)} \\ \vdots \\ (z.z_{\delta_n})^{(\frac{M}{2}-1)(p+lM)} \\ (z.z_{\delta_n})^{\frac{M}{2}(p+lM)} \end{bmatrix}, \quad z = e^{j\frac{2\pi}{M}} \text{ and } z_{\delta_n} = e^{-j\frac{2\pi}{M}\delta_T^n} \tag{7.31}$$

$$\widetilde{\boldsymbol{B}} = \text{diag}[\widetilde{b}_{-\frac{M}{2}} \dots \widetilde{b}_{\frac{M}{2}}] \tag{7.32}$$

$$\boldsymbol{C} = \begin{bmatrix} \boldsymbol{c}(\tau_1) & \boldsymbol{c}(\tau_2) & \dots & \boldsymbol{c}(\tau_q) \end{bmatrix} \tag{7.33}$$

$$\boldsymbol{c}(\tau) = \begin{bmatrix} 1 \\ z_\tau \\ z_\tau^2 \\ \vdots \\ z_\tau^{\frac{M}{2}-1} \\ z_\tau^{\frac{M}{2}+1} \\ \vdots \\ z_\tau^M \end{bmatrix}, \qquad z_\tau = e^{-j2\pi\Delta_f\tau} \tag{7.34}$$

$$\boldsymbol{G} = = \text{diag}[\bar{\bar{\gamma}}_1 \dots \bar{\bar{\gamma}}_q], \qquad \bar{\bar{\gamma}}_k = \bar{\gamma}_k e^{j2\pi\frac{M}{2}\Delta_f\tau_k} \tag{7.35}$$

$$\widetilde{\boldsymbol{a}}_n = \begin{bmatrix} \widetilde{a}_n(\theta_1) \\ \vdots \\ \widetilde{a}_n(\theta_q) \end{bmatrix} \tag{7.36}$$

Collecting M time samples for the l^{th} symbol we get

$$\begin{aligned} \boldsymbol{y}_n(l) &= \begin{bmatrix} y_n(1,l) \\ y_n(2,l) \\ \vdots \\ y_n(M,l) \end{bmatrix} \\ &= \begin{bmatrix} \left(e^{j2\pi\epsilon_f^n(1+lM)T_s^n}\right)\left(\widetilde{\boldsymbol{f}}_{1,n}^T(l)\widetilde{\boldsymbol{B}}\boldsymbol{C}\boldsymbol{G}\widetilde{\boldsymbol{a}}_n\right) \\ \left(e^{j2\pi\epsilon_f^n(2+lM)T_s^n}\right)\left(\widetilde{\boldsymbol{f}}_{2,n}^T(l)\widetilde{\boldsymbol{B}}\boldsymbol{C}\boldsymbol{G}\widetilde{\boldsymbol{a}}_n\right) \\ \vdots \\ \left(e^{j2\pi\epsilon_f^n(M+lM)T_s^n}\right)\left(\widetilde{\boldsymbol{f}}_{M,n}^T(l)\widetilde{\boldsymbol{B}}\boldsymbol{C}\boldsymbol{G}\widetilde{\boldsymbol{a}}_n\right) \end{bmatrix} \\ &= \boldsymbol{D}_\epsilon(l)\widetilde{\boldsymbol{F}}(l)\widetilde{\boldsymbol{B}}\boldsymbol{C}\boldsymbol{G}\widetilde{\boldsymbol{a}}_n \end{aligned} \tag{7.37}$$

where

$$\boldsymbol{D}_{\epsilon}(l) = \text{diag}\left[e^{j2\pi\epsilon_f^n(1+lM)T_s^n} \quad \dots \quad e^{j2\pi\epsilon_f^n(M+lM)T_s^n}\right] \tag{7.38}$$

$$\widetilde{\boldsymbol{F}}(l) = \begin{bmatrix} \widetilde{\boldsymbol{f}}_{1,n}^T(l) \\ \widetilde{\boldsymbol{f}}_{2,n}^T(l) \\ \vdots \\ \widetilde{\boldsymbol{f}}_{M,n}^T(l) \end{bmatrix} \tag{7.39}$$

7.1.4 Summary

The sampled l^{th} symbol up to the output of the ADC at the n^{th} antenna is given by

$$\boldsymbol{y}_n(l) = \boldsymbol{D}_{\epsilon}(l)\widetilde{\boldsymbol{F}}(l)\widetilde{\boldsymbol{B}}\boldsymbol{C}\boldsymbol{G}\widetilde{\boldsymbol{a}}_n \tag{7.40}$$

where

- $\boldsymbol{D}_{\epsilon}(l)$ *is given in equation* (7.38). *This matrix captures the CFO on the n^{th} path.*
- $\widetilde{\boldsymbol{F}}(l)$ *is given in equation* (7.39) *and could be defined as the perturbed DFT matrix.*
- $\widetilde{\boldsymbol{B}}$ *is given in equation* (7.32). *This is a diagonal matrix containing the transmit symbols per subcarrier.*
- $\boldsymbol{C}$ *is given in equations* (7.33)-(7.34). *This is the steering matrix to multipaths arriving with delays $\tau_1 \dots \tau_q$.*
- $\boldsymbol{G}$ *is given in equations* (7.35). *This matrix is a diagonal matrix containing complex gains of each multipath.*
- $\widetilde{\boldsymbol{a}}_n$ *is given in equation* (7.36) *and is the perturbed vector of response of only the n^{th} antenna to all path arriving at angles $\theta_1 \dots \theta_q$.*

7.2 Offline calibration approach

In this section, we explain the preprocessing steps done before AoA/ToA estimation. The preprocessing will be done in an offline manner, i.e. the channel is only the cables connecting Tx with Rx.

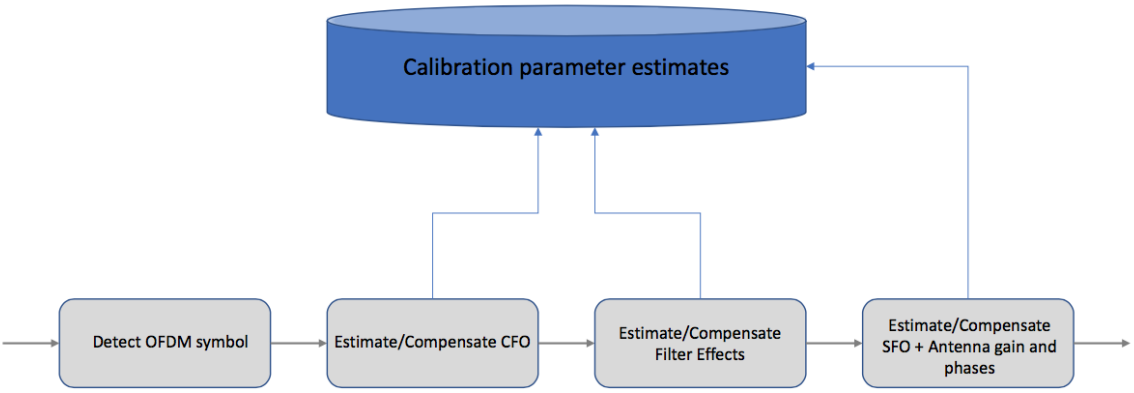

Figure 7.1: Block Diagram of the Offline Calibration approach

7.2.1 Step 1: Detect Frame/Symbol

The first step is to find the beginning of the frame. Let's assume that we have transmitted 31 consecutive LTF symbols, just as in Figure 1, where we can see the received signal sampled at 80 MHz. Our task here is to find which time sample n determines the beginning of the frame.

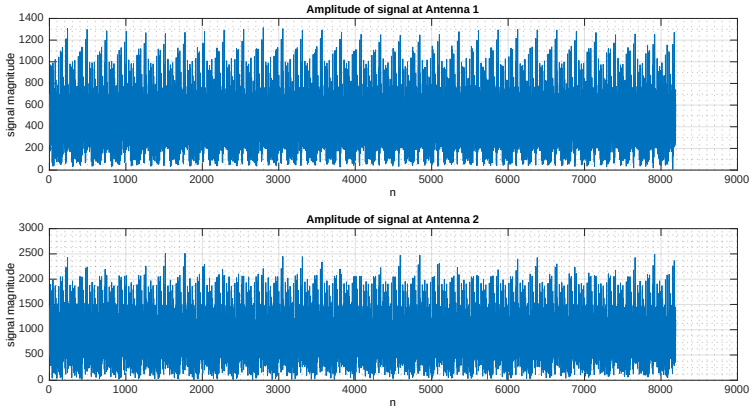

Figure 7.2: An arbitrary chosen frame during Offline Calibration

7.2.2 Step 2: Estimating and Compensating the CFO

Since calibrations are done thru connecting cables, then there doesn't seem to be a multipath channel. In other words, we assume a single direct path of the signal, that is traversing directly thru the cables. Having said that, we shall now write equation (7.40) for a single path, thus the received signal thru the cables read:

$$\begin{aligned} \boldsymbol{y}_n(l) &= \boldsymbol{D}_\epsilon(l)\widetilde{\boldsymbol{F}}(l)\widetilde{\boldsymbol{B}}\boldsymbol{C}\boldsymbol{G}\widetilde{\boldsymbol{a}}_n \\ &= \boldsymbol{D}_\epsilon(l)\widetilde{\boldsymbol{F}}(l)\widetilde{\boldsymbol{B}}\boldsymbol{c}(\tau_0)\bar{\bar{\gamma}}_0\widetilde{a}_n(\theta_0) \end{aligned} \tag{7.41}$$

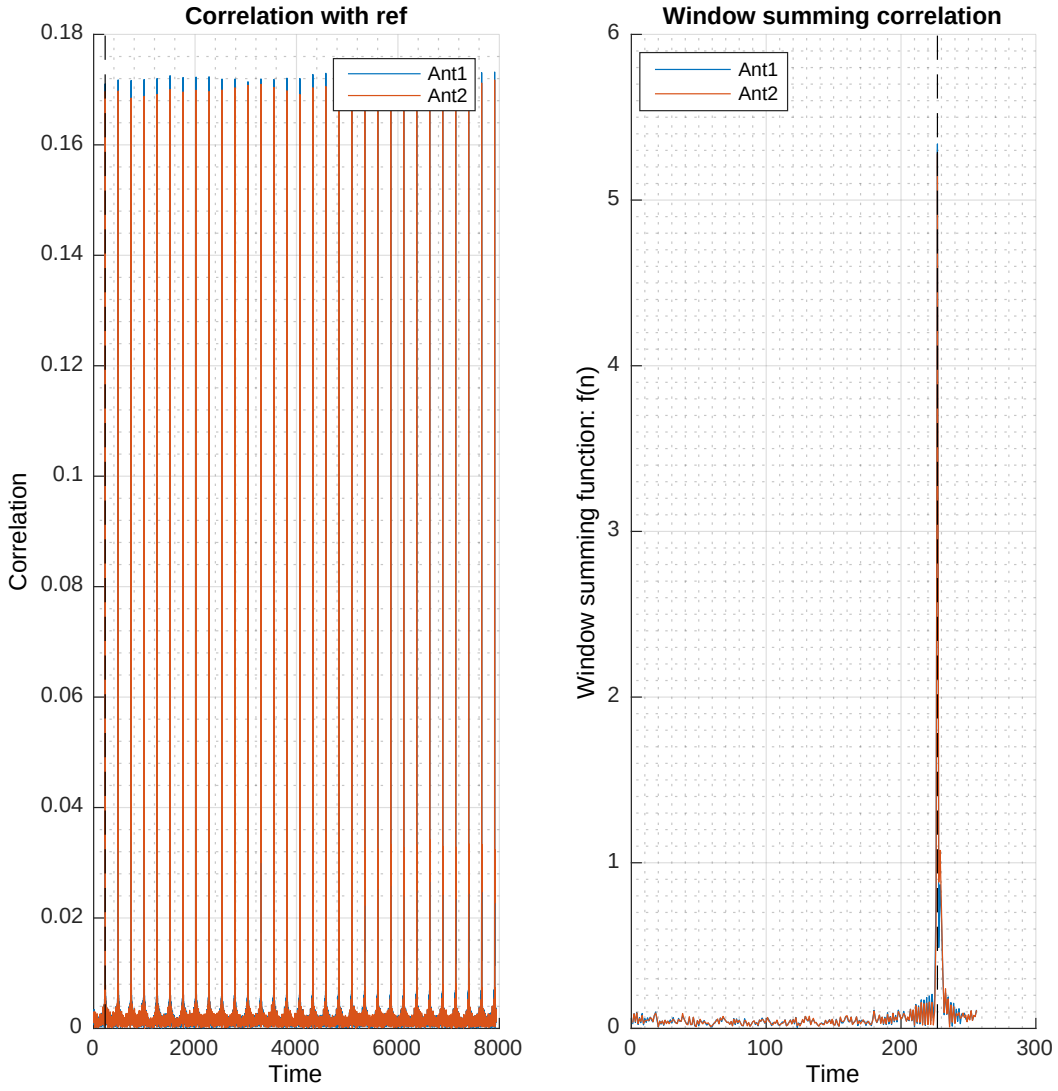

Figure 7.3: Detection of Start Index

But with connected cables, there is no physical meaning of a steering vector $a_n(\theta)$, since ideally the received signal should arrive at the same time instant up till the ADC. However, it is important to include the delays per path, which was given below equation (7.27), which is

$$\widetilde{a}_n(\theta) = e^{j2\pi\beta_n(\epsilon_f^n)} \tag{7.42}$$

Therefore we shall assume $a_n(\theta) = 1$. Also since $\bar{\bar{\gamma}}_0$ is common for all n (i.e. common for all antennas), then we shall assume it to be equal to 1. Let $2\pi\beta_n(\epsilon_f^n) = \phi_n$, therefore equation (7.41) will read

$$\boldsymbol{y}_n(l) = \boldsymbol{D}_\epsilon(l)\widetilde{\boldsymbol{F}}(l)\widetilde{\boldsymbol{B}}\boldsymbol{c}(\tau_0)e^{j\phi_n} \tag{7.43}$$

In this subsection, when we say compensating for CFO, when mean equalizing matrices $\boldsymbol{D}_\epsilon(l)$. The procedure is as follows:

1. We choose a random OFDM symbol as a reference symbol. Let's say we have picked the first symbol, $\boldsymbol{y}_n(0)$ to serve as reference.

2. Let us consider the following inner products $\boldsymbol{y}_n^H(l)\boldsymbol{y}_n(0)$, which can be expressed as

$$\begin{aligned}\boldsymbol{y}_n^H(l)\boldsymbol{y}_n(0) &= \left(\boldsymbol{D}_\epsilon(l)\widetilde{\boldsymbol{F}}(l)\widetilde{\boldsymbol{B}}\boldsymbol{c}(\tau_0)e^{j\phi_n}\right)^H\left(\boldsymbol{D}_\epsilon(0)\widetilde{\boldsymbol{F}}(l)\widetilde{\boldsymbol{B}}\boldsymbol{c}(\tau_0)e^{j\phi_n}\right)\\ &= e^{-j\phi_n}\left(\widetilde{\boldsymbol{F}}(l)\widetilde{\boldsymbol{B}}\boldsymbol{c}(\tau_0)\right)^H\left(\boldsymbol{D}_\epsilon^*(l)\boldsymbol{D}_\epsilon(0)\right)\left(\widetilde{\boldsymbol{F}}(l)\widetilde{\boldsymbol{B}}\boldsymbol{c}(\tau_0)\right)e^{j\phi_n}\\ &= \left(\widetilde{\boldsymbol{F}}(l)\widetilde{\boldsymbol{B}}\boldsymbol{c}(\tau_0)\right)^H\left(\boldsymbol{D}_\epsilon^*(l)\boldsymbol{D}_\epsilon(0)\right)\left(\widetilde{\boldsymbol{F}}(l)\widetilde{\boldsymbol{B}}\boldsymbol{c}(\tau_0)\right)\end{aligned} \tag{7.44}$$

where $\boldsymbol{D}_\epsilon^*(l) = \boldsymbol{D}_\epsilon^H(l)$ since this matrix is diagonal. Using equation (7.38), we get that

$$\begin{aligned}\boldsymbol{D}_\epsilon^*(l)\boldsymbol{D}_\epsilon(0) &= \text{diag}[e^{-j2\pi\epsilon_f^n lMT_s^n}\dots e^{-j2\pi\epsilon_f^n lMT_s^n}]\\ &= e^{-j2\pi\epsilon_f^n lMT_s^n}\,\text{diag}[1\dots 1]\\ &= e^{-j2\pi\epsilon_f^n lMT_s^n}\boldsymbol{I}\end{aligned} \tag{7.45}$$

Plugging (7.45) in (7.44), we get

$$\begin{aligned}\boldsymbol{y}_n^H(l)\boldsymbol{y}_n(0) &= \left(\widetilde{\boldsymbol{F}}(l)\widetilde{\boldsymbol{B}}\boldsymbol{c}(\tau_0)\right)^H\left(e^{-j2\pi\epsilon_f^n lMT_s^n}\boldsymbol{I}\right)\left(\widetilde{\boldsymbol{F}}(l)\widetilde{\boldsymbol{B}}\boldsymbol{c}(\tau_0)\right)\\ &= e^{-j2\pi\epsilon_f^n lMT_s^n}\left(\widetilde{\boldsymbol{F}}(l)\widetilde{\boldsymbol{B}}\boldsymbol{c}(\tau_0)\right)^H\left(\widetilde{\boldsymbol{F}}(l)\widetilde{\boldsymbol{B}}\boldsymbol{c}(\tau_0)\right)\\ &= e^{-j2\pi\epsilon_f^n lMT_s^n}\left\|\widetilde{\boldsymbol{F}}(l)\widetilde{\boldsymbol{B}}\boldsymbol{c}(\tau_0)\right\|^2\end{aligned} \tag{7.46}$$

Now observe that the phase of $\boldsymbol{y}_n^H(l)\boldsymbol{y}_n(0)$ is $2\pi\epsilon_f^n lM$, which allows us to estimate ϵ_f^n. To do this in an optimal manner, we collect all the phases of the $L-1$ inner products in one vector, call it $\boldsymbol{z}$ as follows:

$$\tilde{\boldsymbol{z}}_n = \begin{bmatrix}\angle\boldsymbol{y}_n^H(1)\boldsymbol{y}_n(0)\\ \angle\boldsymbol{y}_n^H(2)\boldsymbol{y}_n(0)\\ \vdots\\ \angle\boldsymbol{y}_n^H(L-1)\boldsymbol{y}_n(0)\end{bmatrix} = \begin{bmatrix}2\pi\epsilon_f^n MT_s^n\\ 2\pi\epsilon_f^n 2MT_s^n\\ \vdots\\ 2\pi\epsilon_f^n(L-1)MT_s^n\end{bmatrix} \tag{7.47}$$

3. We regard $\boldsymbol{z}_n$ as a shifted vector, i.e.

$$\tilde{\boldsymbol{z}}_n = \begin{bmatrix} 2\pi\epsilon_f^n M T_s^n + \phi_n^{(1)} \\ 2\pi\epsilon_f^n 2M T_s^n + \phi_n^{(1)} \\ \vdots \\ 2\pi\epsilon_f^n (L-1) M T_s^n + \phi_n^{(1)} \end{bmatrix} \tag{7.48}$$

where $\phi_n^{(1)}$ should be read as follows: *It is the first attempt of estimating absolute phases at the n^{th} antenna.* This technique actually helped us to resolve phase ambiguities when it came to estimation of ϕ_n. This will be further elaborated on below. Furthermore, we are observing noisy estimates of $\boldsymbol{z}_n$, i.e. we have access to $\boldsymbol{z}'_n$,

$$\boldsymbol{z}'_n = \tilde{\boldsymbol{z}}_n + \boldsymbol{w}_n \tag{7.49}$$

where $\boldsymbol{w}_n$ is noise, *that is not necessarily Gaussian.*

4. Now that the problem is set, we would like to retrieve ϵ_f^n from $\boldsymbol{z}'_n$. Although, there is a small problem, which is that we do not know T_s^n, we know that T_s^n is a perturbed version of T_s according to equation (**??**), we can say that

$$\begin{aligned} \tilde{\boldsymbol{z}}_n &= \begin{bmatrix} 2\pi\epsilon_f^n M T_s^n + \phi_n^{(1)} \\ 2\pi\epsilon_f^n 2M T_s^n + \phi_n^{(1)} \\ \vdots \\ 2\pi\epsilon_f^n (L-1) M T_s^n + \phi_n^{(1)} \end{bmatrix} \\ &= \begin{bmatrix} 2\pi\epsilon_f^n M (T_s - \epsilon_T^n) + \phi_n^{(1)} \\ 2\pi\epsilon_f^n 2M (T_s - \epsilon_T^n) + \phi_n^{(1)} \\ \vdots \\ 2\pi\epsilon_f^n (L-1) M (T_s - \epsilon_T^n) + \phi_n^{(1)} \end{bmatrix} \\ &= \underbrace{\underbrace{2\pi\epsilon_f^n M}_{O(\epsilon)} \begin{bmatrix} T_s + \phi_n^{(1)} \\ 2T_s + \phi_n^{(1)} \\ \vdots \\ (L-1)T_s + \phi_n^{(1)} \end{bmatrix}}_{\boldsymbol{z}_n} \underbrace{- \underbrace{2\pi\epsilon_f^n \epsilon_T^n M}_{O(\epsilon^2)} \begin{bmatrix} 1 \\ 2 \\ \vdots \\ (L-1) \end{bmatrix}}_{\boldsymbol{v}_n} \\ &= \boldsymbol{z}_n + \boldsymbol{v}_n \end{aligned} \tag{7.50}$$

where $\boldsymbol{z}_n$ is seen as the unperturbed vector for ϵ_f^n-estimation and $\boldsymbol{v}_n$ will be regarded as noise because it is of an order $O(\epsilon^2)$ when compared to $\boldsymbol{z}_n$ which is of order $O(\epsilon)$.

5. Plugging (7.50) in (7.49), we get

$$\boldsymbol{z}'_n = \boldsymbol{z}_n + \underbrace{\boldsymbol{v}_n + \boldsymbol{w}_n}_{\boldsymbol{w}'_n} = \boldsymbol{z}_n + \boldsymbol{w}'_n \tag{7.51}$$

Solving via Least Squares means that we optimize the following:

$$\underset{\epsilon_f^n, \phi_n^{(1)}}{\text{minimize}} \|\tilde{\boldsymbol{z}}_n - \boldsymbol{z}_n\| \tag{7.52}$$

yields in

$$\begin{bmatrix} \hat{\epsilon}_f^n \\ \cdots \\ \hat{\phi}_n^{(1)} \end{bmatrix} = (\boldsymbol{\Pi}^T \boldsymbol{\Pi})^{-1} \boldsymbol{\Pi}^T \boldsymbol{z}'_n \tag{7.53}$$

where

$$\boldsymbol{\Pi} = \begin{bmatrix} 2\pi M T_s(1) & 1 \\ 2\pi M T_s(2) & 1 \\ \vdots & \vdots \\ 2\pi M T_s(L-1) & 1 \end{bmatrix} \tag{7.54}$$

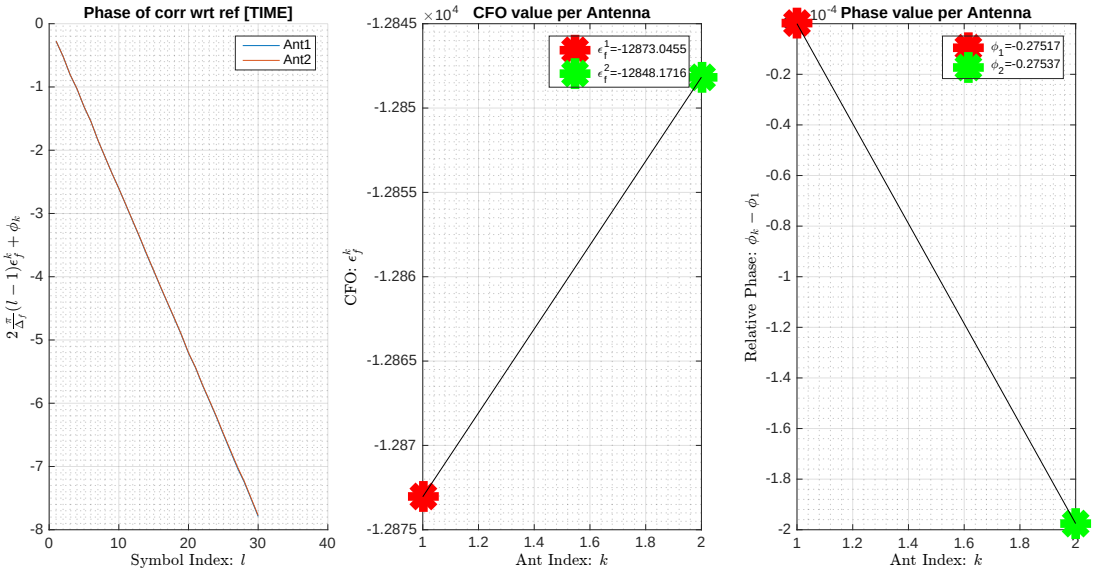

Figure 7.4: 1^{st} Trial: Estimating CFO and phases

Notice that this operation is done twice, to estimate any residual values. The third time we call the function is for verification purposes only.

Note that in Figures 7.4, 7.5, and 7.6, the difference of phases $\phi_1 - \phi_2$ is negligible, i.e. it is of order 10^{-4}. This is natural because the phase has been eliminated due to the usage of a first symbol as reference. Including such a step[5] in this case has not done

[5]Phase offsets ϕ in Least Squares in equation (7.48)

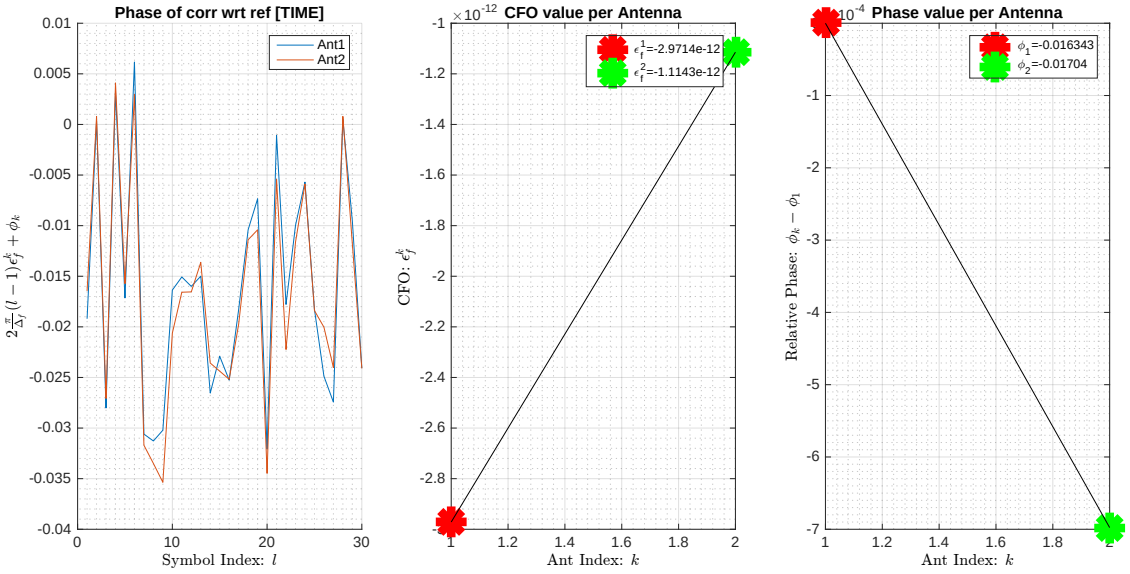

Figure 7.5: 2^{nd} Trial: Estimating CFO and Phases after 1^{st} compensation

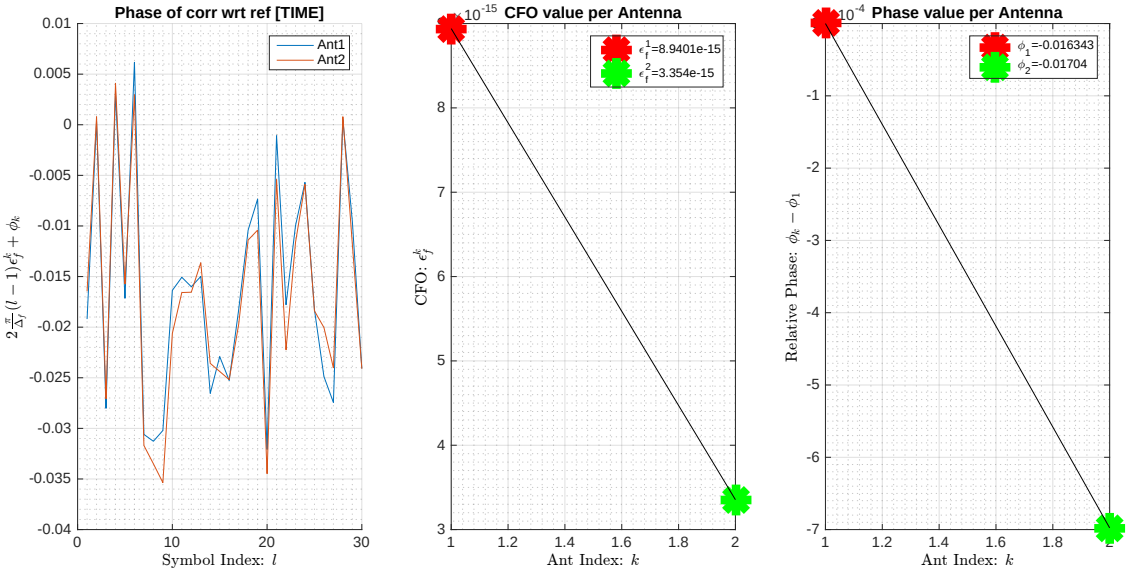

Figure 7.6: 3^{rd} Trial (Verification): Estimating CFO and Phases after 2^{nd} compensation

anything. However, one may choose to use a generated reference signal to form all the inner products in equation (7.47). In that case, including phase offsets ϕ in the LS step is crucial. We have repeated the same experiment but this time by using our own generated reference signal to get Figures 7.7, 7.8, and 7.9.

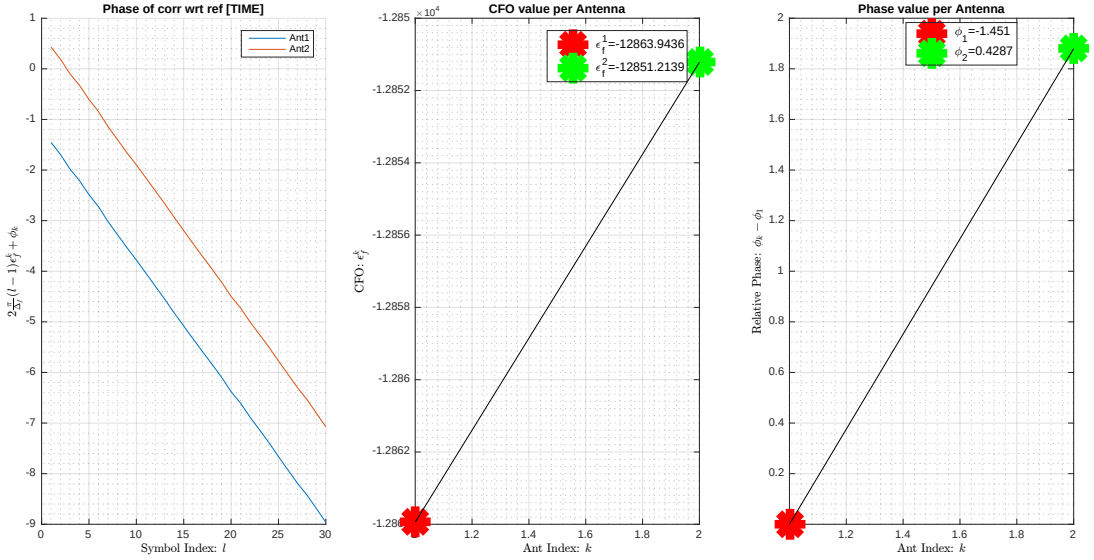

Figure 7.7: 1^{st} Trial: Estimating CFO and phases (Using a generated reference signal)

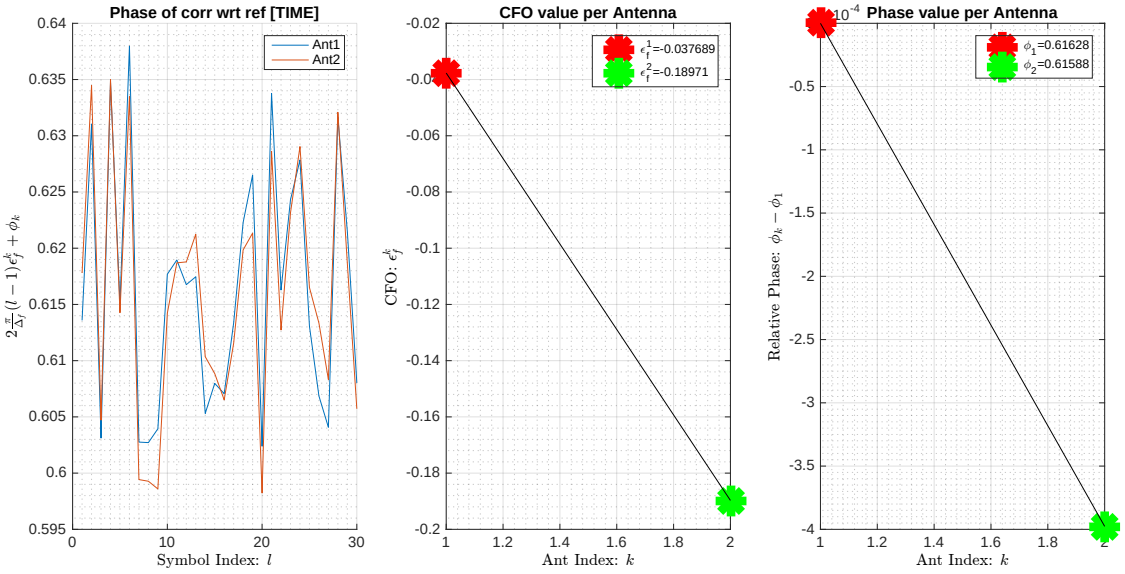

Figure 7.8: 2^{nd} Trial: Estimating CFO and Phases after 1^{st} compensation (Using a generated reference signal)

7.2.3 Step 3: Compensating Tx/Rx Filter Effects

Now we assume that we have compensated the effect of CFO, i.e.

$$\begin{aligned}\bar{\boldsymbol{y}}_n(l) &= \hat{\boldsymbol{D}}_\epsilon^H(l)\boldsymbol{y}_n(l) \\ &= \hat{\boldsymbol{D}}_\epsilon^H(l)\boldsymbol{D}_\epsilon(l)\widetilde{\boldsymbol{F}}(l)\widetilde{\boldsymbol{B}}\boldsymbol{C}\boldsymbol{G}\widetilde{\boldsymbol{a}}_n \\ &\simeq \widetilde{\boldsymbol{F}}(l)\widetilde{\boldsymbol{B}}\boldsymbol{c}(\tau_0)\bar{\bar{\gamma}}_0\widetilde{a}_n(\theta_0) + \underbrace{O(\epsilon_f - \hat{\epsilon}_f)}_{\text{seen as noise}}\end{aligned} \tag{7.55}$$

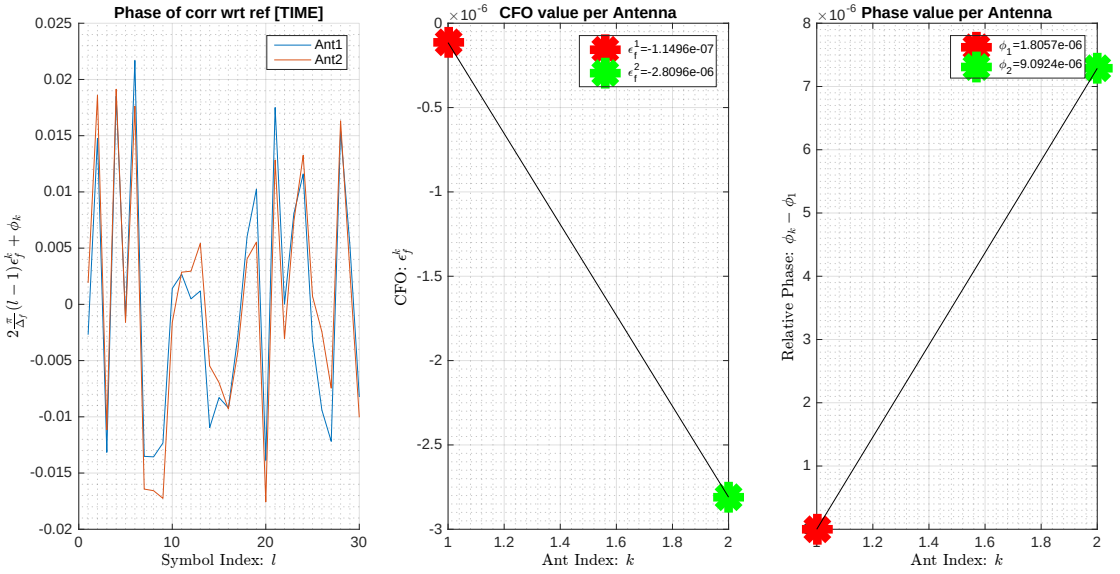

Figure 7.9: 3^{rd} Trial (Verification): Estimating CFO and Phases after 2^{nd} compensation (Using a generated reference signal)

where the $O(\epsilon_f - \hat{\epsilon}_f)$ term comes from a Taylor series expansion of the exponential function in the neighbourhood of 0. To proceed there is an assumption made of matrix $\widetilde{\boldsymbol{F}}(l)$, which is mainly an assumption on the SFO. Let us look at the p^{th} row of $\widetilde{\boldsymbol{F}}(l)$ (equation (7.31)). They are all multiples of a phase shift: $(z.z_{\delta_n})^{(p+lM)}$.

$$\begin{aligned}(z.z_{\delta_n})^{(p+lM)} &= z^{(p+lM)} z_{\delta_n}^{(p+lM)} \\ &= z^p e^{-j\frac{2\pi}{M}(p+lM)\delta_T^n}\end{aligned} \tag{7.56}$$

The approximation here is the following:

$$(p + lM)\delta_T^n \simeq lM\delta_T^n \tag{7.57}$$

this means that we shall assume that the SFO effect has an effect from symbol to symbol only and not within a symbol. Plugging equation (7.57) back in (7.56) gives

$$(z.z_{\delta_n})^{(p+lM)} = z^p e^{-j2\pi l\delta_T^n} \tag{7.58}$$

Thanks to this approximation, now we can say that the perturbed DFT in equation (7.39) becomes

$$\widetilde{\boldsymbol{F}}(l) = e^{-j2\pi l\delta_T^n}\boldsymbol{F} \tag{7.59}$$

where $\boldsymbol{F}$ is the DFT matrix. Now the model in (7.55) becomes[6]:

$$\bar{\boldsymbol{y}}_n(l) = e^{-j2\pi l\delta_T^n}\boldsymbol{F}\widetilde{\boldsymbol{B}}\boldsymbol{c}(\tau_0)\bar{\bar{\gamma}}_0\widetilde{a}_n(\theta_0) \tag{7.60}$$

[6]We do not express noise for presentation's sake

Going to frequency domain means multiplying with $\boldsymbol{F}^H$, i.e.

$$\bar{\boldsymbol{Y}}_n(l) = \boldsymbol{F}^H \bar{\boldsymbol{y}}_n(l) = e^{-j2\pi l \delta_T^n} \boldsymbol{F}^H \boldsymbol{F} \widetilde{\boldsymbol{B}} \boldsymbol{c}(\tau_0) \bar{\bar{\gamma}}_0 \widetilde{a}_n(\theta_0) \tag{7.61}$$

Since $\boldsymbol{F}$ is unitary, then $\boldsymbol{F}^H \boldsymbol{F} = \boldsymbol{I}$, hence

$$\bar{\boldsymbol{Y}}_n(l) = e^{-j2\pi l \delta_T^n} \widetilde{\boldsymbol{B}} \boldsymbol{c}(\tau_0) \bar{\bar{\gamma}}_0 \widetilde{a}_n(\theta_0) \tag{7.62}$$

In this subsection, since our main focus is the $\boldsymbol{B}$ matrix, then we treat all other parameters as nuisance. In other words, we let $\nu_{n,l} = e^{-j2\pi l \delta_T^n} \bar{\bar{\gamma}}_0 \widetilde{a}_n(\theta_0)$ and hence

$$\bar{\boldsymbol{Y}}_n(l) = \nu_{n,l} \widetilde{\boldsymbol{B}} \boldsymbol{c}(\tau_0) \tag{7.63}$$

Recall the form of $\widetilde{\boldsymbol{B}}$ in equation (7.32) and that

$$\widetilde{b}_m = G(m\Delta_f) b_m \tag{7.64}$$

We know what b_m are a priori, therefore we compensate for all such BPSK symbols by a simple diagonal matrix multiplication:

$$\bar{\bar{\boldsymbol{Y}}}_n(l) = \boldsymbol{B}^H \bar{\boldsymbol{Y}}_n(l) = \nu_{n,l} \boldsymbol{B}^H \widetilde{\boldsymbol{B}} \boldsymbol{c}(\tau_0) = \nu_{n,l} \boldsymbol{G} \boldsymbol{c}(\tau_0) \tag{7.65}$$

where

$$\boldsymbol{G} = \text{diag } [G((-\frac{M}{2})\Delta_f) \dots G((\frac{M}{2})\Delta_f)] \tag{7.66}$$

Now plotting the phase of $\bar{\bar{\boldsymbol{Y}}}_n(l)$, we get:
If $\boldsymbol{G} = \boldsymbol{I}$, i.e. no Tx/Rx filters, then we would have observed a straight line with a slope that is decided by the value of τ_0 and an offset that is decided by the phase of $\nu_{n,l}$. Figure 7.10 suggests that there are some filters present in the Transmission and/or Reception chain. The good news is that the phases seem to be static[7]. Observe that we have a *"sinusoidal shape"* in the figure. Indeed one might assume that the phase filter behaves sinusoidally. If we were to assume that, then we have to do a Maximum Likelihood estimator on the amplitude, phase and frequency of the sinusoid that we have. We have proceeded in another manner, i.e. we have divided the set of frequencies into 3 zones, that are separated by vertical dashed lines in Figure 7.10: LeftZone, CenterZone, RightZone. Each zone is parametrised by the following parameters:

- LeftZone: Slope a_1 and offset b_1.
- CenterZone: Slope a_2 and offset b_2.

[7]Variation effects are due to noise of course. We have done exhaustive simulations and found out that the phases are not time-varying.

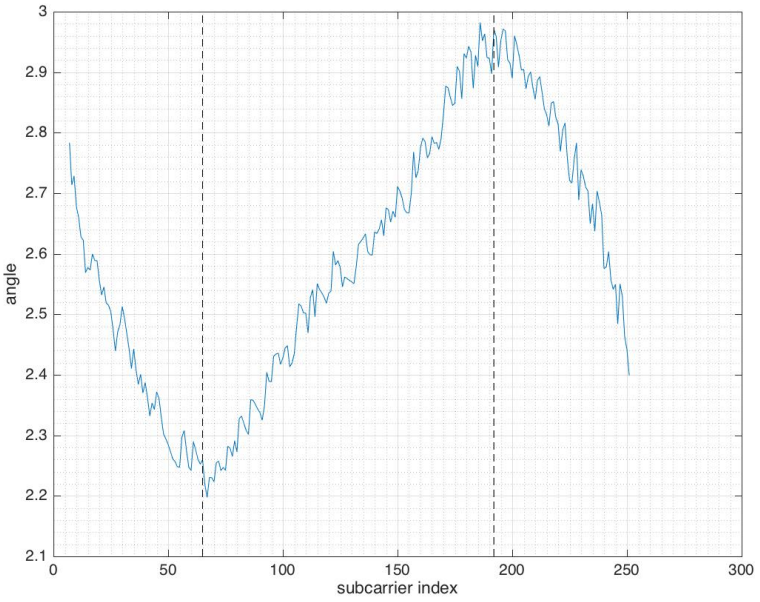

Figure 7.10: Phases of $\bar{\bar{\boldsymbol{Y}}}_n(l_0)$ for some l_0.

- RightZone: Slope a_3 and offset b_3.

Indeed these slopes and offsets change from symbol to other. The change is **not due to the filter effects $\mathbf{G}$, but due to τ_0 and $\nu_{n,l}$.** The former contributes in a change of a **common** slope. However, the latter contributes in an addition of a **common** offset. Therefore, a_1, a_2, a_3 will have a common τ_0 added to their values and b_1, b_2, b_3 will have a common $\angle\nu_{n,l}$ added to their values.

So as to be concise, the task of this subsection is to eliminate any filter slopes/offsets. Hence, we are interested in the relative slopes/offsets rather than the absolute ones. To this extent, let

$$a_{21} = a_2 - a_1 \tag{7.67}$$

$$a_{32} = a_3 - a_2 \tag{7.68}$$

$$b_{21} = b_2 - b_1 \tag{7.69}$$

$$b_{32} = b_3 - b_2 \tag{7.70}$$

To estimate these parameters, we just do a Least Squares fit on each zone separately and then a compensation is done on the angles. Note that we have assumed a flat filter in terms of magnitude, therefore the compensation is done as follows:

$$\bar{\bar{\boldsymbol{Y}}}_n(l) = \boldsymbol{G}^H \bar{\bar{\boldsymbol{Y}}}_n(l) = \nu_{n,l} \boldsymbol{G}^H \boldsymbol{G} \boldsymbol{c}(\tau_0) = \nu_{n,l} \boldsymbol{c}(\tau_0) \tag{7.71}$$

In Figure 7.11, we have plotted the estimated values of a_{21}, a_{32}, b_{21}, and b_{32} on a chosen frame. As one can see, these values tend to be constant as we mentioned. We have averaged the estimates over multiple symbols and frames and obtained their mean values, which we used in the MATLAB code of this block. Note that mean values of estimates are needed for an online phase. In Figure 7.12, we have re-estimated a_{21}, a_{32}, b_{21}, and b_{32} after doing a compensation on the mean values. We can see that the slopes and phases have been at least reduced by 10^{-2} order of magnitude.

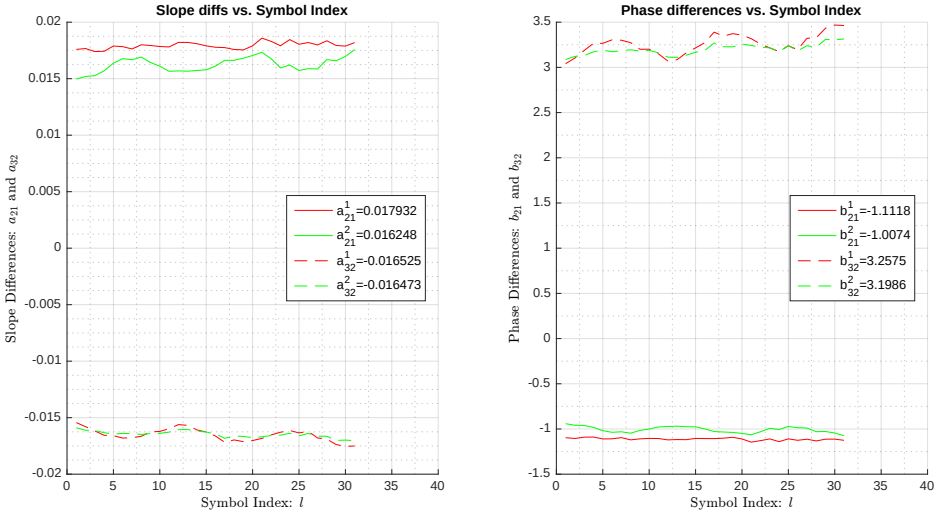

Figure 7.11: Estimation of a_{21}, a_{32}, b_{21}, and b_{32} on a chosen frame per antenna.

Note that we have finally chosen values a_{21}, a_{32}, b_{21}, and b_{32} which were obtained by averaging multiple frames and symbols.

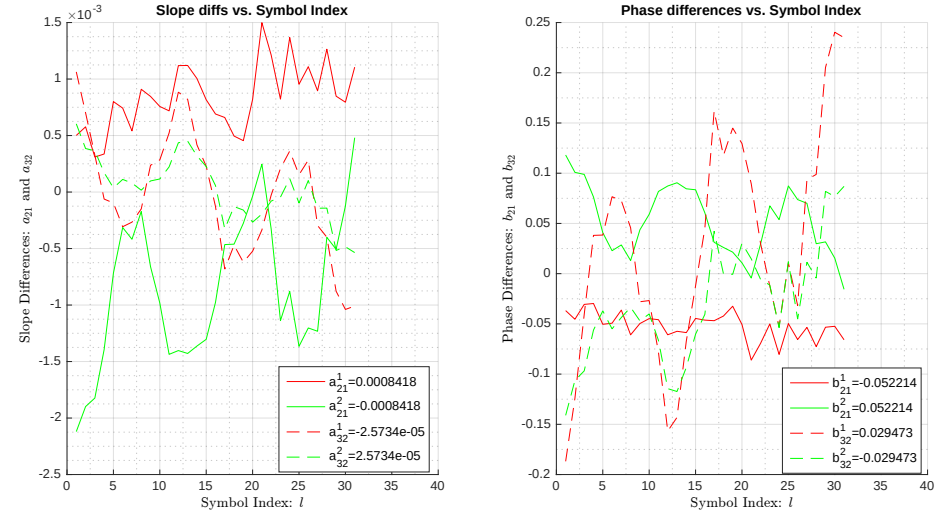

Figure 7.12: Verification of estimates of a_{21}, a_{32}, b_{21}, and b_{32} per antenna after compensating by their means over multiple frames and symbols

7.2.4 Step 4: Estimating and Compensating the SFO and antenna phases

Now that we have compensated the signal in the past three steps, our signal, more or less, follows the model

$$\bar{\bar{\boldsymbol{Y}}}_n(l) = \nu_{n,l}\boldsymbol{c}(\tau_0) = e^{-j2\pi l\delta_T^n}\bar{\bar{\gamma}}_0\widetilde{a}_n(\theta_0)\boldsymbol{c}(\tau_0) = e^{-j2\pi l\delta_T^n}\bar{\bar{\gamma}}_0 e^{j\phi_n}\boldsymbol{c}(\tau_0) \tag{7.72}$$

Here, the parameters that need to be estimating per antenna, that are

- The SFO δ_T^n
- The antenna phase ϕ_n

We propose a 2-stage Lest Squares fit for this estimation:

1^{st} stage: On a Symbol Level

Let

$$\varrho_{l,n} = 2\pi l\delta_T^n - \phi_n \tag{7.73}$$

and for each $\bar{\bar{\boldsymbol{Y}}}_n(l)$. Notice that the phase of vector in equation (7.73) could be expressed as

$$\angle\bar{\bar{\boldsymbol{Y}}}_n(l) = \begin{bmatrix} 1 \\ 2\pi\Delta_f\tau_0 \\ \vdots \\ 2\pi\Delta_f(M-1)\tau_0 \end{bmatrix} + \begin{bmatrix} \varrho_{l,n} \\ \varrho_{l,n} \\ \vdots \\ \varrho_{l,n} \end{bmatrix} \tag{7.74}$$

Applying LS as in equations (7.47) till (7.49) gives us estimates $\hat{\tau}_0^{(l)}$ and $\hat{\varrho}_{l,n}$. Note that $\hat{\tau}_0^{(l)}$ includes superscript l because each symbol l yields a different τ_0 estimate. Our main focus is the latter, i.e. $\varrho_{l,n}$, which is estimated in the 2^{nd} stage below.

2^{nd} stage: On a Frame Level

Now, let us stack all the collected $\hat{\varrho}_{l,n}$ per antenna, namely

$$\begin{bmatrix} \hat{\varrho}_{1,n} \\ \hat{\varrho}_{2,n} \\ \vdots \\ \hat{\varrho}_{L,n} \end{bmatrix} = \begin{bmatrix} 2\pi\delta_T^n \\ 2\pi 2\delta_T^n \\ \vdots \\ 2\pi L\delta_T^n \end{bmatrix} - \begin{bmatrix} \phi_n \\ \phi_n \\ \vdots \\ \phi_n \end{bmatrix} \tag{7.75}$$

Notice that the slope is the SFO δ_T^n and the phase is the antenna phase ϕ_n, that are estimated via Least Squares as well. Hence we can say that (following equations (7.47) till (7.49)) we get estimates $\hat{\delta}_T^n$ and $\hat{\phi}_n$.

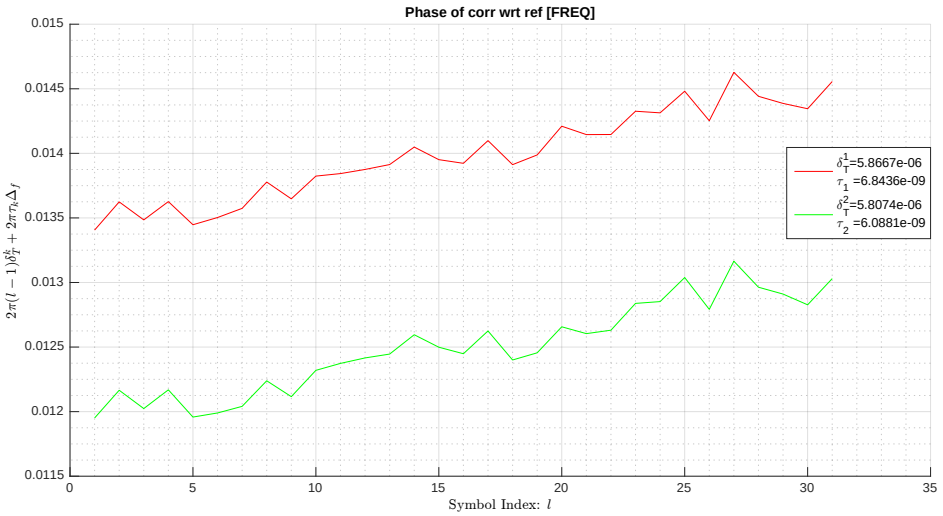

Figure 7.13: Estimation of δ_T^n at a Frame Level

Figure 7.14: Estimation of ϕ_n at a Frame Level

We can see, according to Figure 7.13, that the estimation of δ_T^n lies in the slope of plot as explained in (7.75). The Phase lies in the offset (or difference) of plots in Figure 7.14. **It is worth mentioning that AoA estimation is possible due to the observation that $\phi_2 - \phi_1$ is constant and therefore could be compensated for in the AoA estimation phase**.

7.3 Online method

In this section, we describe the main blocks of the *online* method for our parameter estimation approach, in order to extract the Angle of Arrival of the Line-of-Sight component between the Tx and Wi-Fi Rx.

7.3.1 Why JADED and CSI?

The localisation algorithm that is used to estimate the AoA of the LoS is the CESS-JADED-RIP algorithm, which stands for Joint Angle and Delay Estimation and Detection. It is worth noting the following points of the CESS-JADED-RIP algorithm:

- CESS-JADED-RIP operates for OFDM/ULA systems only.
- CESS-JADED-RIP does not impose the uncorrelated sources assumption. This means that JADED could jointly estimate the Angles and Times of Arrival of multiple coherent sources, which is the case of multipath propagation.
- CESS-JADED-RIP functions properly given a single snapshot, which is what we do here.
- CESS-JADED-RIP does not need prior knowledge of the number of multipath components or number of sources.

Throughout all the conducted experiments, we have used only 2 antennas placed next to each other on the same plane, hence ULA. There was one problem when we look at the OFDM structure we have, i.e. we have a "quasi-OFDM" like structure since the 3 central subcarriers were not used. To overcome this, we have used Cubic Spline Interpolation (CSI) to, more or less, interpolate the 3 missing subcarriers to have a continuous frequency spectrum.

7.3.2 Main blocks

The block diagram depicted below in Fig. 7.15 shows the 4 essential blocks of the online method. Indeed, after detecting the start of the OFDM symbol as described in Section 7.2.1, we should use the stored calibration parameters to calibrate our data before using any parameter estimation model. A Cubic Spline Interpolation is done in frequency domain to solve the "missing subcarriers" problem as described above. Finally, the CESS-JADED-RIP is applied on each symbol to extract the AoA of the LoS component.

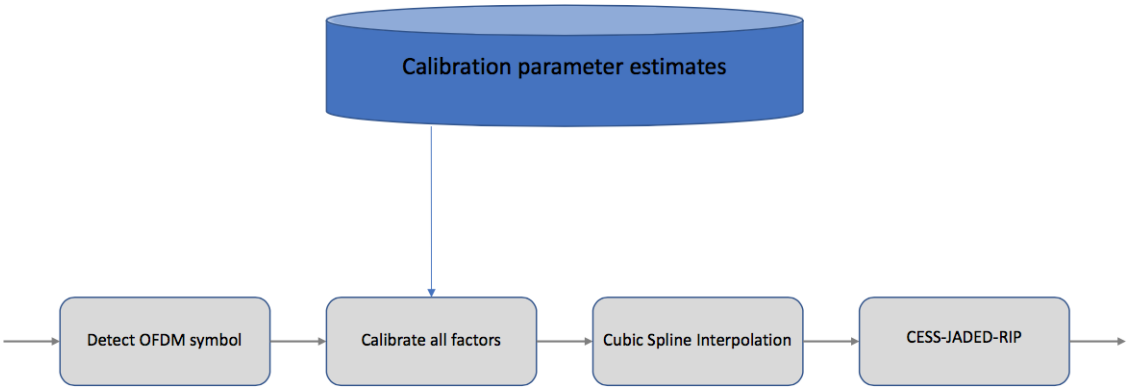

Figure 7.15: Block Diagram of the proposed online method

7.3.3 Real data

To demonstrate that this method actually works, we have set up a campaign shown in Fig. 7.16. As we can see, we have a Wi-Fi Rx equipped with 2 antennas. The signal

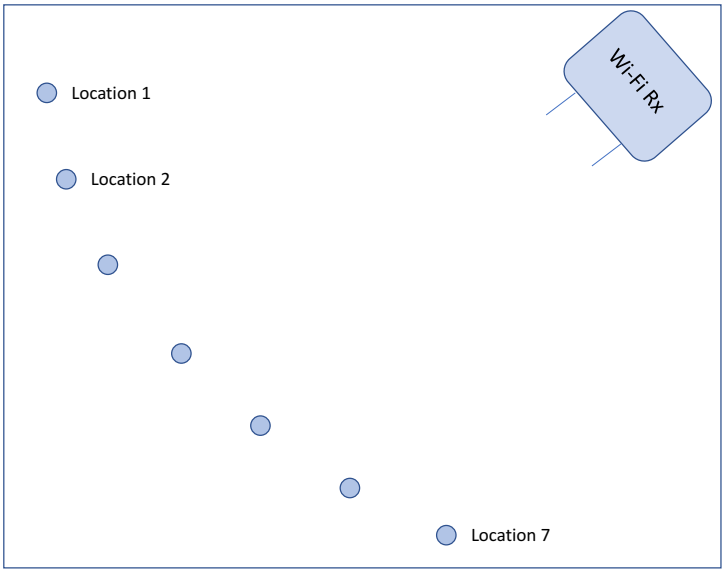

Figure 7.16: Campaign1

transmitted is a 80 MHz OFDM symbol. We have ran the online method described and plotted 3 subplots in Fig. 7.17:

- 1^{st} subplot: The estimated ToA of the LoS as a function of OFDM symbol.
- 2^{nd} subplot: The estimated AoA of the LoS as a function of OFDM symbol.

- 3^{rd} subplot: An accuracy measure that indicates the quality of estimation, which we talk about below.

Also observe the red and black vertical dashed lines, which indicate:

- Red dashed line: indicates moving from one frame to another.
- Black dashed line: indicates moving from one position to another on a circle where the Wi-Fi is acting as the center.

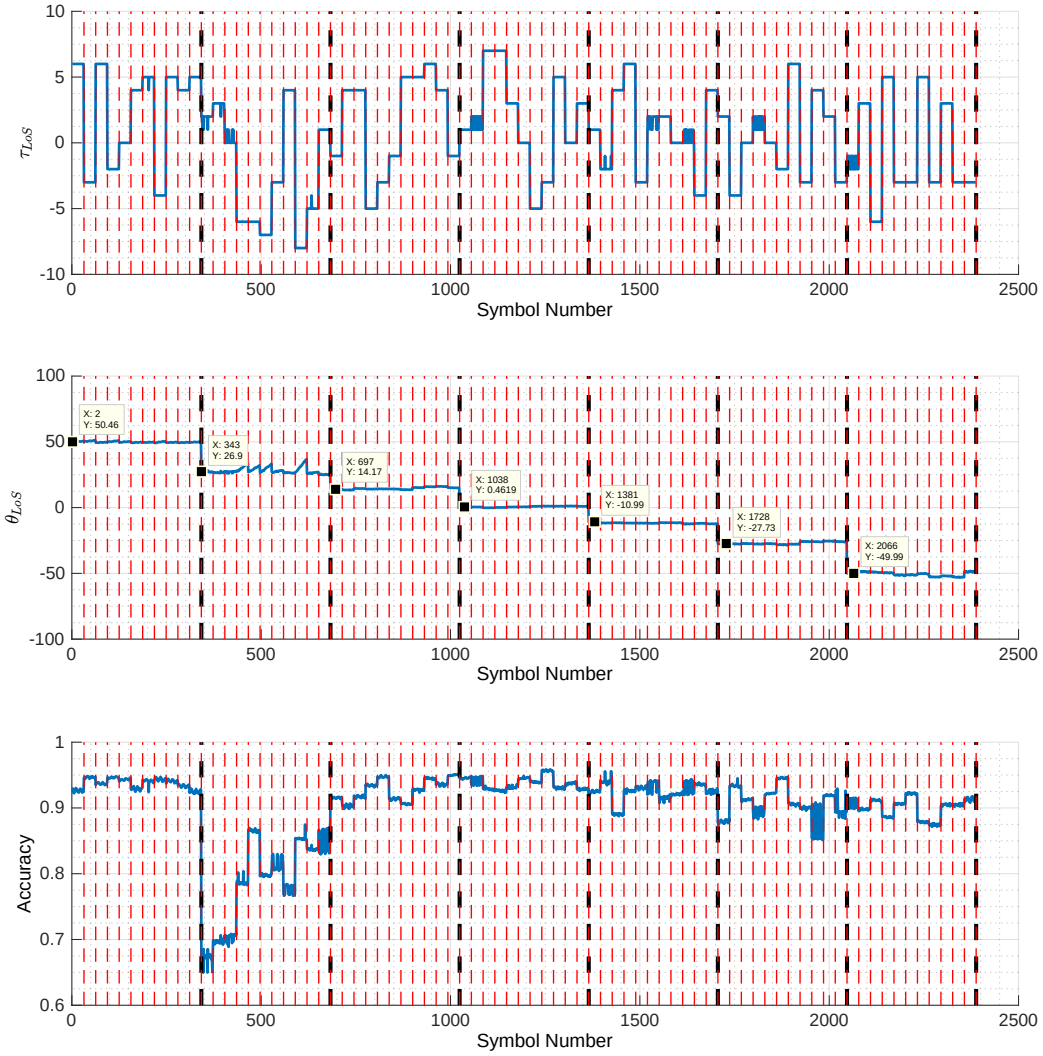

Figure 7.17: Campaign1

We have considered the following cost function:

$$f(\boldsymbol{\Theta}, \boldsymbol{\Gamma}) = \frac{\boldsymbol{x}^H \boldsymbol{P}(\boldsymbol{\Theta}, \boldsymbol{\Gamma}) \boldsymbol{x}}{\boldsymbol{x}^H \boldsymbol{x}} \tag{7.76}$$

where $\boldsymbol{x}$ is the spatio-frequency vector observed and $\boldsymbol{P}(\boldsymbol{\Theta},\boldsymbol{\Gamma})$ is

$$\boldsymbol{P}(\boldsymbol{\Theta},\boldsymbol{\Gamma}) = H(\boldsymbol{\Theta},\boldsymbol{\Gamma})\Big(H^H(\boldsymbol{\Theta},\boldsymbol{\Gamma})H(\boldsymbol{\Theta},\boldsymbol{\Gamma})\Big)^{-1}H^H(\boldsymbol{\Theta},\boldsymbol{\Gamma}) \tag{7.77}$$

where

$$H(\boldsymbol{\Theta},\boldsymbol{\Gamma}) = \boldsymbol{A}(\boldsymbol{\Theta}) \boxtimes \boldsymbol{C}(\boldsymbol{\Theta}) \tag{7.78}$$

with

$$\boldsymbol{A}(\boldsymbol{\Theta}) = \Big[\boldsymbol{a}(\theta_1)\dots\boldsymbol{a}(\theta_q)\Big] \tag{7.79}$$

and

$$\boldsymbol{C}(\boldsymbol{\Gamma}) = \Big[\boldsymbol{c}(\tau_1)\dots\boldsymbol{c}(\tau_q)\Big] \tag{7.80}$$

and $\boxtimes$ denotes column-wise Kronecker product. Note that $\boldsymbol{\Theta} = [\theta_1 \dots \theta_q]$ and $\boldsymbol{\Gamma} = [\tau_1 \dots \tau_q]$ are the AoAs/ToAs, respectively, estimated by the JADED algorithm. The numerator of $f(\boldsymbol{\Theta},\boldsymbol{\Gamma})$ is nothing other than the Maximum Likelihood cost function, which should be maximized in order to estimate the AoAs and ToAs. In the absence of noise and in an ideal case, we have that

$$\boldsymbol{x}^H\boldsymbol{P}(\boldsymbol{\Theta},\boldsymbol{\Gamma})\boldsymbol{x} = \boldsymbol{x}^H\boldsymbol{x} \tag{7.81}$$

since the $\boldsymbol{x}$ vector fully resides in the subspace of $H(\boldsymbol{\Theta},\boldsymbol{\Gamma})$ and therefore

$$\boldsymbol{P}(\boldsymbol{\Theta},\boldsymbol{\Gamma})\boldsymbol{x} = \boldsymbol{x} \tag{7.82}$$

Hence in the absence of noise $f(\boldsymbol{\Theta},\boldsymbol{\Gamma}) = 1$. In case of no signal and pure noise, we have that

$$f(\boldsymbol{\Theta},\boldsymbol{\Gamma}) \simeq 0 \tag{7.83}$$

We can see a good AoA estimation in almost all OFDM symbols in this Campaign as it reflects the actual physical location of the user. We would like to mention that the closer we are to angle $\theta \simeq 90°$, we can see some perturbations going back to $\sim -90°$. This is normal as this is one characteristic of ULAs. Also when the WiFi is mounted in a corner of a room, we think that this issue can be resolved. Also, we have done other campaigns and we have obtained similar results.

7.4 Conclusions and future directions

In this chapter, we have seen multiple scenarios where we could indeed estimate the AoA of the LoS component in the presence of multipath. Herein, we have taken into account all factors that perturb the Joint Angle and Delay estimation problem and formulated

a system model accordingly. These factors are: Sampling Frequency Offset (SFO), Carrier Frequency Offset (CFO), Phase and Delay offsets at each antenna. To compensate for the effect of these critical factors, we propose an offline calibration method to compensate for all their effects. Lastly and most importantly, and with the help of the CESS-JADED-RIP algorithm and the Cubic Spline Interpolation technique, we have successfully been able to estimate the Angles and Times of Arrival of all the multipath components, which allowed for the extraction of the AoA of the LoS component.

Our last work related to this issue is trying to verify whether AoA estimation between a transmitter and receiver could be done in Non LoS (NLoS) scenarios. Some data show the possibility of this attempt. Future work must also be oriented towards a more computationally efficient way of applying the CESS-JADED-RIP method.

Chapter 8

Conclusions

First in Chapter 2, and with the help of random matrix tools, we have presented a modified MDL (MMDL) estimator for detecting the number of superimposed signals. This MMDL estimator dominates the traditional MDL especially at the low number of snapshots regime, i.e. when $L = \mathcal{O}(N)$. Simulation results have shown the potential of MMDL over the traditional MDL. Furthermore, in Chapter 3, and with the help of latent variables and Variational Bayes, we have derived an iterative algorithm that could estimate the Angles of Arrival (AoA) of the incoming sources with a single snapshot, without the knowledge of the number of sources, and with closely spaced sources at high SNR. We have also seen that it is possible that the proposed Newton-type forward backward greedy method performs faster, in terms of convergence and number of operations, and better, in terms of Mean-Squared-Error (MSE) of AoAs. In Chapter 4, we have presented two techniques to solve the highly nonlinear DML algorithm for joint times and angles of arrival: 2D-IQML and 2D-DIQML. Asymptotic performance analysis of both techniques were provided. It has been shown that 2D-IQML gives biased estimates of ToA/AoA and performs poorly at low SNR due to noise. An original "denoising" strategy is proposed, which constrains the Hessian of the cost function to be positive semi-definite. This "denoising" strategy is called 2D-DIQML that has been shown to be globally convergent. Furthermore, 2D-DIQML outperforms 2D-IQML because the former behaves asymptotically at any SNR as the latter behaves at high SNR. Finally, for localisation purposes, joint AoA and ToA information could be used to form a database, where a mapping is done between ToA/AoA vectors and location. Then, this database could be used in an online stage, where joint AoA/ToA estimation is done using the proposed algorithms, followed by a matching criteria that finds the best match in the database to obtain an estimate of the location of a wireless transmitter. We have also presented two algorithms based on 2D Matrix Pencils. These two algorithms allow joint

estimation of times and angles of arrival of multiple paths using only one snapshot. Algorithm 1 resolves more sources than Algorithm 2 in the case where the number of subcarriers is much larger than the number of antennas, which is the case of most Wi-Fi systems. The performance of Algorithm 1 as a function of SNR was studied through simulations. The final aspect of Chapter 4 is that we have presented a 2D smoothing preprocessing technique, applied to a *Spatial-Frequential* array, to "decorrelate" multipath components. Then, any 2D subspace algorithm could be applied to estimate the times and angles of arrivals of the different paths. The 2D smoothing technique presented here, naturally, offers more subarrays to smooth over and, therefore, one could be able to resolve more coherent paths. In Chapter 5, there are some contributions that should be highlighted: We have proposed a novel approach for joint estimation and detection of Angles and Times of arrival, i.e. JADED. Two methods were derived so as to solve the JADED problem using Rotational Invariance Properties (RIP), which arises when a ULA receives known OFDM symbols. The JADED-RIP method performs a 2D search of a suitable cost function, where each peak indicates a present source with corresponding ToA/AoA. The second algorithm, CESS-JADED-RIP, is a faster version of JADED-RIP, which can be used for single snapshot scenarios only. The algorithms function properly in the presence of coherent sources, since subspace extraction is not needed, as in the case of MUSIC, ESPRIT, and other subspace methods. In Chapter 6, we study an important aspect that perturbs Angle-of-Arrival estimation, due to antenna coupling, also known as "Mutual Coupling". First, we derive a sub-optimal algorithm that could estimate AoAs in the presence of mutual coupling; then, we show why this sub-optimal algorithm, along with other ones, are indeed suboptimal, in the sense that there is an upper bound on the coupling parameters allowed in the model. Moreover, we further improve the sub-optimal algorithm and propose an optimal one, in the sense that more coupling parameters are allowed in the model. We have been able to refine the estimates of the optimal algorithm by modifying some constraints of the optimization problem considered. We derive the MSE expression of the optimal algorithm and show that, in some cases, we can attain the *Cramér-Rao* bound of the problem of joint coupling parameters and AoA estimation. Finally in Chapter 6, we derive an iterative method that could give Maximum Likelihood (ML) estimates of the AoAs, and therefore allowing the presence of coherent sources, which is not the case of all the previous algorithms. In Chapter 7, we have seen multiple scenarios where we could indeed estimate the AoA of the LoS component in the presence of multipath. Herein, we have taken into account all factors that perturb the Joint Angle and Delay estimation problem and formulated a system model accordingly. These factors are: Sampling Frequency Offset (SFO), Carrier Frequency Offset (CFO), Phase and Delay offsets at each antenna. To compensate for the effect of these critical factors, we propose an offline calibration method to compensate for all their effects. Lastly and most importantly, and

with the help of the CESS-JADED-RIP algorithm and the Cubic Spline Interpolation technique, we have successfully been able to estimate the Angles and Times of Arrival of all the multipath components, which allowed for the extraction of the AoA of the LoS component.

Chapter 9

Résumé en Français

9.1 Motivation

9.1.1 Bref historique

La localisation se réfère au processus de localisation des objets visés dans l'espace. Bien que le plus souvent associé à la technologie moderne, il existe des méthodes de localisation plus primitive. En fait, les techniques de localisation les plus élémentaires pourraient être obtenues sans utiliser d'instruments spéciaux; Les marins ont utilisé des objets célestes pour la localisation en mer depuis quelques milliers d'années. De nombreux outils spécialisés ont été développés pour aider à fournir une localisation plus précise, y compris l'astrolabe, le chronomètre, le sextant et la boussole, ainsi que des cartes et cartes maritimes détaillées [1]. À la fin des années 1960, le Département de la défense des États-Unis (DoD) a entrepris un projet visant à construire un système de localisation par satellite à des fins militaires; Connu aujourd'hui comme système de positionnement global, ou simplement GPS. Le système a connu sa première utilisation en combat pendant la guerre du Golfe Persique en 1990. De plus, le GPS se compose d'une constellation de 24 satellites qui diffusent des signaux précis. Lorsque les satellites sont en vue d'un récepteur GPS approprié, ces signaux aident la position-emplacement, la navigation et le timing de précision [1]. Ce n'est qu'en 1983 que le GPS a commencé à évoluer bien au-delà de ses origines militaires et a commencé à migrer vers le secteur public. Il s'agit maintenant d'une ressource d'information mondiale qui soutient une large gamme de fonctions civiles, scientifiques et commerciales, allant du contrôle du trafic aérien et de la navigation en temps réel sur la route

jusqu'à la découverte du café dans votre bloc.

En réponse et en 1990, la DoD a activé la disponibilité sélective (SA), une dégradation délibérée du signal GPS civil, qui a limité la précision de la plupart des unités GPS civiles à environ 100 mètres. Luckily SA a été déclenchée en raison du fait que le DoD a reconnu le rôle important joué par le GPS dans de nombreuses activités commerciales. Grâce à la désactivation de SA, avec l'emploi d'autres technologies telles que le GPS différentiel, permettent maintenant aux unités GPS civiles d'obtenir une précision de 10 mètres ou mieux. Ainsi, pour la localisation dans un environnement extérieur, le GPS fonctionne très bien, étant donné qu'il existe une ligne de visée dégagée sur quatre satellites GPS ou plus. Cependant, le signal du GPS est trop faible pour pénétrer la plupart des bâtiments, donc le GPS est inutile à l'intérieur; Une motivation pour rechercher d'autres techniques de localisation à l'intérieur.

Un système de positionnement intérieur, ou simplement IPS, est un système d'acquisition de données fournissant des informations sur des personnes ou des objets dans l'environnement intérieur et l'obtention de données sur les occupants pour faciliter la recherche. Dit différemment et de manière informelle, un IPS est un *mini-GPS* travaillant à l'intérieur, où un *mini-GPS* peut se référer à un récepteur Wi-Fi. Alors que le GPS dépend des satellites, IPS est basé sur des "ancres de référence" qui sont des noeuds de réseau avec une position fixe connue dans l'environnement intérieur. Ces "ancres" coopèrent les uns avec les autres pour identifier la position du noeud prévu. Une approche de l'architecture d'IPS est "Bluetooth Beaconing". Bluetooth a d'abord été inventé en 1994 pour remplacer les câbles courts. Tout grâce aux smartphones Bluetooth et aux balises Bluetooth qui peuvent fournir l'emplacement des utilisateurs de smartphones. En 2010, Nokia a introduit un IPS basé sur la technologie Bluetooth Low Energy (BLE), qui était l'une des dernières technologies Bluetooth fonctionnant à faible puissance avec une faible latence dans les communications. D'autre part, beaucoup de systèmes utilisent une infrastructure Wi-Fi améliorée pour fournir des informations de localisation [4–6]. Le positionnement Wi-Fi profite de la croissance rapide au début du 21ème siècle des points d'accès sans fil dans les zones urbaines.

Ladd *et al.* présentent une nouvelle technique par laquelle la localisation est réalisée en utilisant l'IEEE 802.11b, connu sous le nom Ethernet Ethernet [2]. Dans leur document, Ladd et al proposent l'utilisation de la puissance de signal

mesurée des paquets Ethernet comme capteur pour un système de localisation. La norme sans fil 802.11b intègre un mécanisme par lequel une carte réseau sans fil peut mesurer la puissance du signal de toutes les stations de base dans sa gamme de diffusion [3]. Par conséquent, un système mobile peut utiliser ces informations afin de déterminer sa distance à partir de ces stations à base fixe. Compte tenu de ces distances et de la connaissance préalable de l'emplacement des stations de base, le système mobile peut estimer sa propre position actuelle. La perturbation de la position réelle du système mobile entraînera une modification de la position réelle du système mobile entraînant une modification des intensités de signal mesurées et donc une modification de la position estimée. L'idée est simplement indiquée, mais l'implémentation réelle est beaucoup plus compliquée où Ladd et al utilisent la localisation dite d'inférence Bayésienne. Ils ont mis en œuvre cette approche pour atteindre une précision d'environ un mètre.

Malheureusement, la principale difficulté de localisation avec Ethernet sans fil prédit la puissance du signal. "La puissance du signal de fréquence radio mesurée à l'intérieur est non linéaire avec la distance. En outre, il présente un bruit non Gaussien résultant d'effets multi-voies et d'effets environnementaux, tels que la géométrie du bâtiment, le trafic réseau, la présence de personnes et les conditions atmosphériques" [2]. En outre, la norme IEEE 802.11b fonctionne dans la bande de fréquences 2,4 GHz, ce qui signifie que "les fours à micro-ondes, les appareils Bluetooth, les téléphones sans fil 2,4 GHz et les équipements de soudage peuvent être des sources d'interférence. Ladd et al ont trouvé une idée où Ils ont séparé la zone d'intérêt dans les cellules, puis ont pris des lectures de force du signal dans chaque cellule, en train d'entraîner efficacement le système. Un système mobile pourrait alors prendre des mesures de force du signal, comparer les données mesurées à l'ensemble de formation et utiliser l'inférence Bayésienne pour déterminer L'emplacement qui produirait le plus souvent ces mesures.

Ladd *et al.* identifient un certain nombre de domaines pour des recherches futures [2]. Leurs études ont été effectuées la nuit, quand il y avait relativement peu de trafic humain ou réseau. De plus, les expériences ont eu lieu dans les couloirs, ce qui signifie que leur mouvement était restreint aux lignes droites relativement étroites. Il serait intéressant d'étudier le comportement du système dans un environnement plus dynamique ou plus géométriquement irrégulier, ou les deux. Les avantages de la localisation Ethernet sans fil sont clairs. Contrairement au GPS, le système fonctionnera dans n'importe quel endroit avec accès à plusieurs stations de base sans fil, que ce soit à l'intérieur ou à l'extérieur. En outre, comme la

plupart des systèmes qui utiliseraient potentiellement cette technologie utilisent déjà une carte réseau sans fil, il n'y a pas de coût de matériel associé.

9.1.2 Paramètres inferring location

Puissance reçue

Le pouvoir reçu est l'un des principes de mesure basiques et les plus anciens pour calculer la distance entre un émetteur et son récepteur correspondant. Cette relation est donnée par l'équation de perte de chemin d'espace libre à l'aide d'antennes rayonnantes isotropes [7]:

$$P_R = \frac{P_T G_T G_R}{(4\pi d/\lambda)^2}$$

où P_R et P_T Sont la puissance reçue et transmise, respectivement; G_R et G_T sont les gains d'antennes de réception et d'émission, respectivement; λ est la longueur d'onde du signal de propagation; et d est la distance de séparation entre l'émetteur et le récepteur.
En conséquence, un indicateur largement utilisé pourrait être dérivé qui est connu sous le nom de Indicateur de résistance du signal reçu (RSSI). Il s'agit d'un entier signé de 8 bits qui indique si le niveau de puissance reçu est inférieur ou inférieur à la plage de puissance du récepteur d'or (GRPR) [8]. RSSI indique 0 si la puissance reçue se trouve dans le GRPR; Positif s'il est au-dessus et négatif s'il est ci-dessous. Bien que RSSI soit destiné à des fins de contrôle de puissance [9], de nombreux périphériques Bluetooth, tels que Bluetooth 1.2, utilisent RSSI pour découvrir tous les périphériques proches [10] et estiment la distance de séparation. Cependant, comme testé dans [8], RSSI ne correspond pas bien avec la distance. Les raisons pour lesquelles RSSI est une version quantifiée de la puissance reçue fournie et, par conséquent, la précision dépendrait principalement de la résolution de la quantification. En outre, RSSI est fortement affecté par multipath, qui est une caractéristique principale des environnements intérieurs.

Temps d'arrivée

La distance d entre la cible mobile à l'unité de mesure est directement proportionnelle au temps de propagation Δt. Donc, en mesurant Δt, on pourrait facilement calculer la distance de séparation entre la cible mobile et l'unité de mesure en:

$$d = c\Delta t$$

où c est la vitesse de la lumière sous vide. Cependant, une synchronisation de synchronisation précise est requise entre les horloges de l'émetteur et du récepteur pour effectuer une estimation ToA [11].

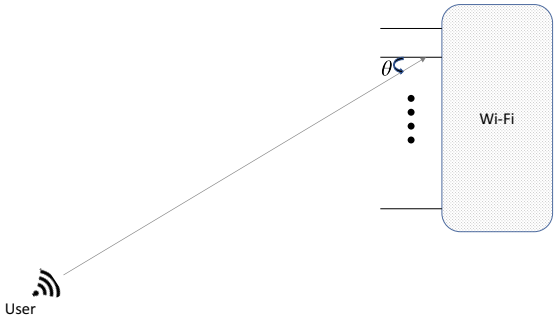

Figure 9.1: L'utilisateur transmet à Wi-Fi à l'angle θ

Angle de Arrivée

Angle de Arrivée (ou AoA) est une technique basée sur le retard temporel relatif par rapport à une antenne arbitraire choisie comme référence, c'est-à-dire que le retard temporel à cette antenne de référence est nul. Assume the SIMO case, as shown in Fig. 9.1, where the user is equipped with one antenna and receive antennas. Let the transmitted signal at any time be $s(t)$ where it is of the form

$$s(t) = Ae^{j2\pi f_c t}$$

La forme de $s(t)$ Dans l'équation ci-dessus est une forme valide d'un signal transmis électromagnétique ayant deux composants orthogonaux, qui sont l'Inphase (ou I) et la Quadrature (ou Q). Ce signal est transmis avec une amplitude A et est en oscillation sur la fréquence f_c. Suivant [12], il est facile de montrer que le signal reçu est sous la forme

$$\boldsymbol{r}(t) = \boldsymbol{a}(\theta)s(t)$$

où $\boldsymbol{a}(\theta)$ est le *steering vector*, qui est fonction de la position des antennes et de l'AoA, θ.

Après θ est estimé par une méthode textit Parameter-Estimation appropriée par, par exemple, deux stations (ou WiFis) telles que représentées dans Fig. 9.2,

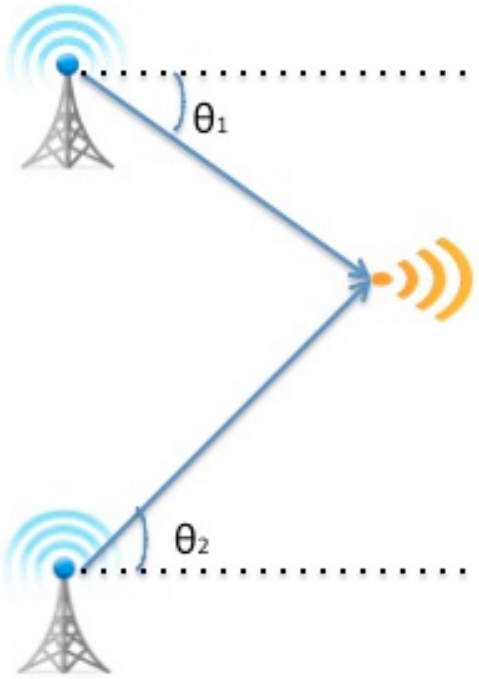

Figure 9.2: Localisation à angle

Figure 9.3: Les deux étapes fondamentales pour l'estimation de position

alors la position de l'utilisateur pourrait être facilement déterminée. Cela signifie qu'une procédure en deux étapes est requise pour déterminer la position d'un utilisateur: a *(i) Éstimation des paramètres* étape suivie d'un *(ii)Emplacement-estimation* étape. *Dans cette thèse, nous nous concentrons sur le premier bloc, c'est-à-dire que nous sommes très intéressés à dériver des méthodes appropriées qui pourraient fournir des estimations de paramètres, ce qui détermine la position de l'utilisateur en présence de bruit, d'imperfections, d'altérations et d'autres difficultés, qui seront Abordé dans la section suivante.*

9.2 Éstimation des paramètres: problèmes et méthodes

Le terme *Éstimation des paramètres* se réfère au processus d'utilisation de données d'échantillonnage pour estimer les paramètres d'intérêt dans un certain modèle,

sous certaines hypothèses. Il vaut la peine de prendre un moment et de mettre en évidence trois mots clés dans l'énoncé précédent: *modèle*, *paramètre* et *hypothèses*. Une difficulté dans la localisation à l'intérieur confirme un modèle. Par exemple, Saleh et Valenzuela [13] ont modélisé le canal multipath comme diffuse, à savoir chaque composant multipath est un groupe de rayons. Sur la base de leurs résultats, ils ont modelé les ToAs des clusters en tant que processus de Poisson avec des taux différents, mais fixes. La thèse dans [14], inspirée de [13], modélise les AoAs des clusters en tant que distribution laplacienne. Cependant, la plupart des méthodes de localisation (sinon toutes), telles que [15–18] supposent un canal multipath spéculaire, c'est-à-dire que chaque composant multi-voies n'est qu'un seul rayon. Cela semble acceptable en raison des problèmes de résolution [1] et donc des sources étroitement espacées pourraient être considérées comme la source.

Après avoir confirmé un modèle ou une famille de modèles, les paramètres impliqués dans ces modèles doivent être estimés. C'est là que les méthodes d'estimation des paramètres entrent. Le maximum de vraisemblance (ML) était l'une des premières méthodes à étudier [20]. Même si la méthode ML est optimale, dans le sens où les paramètres estimés minimisent l'erreur moyenne de niveau (MSE), il n'a pas reçu beaucoup d'attention en raison de la charge informatique élevée du problème de minimisation non linéaire multivarié impliqué, car il nécessite une q-Dimensionnel cherche, où q est le nombre de paramètres qui entrent dans le modèle sous une forme non linéaire. Ensuite, un certain nombre de méthodes de formage de faisceau intéressantes ont été mises en œuvre, en tant que solutions à certains problèmes d'optimisation appropriés, tels que le formateur de faisceau Bartlett [21] et le formateur de faisceau de Capon [22]. Ces formateurs de faisceau nécessitent une 1–Dimensionnel (1D) cherche et sont donc considérés comme rapides. Cependant, la résolution de ces méthodes n'est pas acceptable avec un faible nombre d'antennes, de snapshots et de SNR, ce qui nécessite des méthodes avec une précision supérieure, tout en maintenant une vitesse de calcul acceptable. Les années 80 ont été témoins d'une révolution de la *subspace methods*, qui reposent sur une véritable idée: *"Le sous-espace parcouru par les vecteurs de direction des sources est orthogonal au sous-espace de bruit"*[2] La méthode de sous-espace la plus populaire est la MUltiple SIgnal Classification algorithm, aussi connu sous le nom MUSIC [24] par Schmidt, qui nécessite uniquement une recherche 1D. Un root-MUSIC [25] est un méthode qui a été implémentée par Barabell pour remplacer la

[1] Dans le contexte du traitement de la matrice, la résolution se réfère à la capacité de discriminer entre deux sources étroitement espacées, compte tenu d'un certain SNR [19]

[2] Ceci est expliqué en détail dans le Chapitre 6.

recherche 1D de MUSIC par un critère de recherche racine polynomiale. Paulraj et Kailath a inventé l'ESPRIT [26] (Estimation of Signal Parameters Via Rotational Invariance Techniques) méthode, qui est basé sur l'ajustement des moindres carrés; Cependant, il ne fonctionne que pour les ensembles linéaires uniformes (ULAs). Bien que ces méthodes dominent les formateurs de faisceau susmentionnés en termes de résolution, il existe des cas où les méthodes sous-espace ne fonctionnent pas, telles que:

- Sources cohérentes: c'est le cas du brouillage intelligent ou de la propagation multi-voies. Un exemple très simple de deux sources cohérentes est $s_1(t)$ et $s_2(t) = \alpha s_1(t)$, oú α est un nombre complexe.
- Instantané unique: car aucun sous-espace ne peut être formé par un seul instantané.

Il convient de mentionner qu'il existe un grand nombre de recherches récentes effectuées sur les méthodes sous-espace; Nous renvoyons le lecteur aux articles suivants [27–29].

Une autre classe de méthodes d'estimation de paramètres travaille sur l'approximation de la fonction de coût de ML, qui sont également attrayantes sur le plan du calcul, mais pas aussi attrayantes que les méthodes de sous-espace. Par exemple, la méthode par Ziskind et Wax [30] Atteint l'estimation ML par plusieurs recherches 1D, qui sont décrites comme Projections alternées (AP). Une autre technique populaire est le Iterative Quadratic ML (IQML) développé par Bresler et Macovski dans [31], où, avec un paramétrage linéaire du sous-espace de bruit, la fonction de coût ML à chaque itération est considérée comme une fonction de coût LS pondérée, Qui est quadratique dans le vecteur de paramètres d'intérêt, et donc les expressions de forme fermée pourraient être dérivées. Cependant, la pondération dépend du paramètre et, par conséquent, des itérations à point fixe sont nécessaires.

En plus des méthodes d'estimation de paramètres, l'un est limité par le nombre de composants multi-voies autorisés dans le modèle. Plus précisément, laisser q désignent le nombre de composants multipath et N indique le nombre d'antennes à la Wi-Fi; puis $q < N$ devrait être satisfaite, sinon le problème d'estimation est sous-déterminé et la solution estimée ne sera pas unique. Il y a beaucoup de travail effectué par Pal et Vaidyanathan, tel que [32, 33], où ils tentent d'estimer

les accords de q sources, où $q > N$. Ceci est réalisé par échantillonnage coprime, c'est-à-dire en divisant le N antennes en deux sous-réseaux de tailles N_1 et N_2, où $N = N_1 + N_2$ et (N_1, N_2) sont co-prime. L'approche d'échantillonnage coprime suggère des configurations de réseau d'antenne spécifiques, appelé coprime arrays. Il est avantageux que nous ayons maintenant plus de degrés de liberté, c'est-à-dire que le nombre de sources pourrait augmenter $q < O(N_1 N_2)$. Cependant, cette approche présente de multiples inconvénients, lorsque notre intérêt est orienté vers la localisation à l'intérieur via WiFi:

- Les sources sont supposées être totalement non corrélées, ce qui n'est pas valable pour les sources multi-voies. Au contraire, les composants multi-voies sont connus pour être cohérents.
- Avec un petit nombre d'antennes, disons $N = 3$ antennes, on ne pouvait pas s'attendre à améliorer les degrés de liberté en choisissant, par exemple, $N_1 = 2$ et $N_2 = 1$.
- L'AoA entre l'émetteur et le récepteur ne pouvait être déduit que par les informations de l'AoA uniquement.

D'autre part, Vanderveen, Papadias et Paulraj a introduit une nouvelle approche appelée JADE [34], qui signifie Joint Angle and Delay Estimation. Ils proposent de transmettre un signal connu par un canal multi-voies, qui est reçu à travers N antennes au récepteur et M Des échantillons de temps sont collectés à chaque antenne. Cette idée présente de multiples avantages dans le contexte de la localisation à l'intérieur via WiFi:

- Les degrés de liberté du nombre de composants multi-voies pourraient aller jusqu'à $q < MN$.
- Il n'y a pas de limitation sur la géométrie des antennes.

On remarque que JADE N'est en aucun cas une méthode. C'est simplement une façon intelligente de collecter des données pour augmenter le nombre de composants qui pourraient être résolus. Par conséquent, il est naturel de proposer des méthodes basées sur JADE, telles que JADE-ML et JADE-MUSIC in [34] et JADE-ESPRIT en [35]. Il convient de noter que la partie de la cohérence n'a pas été abordée.

Outre les degrés de liberté et la cohérence des sources, un autre aspect important à considérer est la perturbation du tableau. Ceci est dû à plusieurs facteurs, tels que l'incertitude de position de l'antenne [36], Gains/phases inconnus entre différentes antennes [37], et couplage mutuel entre les antennes [38]. Nous abordons ce sujet en détail dans les chapitres 6 et 7.

9.3 Contributions de cette dissertation

Dans cette thèse, nous abordons tous les problèmes abordés dans la section précédente afin de dériver certaines méthodes qui effectuent l'estimation des paramètres. En particulier,

Chapitre 2. Au chapitre 2, nous abordons un problème bien connu impliqué dans le traitement du signal de tableau, qui est la détection du nombre de signaux présents dans le modèle. En effet, toutes les méthodes mentionnées précédemment exigent le nombre de signaux à connaître a priori. Longueur de description minimale, ou MDL [39], Est une méthode bien connue pour cette question, mais elle subit une dégradation des performances lorsque le nombre d'instantanés disponibles est relativement faible. Nous tirons un estimateur MDL modifié, avec l'aide d'RMT [41–43], ce qui améliore l'estimation du nombre de sources lorsqu'un petit nombre d'instantanés $L = \mathcal{O}(N)$ est disponible.

Les publications relatives à ce chapitre sont les suivantes:

- A. Bazzi, D. T.M. Slock, L. Meilhac, "Detection of the number of Superimposed Signals using Modified MDL Criterion : A Random Matrix Approach," *IEEE International Conference on Acoustics, Speech, and Signal Processing* (ICASSP), March, 2016.

Chapitre 3. Dans le chapitre 3, nous abordons le problème d'estimation de l'AoA d'un point de vue de détection comprimé. Les contributions de ce chapitre sont résumées comme suit:

1. Après une revue de la littérature sur certaines méthodes populaires de détection comprimée, nous proposons une méthode Variational Bayes (VB) qui permet une récupération sparse des signaux transmis désirés, ce qui permet d'estimer leurs acceptations correspondantes.

2. Nous montrons que cette méthode VB itérative dépasse les méthodes de détection comprimée existantes, telles que Matching Pursuit (MP) [50], Orthogonal MP (OMP) [51], et d'autres méthodes.

3. Nous dérivons également une méthode Newward de type Newward Forward Forward Greedy qui effectue une récupération sparse, compte tenu des données.

4. Nous montrons, grâce à des simulations exhaustives, que la méthode de type Newton proposée n'est pas seulement plus rapide, mais atteint une MSE inférieure par rapport à des méthodes telles que Fast Matching Bayesian Pursuit (FBMP) [67] et Basis Pursuit Denoising (BPDN) [53].

Les publications relatives à ce chapitre sont les suivantes:

- A. Bazzi, D. T.M. Slock, L. Meilhac, S. Panneerselvan, "A Comparative Study of Sparse Recovery and Compressed Sensing Algorithms with Application to AoA Estimation," *IEEE International Workshop on Signal Processing advances in Wireless Communications* (SPAWC), 2016.

- A. Bazzi, D. T.M. Slock, L. Meilhac, "Sparse Recovery using an Iterative Variational Bayes Algorithm and Application to AoA Estimation," *IEEE Symposium on Signal Processing and Information Technology* (ISSPIT), 2016.

- A. Bazzi, D. T.M. Slock, L. Meilhac, "A Newton-type Forward Backward Greedy Method for Multi-Snapshot Compressed Sensing," *Asilomar conference on signals, systems, and computers* (ASILOMAR), 2017.

Chapitre 4. Dans le chapitre 4, nous nous concentrons sur le problème Joint Angle and Delay Estimation (JADE) à des fins de localisation. Plus précisément, nous abordons les problèmes d'instantané unique et de cohérence mentionnés dans la section précédente. Les contributions de ce chapitre pourraient être résumées comme suit:

1. Nous dérivons un algorithme qui est une modification de l'algorithme ML (2D-IQML) itératif itératif bidimensionnel, où une contrainte supplémentaire est ajoutée pour l'estimation conjointe de ToA et AoA et nous montrons que 2D-IQML donne des estimations biaisées de ToAs / AoAs et effectue Mal à faible SNR en raison du biais induit par le bruit.

2. Nous proposons un IQML Denoisé bidimensionnel (2D-DIQML) qui donne des estimations cohérentes et surperforme le 2D-IQML; nous montrons que

2D-DIQML est asymptotiquement globalement convergent et donc insensible à l'initialisation.

3. En outre, deux algorithmes, basés sur 2D Matrix Pencils (MP), pour le cas d'un seul symbole OFDM instantané observé par plusieurs antennes dans une configuration ULA sont introduits.

4. Pour le problème de cohérence, nous dérivons une technique de lissage "Spatio-Frequential", lorsque le symbole OFDM d'émission est reçu à travers de multiples signaux cohérents en utilisant un réseau d'antennes linéaire uniforme, ce qui est le cas d'un canal multi-voies intérieur. Cette méthode de lissage est inspirée de [81] et pourrait être considérée comme une généralisation 2D de la technique de lissage spatial traditionnelle.

5. Nous prouvons dans le Théorème 4.3 que nous pourrions *"ascenseur"* Le rang de la matrice de covariance de l'échantillon, afin que nous puissions discriminer entre des sources cohérentes, et donc appliquer des méthodes sous-espace telles que JADE-MUSIC et JADE-ESPRIT.

Théorème 4.3: *Si le nombre de sous-réseaux formés conjointement sur l'espace et la fréquence est supérieur au nombre de composants multi-voies, c'est-à-dire* $q \leq K_M K_N$*, et le nombre maximum de chemins arrivant en même temps mais avec des angles différents est inférieur à* K_N*, i.e.* $\max_i Q_i \leq K_N$*, et le nombre maximum de chemins arrivant aux mêmes angles mais avec des temps différents est inférieur à* K_M*, i.e.* $\max_i P_i \leq K_M$*, alors* $\bar{\boldsymbol{R}}_{\gamma\gamma}$ *est de rang* q*.*

Proof. Voir l'Annexe A □

Les publications relatives à ce chapitre sont les suivantes:

- A. Bazzi, D. T.M. Slock, L. Meilhac, "Efficient Maximum Likelihood Joint Estimation of Angles and Times of Arrival of Multi Paths," *IEEE GLOBAL Communications Conference* (GLOBECOM), Localization and Tracking : Indoors, Outdoors, and Emerging Networks (LION) Workshop, December, 2015.

- A. Bazzi, D. T. M. Slock, and L. Meilhac, "Single Snapshot Joint Estimation of Angles and Times of Arrival: A 2D Matrix Pencil Approach," *IEEE International Conference on Communications*, 2016.

- A. Bazzi, D. T.M. Slock, L. Meilhac, "On Spatio-Frequential Smoothing for Joint Angles and Times of Arrival Estimation of Multipaths," *IEEE International Conference on Acoustics, Speech, and Signal Processing* (ICASSP), March, 2016.

Chapitre 5. Au chapitre 5, nous proposons une approche novatrice, qui s'habille sur JADE, intitulée Joint Angle and Delay Estimation and Detection, ou simplement JADED. Les contributions de ce chapitre sont résumées comme suit:

1. Grâce à cette approche, nous pouvons maintenant estimer les angles et les horaires d'arrivée des chemins multiples, sans connaissance préalable du nombre de composants multi-voies. À notre connaissance, ce problème n'a pas été abordé dans la littérature ouverte.
2. Une méthode appelée JADED-RIP utilise les Propriétés d'Invariance Rotationnelle (RIP) des ULA et des symboles OFDM, détecte le nombre de composants multi-voies et estime les angles et les heures d'arrivée de chaque chemin en effectuant une recherche 2D.
3. Une autre méthode est une version CESS (Simple Instant Effet Computationally Efficient) du JADED-RIP, appelée CESS-JADED-RIP. Cette méthode nécessite une recherche 1D suivie d'un ajustement des moindres carrés et ne peut être utilisée que lorsqu'un seul symbole OFDM est disponible.

L'inconvénient des deux méthodes proposées est qu'ils ne fonctionnent que pour les systèmes ULA / OFDM et qu'ils sont sous-optimaux dans le sens où ils pourraient être encore améliorés en considérant le bruit coloré, ce qui conduit à un estimateur ML-JADED.

Les publications relatives à ce chapitre sont les suivantes:

- A. Bazzi, D. T.M. Slock, L. Meilhac, "JADED-RIP: Joint Angle and Delay Estimator and Detector via Rotational Invariance Properties," *IEEE International Symposium on Signal Processing and Information Technology*, (ISSPIT), 2016.

Chapitre 6. Dans le chapitre 6, nous abordons un aspect important qui perturbe l'estimation de l'angle d'arrivée, en raison du couplage de l'antenne, également appelé "couplage mutuel". Les contributions de ce chapitre sont résumées comme suit:

1. Nous dérivons un algorithme sous-optimal qui pourrait estimer les AAS en présence d'un couplage mutuel.

2. Nous montrons pourquoi cet algorithme sous-optimal, avec d'autres [88–92], Sont en effet suboptimiques, en ce sens qu'il existe une limite supérieure sur les paramètres de couplage autorisés dans le modèle qui peut être amélioré. Cela n'aurait pas été clair sans Théorème 6.6:

   Théorème 6.6: Pour les configurations de types de matrices linéaires uniformes, c'est-à-dire $\boldsymbol{a}(\theta) = [1, z_\theta, \dots z_\theta^{N-1}]^{\mathrm{T}}$ avec $z_\theta = e^{-j2\pi \frac{d}{\lambda}\sin(\theta)}$. Définissez les ensembles suivants:

$$\boldsymbol{\Theta_+} = \left\{ \sin^{-1}\left(\frac{k\lambda}{Nd}\right), \quad k = -\frac{N}{2} \dots \frac{N}{2} \right\} \tag{9.1}$$

$$\boldsymbol{\Theta_-} = \left\{ \sin^{-1}\left(\frac{(k+\frac{1}{2})\lambda}{Nd}\right), \quad k = -\frac{N}{2} \dots \frac{N}{2} \right\} \tag{9.2}$$

$$\boldsymbol{\Theta_\pm} = \left\{ \boldsymbol{\Theta_+} \cup \boldsymbol{\Theta_-} \right\} \tag{9.3}$$

   La matrice $\boldsymbol{B}(\theta) = \mathcal{G}_p(\boldsymbol{a}(\theta))$ présente les caractéristiques suivantes:

   - Si $p < \frac{N+2}{2}$, la matrice $\boldsymbol{B}(\theta)$ est un rang de colonne complet.
   - When $p \geq \frac{N+2}{2}$, nous distinguons les cas suivants:
     - Si N est pair et $\theta \in \boldsymbol{\Theta_+}$, puis $\mathrm{rank}(\boldsymbol{B}(\theta)) = \frac{N}{2}$.
     - Si N est pair et $\theta \in \boldsymbol{\Theta_-}$, puis $\mathrm{rank}(\boldsymbol{B}(\theta)) = \frac{N}{2} + 1$.
     - Si N est impair et $\theta \in \boldsymbol{\Theta_\pm}$, puis $\mathrm{rank}(\boldsymbol{B}(\theta)) = \frac{N+1}{2}$.
     - Autre $\boldsymbol{B}(\theta)$ est un rang de colonne complet.

   Proof. Voir l'Annexe F □

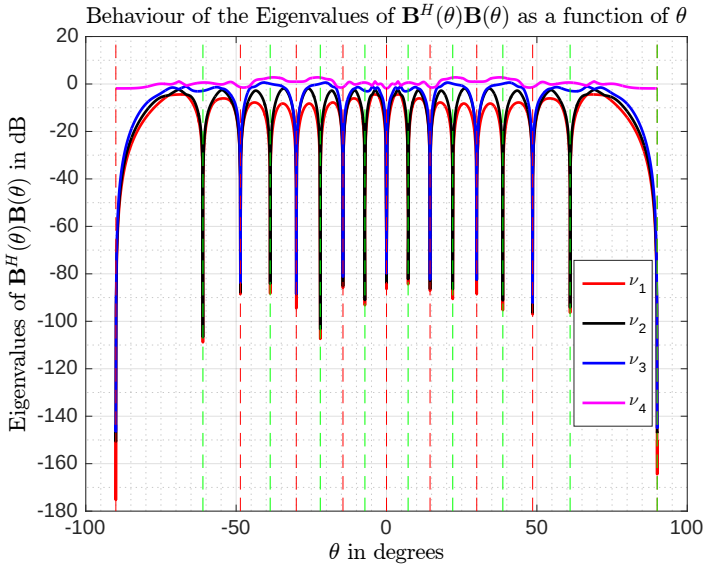

(a) $N = 8$ and $p = 7$

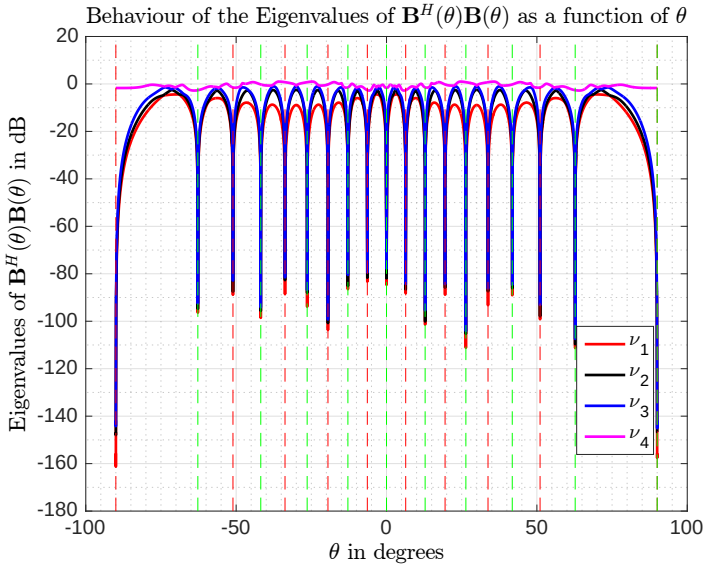

(b) $N = 9$ and $p = 8$

Figure 9.4: Valeurs propres de $\boldsymbol{B}^{\mathrm{H}}(\theta)\boldsymbol{B}(\theta)$ en tant que fonction de θ pour différentes valeurs de N et p.

Il est important de comprendre le comportement de la matrice $\boldsymbol{B}(\theta)$ en fonction de θ. Laisser $\nu_1 \leq \nu_2 \leq \ldots \leq \nu_p$ être la valeur propre de $\boldsymbol{B}^{\mathrm{H}}(\theta)\boldsymbol{B}(\theta)$. Afin de vérifier partiellement ***Théorème 6.6***, nous avons représenté deux chiffres où $p > \frac{N+2}{2}$. En Fig. 9.4a, nous fixons $N = 8$ (pair) and $p = 7$. Les lignes verticales pointillées rouge et verte correspondent à des angles dans $\boldsymbol{\Theta_+}$ et $\boldsymbol{\Theta_-}$, respectivement. Observez cela lorsque θ approche des angles dans $\boldsymbol{\Theta_+}$, nous avons trois valeurs propres, i.e. ν_1, ν_2, et ν_3, tomber à zéro. Cela implique que, lorsque $\theta \in \boldsymbol{\Theta_+}$, le rang de $\boldsymbol{B}(\theta)$ est $p-3 = 4 = \frac{N}{2}$. Cependant, quand $\theta \in \boldsymbol{\Theta_-}$, seulement deux valeurs propres, à savoir ν_1 et ν_2, aller à zéro.

Dans ce cas, le rang de $\boldsymbol{B}(\theta)$ est $p-2=5=\frac{N}{2}+1$. Notez également que ν_4 est strictement positif. En Fig. 9.4b, nous fixons $N=9$ (impair) est $p=8$. Encore, ν_4 est strictement positif. Quand $\theta \in \boldsymbol{\Theta_{\pm}}$, trois valeurs propres vont à zéro, ce qui implique que le rang de $\boldsymbol{B}(\theta)$ est $p-3=5=\frac{N+1}{2}$.

3. Ensuite, nous améliorons encore l'algorithme sous-optimal et proposons un optimum, dans le sens où plus de paramètres de couplage sont autorisés dans le modèle.

4. En outre, nous affinons les estimations de l'algorithme optimal en modifiant certaines contraintes du problème d'optimisation considéré.

5. Nous dérivons l'expression MSE de l'algorithme optimal et montrons que, dans certains cas, nous pouvons atteindre *Cramér-Rao* bound du problème des paramètres de couplage articulaire et de l'estimation de l'AoA. Les théorèmes connexes sont le Théorème 6.7, Théorème 6.9 et Théorème 6.10.

6. Enfin, nous dérivons une méthode itérative qui pourrait donner des estimations de la vraisemblance maximale (ML) des AoAs et donc permettre la présence de sources cohérentes, ce qui n'est pas le cas de tous les algorithmes précédents.

Les publications relatives à ce chapitre sont les suivantes:

- A. Bazzi, D. T.M. Slock, L. Meilhac, "Online Angle of Arrival Estimation in the Presence of Mutual Coupling," *IEEE International Workshop on Statistical Signal Processing* (SSP), 2016.

- A. Bazzi, D. T.M. Slock, L. Meilhac, "On Mutual Coupling for ULAs: Estimating AoAs in the presence of more coupling parameters," *IEEE International Conference on Acoustics, Speech, and Signal Processing* (ICASSP), 2017.

- A. Bazzi, D. T.M. Slock, L. Meilhac, "Performance Analysis of an AoA estimator in the presence of more mutual coupling parameters," *IEEE International Conference on Acoustics, Speech, and Signal Processing* (ICASSP), 2017.

- A. Bazzi, D. T.M. Slock, L. Meilhac, "On a Mutual Coupling Agnostic Maximum Likelihood Angle of Arrival Estimator by Alternating Projection," *IEEE Global Conference on Signal and Information Processing* (GlobalSIP), 2016.

- A. Bazzi, D. T.M. Slock, L. Meilhac, "A Mutual Coupling Resilient Algorithm for Joint Angle and Delay Estimation," *IEEE Global Conference on Signal and Information Processing* (GlobalSIP), 2016.

Chapitre 7. Dans le chapitre 7, nous visons à construire un système réel qui pourrait effectuer l'angle d'articulation et l'Étude de retard d'arrivée et la détection des composants multi-voies. Ceci est tout simplement fait, afin que nous puissions extraire l'angle de l'arrivée du composant Line-of-Sight (LoS) entre l'émetteur et le récepteur.

1. Nous prenons en compte tous les facteurs critiques qui perturbent le problème d'estimation de l'angle articulaire et du retard et formulons un modèle de système en conséquence.

2. Nous proposons une méthode d'étalonnage hors ligne pour compenser tous ces facteurs. Sur la Fig. 9.5, on peut voir que la méthode d'étalonnage

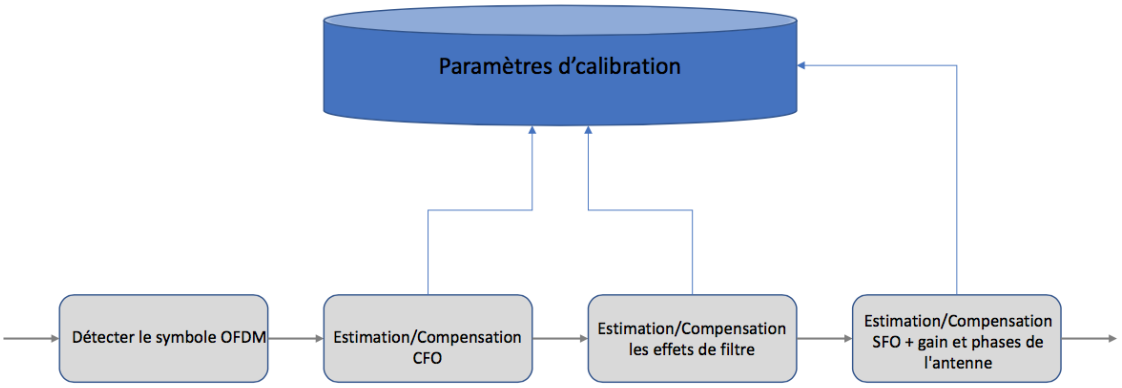

Figure 9.5: Diagramme à blocs de l'approche d'étalonnage hors-ligne

hors ligne. Tout d'abord, nous devons détecter le début du symbole OFDM avant d'estimer tout paramètre. Ensuite, nous devons estimer et compenser le CFO. Notez qu'après avoir estimé le CFO, il est sauvegardé dans la base de données pour les paramètres d'étalonnage. Ensuite, nous estimons les effets de filtre d'émission / réception et compensons leurs effets. De plus, nous sauvegardons les paramètres du filtre dans la base de données. Enfin, nous estimons l'SFO et les paramètres de phase et de gain et leurs effets sont enregistrés dans une base de données.

3. Avec l'aide de l'algorithme CESS-JADED-RIP, nous avons réussi à estimer les angles et les temps d'arrivée de tous les composants multi-voies, ce qui a permis d'extraire l'AoA du composant LoS. L'algorithme de localisation

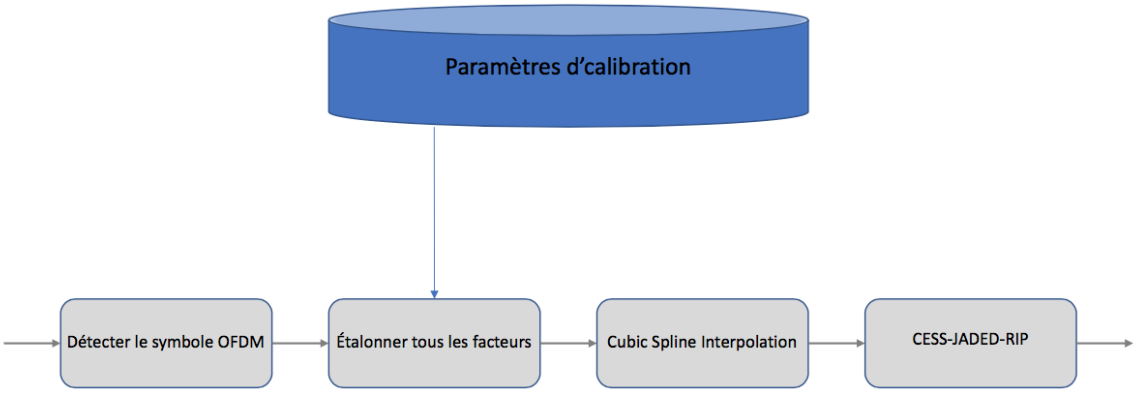

Figure 9.6: Diagramme séquentiel de la méthode en ligne proposée

utilisé pour estimer l'AoA du LoS est l'algorithme CESS-JADED-RIP, qui correspond à l'estimation et au dépistage des angles et des retards. Il convient de noter les points suivants de l'algorithme CESS-JADED-RIP:

- CESS-JADED-RIP fonctionne pour OFDM/ULA systèmes seulement.
- CESS-JADED-RIP n'impose pas l'hypothèse des sources non corrélées. Cela signifie que JADED pourrait estimer conjointement les angles et les temps d'arrivée de multiples sources cohérentes, ce qui est le cas de la propagation multi-voies.
- CESS-JADED-RIP les fonctions sont correctement fournies avec un instantané unique, ce que nous faisons ici.
- CESS-JADED-RIP n'a pas besoin d'une connaissance préalable du nombre de composants multi-voies ou du nombre de sources.

Tout au long de toutes les expériences conduites, nous avons utilisé seulement 2 antennes placées l'une à côté de l'autre sur le même plan, donc ULA. Il y a eu un problème lorsque nous examinons la structure OFDM que nous avons, c'est-à-dire que nous avons une structure "quasi-OFDM" puisque les 3 sous-porteuses centrales n'étaient pas utilisées. Pour remédier à cela, nous avons utilisé Cubic Spline Interpolation (CSI) pour, plus ou moins, interpoler les 3 sous-porteuses manquantes pour avoir un spectre de fréquence continu.

Il n'y a pas de matériel publié concernant ce chapitre.

Autre travail. Par souci de cohérence de cette thèse, nous avons omis trois publications, qui sont les suivantes:

- A. Bazzi, D. T.M. Slock, L. Meilhac, "On the Effect of Random Snapshot Timing Jitter on the Covariance Matrix for JADE Estimation," *European Signal Processing Conference* (EUSIPCO), September, 2015.
- A. Bazzi, D. T.M. Slock, L. Meilhac, "On Joint Angle and Delay Estimation in the Presence of Local Scattering," *IEEE International Conference on Communications* (ICC), Workshop on Advances in Network Localization and Navigation, 2016.
- L. Meilhac and A. Bazzi, "Downlink transmit beamsteering Apparatus for a multi-user MIMO transmission," Patent in Preparation, 2017.

9.4 Conclusions

Tout d'abord au chapitre 2, et avec l'aide d'outils matriciels aléatoires, nous avons présenté un estimateur MDL modifié (MMDL) pour détecter le nombre de signaux superposés. Cet estimateur de MMDL domine le MDL traditionnel surtout au faible nombre de régime d'instantanés, c'est-à-dire quand $L = \mathcal{O}(N)$. Les résultats de simulation ont montré le potentiel de MMDL sur le MDL traditionnel. En outre, dans le chapitre 3, et à l'aide de variables latentes et de Variation Bayes, nous avons dérivé un algorithme itératif qui pourrait estimer les Angles of Arrival (AoA) des sources entrantes avec un seul instantané, sans connaissance du nombre de sources , Et avec des sources étroitement espacées à haute SNR. Nous avons également vu qu'il est possible que la méthode codée vers l'arrière avance de type newton soit plus rapide, en termes de convergence et de nombre d'opérations, et mieux, en termes de Mean-Squared-Error (MSE) de AoAs. Dans le chapitre 4, nous avons présenté deux techniques pour résoudre l'algorithme DML hautement non linéaire pour les temps de joint et les angles d'arrivée: 2D-IQML et 2D-DIQML. Une analyse de performance asymptotique des deux techniques a été fournie. Il a été démontré que 2D-IQML donne des estimations biaisées de ToA / AoA et fonctionne mal à faible SNR en raison du bruit. Une stratégie "denoising" originale est proposée, ce qui contraint le Hessian de la fonction de coût à être semi-définitif positif. Cette stratégie de "déconcentration" s'appelle 2D-DIQML qui s'est révélée globalement convergente. En outre, 2D-DIQML surpasse 2D-IQML car le premier se comporte de manière asymptotique à n'importe

quel SNR car celui-ci se comporte à haute SNR. Enfin, à des fins de localisation, les informations conjointes AoA et ToA pourraient être utilisées pour former une base de données, où une cartographie est effectuée entre les vecteurs ToA / AoA et l'emplacement. Ensuite, cette base de données pourrait être utilisée en ligne, où l'estimation conjointe AoA / ToA se fait à l'aide des algorithmes proposés, suivie d'un critère correspondant à la meilleure concordance dans la base de données pour obtenir une estimation de l'emplacement d'un émetteur sans fil. Nous avons également présenté deux algorithmes basés sur 2D Matrix Pencils. Ces deux algorithmes permettent une estimation conjointe des temps et des angles d'arrivée de plusieurs chemins en utilisant un seul instantané. Algorithme 1 résout plus de sources que l'Algorithme 2 dans le cas où le nombre de sous-porteuses est beaucoup plus grand que le nombre d'antennes, ce qui est le cas de la plupart des systèmes Wi-Fi. La performance de l'Algorithme 1 en fonction de SNR a été étudiée par des simulations. L'aspect final du chapitre 4 est que nous avons présenté une technique de prétraitement de lissage 2D, appliquée à un *Spatial-Frequential* Array, pour "décénérer" les composants multipath. Ensuite, tout algorithme de sous-espace 2D pourrait être appliqué pour estimer les temps et les angles d'arrivée des différents chemins. La technique de lissage 2D présentée ici, naturellement, offre plus de sous-réseaux pour se lisser et, par conséquent, on pourrait pouvoir résoudre des chemins plus cohérents. Au chapitre 5, il faut souligner certaines contributions: Nous avons proposé une nouvelle approche pour l'estimation conjointe et la détection des angles et des temps d'arrivée, à savoir JADED. Deux méthodes ont été dérivées afin de résoudre le problème JADED en utilisant les propriétés d'invariance de rotation (RIP), qui survient lorsqu'un ULA reçoit des symboles OFDM connus. La méthode JADED-RIP effectue une recherche 2D d'une fonction de coût appropriée, où chaque pic indique une source actuelle avec ToA / AoA correspondant. Le deuxième algorithme, CESS-JADED-RIP, est une version plus rapide de JADED-RIP, qui peut être utilisée uniquement pour des scénarios simples. Les algorithmes fonctionnent correctement en présence de sources cohérentes, car l'extraction sous-espace n'est pas nécessaire, comme dans le cas de MUSIC, ESPRIT et d'autres méthodes sous-espace. Au chapitre 6, nous étudions un aspect important qui perturbe l'estimation de l'angle d'arrivée, en raison du couplage de l'antenne, également appelé "couplage mutuel". Tout d'abord, nous dérivons un algorithme sous-optimal qui pourrait estimer les AAS en présence d'un couplage mutuel; Ensuite, nous montrons pourquoi cet algorithme sous-optimal, avec d'autres, est en effet sous-optimal, en ce sens qu'il existe une limite supérieure sur les paramètres de couplage autorisés dans le modèle.

En outre, nous améliorons encore l'algorithme sous-optimal et proposons un optimum, dans le sens où d'autres paramètres de couplage sont autorisés dans le modèle. Nous avons réussi à affiner les estimations de l'algorithme optimal en modifiant certaines contraintes du problème d'optimisation considéré. Nous dérivons l'expression MSE de l'algorithme optimal et montrons que, dans certains cas, nous pouvons atteindre *Cramér-Rao* bound du problème des paramètres de couplage articulaire et de l'estimation de l'AoA. Enfin, dans le chapitre 6, nous dérivons une méthode itérative qui pourrait donner des estimations de la vraisemblance maximale (ML) des AoAs, et donc permettre la présence de sources cohérentes, ce qui n'est pas le cas de tous les algorithmes précédents. Dans le chapitre 7, nous avons vu plusieurs scénarios où nous pourrions en effet estimer l'AoA du composant LoS en présence de multipath. Dans ce cas, nous avons pris en compte tous les facteurs qui perturbent le problème d'estimation de l'angle articulaire et du délai et formulé un modèle de système en conséquence. Ces facteurs sont: le décalage de fréquence d'échantillonnage (OFS), le décalage de fréquence de porteuse (CFO), la phase et les décalages de retard sur chaque antenne. Pour compenser l'effet de ces facteurs critiques, nous proposons une méthode d'étalonnage hors ligne pour compenser tous leurs effets. Enfin et surtout, et avec l'aide de l'algorithme CESS-JADED-RIP et de la technique d'interpolation cubique cubique, nous avons réussi à estimer les angles et les temps d'arrivée de tous les composants multi-voies, ce qui a permis d'extraire le AoA du composant LoS.

Appendix A

Proof of Theorem 4.3

Using (4.79), $\bar{\boldsymbol{R}}_{\gamma\gamma}$ could be written as

$$\bar{\boldsymbol{R}}_{\gamma\gamma} = \boldsymbol{D}\boldsymbol{Q}\boldsymbol{D}^H \tag{A.1}$$

where $\boldsymbol{D}$ is a $q \times qK_MK_N$ matrix given by

$$\boldsymbol{D} = \begin{bmatrix} \boldsymbol{T} & | & \boldsymbol{D}_\theta\boldsymbol{T} & | & \dots & | & \boldsymbol{D}_\theta^{K_N-1}\boldsymbol{T} \end{bmatrix} \tag{A.2a}$$

and

$$\boldsymbol{T} = \begin{bmatrix} \boldsymbol{I}_q & | & \boldsymbol{D}_\tau & | & \dots & | & \boldsymbol{D}_\tau^{K_M-1} \end{bmatrix} \tag{A.2b}$$

and $\boldsymbol{Q}$ is a block diagonal $qK_MK_N \times qK_MK_N$ matrix expressed as

$$\boldsymbol{Q} = \frac{1}{K_MK_N}\boldsymbol{I}_{K_MK_N} \otimes \boldsymbol{R}_{\gamma\gamma} \tag{A.3}$$

Equation (A.1) can be expressed as follows

$$\bar{\boldsymbol{R}}_{\gamma\gamma} = \boldsymbol{W}\boldsymbol{W}^H \tag{A.4}$$

with

$$\boldsymbol{W} = \begin{bmatrix} \boldsymbol{T}_c & | & \boldsymbol{D}_\theta\boldsymbol{T}_c & | & \dots & | & \boldsymbol{D}_\theta^{K_N-1}\boldsymbol{T}_c \end{bmatrix} \tag{A.5a}$$

and

$$\boldsymbol{T}_c = \begin{bmatrix} \boldsymbol{C} & | & \boldsymbol{D}_\tau\boldsymbol{C} & | & \dots & | & \boldsymbol{D}_\tau^{K_M-1}\boldsymbol{C} \end{bmatrix} \tag{A.5b}$$

where $\boldsymbol{C}$ is the square root of $\frac{1}{K_M K_N}\boldsymbol{R}_{\gamma\gamma}$:

$$\frac{1}{K_M K_N}\boldsymbol{R}_{\gamma\gamma} = \boldsymbol{C}\boldsymbol{C}^H \tag{A.6}$$

The rank of $\bar{\boldsymbol{R}}_{\gamma\gamma}$ is equal to the rank of $\boldsymbol{W}$. Now, using the fact that the rank of a matrix is unchanged under column permutations, then we can write the following:

$$\text{rank } \boldsymbol{W} = \text{rank} \begin{pmatrix} c_{11}\boldsymbol{v}_1 \otimes \boldsymbol{t}_1 & \cdots & c_{1q}\boldsymbol{v}_1 \otimes \boldsymbol{t}_1 \\ \vdots & \ddots & \vdots \\ c_{q1}\boldsymbol{v}_q \otimes \boldsymbol{t}_q & \cdots & c_{qq}\boldsymbol{v}_q \otimes \boldsymbol{t}_q \end{pmatrix} \tag{A.7}$$

where c_{ij} is the $(i,j)^{th}$ entry of $\boldsymbol{C}$. Vectors $\boldsymbol{v}_i$ and $\boldsymbol{t}_i$ $(i = 1 \ldots q)$ are of sizes $1 \times K_N$ and $1 \times K_M$, respectively, given as

$$\boldsymbol{v}_i = [1, e^{-j\pi sin(\theta_i)}, \ldots, e^{-j\pi(K_N-1)sin(\theta_i)}] \tag{A.8a}$$

$$\boldsymbol{t}_i = [1, e^{-j2\pi\triangle_f\tau_i}, \ldots, e^{-j2\pi\triangle_f(K_M-1)\tau_i}] \tag{A.8b}$$

To prove that, for $q \leq K_M K_N$, $\max_i Q_i \leq K_N$, and $\max_i P_i \leq K_M$, the matrix $\boldsymbol{W}$ is of rank q, we should prove the following:
(a) $\boldsymbol{W}$ does not have an all-zero row, i.e. for a given row i, there exists at least one j such that $c_{ij} \neq 0$.
(b) The vectors $\{\boldsymbol{v}_i \otimes \boldsymbol{t}_i\}_{i=1}^{q}$ are linearly independent.
The proof of **(a)** is found in [81]. As for **(b)**, let $\boldsymbol{H}$ be a $K_M K_N \times q$ matrix of columns $\{\boldsymbol{v}_i \otimes \boldsymbol{t}_i\}_{i=1}^{q}$. The matrix $\boldsymbol{H}$ is full column rank under the following three conditions:

- **(i)** $q \leq K_M K_N$. (Similar to Condition 1 in Remark 4.2)
- **(ii)** $\max_i Q_i \leq K_N$. (Similar to Condition 2 in Remark 4.2)
- **(iii)** $\max_i P_i \leq K_M$. (Similar to Condition 3 in Remark 4.2)

Appendix B

Proof of Theorem 6.1

The matrix $\boldsymbol{T}(\boldsymbol{\alpha})$ could be re-written as

$$\boldsymbol{T}(\boldsymbol{\alpha}) = \boldsymbol{I_N} + \sum_{i=1}^{p-1} \alpha_i \boldsymbol{S}_i \tag{B.1}$$

Using the above expression of $\boldsymbol{T}(\boldsymbol{\alpha})$, we can now say

$$\begin{aligned} \boldsymbol{T}(\boldsymbol{\alpha})\boldsymbol{a} &= \Big(\boldsymbol{I_N} + \sum_{i=1}^{p-1} \alpha_i \boldsymbol{S}_i\Big)\boldsymbol{a} \\ &= \Big[\ \boldsymbol{a} \ \Big|\ \boldsymbol{S}_1\boldsymbol{a} \ \Big|\ \ldots \ \Big|\ \boldsymbol{S}_{p-1}\boldsymbol{a} \ \Big]\, \boldsymbol{\alpha} \\ &= \boldsymbol{B}_p\boldsymbol{\alpha} \end{aligned} \tag{B.2}$$

Appendix C

Proof of Theorem 6.3

We shall seek the conditions under which the assumptions of Lemma 6.2 hold true. Clearly, *Assumption 1* is satisfied for any p. As for *Assumption 2*, let $\mathbf{z} \in \mathbb{C}^{\mathrm{p}\times 1}$ be a vector such that $\mathbf{e_1^H z} = \mathbf{0}$, then:

$$\mathbf{z} \in \operatorname{span}\{\mathbf{e_2}, \ldots, \mathbf{e_p}\} = \mathcal{N}(\mathbf{E}) \tag{C.1}$$

In other words, there exists $\beta_2 \ldots \beta_p \in \mathbb{C}$ such that

$$\mathbf{z} = [0, \beta_2 \ldots \beta_p]^{\mathrm{T}} \tag{C.2}$$

Now, we seek a condition under which a vector $\mathbf{z} \in \mathcal{N}(\mathbf{e_1^H})$ satisfies $\mathbf{z}^{\mathrm{H}}\mathbf{K}(\theta)\mathbf{z} = 0$. Since $\mathbf{B}(\theta)$ is full column rank for any p satisfying $p \leq \frac{N}{2}$, then

$$\begin{aligned} \operatorname{rank}\Big(\mathbf{K}(\theta)\Big) = \operatorname{rank}\Big(\mathbf{B}^{\mathrm{H}}(\theta)\hat{\mathbf{U}}_{\mathbf{n}}\hat{\mathbf{U}}_{\mathbf{n}}^{\mathrm{H}}\mathbf{B}(\theta)\Big) &= \operatorname{rank}\Big(\hat{\mathbf{U}}_{\mathbf{n}}\hat{\mathbf{U}}_{\mathbf{n}}^{\mathrm{H}}\Big) \\ &= N - q \end{aligned} \tag{C.3}$$

Therefore, $\mathbf{K}(\theta)$ admits $N - q$ linearly independent columns. Recall that the number of possibly non-zero elements of $\mathbf{z}$ is $p-1$. This immediately implies that there exists a vector $\mathbf{z}$ such that $\mathbf{z}^{\mathrm{H}}\mathbf{K}(\theta)\mathbf{z} = 0$ if and only if

$$p - 1 \geq N - q \tag{C.4}$$

Finally, for every $\mathbf{z} \in \mathcal{N}(\mathbf{E})$ such that $\mathbf{z}^{\mathrm{H}}\mathbf{K}(\theta)\mathbf{z} \neq 0$ is satisfied if and only if $p + q < N + 1$ and $p \leq \frac{N}{2}$. And the proof is done. Note that when $p = 1$ (absence of mutual coupling), we get the traditional identifiability, i.e. $q < N$.

Appendix D

Proof of Theorem 6.4

We shall prove this theorem by mathematical recurrence. Clearly, the theorem is true when $p = 1$ for any $N \geq 1$. Assume equality (6.33) holds true for $p-1$. Our task is to prove the same equality for p. Using Theorem 6.1, we can say

$$\begin{aligned}
\boldsymbol{T}(\boldsymbol{\alpha}_p)\boldsymbol{a} &= \boldsymbol{B}_p\boldsymbol{\alpha}_p \\
&= \boldsymbol{B}_{p-1}\boldsymbol{\alpha}_{p-1} + \alpha_{p-1}\boldsymbol{S}_{p-1}\boldsymbol{a} \\
&= g(z,\boldsymbol{\alpha}_{p-1})\boldsymbol{a} - \boldsymbol{M}_{p-1}\widetilde{\boldsymbol{\alpha}}_{p-1} + \alpha_{p-1}\boldsymbol{S}_{p-1}\boldsymbol{a} \\
&= g(z,\boldsymbol{\alpha}_p)\boldsymbol{a} - \alpha_{p-1}(z^{p-1} + z^{-(p-1)})\boldsymbol{a} - \boldsymbol{M}_{p-1}\tilde{\boldsymbol{\alpha}}_{p-1} \\
&+ \alpha_{p-1}\boldsymbol{S}_{p-1}\boldsymbol{a} \\
&= g(z,\boldsymbol{\alpha}_p)\boldsymbol{a} - \left[\begin{array}{c|c} \boldsymbol{M}_{p-1} & \boldsymbol{m}_{p-1} \end{array}\right]\widetilde{\boldsymbol{\alpha}}_p
\end{aligned} \tag{D.1}$$

where $\boldsymbol{B}_p = \mathcal{G}_p(\boldsymbol{\alpha}_p)$ and $\boldsymbol{S}_{p-1}$ are given in Theorem 6.1. The vector $\boldsymbol{m}_{p-1}$ is given as

$$\boldsymbol{m}_{p-1} = \Big((z^{p-1} + z^{-(p-1)})\boldsymbol{I}_N - \boldsymbol{S}_{p-1}\Big)\boldsymbol{a} = \boldsymbol{u}_{p-1} + \boldsymbol{l}_{p-1} \tag{D.2}$$

where

$$\boldsymbol{u}_{p-1} = \left[\begin{array}{c|c|c|c} z^{-(p-1)} & \ldots & z^{-1} & \boldsymbol{0}_{[1\times(N-p+1)]} \end{array}\right]^{\mathrm{T}} \tag{D.3a}$$

and

$$\boldsymbol{l}_{p-1} = \left[\begin{array}{c|c|c|c} \boldsymbol{0}_{[1\times(N-p+1)]} & z^{N} & \ldots & z^{N+p-2} \end{array}\right]^{\mathrm{T}} \tag{D.3b}$$

Notice that $\boldsymbol{u}_{p-1}$ and $\boldsymbol{l}_{p-1}$ are the last columns of $\boldsymbol{U}_p$ and $\boldsymbol{L}_p$, respectively. And the proof is done.

Appendix E

Proof of Theorem 6.5

Using ***Theorem 1*** and ***Theorem 2***, then for any $1 \leq p \leq N$ and $\boldsymbol{\alpha} = [\alpha_0, \alpha_1 \dots \alpha_{p-1}]^{\mathrm{T}}$ we could say

$$\boldsymbol{B}_p\boldsymbol{\alpha} = \boldsymbol{T}(\boldsymbol{\alpha})\boldsymbol{a} = g(z, \boldsymbol{\alpha})\boldsymbol{a} - \boldsymbol{M}_p\widetilde{\boldsymbol{\alpha}} \tag{E.1}$$

where quantities have been previously defined in their corresponding theorems.

Case 1: Here, we should prove that $\boldsymbol{B}_p\boldsymbol{\alpha} = \boldsymbol{0}$ implies $\boldsymbol{\alpha} = \boldsymbol{0}$. For $p \leq \frac{N+1}{2}$, the matrix $\boldsymbol{M}_p$ could be alternatively expressed as

$$\boldsymbol{M}_p = \begin{bmatrix} \boldsymbol{U}_p \\ \hline \boldsymbol{0}_{[(N-2p+2)\times(p-1)]} \\ \hline \boldsymbol{L}_p \end{bmatrix} \tag{E.2}$$

Note the "zero" gap in matrix $\boldsymbol{M}_p$. This gap exists when $N - 2p + 2 \geq 1$, or equivalently $p \leq \frac{N+1}{2}$. In this case, the system of equations $\boldsymbol{B}_p\boldsymbol{\alpha} = \boldsymbol{0}$, and in particular the "zero" gap, suggest that the polynomial $g(z, \boldsymbol{\alpha}) = 0$. Now, the $(p-1)^{th}$ row gives

$$\alpha_{p-1}z^{-1} = 0 \Rightarrow \alpha_{p-1} = 0 \tag{E.3}$$

By backward substitution from rows $p-2$ till 1 in matrix $\boldsymbol{M}_p$, one gets the following

$$\alpha_{p-1} = \dots = \alpha_1 = 0 \tag{E.4}$$

which, in turn, by plugging in $g(z, \boldsymbol{\alpha})$ gives $\alpha_0 = 0$.

Case 2: Fix $p = \frac{N+2}{2}$ and N is even. The matrices $\boldsymbol{U}_p$ and $\boldsymbol{L}_p$ that are embedded in $\boldsymbol{M}_p$ do not overlap, but the "zero" gap doesn't exist, viz.

$$\boldsymbol{M}_p = \left[\begin{array}{c} \boldsymbol{U}_p \\ \hline \boldsymbol{L}_p \end{array}\right] \tag{E.5}$$

Assume $\boldsymbol{B}_p\boldsymbol{\alpha} = \boldsymbol{0}$. The $(p-1)^{th}$ row implies

$$z^{p-2}g(z,\boldsymbol{\alpha}) = z^{-1}\alpha_{p-1} \tag{E.6}$$

Plugging equation (E.6) in the equation given by row $p-2$ gives $\alpha_{p-1} = 0$. By backward substitution from rows $p-3$ till 1, we get

$$\alpha_{p-2} = \ldots = \alpha_1 = 0 \tag{E.7}$$

Now, the polynomial $g(z,\boldsymbol{\alpha})$ is given as

$$g(z,\boldsymbol{\alpha}) = \alpha_0 + \alpha_{p-1}(z^{p-1} + z^{-(p-1)}) \tag{E.8}$$

Therefore, using equation (E.6), row $(p-1)$ gives

$$\alpha_0 = -\alpha_{p-1}z^{p-1} \tag{E.9}$$

Similarly, the p^{th} row and using $z^{2(p-1)} = z^N$ since $p = \frac{N+2}{2}$, we get

$$\alpha_0 = -\alpha_{p-1}z^{-(p-1)} \tag{E.10}$$

Equations (E.9) and (E.10) together give $z^N = 1$ if $\alpha_{p-1} \neq 0$. Moreover, equations (E.9) and (E.10) give us the null space of $\boldsymbol{B}_p$, namely

$$\mathcal{N}(\boldsymbol{B}_p) = \{\boldsymbol{\beta} \in \mathbb{C}^{p\times 1}, z \in \mathbb{C}^* | \boldsymbol{\beta} = [1, 0 \ldots 0, -z^{p-1}]^{\mathrm{T}}\} \tag{E.11}$$

Therefore, the rank of $\boldsymbol{B}_p$ is $p-1$.

Case 3(a): Here, N is even and $p > \frac{N+2}{2}$. Fix $k = p - \frac{N+2}{2}$. In this case, the matrices $\boldsymbol{U}_p$ and $\boldsymbol{L}_p$ overlap. Furthermore, the structure of $\boldsymbol{M}_p$ is given as follows

$$\boldsymbol{M}_p = \left[\begin{array}{c|c} \boldsymbol{U}_{p-k} & \boldsymbol{V} \\ \hline \boldsymbol{L}_{p-k} & \end{array}\right] \tag{E.12}$$

The i^{th} column of $\boldsymbol{V} \in \mathbb{C}^{N\times k}$ is

$$\boldsymbol{v}_i = \left[\begin{array}{c|c|c} \boldsymbol{u}_i^{\mathrm{T}} & \boldsymbol{m}_i^{\mathrm{T}} & \boldsymbol{b}_i^{\mathrm{T}} \end{array}\right]^{\mathrm{T}} \tag{E.13}$$

where

$$\boldsymbol{u}_i = [z^{-(\frac{N}{2}+i)}, z^{-(\frac{N}{2}+i)+1} \dots z^{-(2i+1)}]^{\mathrm{T}} \tag{E.14}$$

$$\boldsymbol{m}_i = [z^{-2i} + z^N, z(z^{-2i} + z^N) \dots z^{2i-1}(z^{-2i} + z^N)]^{\mathrm{T}} \tag{E.15}$$

$$\boldsymbol{b}_i = [z^{N+2i}, z^{N+2i+1} \dots z^{\frac{3N}{2}-1+i}]^{\mathrm{T}} \tag{E.16}$$

Realising the above equations, the system of equations $\boldsymbol{B}_p\boldsymbol{\alpha} = \boldsymbol{0}$ could be partitioned into 4 subsystems of equations given as follows:

Rows $1 \dots \frac{N}{2} - k$ of $\boldsymbol{B}_p\boldsymbol{\alpha} = \boldsymbol{0}$ are given by system $\mathcal{S}_1$

$$\mathcal{S}_1 : \quad \boldsymbol{g}(z, \boldsymbol{\alpha}) = \sum_{i=l}^{\frac{N}{2}+k} \alpha_i z^{-i}, \quad l = 1 \dots \frac{N}{2} - k \tag{E.17}$$

Rows $\frac{N}{2} - k + 1 \dots \frac{N}{2}$ of $\boldsymbol{B}_p\boldsymbol{\alpha} = \boldsymbol{0}$ are given by system $\mathcal{S}_2$

$$\mathcal{S}_2 : \quad \boldsymbol{g}(z, \boldsymbol{\alpha}) = \sum_{i=\frac{N}{2}-k+l}^{\frac{N}{2}+k-l} \alpha_i z^{-i} + \sum_{i=\frac{N}{2}-k-l+1}^{\frac{N}{2}+k} \alpha_i (z^i + z^{-i}), \quad l = 1 \dots k \tag{E.18}$$

Rows $\frac{N}{2} + 1 \dots \frac{N}{2} + k$ of $\boldsymbol{B}_p\boldsymbol{\alpha} = \boldsymbol{0}$ are given by system $\mathcal{S}_3$

$$\mathcal{S}_3 : \quad \boldsymbol{g}(z, \boldsymbol{\alpha}) = \sum_{i=\frac{N}{2}-k+l}^{\frac{N}{2}+k-l} \alpha_i z^{i} + \sum_{i=\frac{N}{2}-k-l+1}^{\frac{N}{2}+k} \alpha_i (z^i + z^{-i}), \quad l = 1 \dots k \tag{E.19}$$

Rows $\frac{N}{2} + k + 1 \dots N$ of $\boldsymbol{B}_p\boldsymbol{\alpha} = \boldsymbol{0}$ are given by system $\mathcal{S}_4$

$$\mathcal{S}_4 : \quad \boldsymbol{g}(z, \boldsymbol{\alpha}) = \sum_{i=l}^{\frac{N}{2}+k} \alpha_i z^{i}, \quad l = 1 \dots \frac{N}{2} - k \tag{E.20}$$

Now, system $\mathcal{S}_1$ (or equivalently $\mathcal{S}_4$) imply the following

$$\alpha_1 = \dots = \alpha_{\frac{N}{2}-k-1} = 0 \tag{E.21}$$

which is carried on by backward substitution. Therefore, systems $\mathcal{S}_1$ and $\mathcal{S}_4$ each break down to one and only one equation (for $l = \frac{N}{2} - k$). Furthermore, for $l = k$,

system $\mathcal{S}_2$ gives

$$\alpha_{\frac{N}{2}} z^{-\frac{N}{2}}(z^N - 1) = 0 \tag{E.22}$$

According to equation (E.22), two cases arise:

$$\boxed{\alpha_{\frac{N}{2}} = 0 \text{ and } z^N \neq 1}$$

Using systems $\mathcal{S}_1$ and $\mathcal{S}_2$, we get

$$\sum_{i=\frac{N}{2}-k}^{\frac{N}{2}-k+l-1} \alpha_i z^{-i} = \sum_{i=\frac{N}{2}+k-l+1}^{\frac{N}{2}+k} \alpha_i z^i, \quad l = 1 \dots k \tag{E.23}$$

Similarly, systems $\mathcal{S}_3$ and $\mathcal{S}_4$ give

$$\sum_{i=\frac{N}{2}-k}^{\frac{N}{2}-k+l-1} \alpha_i z^{i} = \sum_{i=\frac{N}{2}+k-l+1}^{\frac{N}{2}+k} \alpha_i z^{-i}, \quad l = 1 \dots k \tag{E.24}$$

Equation (E.23) reads

$$\alpha_{\frac{N}{2}-k+l-1} = \alpha_{\frac{N}{2}+k-l+1} z^N, \qquad l = 1 \dots k \tag{E.25}$$

Equation (E.24) gives

$$\alpha_{\frac{N}{2}-k+l-1} = \alpha_{\frac{N}{2}+k-l+1} z^{-N}, \qquad l = 1 \dots k \tag{E.26}$$

Equations (E.25) and (E.26) together give

$$\alpha_{\frac{N}{2}+k-l+1}(1 - z^N)(1 + z^{-N}) = 0 \tag{E.27}$$

Based on assumption $z^N \neq 1$, equation (E.27) gives two subcases:

Case 3(a.i): $\{\alpha_{\frac{N}{2}+k-l+1} = 0\}_{l=1}^{k}$ and $z^N \neq -1$. In this case, one could easily verify that $\alpha_0 = \ldots = \alpha_{p-1} = 0$. Hence, iff $z^N \neq \pm 1$, the matrix $\boldsymbol{B}_p$ is full rank.

Case 3(a.ii): $\{\alpha_{\frac{N}{2}+k-l+1} \neq 0\}_{l=1}^{k}$ and $z^N = -1$. In this case, equation (E.26) gives

$$\alpha_{\frac{N}{2}-k+l-1} = -\alpha_{\frac{N}{2}+k-l+1}, \qquad l = 1 \dots k \tag{E.28}$$

Systems $\mathcal{S}_1$ and $\mathcal{S}_4$ now give

$$\alpha_0 = -z^{\frac{N}{2}} \sum_{i=1}^{k} \alpha_{\frac{N}{2}+i}(z^i - z^{-i}) \tag{E.29}$$

The dimension of the corresponding null space is $(2k+1) - (k+1) = k$. Note that the quantity $(2k+1)$ is the number of non-zero variables and $(k+1)$ is the number of linearly independent equations. The null space of $\boldsymbol{B}_p$ when $z^N = -1$ is given by

$$\mathcal{N}(\boldsymbol{B}_p) = \left\{ \boldsymbol{b} \in \mathbb{C}^{p\times 1}, \boldsymbol{\beta} \neq \boldsymbol{0} \middle| \boldsymbol{b} = \begin{bmatrix} h_-(\boldsymbol{\beta}) \\ \boldsymbol{0} \\ -\boldsymbol{J}_k\boldsymbol{\beta} \\ 0 \\ \boldsymbol{\beta} \end{bmatrix} \right\} \tag{E.30a}$$

where $\boldsymbol{\beta} = [\beta_1 \dots \beta_k]^{\mathrm{T}}$ and

$$h_-(\boldsymbol{\beta}) = -z^{\frac{N}{2}} \sum_{i=1}^{k} \beta_i(z^i - z^{-i}) \tag{E.30b}$$

Therefore,

$$\operatorname{rank}(\boldsymbol{B}_p) = p - k = \frac{N}{2} + 1 \tag{E.31}$$

$$\boxed{\alpha_{\frac{N}{2}} \neq 0 \text{ and } z^N = 1}$$

Following the same steps as Case 3(a.1), one reaches equation (E.25) and concludes

$$\alpha_{\frac{N}{2}-k+l-1} = \alpha_{\frac{N}{2}+k-l+1}, \qquad l = 1 \dots k \tag{E.32}$$

Also, as previously done, systems $\mathcal{S}_1$ and $\mathcal{S}_4$ imply

$$\alpha_0 = -z^{\frac{N}{2}} \left(\alpha_{\frac{N}{2}} + \sum_{i=1}^{k} \alpha_{\frac{N}{2}+i}(z^i + z^{-i}) \right) \tag{E.33}$$

The null space therefore spans $k+1$ dimensions, namely

$$\mathcal{N}(\boldsymbol{B}_p) = \left\{ \boldsymbol{b} \in \mathbb{C}^{p\times 1}, [\boldsymbol{\beta}, \gamma]^{\mathrm{T}} \neq \boldsymbol{0} \middle| \boldsymbol{b} = \begin{bmatrix} h_+(\boldsymbol{\beta}, \gamma) \\ \boldsymbol{0} \\ \boldsymbol{J}_k\boldsymbol{\beta} \\ \gamma \\ \boldsymbol{\beta} \end{bmatrix} \right\} \tag{E.34a}$$

$$h_+(\boldsymbol{\beta},\gamma) = -z^{\frac{N}{2}}\Big(\gamma + \sum_{i=1}^{k}\beta_i(z^i + z^{-i})\Big) \tag{E.34b}$$

Hence, we conclude that the rank of $\boldsymbol{B}_p$ is $\frac{N}{2}$. This completes the proof of ***Case 3(a.iii)***.

Case 3(b): Here, N is odd and $p > \frac{N+2}{2}$. Fix $k = p - \frac{N+1}{2}$. The proof follows similar steps as ***Case 3(a)***. The null space is given as follows

$$\mathcal{N}(\boldsymbol{B}_p) = \Big\{\boldsymbol{b} \in \mathbb{C}^{p\times 1}, \boldsymbol{\beta} \neq \mathbf{0}\Big|\boldsymbol{b} = \begin{bmatrix} y(\boldsymbol{\beta}) \\ \mathbf{0} \\ -z^N\boldsymbol{J}_k\boldsymbol{\beta} \\ \boldsymbol{\beta} \end{bmatrix}\Big\} \tag{E.35a}$$

$$y(\boldsymbol{\beta}) = -z^{\frac{N}{2}}\sum_{i=1}^{k}\beta_i\Big(z^{(i+\frac{1}{2})} - z^N z^{-(i+\frac{1}{2})}\Big) \tag{E.35b}$$

Appendix F

Proof of Theorem 6.6

Using the results of ***Theorem 3*** and restricting ourselves with $z = z_\theta = e^{-j2\pi \frac{d}{\lambda}\sin(\theta)}$, it suffices to derive the two sets, $\mathbf{\Theta_+}$ and $\mathbf{\Theta_-}$. The equation $z_\theta^N = 1$ reads the following

$$e^{-j2\pi \frac{d}{\lambda} N\sin(\theta)} = e^{j2k\pi}, \quad k = -\frac{N}{2} \cdots \frac{N}{2} \tag{F.1}$$

With some straightforward algebra, equation (F.1) implies that $\theta \in \mathbf{\Theta_+}$. In a similar manner, $z_\theta^N = -1$ implies $\theta \in \mathbf{\Theta_-}$. Combining ***Theorem 3*** with the above completes the proof.

Appendix G

Proof of Property 2

- The first two cases are a direct consequence of equation (6.19).
- The third case is a result of ***Consequence 1*** and equation (6.19).
- As for the fourth case, assume that the sets $\boldsymbol{\Theta}$ and $\boldsymbol{\Theta}_{\pm}$ overlap and $\frac{N+2}{2} \leq p < N$. Let $\theta_i \in \boldsymbol{\Theta} \cap \boldsymbol{\Theta}_{\pm}$. Therefore, $\boldsymbol{K}(\theta_i)\boldsymbol{\alpha} = \mathbf{0}$ only when $\boldsymbol{\alpha} \in \mathcal{N}\big(\boldsymbol{B}(\theta_i)\big)$ or $\boldsymbol{\alpha} = \boldsymbol{c}$. It suffices to prove that the set $\boldsymbol{c}$ is linearly independent from the span of $\mathcal{N}\big(\boldsymbol{B}(\theta_i)\big)$.
  Let Δ be the dimension of $\mathcal{N}\big(\boldsymbol{B}(\theta_i)\big)$. Furthermore, let $\boldsymbol{\gamma} \in \mathbb{C}^{(\Delta+1)\times 1}$ be an arbitrary vector and $\boldsymbol{E} \in \mathbb{C}^{p\times(\Delta+1)}$ be a matrix where the first Δ columns span $\mathcal{N}\big(\boldsymbol{B}(\theta_i)\big)$ and the last column is the vector $\boldsymbol{c}$. It remains to show that $\boldsymbol{E}\boldsymbol{\gamma} = \mathbf{0} \Rightarrow \boldsymbol{\gamma} = \mathbf{0}$. Under the assumption that $p < N$ and using the structure of the null space of $\boldsymbol{B}(\theta_i)$ given in equations (E.11), (E.30), (E.34), and (E.35), one could easily verify that the second row of $\boldsymbol{E}$ is given as

$$[\underbrace{0 \ldots 0}_{\Delta}, c_1] \tag{G.1}$$

  which implies that the last element of $\boldsymbol{\gamma}$ is 0, since by construction $c_1 \neq 0$, for $p \geq 2$. Hence, $\boldsymbol{\gamma} = \mathbf{0}$ because the first Δ columns of $\boldsymbol{E}$ are linearly independent.

Appendix H

Proof of Property 3

Let the function $f_\epsilon(\theta)$ be defined as follows:

$$f_\epsilon(\theta) = \boldsymbol{a}_p^{\mathrm{T}}(\theta)\big(\boldsymbol{K}(\theta) + \epsilon \boldsymbol{I}\big)^{-1}\boldsymbol{a}_p^*(\theta) \tag{H.1}$$

and therefore

$$\lim_{\epsilon \to 0} f_\epsilon(\theta) = f(\theta) \tag{H.2}$$

By spectral decomposition,

$$\boldsymbol{K}(\theta) = \boldsymbol{V}\boldsymbol{\Phi}\boldsymbol{V}^{\mathrm{H}} \tag{H.3}$$

where the k^{th} column of $\boldsymbol{V}$ is the k^{th} normalized eigenvector[1] of $\boldsymbol{K}(\theta)$, denoted as $\boldsymbol{v}_k$ and its corresponding eigenvalue is the k^{th} smallest eigenvalue found in the k^{th} diagonal entry of $\boldsymbol{\Phi}$, denoted as λ_k. We could then express $f_\epsilon(\theta)$ as

$$f_\epsilon(\theta) = \boldsymbol{a}_p^{\mathrm{T}}(\theta)\boldsymbol{V}\big(\boldsymbol{\Phi} + \epsilon \boldsymbol{I}\big)^{-1}\boldsymbol{V}^{\mathrm{H}}\boldsymbol{a}_p^*(\theta) \tag{H.4}$$

- When $\theta \notin \boldsymbol{\Theta}$, we distinguish two sub-cases:
  - If $\theta \notin \boldsymbol{\Theta}_\pm$, then $\boldsymbol{K}(\theta)$ is full rank according to ***Property 2*** and hence $\lambda_k > 0$ for all k, so

$$f(\theta) = \|\boldsymbol{\Phi}^{-1/2}\boldsymbol{V}^{\mathrm{H}}\boldsymbol{a}_p^*(\theta)\|^2 < \infty \tag{H.5}$$

  - If $\theta \in \boldsymbol{\Theta_\pm}$, then $\boldsymbol{K}(\theta)$ is full rank (if $p < \frac{N+2}{2}$) and the preceeding argument holds. However, if $p \geq \frac{N+2}{2}$, then $\boldsymbol{K}(\theta)$ admits the same null-space as that of $\boldsymbol{B}(\theta)$ according to ***Property 2***. As before, let Δ be the

[1] Indeed, $\boldsymbol{V}$ and $\boldsymbol{\Phi}$ are functions of θ. This is omitted for the sake of compact exposition.

dimension of $\boldsymbol{K}(\theta)$, therefore $f_\epsilon(\theta)$ behaves as

$$f_\epsilon(\theta) \backsim \sum_{k=1}^{\Delta} \frac{1}{\lambda_k + \epsilon} \|\boldsymbol{a}_p^{\mathrm{T}}(\theta)\boldsymbol{v}_k\|^2 = \sum_{k=1}^{\Delta} \frac{1}{\epsilon} \|\boldsymbol{e}_1^{\mathrm{T}}\boldsymbol{B}(\theta)\boldsymbol{v}_k\|^2 \tag{H.6}$$

Note that $\{\boldsymbol{v}_k\}_{k=1}^{\Delta}$ span the null space of $\boldsymbol{B}(\theta)$ and therefore $\boldsymbol{B}(\theta)\boldsymbol{v}_k = \boldsymbol{0}$. So, $f_\epsilon(\theta) = f(\theta) = 0 < \infty$.

- When $\theta \in \boldsymbol{\Theta}$, we also distinguish the same sub-cases:
  - If $\theta \notin \boldsymbol{\Theta}_\pm$, then there is only one singularity in $\boldsymbol{K}(\theta)$ according to ***Property 2***, i.e. $\lambda_1 = 0$, $\boldsymbol{v}_1 = \frac{\boldsymbol{c}}{\|\boldsymbol{c}\|}$, and $\lambda_k > 0$ for all $k \geq 2$. Hence

$$f_\epsilon(\theta) \backsim \frac{1}{\epsilon} \frac{\|\boldsymbol{a}_p^{\mathrm{T}}(\theta)\boldsymbol{c}\|^2}{\|\boldsymbol{c}\|^2} \tag{H.7}$$

    Notice that the term $\boldsymbol{a}_p^{\mathrm{T}}(\theta)\boldsymbol{c}$ is a polynomial of degree $p-1$ evaluated at the unit circle. For a polynomial with non-zero coefficients to have zeros on the unit-circle, the coefficient vector $\boldsymbol{c}$ must be conjugate-symmetric [97], which is not the case according to equation (2.10). Therefore, $\boldsymbol{a}_p^{\mathrm{T}}(\theta)\boldsymbol{c} \neq 0$ and thus

$$f(\theta) = \lim_{\epsilon \to 0} f_\epsilon(\theta) = \infty \tag{H.8}$$

  - If $\theta \in \boldsymbol{\Theta_\pm}$, then the null space of $\boldsymbol{K}(\theta)$ is spanned by $\Delta + 1$ vectors given in ***Property 2***, and we have

$$f_\epsilon(\theta) \backsim \sum_{k=1}^{\Delta} \frac{1}{\epsilon} \|\boldsymbol{e}_1^{\mathrm{T}}\boldsymbol{B}(\theta)\boldsymbol{v}_k\|^2 + \frac{1}{\epsilon} \frac{\|\boldsymbol{a}_p^{\mathrm{T}}(\theta)\boldsymbol{c}\|^2}{\|\boldsymbol{c}\|^2} \tag{H.9}$$

    Using the same argument as before, as ϵ goes to zero, the 1^{st} term of the above expression goes to zero, whereas the 2^{nd} term goes to ∞.

Appendix I

Proof of Property 5

The 1^{st} order derivative is computed as

$$f'(\theta) = 2\mathrm{Re}\{\boldsymbol{a}_p^{\mathrm{T}}(\theta)\widehat{\boldsymbol{K}}^{-1}(\theta)\frac{\partial \boldsymbol{a}_p^*(\theta)}{\partial\theta}\} + \boldsymbol{a}_p^{\mathrm{T}}(\theta)\frac{\partial \widehat{\boldsymbol{K}}^{-1}(\theta)}{\partial\theta}\boldsymbol{a}_p^*(\theta) \tag{I.1}$$

Denoting

$$\boldsymbol{d}_p(\theta) = \frac{\partial \boldsymbol{a}_p(\theta)}{\partial\theta} \tag{I.2}$$

$$\boldsymbol{D}(\theta) = \frac{\partial \boldsymbol{B}(\theta)}{\partial\theta} = \mathcal{G}_p(\frac{\partial \boldsymbol{a}(\theta)}{\partial\theta}) \tag{I.3}$$

and using the following identity [98]

$$\frac{\partial \widehat{\boldsymbol{K}}^{-1}(\theta)}{\partial\theta} = -\widehat{\boldsymbol{K}}^{-1}(\theta)\frac{\partial \widehat{\boldsymbol{K}}(\theta)}{\partial\theta}\widehat{\boldsymbol{K}}^{-1}(\theta) \tag{I.4}$$

then $f'(\theta) = g_1(\theta) + g_2(\theta)$, where

$$g_1(\theta) = 2\mathrm{Re}\{\boldsymbol{a}_p^{\mathrm{T}}(\theta)\widehat{\boldsymbol{K}}^{-1}(\theta)\boldsymbol{d}_p^*(\theta)\} \tag{I.5a}$$

$$g_2(\theta) = -2\mathrm{Re}\{\boldsymbol{a}_p^{\mathrm{T}}(\theta)\widehat{\boldsymbol{K}}^{-1}(\theta)\widehat{\boldsymbol{G}}(\theta)\widehat{\boldsymbol{K}}^{-1}(\theta)\boldsymbol{a}_p^*(\theta)\} \tag{I.5b}$$

and

$$\widehat{\boldsymbol{G}}(\theta) = \boldsymbol{B}^{\mathrm{H}}(\theta)\widehat{\boldsymbol{U}}_{\boldsymbol{n}}\widehat{\boldsymbol{U}}_{\boldsymbol{n}}^{\mathrm{H}}\boldsymbol{D}(\theta) \tag{I.5c}$$

In a similar manner, after some straightforward, but lengthy, calculations, one could verify that $f''(\theta) = h_1(\theta) + h_2(\theta) + h_3(\theta)$, where $h_k(\theta)$ are given as

$$h_1(\theta) = 2\mathrm{Re}\Big\{\boldsymbol{d}_p^{\mathrm{T}}(\theta)\widehat{\boldsymbol{K}}^{-1}(\theta)\boldsymbol{d}_p^*(\theta) + \boldsymbol{a}_p^{\mathrm{T}}(\theta)\widehat{\boldsymbol{K}}^{-1}(\theta)\frac{\partial \boldsymbol{d}_p^*(\theta)}{\partial\theta}\Big\} \tag{I.6a}$$

$$\begin{aligned} h_2(\theta) = &- 4\mathrm{Re}\Big\{\boldsymbol{a}_p^{\mathrm{T}}(\theta)\widehat{\boldsymbol{K}}^{-1}(\theta)\Big(\widehat{\boldsymbol{G}}(\theta)+\widehat{\boldsymbol{G}}^{\mathrm{H}}(\theta)\Big)\widehat{\boldsymbol{K}}^{-1}(\theta)\boldsymbol{d}_p^{*}(\theta)\Big\} \\ &- 2\mathrm{Re}\Big\{\boldsymbol{a}_p^{\mathrm{T}}(\theta)\widehat{\boldsymbol{K}}^{-1}(\theta)\boldsymbol{B}^{\mathrm{H}}(\theta)\widehat{\boldsymbol{U}}_{\boldsymbol{n}}\widehat{\boldsymbol{U}}_{\boldsymbol{n}}^{\mathrm{H}}\frac{\partial \boldsymbol{D}(\theta)}{\partial\theta}\widehat{\boldsymbol{K}}^{-1}(\theta)\boldsymbol{a}_p^{*}(\theta)\Big\} \\ &- 2\boldsymbol{a}_p^{\mathrm{T}}(\theta)\widehat{\boldsymbol{K}}^{-1}(\theta)\boldsymbol{D}^{\mathrm{H}}(\theta)\widehat{\boldsymbol{U}}_{\boldsymbol{n}}\widehat{\boldsymbol{U}}_{\boldsymbol{n}}^{\mathrm{H}}\boldsymbol{D}(\theta)\widehat{\boldsymbol{K}}^{-1}(\theta)\boldsymbol{a}_p^{*}(\theta) \end{aligned} \tag{I.6b}$$

$$h_3(\theta) = 4\mathrm{Re}\Big\{\boldsymbol{a}_p^{\mathrm{T}}(\theta)\widehat{\boldsymbol{K}}^{-1}(\theta)\Big(\widehat{\boldsymbol{G}}(\theta)\widehat{\boldsymbol{K}}^{-1}(\theta)\widehat{\boldsymbol{G}}(\theta)+\widehat{\boldsymbol{G}}^{\mathrm{H}}(\theta)\widehat{\boldsymbol{K}}^{-1}(\theta)\widehat{\boldsymbol{G}}(\theta)\Big)\widehat{\boldsymbol{K}}^{-1}(\theta)\boldsymbol{a}_p^{*}(\theta)\Big\} \tag{I.6c}$$

Appendix J

Proof of Theorem 6.7

$\boldsymbol{K}(\theta_k)$ could, also, be decomposed as follows

$$\widehat{\boldsymbol{K}}(\theta_k) = \boldsymbol{K}(\theta_k) + \widetilde{\boldsymbol{K}}(\theta_k) \tag{J.1}$$

where $\boldsymbol{K}(\theta_k) = \boldsymbol{B}^{\mathrm{H}}(\theta_k)\boldsymbol{U_n}\boldsymbol{U_n}^{\mathrm{H}}\boldsymbol{B}(\theta_k)$ and

$$\widetilde{\boldsymbol{K}}(\theta_k) = 2\mathrm{Re}\big\{\boldsymbol{B}^{\mathrm{H}}(\theta_k)\widetilde{\boldsymbol{U}}_{\boldsymbol{n}}\boldsymbol{U_n}^{\mathrm{H}}\boldsymbol{B}(\theta_k)\big\} + \boldsymbol{B}^{\mathrm{H}}(\theta_k)\widetilde{\boldsymbol{U}}_{\boldsymbol{n}}\widetilde{\boldsymbol{U}}_{\boldsymbol{n}}^{\mathrm{H}}\boldsymbol{B}(\theta_k) \tag{J.2}$$

Using well-known results in *Perturbation Theory*[100, 101], we seek to use the following methodology: Given two Hermitian positive semi-definite matrices $\boldsymbol{K}(\theta_k)$ and $\widetilde{\boldsymbol{K}}(\theta_k)$, where the latter perturbs the former, each $\widehat{\lambda}_j$ and $\widehat{\boldsymbol{v}}_j$ could be approximated by a linear combination as follows:

$$\widehat{\lambda}_j = \lambda_j + \boldsymbol{v}_j^{\mathrm{H}}\widetilde{\boldsymbol{K}}(\theta_k)\boldsymbol{v}_j + \sum_{i\neq j}\frac{|\boldsymbol{v}_i^{\mathrm{H}}\widetilde{\boldsymbol{K}}(\theta_k)\boldsymbol{v}_j|^2}{\lambda_j - \lambda_i} + \mathcal{O}(\|\widetilde{\boldsymbol{K}}\|^3) \tag{J.3}$$

and

$$\widehat{\boldsymbol{v}}_j = \boldsymbol{v}_j + \sum_{i\neq j}\frac{\boldsymbol{v}_i^{\mathrm{H}}\widetilde{\boldsymbol{K}}(\theta_k)\boldsymbol{v}_j}{\lambda_j - \lambda_i}\boldsymbol{v}_i + \mathcal{O}(\widetilde{\boldsymbol{K}}^2) \tag{J.4}$$

This approximation is valid if the the eigenvalue λ_j is non-degenerate. In our case, $\lambda_1 = 0$ is non-degenerate as long as $p \leq \frac{N+2}{2}$ or $\{p > \frac{N+2}{2}$ *and* $\theta_k \notin \boldsymbol{\Theta_{\pm}}\}$ according to ***Consequence 1***. In that case, applying equation (J.3) to $\widehat{\lambda}_1$ and denoting

$\boldsymbol{B} = \boldsymbol{B}(\theta_k)$ and $\boldsymbol{K} = \boldsymbol{K}(\theta_k)$ for short, we get

$$\begin{aligned}
\widehat{\lambda}_1 &= \frac{1}{\|\boldsymbol{c}\|^2}\Big(\boldsymbol{c}^{\mathrm{H}}\widetilde{\boldsymbol{K}}\boldsymbol{c} - \sum_{i=2}^{p}\frac{|\boldsymbol{v}_i^{\mathrm{H}}\widetilde{\boldsymbol{K}}\boldsymbol{c}|^2}{\lambda_i}\Big) + \mathcal{O}(\|\widetilde{\boldsymbol{K}}\|^3) \\
&= \frac{1}{\|\boldsymbol{c}\|^2}\Big(\boldsymbol{c}^{\mathrm{H}}\boldsymbol{B}^{\mathrm{H}}\widetilde{\boldsymbol{U}}_{\boldsymbol{n}}\widetilde{\boldsymbol{U}}_{\boldsymbol{n}}^{\mathrm{H}}\boldsymbol{B}\boldsymbol{c} - \sum_{i=2}^{p}\frac{|\boldsymbol{v}_i^{\mathrm{H}}\boldsymbol{B}^{\mathrm{H}}\boldsymbol{U}_{\boldsymbol{n}}\widetilde{\boldsymbol{U}}_{\boldsymbol{n}}^{\mathrm{H}}\boldsymbol{B}\boldsymbol{c}|^2}{\lambda_i}\Big) + \dots \\
&= \frac{1}{\|\boldsymbol{c}\|^2}\boldsymbol{c}^{\mathrm{H}}\boldsymbol{B}^{\mathrm{H}}\widetilde{\boldsymbol{U}}_{\boldsymbol{n}}\Big(\boldsymbol{I} - \boldsymbol{U}_{\boldsymbol{n}}^{\mathrm{H}}\boldsymbol{B}\big(\underbrace{\sum_{i=2}^{p}\frac{\boldsymbol{v}_i\boldsymbol{v}_i^{\mathrm{H}}}{\lambda_i}}_{\boldsymbol{K}^+}\big)\boldsymbol{B}^{\mathrm{H}}\boldsymbol{U}_{\boldsymbol{n}}\Big)\widetilde{\boldsymbol{U}}_{\boldsymbol{n}}^{\mathrm{H}}\boldsymbol{B}\boldsymbol{c} \\
&= \frac{1}{\|\boldsymbol{c}\|^2}\boldsymbol{c}^{\mathrm{H}}\boldsymbol{B}^{\mathrm{H}}\widetilde{\boldsymbol{U}}_{\boldsymbol{n}}\Big(\boldsymbol{I} - \boldsymbol{P}_k\Big)\widetilde{\boldsymbol{U}}_{\boldsymbol{n}}^{\mathrm{H}}\boldsymbol{B}\boldsymbol{c} + \mathcal{O}(\|\widetilde{\boldsymbol{U}}_{\boldsymbol{n}}\|^3) \\
&= \frac{1}{\|\boldsymbol{c}\|^2}\boldsymbol{c}^{\mathrm{H}}\boldsymbol{B}^{\mathrm{H}}\widetilde{\boldsymbol{U}}_{\boldsymbol{n}}\boldsymbol{P}_k^{\perp}\widetilde{\boldsymbol{U}}_{\boldsymbol{n}}^{\mathrm{H}}\boldsymbol{B}\boldsymbol{c} + \mathcal{O}(\|\widetilde{\boldsymbol{U}}_{\boldsymbol{n}}\|^3)
\end{aligned} \tag{J.5}$$

In a similar manner, using equation (J.4), $\widehat{\boldsymbol{v}}_{\mathbf{1}}$ could be written as

$$\begin{aligned}
\widehat{\boldsymbol{v}}_1 &= \frac{1}{\|\boldsymbol{c}\|}\Big(\boldsymbol{c} - \sum_{i=2}^{p}\frac{\boldsymbol{v}_i^{\mathrm{H}}\widetilde{\boldsymbol{K}}\boldsymbol{c}}{\lambda_i}\boldsymbol{v}_i\Big) + \mathcal{O}(\widetilde{\boldsymbol{K}}^2) \\
&= \frac{1}{\|\boldsymbol{c}\|}\Big(\boldsymbol{c} - \sum_{i=2}^{p}\frac{\boldsymbol{v}_i^{\mathrm{H}}\boldsymbol{B}^{\mathrm{H}}\boldsymbol{U}_{\boldsymbol{n}}\widetilde{\boldsymbol{U}}_{\boldsymbol{n}}^{\mathrm{H}}\boldsymbol{B}\boldsymbol{c}}{\lambda_i}\boldsymbol{v}_i\Big) + \mathcal{O}(\widetilde{\boldsymbol{U}}_{\boldsymbol{n}}^2)
\end{aligned} \tag{J.6}$$

As for the degenerate case, i.e. $\lambda_1 = \ldots = \lambda_{\Delta+1} = 0$, which occurs when $p > \frac{N+2}{2}$ and $\theta_k \in \boldsymbol{\Theta}_{\boldsymbol{\pm}}$; we follow similar steps and use the approximations given in [102].

Appendix K

Proof of Theorem 6.9

Let's call

$$\widetilde{\boldsymbol{\omega}}_k \triangleq \widetilde{\boldsymbol{U}}_{\boldsymbol{n}}^{\mathrm{H}} \boldsymbol{B}(\theta_k)\boldsymbol{c} = \widetilde{\boldsymbol{U}}_{\boldsymbol{n}}^{\mathrm{H}} \boldsymbol{U}_{\boldsymbol{s}} \boldsymbol{U}_{\boldsymbol{s}}^{\mathrm{H}} \boldsymbol{B}(\theta_k)\boldsymbol{c} \tag{K.1}$$

where the second equality is due to the fact that $\boldsymbol{B}(\theta_k)\boldsymbol{c} = \bar{\boldsymbol{a}}(\theta_k) = \boldsymbol{T}(\boldsymbol{c})\boldsymbol{a}(\theta_k)$. Using ***Lemma 1***, it is easy to see that $\widetilde{\boldsymbol{\omega}}_k$ is Gaussian distributed with zero mean and covariance matrix

$$\begin{aligned}
\Big(\mathbb{E}\{\widetilde{\boldsymbol{\omega}}_k \widetilde{\boldsymbol{\omega}}_k^{\mathrm{H}}\}\Big)_{i,j} &= \mathbb{E}\Big\{ \big(\boldsymbol{U}_{\boldsymbol{s}} \boldsymbol{U}_{\boldsymbol{s}}^{\mathrm{H}} \widetilde{\boldsymbol{n}}_i\big)^{\mathrm{H}} \bar{\boldsymbol{a}}(\theta_k) \bar{\boldsymbol{a}}^{\mathrm{H}}(\theta_k) \big(\boldsymbol{U}_{\boldsymbol{s}} \boldsymbol{U}_{\boldsymbol{s}}^{\mathrm{H}} \widetilde{\boldsymbol{n}}_j\big) \Big\} \\
&= \bar{\boldsymbol{a}}^{\mathrm{H}}(\theta_k) \mathbb{E}\Big\{ \big(\boldsymbol{U}_{\boldsymbol{s}} \boldsymbol{U}_{\boldsymbol{s}}^{\mathrm{H}} \widetilde{\boldsymbol{n}}_j\big) \big(\boldsymbol{U}_{\boldsymbol{s}} \boldsymbol{U}_{\boldsymbol{s}}^{\mathrm{H}} \widetilde{\boldsymbol{n}}_i\big)^{\mathrm{H}} \Big\} \bar{\boldsymbol{a}}(\theta_k) \\
&= \underbrace{\frac{\sigma^2}{L} \bar{\boldsymbol{a}}^{\mathrm{H}}(\theta_k) \boldsymbol{U} \bar{\boldsymbol{a}}(\theta_k)}_{\widetilde{\sigma}_k^2} \delta_{i,j}
\end{aligned} \tag{K.2}$$

where the last equality is a result of equation (6.68). Therefore, $\widetilde{\boldsymbol{\omega}}_k \sim \mathcal{CN}(\boldsymbol{0}, \widetilde{\sigma}_k^2 \boldsymbol{I})$. Similarly, $\mathbb{E}\{\widetilde{\boldsymbol{\omega}}_k \widetilde{\boldsymbol{\omega}}_k^{\mathrm{T}}\} = \boldsymbol{0}$. Using the moments of $\widetilde{\boldsymbol{\omega}}_k$, we have

$$\begin{aligned}
\mathbb{E}\big\{(\widetilde{\theta}_k)\big\} &= \mathbb{E}\Big\{\frac{\mathrm{Re}\{\widetilde{\rho}_k\}}{\upsilon_k}\Big\} \\
&= \frac{1}{2\upsilon_k}\Big(\bar{\boldsymbol{d}}^{\mathrm{H}}(\theta_k) \boldsymbol{U}_{\boldsymbol{n}} \boldsymbol{P}_k^{\perp} \mathbb{E}\{\widetilde{\boldsymbol{\omega}}_k\} + \mathbb{E}\{\widetilde{\boldsymbol{\omega}}_k^{\mathrm{H}}\} \boldsymbol{P}_k^{\perp} \boldsymbol{U}_{\boldsymbol{n}}^{\mathrm{H}} \bar{\boldsymbol{d}}(\theta_k)\Big) \\
&= 0
\end{aligned} \tag{K.3}$$

$$
\begin{aligned}
\mathbb{E}\big\{(\widetilde{\theta}_k)^2\big\} &= \mathbb{E}\Big\{\frac{\big(\mathrm{Re}\{\widetilde{\rho}_k\}\big)^2}{\upsilon_k^2}\Big\} \\
&= \frac{1}{2\upsilon_k^2}\mathbb{E}\big\{|\widetilde{\rho}_k|^2\big\} \\
&= \frac{1}{2\upsilon_k^2}\bar{\boldsymbol{d}}^{\mathrm{H}}(\theta_k)\boldsymbol{U}_{\boldsymbol{n}}\boldsymbol{P}_k^{\perp}\mathbb{E}\big\{\widetilde{\boldsymbol{\omega}}_k\widetilde{\boldsymbol{\omega}}_k^{\mathrm{H}}\big\}\boldsymbol{P}_k^{\perp}\boldsymbol{U}_{\boldsymbol{n}}^{\mathrm{H}}\bar{\boldsymbol{d}}(\theta_k) \\
&= \frac{\widetilde{\sigma}_k^2}{2\upsilon_k^2}\bar{\boldsymbol{d}}^{\mathrm{H}}(\theta_k)\boldsymbol{U}_{\boldsymbol{n}}\boldsymbol{P}_k^{\perp}\boldsymbol{U}_{\boldsymbol{n}}^{\mathrm{H}}\bar{\boldsymbol{d}}(\theta_k) = \frac{\widetilde{\sigma}_k^2}{2\upsilon_k} \\
&= \frac{\sigma^2}{2L}\frac{\bar{\boldsymbol{a}}^{\mathrm{H}}(\theta_k)\boldsymbol{U}\bar{\boldsymbol{a}}(\theta_k)}{\upsilon_k}
\end{aligned}
\tag{K.4}
$$

where we have used

$$
\big(\mathrm{Re}\{z\}\big)^2 = \frac{1}{2}\big(|z|^2 + \mathrm{Re}\{z^2\}\big) \tag{K.5}
$$

and $\mathbb{E}\big\{\mathrm{Re}\{\widetilde{\rho}_k^2\}\big\} = 0$ since $\mathbb{E}\{\widetilde{\boldsymbol{\omega}}_k\widetilde{\boldsymbol{\omega}}_k^{\mathrm{T}}\} = \boldsymbol{0}$.

Appendix L

Proof of Theorem 6.10

The terms $\boldsymbol{B}^{\mathrm{H}}(\theta_k)\boldsymbol{B}(\theta_l)$, $\boldsymbol{B}^{\mathrm{H}}(\theta_k)\boldsymbol{D}(\theta_l)$, and $\boldsymbol{D}^{\mathrm{H}}(\theta_k)\boldsymbol{D}(\theta_l)$ appear in $\mathrm{var}_f^{(p)}(\widehat{\theta}_k)$ and $\mathrm{var}_{\mathrm{CRB}}(\widehat{\theta}_k)$. We first compute the limits of these three expressions as $\frac{p}{N} \to 0$. With some straightforward calculations, one could verify the following equality

$$\Big(\boldsymbol{B}^{\mathrm{H}}(\theta_k)\boldsymbol{B}(\theta_l)\Big)_{m,n} = \begin{cases} b_{k,l}(m,n), & \text{if } m \geq n \\ b^*_{l,k}(n,m), & \text{else} \end{cases} \tag{L.1}$$

where

$$\begin{aligned} & b_{k,l}(m,n) \\ &= \Big(z_{\theta_k}^{-(m-1)} z_{\theta_l}^{(n-1)} + (1-\delta_{1,m}\delta_{1,n}) z_{\theta_l}^{(m-n)}\Big)\Big(\sum_{i=0}^{N-m} [z^*_{\theta_k} z_{\theta_l}]^i\Big) \\ &+ (1-\delta_{1,n})\Big(z_{\theta_k}^{-(m+n-2)} + z_{\theta_l}^{(m+n-2)}\Big)\Big(\sum_{i=0}^{N-m-n+1} [z^*_{\theta_k} z_{\theta_l}]^i\Big) \end{aligned} \tag{L.2}$$

Using the following identity

$$\frac{1}{m^{k+1}} \sum_{t=1}^{m} t^k e^{jt(w_1-w_2)} \xrightarrow[m\to\infty]{} \frac{1}{k+1}\delta_{w_1,w_2} \tag{L.3}$$

and keeping in mind that p is fixed, we could complete the summation terms appearing in equation (L.2) by a "finite" amount of terms of order p so that the limits of the sum span all integers $i = 0 \dots N$, and therefore we have

$$\frac{\boldsymbol{B}^{\mathrm{H}}(\theta_k)\boldsymbol{B}(\theta_l)}{N} \xrightarrow[\frac{p}{N}\to 0]{} \boldsymbol{h}_k \boldsymbol{h}_k^{\mathrm{H}} \delta_{k,l} \tag{L.4a}$$

which is a rank-one contribution, and $\boldsymbol{h}_k$ is given in equation (6.6). In a very similar manner, we can prove

$$\frac{\boldsymbol{B}^{\mathrm{H}}(\theta_k)\boldsymbol{D}(\theta_l)}{N^2} \xrightarrow[\frac{p}{N}\to 0]{} \frac{j}{2}\boldsymbol{h}_k\boldsymbol{h}_k^{\mathrm{H}}\delta_{k,l} \tag{L.4b}$$

and

$$\frac{\boldsymbol{D}^{\mathrm{H}}(\theta_k)\boldsymbol{D}(\theta_l)}{N^3} \xrightarrow[\frac{p}{N}\to 0]{} \frac{1}{3}\boldsymbol{h}_k\boldsymbol{h}_k^{\mathrm{H}}\delta_{k,l} \tag{L.4c}$$

With those limits in hand, we could verify the following

$$\frac{1}{N^3}\bar{\boldsymbol{D}}^{\mathrm{H}}\boldsymbol{P}_{\bar{\boldsymbol{A}}}^{\perp}\bar{\boldsymbol{D}} \xrightarrow[\frac{p}{N}\to 0]{} \frac{1}{12}\begin{bmatrix} |\boldsymbol{h}_1^{\mathrm{H}}\boldsymbol{c}|^2 & 0 & \cdots & 0 \\ 0 & |\boldsymbol{h}_2^{\mathrm{H}}\boldsymbol{c}|^2 & \cdots & 0 \\ \vdots & \ddots & \ddots & \vdots \\ 0 & \cdots & 0 & |\boldsymbol{h}_q^{\mathrm{H}}\boldsymbol{c}|^2 \end{bmatrix} \tag{L.5}$$

Note that, when $p = 1$, the above diagonal matrix is the identity matrix, which coincides with the result in [95]. Plugging the limit of equation (L.5) in the CRB expression given in equation (6.1), we get equation (6.81). To verify equation (6.82), we expand the denominator of equation (6.4) as follow

$$\begin{aligned} &\bar{\boldsymbol{d}}^{\mathrm{H}}(\theta_k)\boldsymbol{U}_{\boldsymbol{n}}\boldsymbol{P}_k^{\perp}\boldsymbol{U}_{\boldsymbol{n}}^{\mathrm{H}}\bar{\boldsymbol{d}}(\theta_k) \\ &= \boldsymbol{c}^{\mathrm{H}}\Big[\boldsymbol{D}^{\mathrm{H}}(\theta_k)\boldsymbol{U}_{\boldsymbol{n}}\boldsymbol{U}_{\boldsymbol{n}}^{\mathrm{H}}\boldsymbol{D}(\theta_k) - \big(\boldsymbol{D}^{\mathrm{H}}(\theta_k)\boldsymbol{U}_{\boldsymbol{n}}\boldsymbol{U}_{\boldsymbol{n}}^{\mathrm{H}}\boldsymbol{B}(\theta_k)\big) \\ &\big(\boldsymbol{B}^{\mathrm{H}}(\theta_k)\boldsymbol{U}_{\boldsymbol{n}}\boldsymbol{U}_{\boldsymbol{n}}^{\mathrm{H}}\boldsymbol{B}(\theta_k)\big)^{+}\big(\boldsymbol{B}^{\mathrm{H}}(\theta_k)\boldsymbol{U}_{\boldsymbol{n}}\boldsymbol{U}_{\boldsymbol{n}}^{\mathrm{H}}\boldsymbol{D}(\theta_k)\big)\Big]\boldsymbol{c} \end{aligned} \tag{L.6}$$

By using the limits computed in (L.4), we have

$$\frac{\boldsymbol{B}^{\mathrm{H}}(\theta_k)\boldsymbol{U}_{\boldsymbol{n}}\boldsymbol{U}_{\boldsymbol{n}}^{\mathrm{H}}\boldsymbol{B}(\theta_k)}{N} \xrightarrow[\frac{p}{N}\to 0]{} \boldsymbol{0} \tag{L.7a}$$

$$\frac{\boldsymbol{B}^{\mathrm{H}}(\theta_k)\boldsymbol{U}_{\boldsymbol{n}}\boldsymbol{U}_{\boldsymbol{n}}^{\mathrm{H}}\boldsymbol{D}(\theta_k)}{N^2} \xrightarrow[\frac{p}{N}\to 0]{} \boldsymbol{0} \tag{L.7b}$$

$$\frac{\boldsymbol{D}^{\mathrm{H}}(\theta_k)\boldsymbol{U}_{\boldsymbol{n}}\boldsymbol{U}_{\boldsymbol{n}}^{\mathrm{H}}\boldsymbol{D}(\theta_k)}{N^3} \xrightarrow[\frac{p}{N}\to 0]{} \frac{1}{12}\boldsymbol{h}_k\boldsymbol{h}_k^{\mathrm{H}} \tag{L.7c}$$

and therefore

$$\frac{1}{N^3}\bar{\boldsymbol{d}}^{\mathrm{H}}(\theta_k)\boldsymbol{U}_{\boldsymbol{n}}\boldsymbol{P}_k^{\perp}\boldsymbol{U}_{\boldsymbol{n}}^{\mathrm{H}}\bar{\boldsymbol{d}}(\theta_k) \xrightarrow[\frac{p}{N}\to 0]{} \frac{1}{12}|\boldsymbol{h}_k^{\mathrm{H}}\boldsymbol{c}|^2 \tag{L.8}$$

Equations (L.7) directly imply that $\gamma_k \xrightarrow[\frac{p}{N}\to 0]{} 0$. Now, using equation (L.4a), we can verify that the second term in the numerator of equation (6.4) goes to zero,

viz.

$$\left(\boldsymbol{R}_{\boldsymbol{ss}}^{-1}(\bar{\boldsymbol{A}}^{\mathrm{H}}\bar{\boldsymbol{A}})^{-1}\boldsymbol{R}_{\boldsymbol{ss}}^{-1}\right)_{k,k} \xrightarrow[\frac{p}{N}\to 0]{} 0 \tag{L.9}$$

Another proof could be done by using the asymptotic equivalence between *Toeplitz* and *Circulant* type matrices [99].

Bibliography

[1] S. Pace, et al, "The global positioning system: assessing national policies," No. RAND-MR-614-OSTP. RAND CORP SANTA MONICA CA, 1995.

[2] A. M. Ladd, et al. "On the feasibility of using wireless ethernet for indoor localization," *IEEE Transactions on Robotics and Automation*, 20.3: 555-559, 2004.

[3] A. Haeberlen, et al. "Practical robust localization over large-scale 802.11 wireless networks." *Proceedings of the 10th annual international conference on Mobile computing and networking. ACM*, 2004.

[4] N. Chang, R. Rashidzadeh, and M. Ahmadi. "Robust indoor positioning using differential Wi-Fi access points." *IEEE Transactions on Consumer Electronics*, 56.3, 2010.

[5] Y. S. Chiou, C-L. Wang, and S-C. Yeh. "An adaptive location estimator using tracking algorithms for indoor WLANs." *Wireless Networks*, 16.7 1987-2012, 2010.

[6] H. Lim, *et al.* "Zero-configuration indoor localization over IEEE 802.11 wireless infrastructure." *Wireless Networks*, 16.2, 405-420, 2010.

[7] J. Hightower, and G. Borriello. "Location systems for ubiquitous computing." *Computer*, 34.8: 57-66, 2001.

[8] K. Pahlavan, X. Li, and J-P. Makela, "Indoor geolocation science and technologym" *IEEE Communications Magazine*, 40.2: 112-118, 2002.

[9] J. G. Proakis and M. Salehi, "Communication systems engineering," Vol. 2. New Jersey: Prentice Hall, 1994.

[10] A. K. M. M. Hossain, and W.-S. Soh, "A comprehensive study of bluetooth signal parameters for localization," *IEEE 18th International Symposium on. Personal, Indoor and Mobile Radio Communications*, 2007.

[11] H. Liu, *et al.* "Survey of wireless indoor positioning techniques and systems," *IEEE Transactions on Systems, Man, and Cybernetics, Part C (Applications and Reviews)*, 37.6: 1067-1080, 2007.

[12] F. Li, and R. J. Vaccaro. "Unified analysis for DOA estimation algorithms in array signal processing," *Signal Processing*, 25.2: 147-169, 1991.

[13] A. AM. Saleh, and R. Valenzuela, "A statistical model for indoor multipath propagation," *IEEE Journal on selected areas in communications* 5.2: 128-137, 1987.

[14] Q. H. Spencer *et al,* "Modeling the statistical time and angle of arrival characteristics of an indoor multipath channel," *IEEE Journal on Selected areas in communications*, 18.3: 347-360, 2000.

[15] S. Sen *et al.* "Avoiding multipath to revive inbuilding WiFi localization." *Proceeding of the 11th annual international conference on Mobile systems, applications, and services.* ACM, 2013.

[16] A. T. Mariakakis *et al.* "Sail: Single access point-based indoor localization." *Proceeding of the 12th annual international conference on Mobile systems, applications, and services.* ACM, 2014.

[17] M. Kotaru *et al.* "Spotfi: Decimeter level localization using wifi." *ACM SIGCOMM Computer Communication Review.* Vol. 45. No. 4. ACM, 2015.

[18] D. Vasisht, S. Kumar, and D. Katabi. "Decimeter-Level Localization with a Single WiFi Access Point." *NSDI.* 2016.

[19] M. Shahram and P. Milanfar. "On the resolvability of sinusoids with nearby frequencies in the presence of noise." *IEEE Transactions on Signal Processing*, 53.7: 2579-2588, 2005.

[20] F. C. Schweppe, "Sensor array data processing for multiple signal sources," *IEEE Transactions on Information Theory*, vol. IT, 14, pp. 294-305, 1968.

[21] M.S. Bartlett, "Smoothing Periodograms from Time Series with Continuous Spectra," *Nature*, 161:686-687, 1948.

[22] J . Capon, "High-resolution frequency-wavenumber spectrum analysis," *Proceedings of the IEEE*, 57.8: 1408-1418, 1969.

[23] H. L. Van Trees, "Detection, Estimation, and Modulation Theory," Part IV, Optimum Array Processing. New York: Wiley, 2002.

[24] R. 0 . Schmidt, "Multiple emitter location and signal parameter estimation," *IEEE Trans. Antennas and Propagation*, vol. AP-34, pp. 276- 280, 1986.

[25] A. Barabell, "Improving the resolution performance of eigenstructure-based direction-finding algorithms," *IEEE International Conference on Acoustics, Speech, and Signal Processing*, ICASSP'83, Vol. 8, 1983.

[26] R. Roy and T. Kailath, "ESPRIT-Estimation of signal parameters via rotational invariance techniques," *IEEE International Conference on Acoustics, Speech, and Signal Processing*, ICASSP'89, vol.37, no. 7, pp. 984-995, July 1989.

[27] F. Gao, and A. B. Gershman. "A generalized ESPRIT approach to direction-of-arrival estimation." *IEEE signal processing letters*, 12.3: 254-257, 2005.

[28] M. L. McCloud, and L. L. Scharf. "A new subspace identification algorithm for high-resolution DOA estimation." *IEEE Transactions on Antennas and Propagation* 50.10: 1382-1390, 2002.

[29] W.-K. Ma, T.-H. Hsieh, and C.-Y. Chi. "DOA estimation of quasi-stationary signals via Khatri-Rao subspace." *IEEE International Conference on Acoustics, Speech and Signal Processing*, ICASSP, 2009.

[30] I. Ziskind and M. Wax, "Maximum likelihood localization of multiple sources by alternating projection," *IEEE Trans. Acoust., Speech, Signal Processing*, vol. ASSP-36, pp.1553–1560, 1988.

[31] Y. Bresler and A. Macovski, "Exact Maximum Likelihood Parameter Estimation of Superimposed Exponential Signals in Noise," *IEEE Transactions on Acoustics, Speech, Signal Processing*, vol. 35, no. 10, pp. 1081–1089, Oct. 1986.

[32] P. Pal, and P. P. Vaidyanathan. "Coprime sampling and the MUSIC algorithm." *Digital Signal Processing Workshop and IEEE Signal Processing Education Workshop (DSP/SPE)*, IEEE, 2011.

[33] P. Pal, and P. P. Vaidyanathan. "Nested arrays: A novel approach to array processing with enhanced degrees of freedom." *IEEE Transactions on Signal Processing*, 58.8: 4167-4181, 2010.

[34] M. C. Vanderveen, C. B. Papadias, and A. Paulraj. "Joint angle and delay estimation (JADE) for multipath signals arriving at an antenna array," *IEEE Communications letters*, 1.1: 12-14, 1997.

[35] A-J. Van der Veen, M. C. Vanderveen, and A. Paulraj. "Joint angle and delay estimation using shift-invariance techniques." *IEEE Transactions on Signal Processing 46.2*, 405-418, 1998.

[36] C-MS. See and B-K. Poh, "Parametric sensor array calibration using measured steering vectors of uncertain locations," *IEEE Transactions on Signal Processing*, vol. 47, no. 4, pp. 1133-1137, 1999.

[37] A. Liu, G. Liao, C. Zeng, Z. Yang, and Q. Xu, "An eigenstructure method for estimating DOA and sensor gain-phase errors," *IEEE Transactions on Acoustics, Speech, Signal Processing*, vol. 59, no. 12, pp. 5944-5956, 2011.

[38] T. Svantesson, "The effects of mutual coupling using a linear array of thin dipoles of finite length," *IEEE Statistical Signal and Array Processing Workshop*, 1998.

[39] M. Wax, T. Kailath, "Detection of Signals by Information Theoretic Criteria," IEEE Transactions on Acoustics, Speech, and Signal Processing, VOL. ASSP-3, No. 2, APRIL 1985.

[40] T. W. Anderson, "Asymptotic theory for principal component analysis," Ann. J. Math. Stat., vol. 34, pp. 122-148, 1963.

[41] X. Mestre, "On the asymptotic behavior of the sample estimates of eigenvalues and eigenvectors of covariance matrices," IEEE Trans. Signal Process., vol. 56, no. 11, Nov. 2008.

[42] X. Mestre, "Improved estimation of eigenvalues and eigenvectors of covariance matrices using their sample estimates," IEEE Transactions on Information Theory, vol. 54, no. 11, pp. 5113–5129, Nov. 2008.

[43] R. Couillet and M. Debbah, "Random Matrix Methods for Wireless Communications," 1st ed. Cambridge, UK: Cambridge University Press, 2011.

[44] D. L. Donoho and M. Elad, "Optimally sparse representation in general (nonorthogonal) dictionaries via l_1 minimization," *Proc. Natl. Acad. Sci.* USA 100 (2003), 2197–2202.

[45] W. J. Fu, "Penalized regressions: the bridge versus the LASSO," *Journal of Computational and Graphical Statistics*, vol. 7, no. 3, Sept. 1998.

[46] A. Cohen, W. Dahmen, and R. DeVore, "Compressed sensing and best k-term approximation," *J. Am. Math. Soc.*, 22:211–231, 2009.

[47] M. Elad and A. M. Bruckstein, "A generalized uncertainty principle and sparse representation in pairs of bases," *IEEE Transactions on Information Theory*, 48:2558–2567, 2002.

[48] D. L. Donoho and J. Tanner, "Neighborliness of Randomly-Projected Simplices in High Dimensions," *Proc. Natl. Acad. Sci.* USA, 102:9452–9457, 2005.

[49] D. L. Donoho and J. Tanner, "Sparse Nonnegative Solutions of Underdetermined Linear Equations by Linear Programming," *Proc. Natl. Acad. Sci.* USA, 102:9446–9451, 2005.

[50] S. G. Mallat and Z. Zhang, "Matching pursuits with time-frequency dictionaries," *IEEE Transactions on Signal Processing*, 41:3397–3415, 1993.

[51] Y. C. Pati, R. Rezaiifar, and P. S. Krishnaprasad, "Orthogonal matching pursuit: Recursive function approximation with applications to wavelet decomposition," In *Proc. of the 27th Asilomar Conference on Signals, Systems and Computers*, 1:40-44, 1993.

[52] T. Blumensath and M. Davies, "Gradient pursuits," *IEEE Transactions on Signal Processing*, 56(6):2370–2382, 2008.

[53] S. Chen, D. Donoho, and M. Saunders, "Atomic decomposition by basis pursuit," *SIAM J. Sci. Comput.*, 20,pp. 33-61, 1998.

[54] M. Mishali and Y. C. Eldar, "Compressed Sensing: Theory and Applications," *Cambridge*, 2012.

[55] R. Baraniuk, "Compressive sensing," *IEEE Signal Processing Magazine*, vol. 24, no. 4, pp. 118–121, Jul. 2007.

[56] J. A. Tropp, "Greed is good: Algorithmic results for sparse approximation," *IEEE Transactions on Information Theory*, 50:2231–2242, 2004.

[57] D.L. Donoho, M. Elad, and V. Temlyakov, "Stable recovery of sparse overcomplete representations in the presence of noise," *IEEE Trans. Inform. Theory*, 52:6–18, 2006.

[58] T. Blumensath and M. Davies, "Iterative thresholding for sparse approximations," *J. Fourier Anal Appl*, 14(5):629–654, 2008.

[59] J. Portilla, "Image restoration through l0 analysis-based sparse optimization in tight frames," *Proc IEEE Int Conf Image*, 2009.

[60] T. Blumensath and M. E. Davies, "Normalized iterated hard thresholding: guaranteed stability and performance," *IEEE Journal of Selected Topics in Signal Processing*, vol. 4, no. 2, pp. 298 – 309, 2010.

[61] I. Daubechies, M. Defrise, and C. de Mol, "An iterative thresholding algorithm for linear inverse problems with a sparsity constraint," *Comm. Pure Appl. Math.*, 57 (2004), pp. 1413-1457.

[62] P. L. Combettes and V.R. Wajs, "Signal recovery by proximal forward- backward splitting," *Multiscale Model. Simul. 4* , pp. 1168-1200, 2005.

[63] J. J. Moreau, "Proximite et dualite dans un espace hilbertien," *Bull. Soc. Math.*, France 93, 273299, 1965.

[64] T. Blumensath and M. Davies, "Iterative hard thresholding for compressed sensing," *Appl Comput Harmonic Anal*, 27(3):265–274, 2009.

[65] R. Garg and R. Khandekar, "Gradient Descent with Sparsification: an iterative algorithm for sparse recovery with restricted isometry property," *Proc Int Conf Machine Learning*, Montreal, Canada; 2009.

[66] M. Masood and T. Y. Al-Naffouri, "Sparse reconstruction using distribution agnostic Bayesian matching pursuit," *IEEE Transactions on Signal Processing*, vol. 61, no. 21, pp. 5298–5309, Nov. 2013.

[67] P. Schniter, L. C. Potter, and J. Ziniel, "Fast bayesian matching pursuit," in *Proc. Workshop Inform. Theory Appl. (ITA)*, 2008.

[68] D. Wipf, "Bayesian methods for finding sparse representations," Ph. D., Univ. Calif., San Diego, 2006.

[69] D. Wipf, B. D. Rao, and S. Nagarajan, "Latent variable Bayesian models for promoting sparsity," *IEEE Transactions on Information Theory*, 2010.

[70] D. Wipf, J. Palmer, B. Rao, and K. Kreutz-Delgado, "Performance analysis of latent variable models with sparse priors," in *Proc. IEEE Int. Conf. Acoust., Speech, Signal Process.*, Apr. 2007.

[71] M. J. Beal, "Variational algorithms for approximate Bayesian inference," PhD Thesis, University College London, 2003.

[72] C. M. Bishop, "Pattern Recognition and Machine Learning," *Springer*, 2006.

[73] M. J. Beal and Z. Ghahrarmani, "The variational Bayesian EM algorithm for incomplete data: With application to scoring graphical model structures," in Bayesian Statistics. Oxford, U.K.: Oxford Univ. Press, vol. 7, 2002.

[74] T. Zhang, "Adaptive forward-backward greedy algorithm for learning sparse representations." *IEEE transactions on information theory,* 57.7 (2011): 4689-4708.

[75] D. Tse and P. Viswanath, "Fundamentals of Wireless Communication," New York: Cambridge Univ. Press, 2005, pp. 10–42.

[76] D. N. Lawley, "Tests of significance of the latent roots of the covariance and correlation matrices," Biometrica, vol. 43,pp. 128-136,1956.

[77] M. Wax and T. Kailath, "Detection of signals by information theoretic criteria," IEEE Trans. Acoust., Speech, Signal Process., vol. ASSP-33, no. 2, pp. 387–392, Apr. 1985.

[78] M. P. Clark and L. L. Scharf, "A maximum likelihood estimation technique for spatial-temporal modal analysis," in Proceedings of the 25th Asilomar Conference on Signals, Systems and Computers, vol. 1, pp. 257–261, Pacific Grove, Calif, USA, November 1991.

[79] M. Gurelli and C. Nikias, "A New Eigenvector-Based Algorithm for Multichannel Blind Deconvolution of Input Colored Signals," in Proc. ICASSP, 1993, pp. 448–451.

[80] A. Gaber and A. Omar, "A Study of Wireless Indoor Positioning Based on Joint TDOA and DOA Estimation Using 2-D Matrix Pencil Algorithms and IEEE 802.11ac," IEEE Trans. on Wireless Communications, Vol. 14, No. 5, May 2015.

[81] T. J. Shan, M. Wax, and T. Kailath, "On spatial smoothing for direction of arrival estimation of coherent signals," IEEE Trans. ASSP, vol. 33, no.4, pp. 806-811, Apr. 1985.

[82] M. Oziewicz, "On application of MUSIC algorithm to time delay estimation in OFDM channels," IEEE Trans. Broadcasting, vol. 51, no.2, pp. 249–255, June 2005.

[83] S. Boyd and L. Vandenberghe, "Convex Optimization," *Cambridge University Press*, 2009.

[84] B. M. Radich and K. M. Buckley. "Single-snapshot DOA estimation and source number detection," *IEEE Sig. Proc. Letters*, Vol. 4, no. 4, 109-111, 1997.

[85] B. Friedlander, and A. J. Weiss. "Direction finding in the presence of mutual coupling." *IEEE Transactions on Antennas and Propagation*, vol. 39, no. 3, pp. 273-284, 1991.

[86] T. Su, K. Dandekar, and H. Ling, "Simulation of mutual coupling effect in circular arrays for direction-finding applications," *Microwave and optical technology letters*, vol. 26, no. 5, pp. 331-336, 2000.

[87] H. T. Hui, "A new definition of mutual impedance for application in dipole receiving antenna arrays," *IEEE Antennas and Wireless Propagation Letters*, vol. 3, no. 1, 364-367, 2004.

[88] B. Liao, Z.G. Zhang, S.C. Chan, "DOA Estimation and Tracking of ULAs with Mutual Coupling," IEEE Trans on Aerospace and Electronic Systems, vol. 48, 2012, 891-905.

[89] E. W. J. Ding and B. Su, "A new method for DOA estimation in the presence of unknown mutual coupling of an antenna array," *48th Asilomar Conference on Signals, Systems and Computers,* IEEE, 2014.

[90] M. Pesavento, A. B. Gershman, and K. M. Wong, "Direction finding in partly calibrated sensor arrays composed of multiple subarrays." *IEEE Transactions on Signal Processing*, vol. 50, no. 9, pp. 2103-2115, 2002.

[91] W. Bu-Hong, W. Yong-liang, and C. Hui, "A robust DOA estimation algorithm for uniform linear array in the presence of mutual coupling," *IEEE Antennas and Propagation Society International Symposium*, Vol. 3, pp. 924-927, 2003.

[92] J. Dai, X. Bao, N. Hu, C. Chang, and W. Xu "A recursive RARE algorithm for DOA estimation with unknown mutual coupling," *IEEE Antennas and Wireless Propagation Letters* 13, pp. 1593-1596, 2014.

[93] F. Sellone and A. Serra, "A novel online mutual coupling compensation algorithm for uniform and linear arrays," *IEEE Transactions on Signal Processing*, vol. 55, no. 2, pp. 560-573, 2007.

[94] A. Jaffe and M. Wax, "Single-site localization via maximum discrimination multipath fingerprinting," *IEEE Transactions on Signal Processing*, vol. 62, no. 7, pp. 1718-172, 2014.

[95] P. Stoica and A. Nehorai, "MUSIC, Maximum Likelihood and Cramér-Rao bound," *IEEE Transactions on Acoustics, Speech, Signal Processing*, vol. 37, pp. 720-741, 1989.

[96] T. Svantesson, "Antennas and Propagation from a Signal Processing Perspective," PhD thesis, Chalmers University of Technology, Gothenburg, Sweden, 2001.

[97] T. Svantesson, "Modeling and estimation of mutual coupling in a uniform linear array of dipoles," *IEEE International Conference on Acoustics, Speech, and Signal Processing (ICASSP)*, Phoenix, AZ, March 1999.

[98] K. B. Petersen and M. S. Pedersen, "The matrix cookbook,", Version 20070905. [Online]. Available: http://www2.imm.dtu.dk/pubdb/p.php?3274, Feb. 2008.

[99] R. M. Gray, *"Toeplitz and Circulant Matrices : A Review,"* Available online at http://www-ee.stanford.edu/ gray/toeplitz.pdf, 2002.

[100] T. Kato, "Perturbation theory for linear operators," *Springer Science and Business media*, Vol. 132, 2013.

[101] D. Bau and L. Trefethen, "Numerical linear algebra," *Society for Industrial and Applied Mathematics (SIAM)*, Philadelphia, PA, 1997.

[102] J. J. Sakurai and J. Napolitano, "Modern quantum mechanics," *Addison-Wesley*, 2011.

[103] A. Bazzi, D. T.M. Slock, L. Meilhac, "Detection of the number of Superimposed Signals using Modified MDL Criterion : A Random Matrix Approach," *IEEE International Conference on Acoustics, Speech, and Signal Processing* (ICASSP), March, 2016.

[104] A. Bazzi, D. T.M. Slock, L. Meilhac, S. Panneerselvan, "A Comparative Study of Sparse Recovery and Compressed Sensing Algorithms with Application to AoA Estimation," *IEEE International Workshop on Signal Processing advances in Wireless Communications* (SPAWC), 2016.

[105] A. Bazzi, D. T.M. Slock, L. Meilhac, "Sparse Recovery using an Iterative Variational Bayes Algorithm and Application to AoA Estimation," *IEEE Symposium on Signal Processing and Information Technology*, 2016.

[106] A. Bazzi, D. T.M. Slock, L. Meilhac, "A Newton-type Forward Backward Greedy Method for Multi-Snapshot Compressed Sensing," *Asilomar conference on signals, systems, and computers* (ASILOMAR), 2017.

[107] A. Bazzi, D. T.M. Slock, L. Meilhac, "Efficient Maximum Likelihood Joint Estimation of Angles and Times of Arrival of Multi Paths," *IEEE GLOBAL Communications Conference* (GLOBECOM), Localization and Tracking : Indoors, Outdoors, and Emerging Networks (LION) Workshop, December, 2015.

[108] A. Bazzi, D. T. M. Slock, and L. Meilhac, "Single Snapshot Joint Estimation of Angles and Times of Arrival: A 2D Matrix Pencil Approach," *ICC*, 2016.

[109] A. Bazzi, D. T.M. Slock, L. Meilhac, "On Spatio-Frequential Smoothing for Joint Angles and Times of Arrival Estimation of Multipaths," *IEEE International Conference on Acoustics, Speech, and Signal Processing* (ICASSP), March, 2016.

[110] A. Bazzi, D. T.M. Slock, L. Meilhac, "JADED-RIP: Joint Angle and Delay Estimator and Detector via Rotational Invariance Properties," *IEEE International Symposium on Signal Processing and Information Technology*, (ISSPIT), 2016.

[111] A. Bazzi, D. T.M. Slock, L. Meilhac, "Online Angle of Arrival Estimation in the Presence of Mutual Coupling," *IEEE International Workshop on Statistical Signal Processing* (SSP), 2016.

[112] A. Bazzi, D. T.M. Slock, L. Meilhac, "On Mutual Coupling for ULAs: Estimating AoAs in the presence of more coupling parameters," *IEEE International Conference on Acoustics, Speech, and Signal Processing* (ICASSP), 2017.

[113] A. Bazzi, D. T.M. Slock, L. Meilhac, "Performance Analysis of an AoA estimator in the presence of more mutual coupling parameters," *IEEE International Conference on Acoustics, Speech, and Signal Processing* (ICASSP), 2017.

[114] A. Bazzi, D. T.M. Slock, L. Meilhac, "On a Mutual Coupling Agnostic Maximum Likelihood Angle of Arrival Estimator by Alternating Projection," *IEEE Global Conference on Signal and Information Processing* (GlobalSIP), 2016.

[115] A. Bazzi, D. T.M. Slock, L. Meilhac, "A Mutual Coupling Resilient Algorithm for Joint Angle and Delay Estimation," *IEEE Global Conference on Signal and Information Processing* (GlobalSIP), 2016.